STUDIES ON THE THERMAL DECOMPOSITION BEHAVIOUR, KINETICS AND ELECTRICAL CONDUCTIVITY OF THE NON-ISOTHERMAL DECOMPOSITION OF PYRIDINE MONO CARBO-XYLIC ACIDS AND SOME OF THEIR TRANSITION METAL COMPLEXES

Ghareeb Nemir Al-Sousi
Doctor of Philosophy

THE UNIVERSITY OF ASTON IN BIRMINGHAM

January 2000

Thesis Summary

THE UNIVERSITY OF ASTON IN BIRMINGHAM

STUDIES ON THE THERMAL DECOMPOSITION BEHAVIOR, KINETICS AND ELECTRICAL CONDUCTIVITY OF THE NON-ISOTHERMAL DECOMPOSITION OF PYRIDINE MONO CARBO-XYLIC ACIDS AND SOME OF THEIR TRANSITION METAL COMPLEXES.

Ghareeb Nemir Al-Sousi
Doctor of Philosophy
January 2000

The thesis is divided into four chapters. They are: introduction, experimental, results and discussion about the free ligands and results and discussion about the complexes.

The First Chapter, the introductory chapter, is a general introduction to the study of solid state reactions.

The Second Chapter is devoted to the materials and experimental methods that have been used for carrying out the experiments.

The Third Chapter is concerned with the characterisations of free ligands (Picolinic acid, nicotinic acid, and isonicotinic acid) by using elemental analysis, IR spectra, X- ray diffraction, and mass spectra. Additionally, the thermal behaviour of free ligands in air has been studied by means of thermogravimetry (TG), derivative thermogravimetry (DTG), and differential scanning calorimetry (DSC) measurements. The behaviour of thermal decomposition of the three free ligands was not identical. Finally, a computer program has been used for kinetic evaluation of non-isothermal differential scanning calorimetry data according to a composite and single heating rate methods in comparison with the methods due to Ozawa and Kissinger methods. The most probable reaction mechanism for the free ligands was the Avrami-Erofeev equation (A) that described the solid-state nucleation-growth mechanism. The activation parameters of the decomposition reaction for free ligands were calculated and the results of different methods of data analysis were compared and discussed.

The Fourth Chapter, the final chapter, deals with the preparation of cobalt, nickel, and copper with mono-pyridine carboxylic acids in aqueous solution. The prepared complexes have been characterised by analyses, IR spectra, X-ray diffraction, magnetic moments, and electronic spectra. The stoichiometry of these compounds was $ML_2x(H_2O)$, (where M = metal ion, L = organic ligand and x = water molecule). The environments of cobalt, nickel, and copper nicotinates and the environments of cobalt and nickel picolinates were octahedral, whereas the environment of copper picolinate [Cu(PA)2] was tetragonal. However, the environments of cobalt, nickel, and copper isonicotinates were polymeric octahedral structures. The morphological changes that occurred throughout the decomposition were followed by SEM observation. TG, DTG, and DSC measurements have studied the thermal behaviour of the prepared complexes in air. During the degradation processes of the hydrated complexes, the crystallisation water molecules were lost in one or two steps. This was also followed by loss of organic ligands and the metal oxides remained. Comparison between the DTG temperatures of the first and second steps of the dehydration suggested that the water of crystallisation was more strongly bonded with anion in Ni(II) complexes than in the complexes of Co(II) and Cu(II). The intermediate products of decomposition were not identified. The most probable reaction mechanism for the prepared complexes was also Avrami-Erofeev equation (A) characteristic of solid-state nucleation-growth mechanism. The temperature dependence of conductivity using direct current was determined for cobalt, nickel, and copper isonicotinates. An activation energy ($\Delta\bar{E}$), the activation energy (ΔE) were calculated. The temperature and frequency dependence of conductivity, the frequency dependence of dielectric constant, and the dielectric loss for nickel isonicotinate were determined by using alternating current. The value of s parameter and the value of density of state [$N(E_f)$] were calculated.

Keyword Thermal decomposition, kinetic, electrical conduction, pyridine mono-carboxylic acid, complex, transition metal complex.

DEDICATION

To my parents
To my wife
To my sons
To my daughters

ACKNOWLEDGEMENTS

I express my most sincere gratitude to Prof. **Dr. D. J. Miller**, **Prof. Dr. El-Husseiny Diefallah**, and my supervisors for their co-operation advice, and stimulating discussion during the course of this work.

Thank you to **Dr. A. A. El-Bellihi** of the Faculty of Science, King Abdulaziz University, Jeddah, Kingdom of Saudi Arabia, for continuous help.

Thank you to **Prof. Dr. Mohamed T. Makhloof** of the Faculty of Science, Assiut University, Assiut, Egypt, for supplying IR measurements and elemental analysis.

Thank you to **Dr. A. Eifan**, Vice-Dean of the Faculty of Earth Science, King Abdulaziz University, Jeddah, Kingdom of Saudi Arabia, for doing XR measurements.

The author is deeply indebted to **Dr. M. Qurashi** of the Faculty of Applied Science, Omm Al- Kora University, Makah, Kingdom of Saudi Arabia, for doing thermal measurements.

I am also indebted to my colleague **Dr. N. Shash** of the Faculty of Science, Banha University, Banha, Egypt, for his valuable assistance, continual interest, sincere help and guidance, and for sharing his personal experience.

Thank you to **Mr. Ayman A. H. Ghannam** and **MS. Aruua Eid** of the Faculty of Science, University of Jordan, Amman, Jordan, for doing AC current measurements.

CONTENTS

TABLES

FIGURES

CHAPTER 1

INTRODUCTION

INTRODUCTION

1.1 Properties of co-ordination compounds.

Co-ordination compounds conventionally consist of a central atom or ion surrounded by a set of (usually 2 to 9) other atoms, ions, or small molecules, the latter being called ligands. The resulting conglomeration is often called a complex or, if it is charged, a complex ion. The terms "co-ordination compound and "complex" may be broadly defined to embrace all species, charged or uncharged, in which a central atom is surrounded by a set of outer or ligand atoms. The co-ordination number is the number of outer or ligand atoms bound to the central one. The set of ligands need not consist of several small independent sets of atoms (or single atoms), but may involve fairly elaborate arrangements of atoms connecting those few that are directly bound to - or coordinated to - the central atom[1].

Co-ordination compounds have been found useful in many important applications in various fields. They have been used in households, industry, medicine, and biological systems[2]. In water treatment, for example, chelating agents such as tripolyphosphate ions $[P_3O_{10}]^{5-}$ and nitrilotriacetic acid $[N(CH_2)_3(COOH)_3]$ are used to remove Ca^{2+} and Mg^{2+} ions in hard water. These chelating agents form stable water-soluble complexes with undesirable ions. Recent studies have shown that some of the co-ordination complexes of platinum effectively inhibit the growth of cancerous cells. For example: cis-diaminedichloroplatinum $[Pt(NH_3)Cl_2]$, cis-ethylendiaminedichloroplatinum $[Pt(H_2NCH_2CH_2NH_2)Cl_2]$ and cis-dianilinedichloroplatinum $[Pt(C_6H_6NH_2)_2Cl_2]$. The development of new semiconducting and conducting organometallic polymers is an important area of current research because of the potential applications in solid state electro-optical systems. These materials can have prime roles in devices such as sensors, detectors, and electrophotographic units where chemical, photo, and thermal stability are essential [3]. Hydroxyoximates $[2\text{-}OHC_6H_6RCNOH]$ consist of organo-nitrogen, oxygen compounds with

strong binding properties, which are also known to have a significant and extensive application as an analytical reagent in solvent extraction systems and in hydrometallurgy. Such applications are of continuing interest and industrial importance. Moreover, the new application of copper(II) chelates of salicylaldoxime [2-(HO)C_6H_4CH=NOH] and related ligands as anti-proliferative and anti-neoplastic suggests further investigation on the coordination chemistry of hydroxyoximates [4].

Pyridine compounds, ranging in complexity from nicotine to mono-substituted pyridine like nicotinamide and nicotinic acid, play an important role in the metabolism of all living cells. Nicotinamide and nicotinic acid are of biological origin. Nicotinamide is an important compound of the hydrogen-carrying co-enzymes nicotinamide-adenine dinucleotide and nicotinamide-adenine dinucleotide phosphate while nicotinic acid is an essential vitamin[5]. Isonicotinic acid is of biological origin, and it can be produced by cell metabolism from isonicotinic acid hydrazide (isoniazid), a drug widely used in the treatment and prophylaxis of tuberculosis. Several complexes of transition metals with isonicotinic acid have been previously prepared, but only two compounds between a transition metal halide and this ligand have been reported in the literature[6].

The importance of heterocyclic compounds[7] is apparent from the wealth and variety of such compounds that occur naturally or are prepared on commercial scale by the dye and drug industries. Many of these compounds fulfill important physiological functions in plants and animals. Among the most important and most interesting heterocycles are the ones that possess aromatic properties. Pyridine is classified as aromatic on the basis of its properties. It is flat with bond angles of 120°; the four carbon-carbon bonds are of the same length, and so are the two carbon-nitrogen bonds. It resists addition and undergoes electrophilic and nuclophilic substitution.

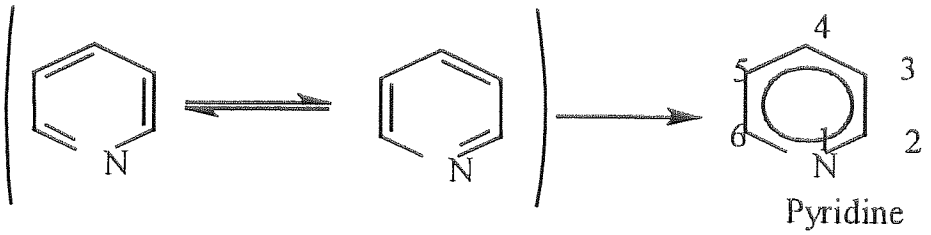

In an electronic configuration the nitrogen atom like each of the carbon atoms is bonded to other members of the ring by the use of sp^2 orbitals and provides one electron for the π cloud. The third sp^2 orbital of each carbon atom is used to form a bond to hydrogen. The third sp^2 orbital of nitrogen simply contains a pair of electrons, which is available for sharing with acid.

Pyridine is found in coal tar. Along with it are found a number of methyl- pyridines, the most important of which are the mono-methyl compounds known as picolines. Oxidation of picolines yields the pyridine carboxylic acids.

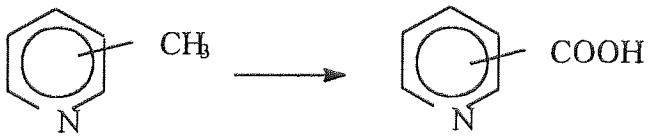

Picoline Pyridine carboxylic acid

The 3-isomer (nicotinic acid or niacin) is a vitamin. The 4- isomer (isonicotinic acid) has been used in the form of its hydrazide in treatment of tuberculosis[8].

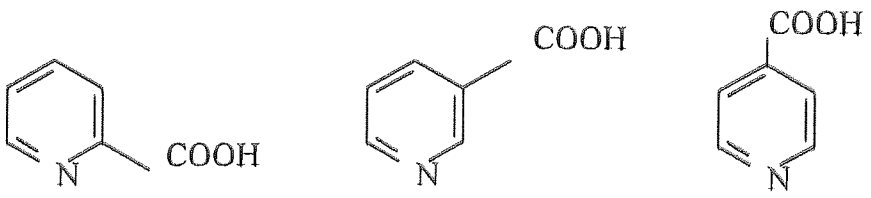

Picolinic acid Nicotinic acid Isonicotinic acid

Isomers of pyridine carboxylic acids

Among the most important " classical " ligands are the halide ions, F^-, Cl^-, Br^-, I^-, the anions of various oxo acid, such as NO_3^-, NO_2^-, RCO_2^-, SO_4^{2-} and neutral molecules in which the donor atoms are usually N or O, the examples being NH_3, RNH_2, H_2O, MeOH, R_2SO and CH_3CN. The simplest role that each of these ligands can play is that of an electron-pair donor to single cation.

Some of these donors occur in sets of two, or more, in a complex ligand that is structurally capable of permitting all the donors simultaneously to form bonds to the same metal atom. This is illustrated for several important types of donor groups in the following. Such ligands are called ***polydenatate*** (or multidentate) ligands and also chelating ligands[1].

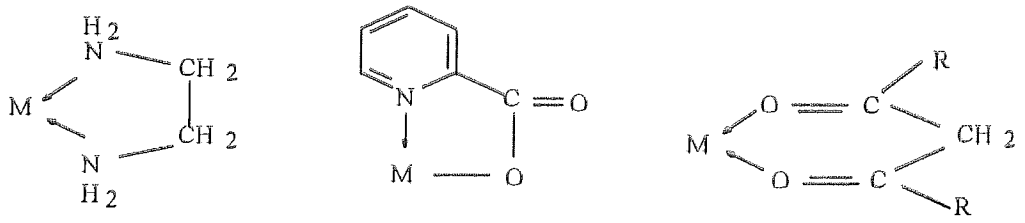

Cyclic ligands having nitrogen, oxygen, and sulfur donor atoms in their structures can act as good chelating agents for transitional and non-transitional metal ions. However, work on cyclic ligand complexes is still very sparse[9]. Cyclic ligands having oxygen or nitrogen donor atoms in their structures can act as good chelating agents for transition and non-transition metal ions. However, works on cyclic ligand complexes are still very rare, and there has been little thermal investigation of cyclic ligand complexes in the solid state[10]. Cyclic molecules containing the group $N(CH_2)_nN$ in their structures are among the best characterized chelating agents for transition metals[11]. Hippuric acid is a monocarboxylic acid with three types of donor sites: the nitrogen and oxygen atoms of the amide group and the oxygen atoms of the carboxylic acid group[12]. The compound 4-(butylamino) benzoic acid has two different sites for

forming bonds with metal ions: the nitrogen atom of the amino group and the oxygen atoms of the carboxylic acid group[13].

1.2 THERMAL ANALYSIS

The term thermal analysis will be defined as those techniques in which some physical parameter of the system is determined as a function of temperature. The physical parameter is recorded as a dynamic function of temperature. Using this definition, the principle techniques of thermal analysis are dynamic thermogravimetry (TG) and differential thermal analysis (DTA). Other less widely employed but useful techniques include evolved gas detection or analysis (EGD or EGA), thermomechanical analysis (TMA), dynamic reflectance spectroscopy (RS), electrical conductivity (EC), and photothermal analysis (PTA);

It should be pointed out that, in many cases, the use of only a single thermal analysis technique may not provide sufficient information about a given system[14]. As with many other analytical methods, complementary or supplementary techniques may be required. For example, it is fairly common to complement all DTA or DSC data with thermogravimetry TG.

The thermal analysis technique of thermogravimetry (TG) is one in which the change in sample mass is recorded as a function of temperature. Three modes of thermogravimetry may be described[14,15]:

(a) Isothermal or static thermogravimetry, in which the sample mass is recorded as a function of time at a constant temperature;

(b) Quasistatic thermogravimetry, in which the sample is heated to constant mass at each of a series of increasing temperatures; and

(c) Dynamic thermogravimetry, in which the sample is heated in an environment whose temperature, is changing in a predetermined manner, preferably at a linear rate.

The resulting mass-change versus temperature curve (which has various synonyms such as thermolysis curve, pyrolysis curve, thermogram, thermogravimetric curve, thermogravimetric analysis curve, and so on) provides information concerning the thermal stability and composition of the initial sample. To yield useful information with this technique, the sample must evolve a volatile product, which can originate by various physical and chemical processes. Except for the mass-change, much of the information obtained from the TG curve is of an empirical nature, in that the transition temperatures are dependent on the instrumental and sample parameters. Thus, it is difficult to make meaningful comparisons between the TG data obtained on different thermobalances in different laboratories. The use of commercially available thermobalances has done much to improve this situation, but it should still be noted that the curve transition temperatures are procedurally obtained temperatures and are not fundamental to the compound as are X-ray d-spacing and infrared absorption band minima. Two temperatures may be selected as characteristics of any single-stage nonisothermal reaction (T_i and T_f). T_i. the initial temperature or procedural decomposition temperature (pdt), is the temperature at which the cumulative mass-change reaches a magnitude that thermobalance can detect. T_f, the final temperature is the temperature at which the cumulative mass-change first reaches its maximum value, corresponding to complete reaction. However, the T_i may be the lowest temperature at which the onset of a mass-change may be observed in a given experiment. At a linear heating rate, T_f must be greater than T_i, and the difference, $T_f - T_i$, is called the reaction interval. For an endothermic decomposition reaction, both T_i and T_f are increased with an increased heating rate, the effect being greater for T_i than T_f.

1.3 KINETICS OF SOLID STATE REACTION

Knowledge of the relevant kinetic behaviour is important for comprehensive evaluation of solid state reaction processes. The kinetic parameters of the decomposition process can be calculated from the relevant non-isothermal thermogravimetric data[16].

Knowledge of the kinetic reaction is important in two respects[17]. First, such kinetics are related to simple mathematical descriptions of the process. Second, they are important data in the evaluation of stability and compatibility for energetic materials and in the study of manufacturing processes for crystalline materials. Since thermal analysis techniques show versatility in studying the kinetics of cases such as those of crystalline and non-crystalline materials, a number of methods for evaluating the kinetic parameters have been developed.

The kinetic treatment of non-isothermal thermoanalytical (TA) data has been a widely discussed topic for many years[18]. The popularity of the non-isothermal method of kinetic analysis of TA data is mainly due to the fact that both analytical and kinetic data can be obtained simultaneously in a relatively short period of time. Unfortunately, the ease with which such data can be obtained has resulted in an increase in the quality of TA research. Therefore, it is not surprising that the usefulness and reliability of kinetic parameters obtained from non-isothermal TA data are questioned. It seems that the problems arise from the uncritical application of standard techniques of TA data processing, not taking into account the basic assumption under which these methods were derived.

Comparison of the results of kinetic processing of data obtained under isothermal and nonisothermal experimental conditions[19] is a source of information about the mechanism of the process. As a rule, the values of the kinetic parameters are compared. It is obvious that such a comparison can yield

only information about the difference of the temperature dependencies of the rate of the process proceeding under isothermal and nonisothermal conditions. Of no less interest is information about the regime of the kinetic experiment on the mechanism of the process. On the face of it, such information can be described in the best way.

The advantages of determining kinetic parameters by non-isothermal methods rather than by conventional isothermal studies are:

(a) That considerably less data are required;

(b) That the kinetics can be calculated over an entire temperature range in a continuous manner;

(c) That when a sample undergoes a considerable reaction in being raised to the required temperature, the results obtained by an isothermal method are often questionable; and

(d) That only a single sample is required[19,20].

A decided disadvantage of nonisothermal compared with isothermal methods is that the reaction mechanism cannot usually be determined, and hence, the meaning of the activation energy, order of reaction, and frequency factor is uncertain.

In an increasing number of areas of technology and industry, progress is recognised as being directly related to understanding the factors influencing the reactivity of solids and how they react and interact in specific environments[20]. In general, reactions, which include solid reactions, are very complex from the kinetic standpoint as they involve several physical and chemical steps.

Many thermal techniques have been applied as valuable tools for studying the kinetics of thermal solid decomposition[14]. In analyzing the kinetic data it is true that the conventional isothermal method is important for estimating the kinetic model and parameters, but the dynamic method has some advantages over it in several respects.

There is considerable diversity in the mechanisms by which solids react and there are a variety of factors which may control, determine, influence or modify the rate-limiting processes. The kinetics of the thermal decomposition of solids are affected by experimental factors and processing parameters. Moreover, the use of different methods of kinetic analysis of isothermal and dynamic TG data obtained on one system usually gives different results[21].

Thermal analytic methods have been used extensively for studying the kinetics of solid powder decomposition reaction. In the analysis of data, it is true that the conventional isothermal method is more precise for estimating the kinetic model and parameters, but dynamic methods have advantages over the conventional isothermal method in several respects. Comparisons of thermal stabilities and reactivity parameters among a series of solids by means of dynamic thermal analysis should be meaningful if the experiments and the data analysis were carried out under identical conditions[22].

Results from TG curves are known to be affected by a number of experimental variables such as heating rate, sample mass, particle size, packing, and atmosphere. Although the dependence of activation energy *(E)* and pre-exponential *(A)* on the sample mass and heating rate is well known, only recently have attempts been made to study the dependence quantitatively. However, no effort seems to have been made so far to explore the possible relation between the type of reaction and kinetic parameters with procedural factors[23].

It has been reported that the kinetic parameters obtained from thermoanalytical (TA) measurements of solid state decompositions change depending on the sample mass examined. The gradients of temperature and partial pressure of the evolved gas in the sample matrix cause the change in the sample mass[24].

In recent years there has been an increase in the determination of the rate dependent parameters of solid state non-isothermal decomposition reactions by

the analysis of TG curves. Several equations have been proposed as a means of analyzing a TG curve and obtaining values for its kinetic parameters. Many authors have discussed the advantages of this method over the conventional isothermal method[25].

There are basically two kinds of methods for evaluating kinetic parameters in thermal analysis. One is the single-heating-rate method and the other is the multi-heating-rate method. In both, there are two routines which are most often used - the differential method and the integral method. There is, however, another method due to Kissinger which is based on the change in the position of the peak maximum with the heating rate being used. Although it was originally deduced from data obtained from differential thermal analysis (DTA), the method allows the reaction rate and the reaction extent to be obtained from the thermogravimetry (TG). However, in general, it is difficult to locate the exact peak maxim positions, and the reaction process is affected by the reaction environment[26].

There is, however, another method proposed by Ozawa[27] which is based on the change in the absolute temperature for different heating rates with the same conversion α values.

1.4 METHODOLOGY OF KINENTIC PARAMETERS AND MECHANISM OF REACTION FROM NON-ISOTHERMALDATA

In many industrial practices and thermal analysis studies the starting material is in a solid state at the commencement. During the heat treatment, the starting solid material may undergo a transition that occurs either completely or partially to the liquid or gas phase, and it is important to recognise this position of the solid phase. There are several possibilities[28]:

$$A_{(solid)} \xrightarrow{\Delta} A_{(Liquid)} \xrightarrow{\Delta} B_{(solid)} + C_{(gases)}$$

$$A_{(solid)} \xrightarrow{\Delta} B_{(solid)} + C_{(gases)}$$

$$A_{(solid)} \xrightarrow{\Delta} A_{(Liquid)} \xrightarrow{\Delta} C_{(gases)}$$

$$A_{(solid)} \xrightarrow{\Delta} C_{(gases)}$$

$$A_{(solid)} \xrightarrow{\Delta} B_{(Liquid)} + C_{(gases)}$$

$$A_{(solid)} + (gases) \xrightarrow{\Delta} C_{(gases)}$$

The kinetics of thermal dehydration of different complexes and salts have recently been extensively studied. Both isothermal and nonisothermal methods have been used to evaluate the kinetic parameters and to elucidate the mechanism of dehydration reaction [29].

Deduction of the kinetic parameters and mechanism of reaction using non-isothermal methods have been discussed by Sestak and Berggeren[30] and by Satava[31]. In thermal analysis, the rate of a decomposition process can be described as the product of two separate functions of temperature and conversion using the following equation[32]:

$$\frac{d\alpha}{dt} = k(T)f(\alpha) \qquad (1)$$

where $k(T)$ is temperature-dependent and $f(\alpha)$ is the conversion function dependent on the mechanism of the reaction. It has been established that the

temperature-dependent function ***k(T)*** is of the Arrhenius type and can be written as the constant k

$$k = Ae^{-(E/RT)} \tag{2}$$

Where A is the pre-exponential factor or frequency factor, E is the activation energy, R is the gas constant, and T is the absolute temperature.

If eqn. (1) is combined with eqn. (2), then

$$\frac{d\alpha}{dt} = f(\alpha)Ae^{(-E/rRT)} \tag{3}$$

By rearrangement of eqn. (3), then

$$\frac{d\alpha}{f(\alpha)} = Ae^{(-E/RT)}dt \tag{4}$$

With constant temperature increase, β= dT/dt, then

$$dt = \frac{dT}{\beta} \tag{5}$$

From eqn. (5) and eqn. (4) can be written the following form:

$$\frac{d\alpha}{f(\alpha)} = \frac{A}{\beta}e^{(-E/RT)}dT \tag{6}$$

$$\int_0^{\alpha} \frac{d\alpha}{f(\alpha)} = g(\alpha) = \frac{A}{\beta}\int_0^{T} e^{(-E/RT)}dT \tag{7}$$

The mathematical treatment of the kinetic equation makes use of one of the following three methods of evaluation: (a) differential, (b) integral, or (c) approximate[14]. Differential methods are used by Friedman[33] and Freeman and Carroll[34]. Integral methods are used by Doyle[35] and Coats and Redfern[36], as well as others[37,38]. Approximation methods were used by Horowitz and Metzger[39].

1.4.1 Differential methods:

1- Friedman[33]:

$$\ln\left(\frac{d\alpha}{dt}\right)_i = \ln Af(\alpha_i) - \frac{E}{RT_i} \tag{8}$$

2- Freeman and Carroll[34]:

$$\ln\left[\left(\frac{d\alpha}{dt}\right)/f(\alpha)\right] = \ln A - \frac{E}{RT} \tag{9}$$

α is the fractional decomposition, **T** is the temperature (K), **A** is the preexponential factor, **E** is the energy of activation, **R** is the gas constant. The subscript *i* refers to the value of the variable at the degree of conversion α_i forming at least two or more experiments under different heating rates.

For equation 8, a plot of left-hand side against $1/T_i$ is obtained by taking the experimental data directly from different heating rate curves at the same α_i value. The linear regression is then made to each α_i value and from the slope the activation energy (E) can be calculated.

For equation 9, by feeding the experimental data from a single heating rate curve a plot of left hand side versus $1/T_i$ is obtained by testing all the functions $f(\alpha)$. The linear regression can be calculated and then the activation energy E and the frequency factor A can be calculated from the slope and intercept of the regression line.

It has been reported that the differential methods give better results than the integral methods because the approximation in integral methods introduces some error in the calculation steps[40]. However, integral methods are generally preferred because they are more reliable and convenient than differential methods[41].

1.4.2 Integral Methods

Coats-Redfern[39]:

$$\ln\left(\frac{g(\alpha)}{T^2}\right) = \ln\left[\frac{AR}{\beta E}\left(1-\frac{2RT}{E}\right)\right] - \left(\frac{E}{RT}\right) \tag{10}$$

1- Modified Coats-Redfern[42]:

$$\ln\left(\frac{g(\alpha)}{T^2}\right) = \ln\left(\frac{AR}{\beta E}\right) - \left(\frac{E}{RT}\right) \tag{11}$$

2- Doyle[35]:

$$\log[g(\alpha)\beta] = \left[\log\left(\frac{AE}{R}\right) - 2.315\right] - \frac{0.4567E}{RT} \tag{12}$$

3- The Madhusudanan et. al[43].

$$\ln\left[\frac{g(\alpha)}{T^{1.921503}}\right] = \ln\left(\frac{AE}{\beta R}\right) + 3.772051 - 1.921503LnE - \frac{E}{RT} \tag{13}$$

4- MacCallum and Tanner[44]:

$$\log[g(\alpha)] = \log\left(\frac{AR}{\beta E}\right) - 0.485E^{0.435} - \frac{(0.449+0.217E)10^3}{T} \tag{14}$$

5- Horowitz-Metzeger[39]:

$$\ln g(\alpha) = \ln\frac{ART_s^2}{\beta E} - \frac{E}{RT_s} + \frac{E\theta}{RT_s^2} \tag{15}$$

6- Kissinger[45]:

$$\ln\left(\frac{\beta}{T_s^l}\right) = C - \frac{E}{RT_s} \tag{16}$$

7- Ozawa[27]:

$$-\log\beta_i = C + 0.4567\frac{E}{T_i} \tag{17}$$

α is the fractional decomposition, **T** is the temperature (K), $\mathbf{T_s}$ is the DSC peak temperature, β is the heating rate (°C min^{-1}), **A** is the preexponential factor, **E** is the energy of activation, **R** is the gas constant, θ is ($T-T_s$), Ti is the absolute temperature for that heating rate with the same conversion α value, and C is a constant.

The plots of the left-hand side of the kinetic equations against 1/T for equations 10, 11, 12, 13 and 14 and against θ for equation 15 were made from a single experimental heating rate curve, and the integral forms of the function $g(\alpha)$ may be tested . The linear regression can be calculated and then the activation energy E and the frequency factor A can be calculated from the slope and intercept of the regression line. In the Kissinger method (equation 16), by changing the heating rate, the peak temperatures can be found and from the linear regression of the $\ln(\beta / T_s^2)$ versus $1/T_s$ plot, the activation energy and other regression parameters can be calculated. According to the Ozawa method (equation 17), at least two experiments with different heating rates must be made. By plotting log β_i against $1/T_i$ the activation energy E is obtained from the slope of the best fitting line.

1.4.3 The composite method[46].

In the composite method of analysis, the results obtained not only at a different heating rate but also with different α values, are superimposed on one master curve. This has been achieved by rewriting the different approximate equations due to different workers for the integral kinetic analysis of nonisothermal data in such a form that the kinetic function g (α) and the linear heating rate β lie on one side of the equation and (1/T) on the other side. In order to do the composite analysis of nonisothermal data, equations 10, 11, 12, 13, 14 and 15 are rewritten in the forms:

Coats-Redfern:

$$\ln\left(\frac{\beta g(\alpha)}{T^2}\right) = \ln\left[\frac{AR}{E}\left(1-\frac{2RT}{E}\right)\right] - \left(\frac{E}{RT}\right) \tag{16}$$

Modified Coats-Redfern:

$$\ln\left(\frac{\beta g(\alpha)}{T^2}\right) = \ln\left(\frac{AR}{E}\right) - \left(\frac{E}{RT}\right) \tag{17}$$

Doyle:

$$\log[g(\alpha)\beta] = \left[\log\left(\frac{AE}{R}\right) - 2.315\right] - \frac{0.4567E}{RT} \tag{18}$$

The Madhusudanan et. al.:

$$\ln\left[\frac{\beta g(\alpha)}{T^{1.921503}}\right] = \ln\left(\frac{AE}{R}\right) + 3.772051 - 1.921503LnE - \frac{E}{RT} \tag{19}$$

MacCallum and Tanner:

$$\log[\beta g(\alpha)] = \log\left(\frac{AR}{E}\right) - 0.485E^{0.435} - \frac{(0.449+0.217E)10^3}{T} \tag{20}$$

Horowitz-Metzeger:

$$\ln(\beta g(\alpha)) = \ln\frac{ART_s^2}{E} - \frac{E}{RT_s} + \frac{E\theta}{RT_s^2} \tag{21}$$

Equations 16, 17, 18, 19, 20, and 21 show that the dependence of the left side of the equation (calculated for different α- values at their respective β-values) on (1/T) should give a single master straight line for the correct form of g(α) and, hence, the activation energy and the frequency factor can be calculated. In general, analysis of nonisothermal kinetic data according to the composite method showed that the different approximate integral equations

gave rise within experimental error to identical values of activation parameters using the same model for the reaction interface [47,48and49].

In solid thermal decompositions it is very difficult to establish isothermal conditions before a substantial degree of the reaction has occurred. That is why experiments with linear temperature changes are preferred. Three methods are usually applied to the analysis of nonisothermal data: differential, difference-differential, and integral methods. The integral methods are the most widely used, but they have two significant limitations: the integration of the integral temperature and the determination of the kinetic model [50]. The use of nonisothermal data to calculate kinetic parameters of solid state processes has been described in the literature for many years [51].

Mathematical treatment of the results of thermogravimetric experiments to determine the kinetic parameters of thermal decomposition of substances is a tedious and time-consuming operation. To overcome those difficulties computer programs have been developed that describe and test many kinetic expressions [52]. The kinetic parameters calculation was also one of the earliest to be computerised and, today, many kinetic analysis programs are available. However, these programs have their limitations and shortcomings[51].

Zsako and Zsako[53] used a FORTRAN program to estimate kinetic parameters (pre-exponential factor, activation energy), the method being limited to the " reaction order " model.

The program written in Basic by Reich and Stivala [54] allows the calculation of pre-exponential factor and activation energy from non-isothermal data in solid-gas decompositions.

A FORTRAN program for the kinetic analysis of transport non-isothermal TG data, which is based upon the Arrhenius, Friedman, and Kissinger analysis procedures and includes a maximum of nine different solid state rate-controlling reactions, has been developed by Elder[55].

Eftimie and Segal[56] reported a BASIC program used to obtain non-isothermal kinetic parameters based upon the Coats-Redfern method; a later FORTRAN - 77 version has been developed[57].

Diefallah et al[48] reported a BASIC program used for the kinetic analysis of nonisothermal thermogravimetric data according to the composite method using the available kinetic model g(α) functions.

Taylor and Khanna[58] have described a program for the kinetic evaluation of TG data from a single non-isothermal experiment using the computerized method of Stvara and Seatak.

Huang and Hill[59] have described a new computer program, KNIS, for the kinetic analysis of non-isothermal thermogravimetric data which enables an automatic regional kinetic analysis of the entire TG data obtained. The program includes 12 theoretically possible solid state decomposition mechanism models. Malek has reported on kinetic analysis software for experimental DSC data[60].

Recently, spreadsheet analysis was successfully applied to a range of material in order to determine various kinetic parameters such as activation energy and reaction order using various algorithms. There are many advantages to the utilisation of spreadsheets. They provide neat formats of data and results, and they possess many desirable built-in functions for single and multiple linear regression analysis. An important development that spreadsheet subsequently provided was the use of macro. These allowed the automatic utilization of a worksheet, so that values such as kinetic parameters could be conveniently determined[61].

There are many spreadsheets which have became commercially available in the past few years. Several such spreadsheets designed for the IBM and compatible computers are listed as follows: Lotus 1-2-3 (Lotus devel-opment Corp., Cambridge, MA), Multiplan 3 (Microsoft Corp., Redmond, CA), Planning Assistant 2 (IBM Corp.), PlanPerfect 3 (WordPerfect Corp., Orem, UT) and SuperCalc 41 (Computer Associates International, Inc., San Jose, CA).

Spreadsheets have been employed in the preparation of business reports, modelling, forecasting, as small database managers, as graphics generators and in electronic circuit simulation. However, they have been utilized little in the field of thermal analysis[62].

Spreadsheet analysis of TG, DTA, or DSC data used for obtaining activation energy E and reaction order n, or E and the mechanism has been used only rarely in the past. Thus, previous determination of E and n generally employed graphical and/or computer methods. However, recently, spreadsheet procedures have been successfully used for the determination of E and n, or E and the mechanism. There are many advantages to using of spreadsheets. They can provide neat formats of data and results and process many built-in functions. Some of these functions (in the case of Lotus 2) are as follows: Summation (SUM), standard deviations (@ STD), maximum and minimum values (@Max and @Min), single and multiple linear regression analysis, graphics, and sorting. Furthermore, macros allows the automatic utilisation of worksheets for the estimation of the kinetic parameters[63].

1.5 ELECTRICAL STUDY OF SOLID

1.5.1 Conductors

Conduction in metallic state or solid crystals is attributed to free mobile electrons[64,65,66], which are called valence electrons in free atoms. These electrons, which are called conduction electrons in metallic state, are no longer attached to a particular atom, and in a solid crystal they belong to the whole crystal. With respect to core electrons those centred around the nuclei do not contribute anything to the electric a conduction. The states of those electrons in a solid state differ little from those in the free atom. The energy spectrum of such electrons assumes a band pattern. Forbidden energy bands separate the energy bands formed from corresponding atomic levels. Fig. (1.1) illustrates the forbidden energy.

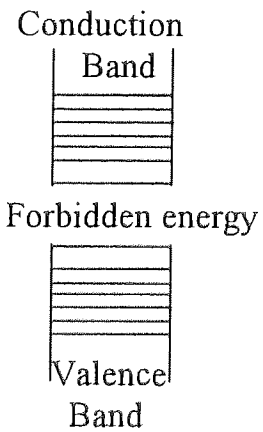

Fig. (1.1): Schematic representation of energy band pattern.

According to the nature of band occupation by electrons, all solids can be classified into two large groups. The *first* group includes bodies in which there is a partially filled band above the completely filled lower bands (Fig 1.2(a)). Such bands are formed from partially filled atomic levels , for instance,

in the case of alkali metals. A partially filled band may also be the result of overlapping of filled and empty or partially filled bands, as is the case with beryllium and alkali-earth metals (Fig 1.2(b)). A partially filled band is a feature of metals. The ***second*** group includes bodies with an empty band above completely filled ones (Fig 1.2(c, d)). Typical examples of such bodies are the elements of Group IV of the periodic table (carbon, silicon germanium and gray tin). This group also includes many chemical compounds (metal oxides, nitrides, carbides, halides of alkali metals, etc).

The solids of the second group are conventionally subdivided into dielectrics and semiconductors according to the width of the forbidden band. Dielectrics include solids with a relatively wide forbidden band. Semiconductors include solids with a relatively narrow forbidden band (Fig. 1.2(d)).

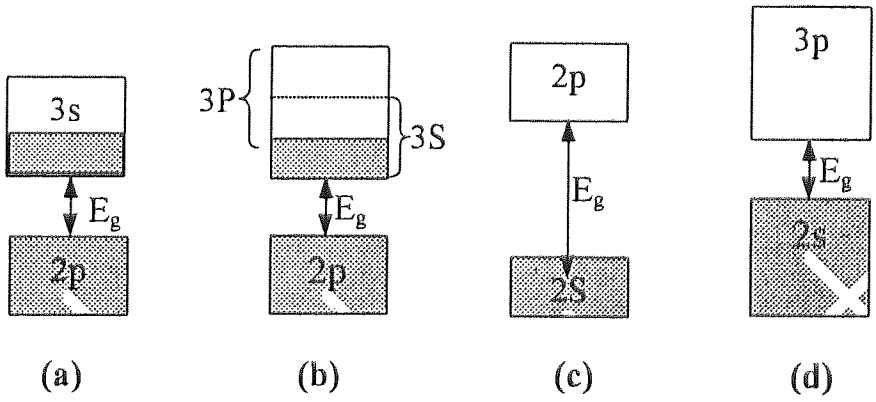

Fig.(1.2): Occupation of bands by electrons: In (a) and (b), there is a partially filled band above the filled band; in (c) and (d), there is an empty band above the filled band.

1.5.2 SEMI-CONDUCTORS

Intrinsic semi-conductors

Semi-conductors containing a negligible amount of electro-active defects (chemical and crystallographic) are termed intrinsic semiconductors. They include some pure chemical elements (germanium, silicon, selenium, tellurium, etc.) and numerous chemical compounds such as gallium arsenide (GaAs), indium arsenide (InAs), indium antimonide (InSb), silicon carbon (SiC), and so on.

In the field of semi-conductors, electrons and holes are usually referred to as free carriers or, simply, carriers because it is these particles which are responsible for carrying the electric current.

Impurity semi-conductors

Semi-conductors, no matter how pure, contain some impurity atoms which create their own energy levels termed impurity levels. Those levels may occupy positions both inside the allowed and the forbidden bands of the semi-conductor at various distances from the top of the valence band and from the bottom of the conduction band. Frequently, the impurities are introduced intentionally to impart specific properties to the semi-conductor. The impurities, which supply electrons, are termed ***donors*** and the energy levels of those impurities ***donor levels***. The semi-conductors doped with donor impurities are termed ***n-type*** semiconductors. The impurities that trap electrons from the valence band are termed ***acceptors*** and the energy levels of such impurities ***acceptor levels***. The semi-conductors doped with such impurities are termed ***p-type*** semi-conductors.

The electrical conductivity, σ, of organic substances has traditionally been described by the equation:

$$\sigma = \sigma_0 \exp(-E_{act.} / kT) \qquad (22)$$

where σ_0 is the constant, k is Boltzmann's constant, T is the absolute temperature, and $E_{act.}$ is the energy obtained from the slope of ln σ versus 1/T plot.

Allan et.al.[67] have reported that it was found in earlier electrical studies that when a C=C group is present in an organic molecule hysteresis was observed. Electrical conductivity of 4-pyridinealdoxime, which contains a C=N group, and some of its metal complexes were studied [68].

1.6 Previous studies

In general, there have been only a few papers published on the preparation, structural characterisation, thermal, electrical studies, and doping of pyridine carboxylic acid complex with the first row of transition elements.

Some complexes of the chloride and bromide complexes of manganese (II), iron (II), cobalt (II), nickel (II), and copper (II) with nicotinamide and nicotinic acid have stoichiometry ML_2X_2 where M is a metal ion, L is an organic ligand, and X is a halide ion. Spectra and magnetic properties indicate that these compounds have octahedral polymeric structures. The decomposition of the complexes was studied by thermogravimetry and differential thermal analysis [5].

Complexes of isonicotinic acid with the bromides and chlorides of cobalt (II), nickel (II), and copper (II) and also with chlorides of manganese (II) and iron (II) have octahedral polymeric structures [6].

Complexes have been prepared between iron (II), copper (II), zinc (II), and cadmium (II) halides and pyridine, α-, β- and γ- picoline, 2,6-lutidine, and 2,4,6-collidine. Where possible, structure types are identified. The present complexes are compared with similar compounds of chromium (II), manganese (II), cobalt (II), and nickel (II). The complexes were prepared either from solution or by thermal decomposition of compounds containing a high ratio of ligand to metal [69].

Pyridine monocarboxylic acid N-oxides coordinate in many different ways with ions in the solid state. For Cu (II), polymeric structures have been described with nicotinic acid N-oxide. Other divalent ions form polymeric species, more willingly as the ionic radius increases. For example, Cd^{2+} forms a chain polymer with isonicotinic acid N-oxide, in which coordination occurs through one of the carboxylic oxygen atoms and the N-oxide oxygen atom. Likewise, lead (II) ions form polymeric compounds with all three of the present monocarboxylic acid N-oxides [70].

Some new compounds of pyridine-2,3-dicarboxylic acid with manganese (II), iron (I), and cobalt (II), have been prepared in aqueous solutions. The thermogravimetry (TG), differential thermal analysis (DTA) and differential scanning calorimetry (DSC) techniques have studied the thermal behaviour of these compounds. The compounds lose the water, and then organic ligand to give the metal oxide [71].

Thermal decomposition of a series of complexes of the type CdCl2(R-py)n (where py = pyridine (py), R = 4-methyl (4Me), 3-methyl (3Me), 2-methyl (2Me), 2-ethyl (2Et), and 4-cyano (4CN); n = 4, 2, or 1) has been studied by means of TG-DTA measurements. The decomposition took place through several steps, and all steps proceeded as a two-dimensional phase boundary reaction. The activation and the rate constant at various temperatures for each step were determined on the basis of thermogravimetry. The thermal stability was mainly dependent on the σ donating power of ligand R-py that is associated with its basicity. In addition to this, thermal stability was considerably affected by the crystal packing structure and the sterical character of the complexes [72].

The thermal decomposition of copper (II) nicotinate and isonicotinate yields in a sharp transition metallic copper as the final solid residue along with the release of carbon dioxide and pyridine. In the case of nicotinate, small amounts of nicotinic acid are also detected. The decomposition is started by

homolytic RC(O)C-Cu bond scission, which is equivalent to an electron transfer from $RC(O)O^-$ to Cu(II) [73].

Compounds of zinc with picolinic acid, nicotinic acid, and isonicotinic acid have been prepared. The thermal behaviour of these compounds, together with that of free pyridine carboxylic acid, has been studied by thermogravimetry and differential thermal analysis. The metal complexes which are all hydrated lose water, then the organic ligand, to give zinc (II) oxide. The IR spectra of the compounds are also discussed [74].

The chloro complexes of manganese, cobalt, nickel, copper and zinc with 2,3-cyclododecenopyridine were prepared in ethanolic solution from which solid compounds were isolated. The suggested structure for the cobalt and zinc is tetrahedral, while for manganese, nickel and copper compounds it is octahedral. The techniques of thermogravimetry and differential thermal analysis show that 2,3-cyclododecenopyridine nickel (II) chloride and bis (2,3-cyclododecenopyridine) copper (II) chloride form intermediate compounds before their metal oxides are produced. The other compounds lose the organic ligand and the halogen to give the metal oxide [75].

In the preparation of cobalt(II)–picoline-bromide and iodide, three different solvents were tested. Some new ternary mixed complexes were prepared containing different picolines using a solid-gas phase preparation method. Thermal and spectroscopic properties of the title compounds were investigated [76].

1.7 Objectives of present study

In the present study an attempt was made to prepare complexes of some divalent metal halides and pyridine mono-carboxylic acid in an aqueous solution. Elemental analysis, infrared spectra, atomic absorption spectrophotometer, x-ray diffraction, and mass spectra measurements were made to characterise each ligand. These measurements, electronic spectra, and magnetic studies were used to characterise each prepared metal complex and to interpret the type of co-ordination, which took place to the metal ion. Electronic scanning microscopy was used for some prepared complexes calcined at different temperatures to examine the chemical phase, morphology, and texture changes which occurred during the thermal decomposition. These are compared and discussed. Thermal analysis studies of 2, 3, or 4-pyridine carboxylic acids together with the complexes formed by the acids and the transition metals cobalt, nickel, and copper have been studied by using thermogravimetry, TG, and differential scanning calorimetry (DSC).

Several heterogeneous solid-state reaction models and computation techniques were used to discuss the kinetics of the isothermal and non-isothermal data. Cobalt picolinate hydrate, cobalt nicotinate hydrate, cobalt isonicotinate hydrate, nickel picolinate hydrate, nickel nicotinate hydrate, and nickel isonicotinate hydrate were chosen as a typical representative of these compounds and free ligands to study the kinetics of thermal decomposition by using nonisothermal techniques. Kinetic analyses of differential scanning calorimetry data were made using these different integral methods: single heating rate, a composite method, and Ozawa and Kissinger methods. The single and composite methods were based on Coats-Redfern, modified Coats-Redfern, Doyle, and Madhusudanan et. al equations. A new computer program was written in Fortran 77 for the kinetic analysis of non-isothermal differential scanning calorimetry data. The program included all the published theoretically possible solid state decomposition mechanism models.

Finally, direct current (D.C.) electrical measurements were used to obtain the temperature dependence of electrical conductivity (σ_{da}) for the cobalt isonicotinic hydrate, nickel isonicotinic hydrate, and copper isonicotinic hydrate complexes. The alternating current (A.C.) electrical measurements were used to obtain the temperature and frequency dependence of conductivity (σ_T) of the nickel isonicotinic hydrate complex. The frequency dependence of each dielectric constant (ε') and dielectric loss (ε'') was obtained for nickel isonicotinic hydrate complex.

CHAPTER II

EXPERIMENTAL:

EXPERIMENTAL

2.1 CHEMICAL MATERIALS

2.1.1- *Pyridine monocarboxylic acids:*

Picolinic acid (HPA), Nicotinic acid (HNA) and Isonicotinic acid (H IA), supplied by Aldrich Chemical Company, Inc., M.W. 123.11 with melting points 139-142°C, 234- 237°C, 310 - 315°C (sublimes) respectively, were used as ligands.

2.1.2- *Divalent Metals*

Cobalt (II) chloride -6 hydrate pure crystal, M.W. 237.93 was supplied by RIEDEL - DE HAEN. Nickel (II) chloride - 6 hydrate, M.W. 237.71, Cupric (II) chloride - 2 hydrate, M.W. 170.48 and Zinc (II) chloride, M.W. 136.28 were supplied by BDH Chemicals Ltd. Poole, England.

2.1.3- *Sodium hydroxide (NaOH)*

Sodium hydroxide chemical, pure pellets, M.W. 40 were supplied by RIEDEL - DE HAEN

2.1.4- *Bidistilled water*

Bidistilled water was prepared using all glass equipment.

2.2 COMPLEXES PREPARATION

2.2.1- *Introduction*

Complexes of cobalt (II), nickel (II), and copper (II) with picolinic acid (HPA), Nicotinic acid (HNA) and Isonicotinic acid (HIA) were prepared. These complexes appeared to have stoichiometry $ML_2.xH_2O$; where M is a metal ion, L is an organic ligand, and x is the number of water molecules.

In the present investigation, complexes consisted mainly of divalent metal with pyridine monocarboxylic acid with a 1: 2 molar ratio.

2.2.- *Complex preparations*

The complexes were generally prepared by published procedures[73,77].

1- A known weight of pyridine monocarboxylic acid (10 gm or the equivalent of 1M), and a suitable stoichiometric amount of sodium hydroxide (3.249 gm or the equivalent of 1M) was dissolved in a minimum amount of bidistilled water pH (5-6).

2 - A known weight of metal salt (see Table 2.1) in the form of soluble salt (the equivalent of 0.5 M) was slowly added dropwise while the pyridine mono-carboxylate salt was stirred. The colored complex precipitated immediately.

3 - The suspension (solution) was stirred for one hour. The pH of the final solution was in the range 4 - 5.

4 - The solution was suction filtered, and the precipitated complexes were washed several times with bidistilled water.

5 - The solids were dried over $CaCl_2$ under a vacuum for 24 hours and then stored in a dissector.

Table 2.1

Weight of metal salts for preparation of complexes

Sr.	Metal salt	Weight ([M.W./12.31195]/2)
1	$CoCl_2\ 6H_2O$	9.663
2	$NiCl_2.6H_2O$	9.654
3	$CuCl_2.2H_2O$	6.923
4	$ZnCl_2$	5.535

2.3- IDENTIFICATION OF PREPARED COMPLEXES

2.3.1- *ATOMIC ABSORPTION SPECTROPHOTOMETER*

The complexes prepared had been digestions by published procedure [78] according to the following procedures:

Weigh a sample of 5-10 mg into a 50-ml digestion flask and add 3 ml of concentrated sulfuric acid (M. A. R. grade) and 3 ml of 100-vol. hydrogen peroxide (M. A. R. grade). Heat gently to fumes and then boil for 5-10 minutes, adding more hydrogen peroxide if necessary. Cool the mixture as required. Transfer to a measuring flask and carefully add distilled water.

The concentrations of the metal ions were obtained using the Perkin - Elmer 2380 atomic absorption spectrophotometer with air-acetylene fuel at Aston University, Birmingham, United Kingdom.

2.3.2- *Elemental Analysis*

The analyses of carbon, nitrogen, and hydrogen were determined using the Perkin Elmer 240C microanalyser at Assiut University, Assiut, Egypt.

2.3.3- *IR. Spectra*

The IR. spectra were obtained using KBr discs, 4000- 200 cm^{-1}, on a SHMADZU 407 at Assiut University, Assiut, Egypt.

2.3.4- *X - ray diffraction*

The X-ray powder diffraction patterns were recorded on an X - ray diffraction system, semiautomatic with Ni- filtered Cu Kα radiation, λ=1.5418A°, type pw. 1840, Philips. The experimental conditions, for all patterns taken, were: working voltage, 30 k, working current. 20 mA; 2θ = 5° - 70° by means of the Debye- Scherrer method [79]; continuous scan with a speed of 1.2°2θ/s, chart 10 mm / 2θ; Range 5 x 10^{-3} c/s, slit 0.2 m and T.c 1 s.

The measurements were taken at room temperature in air under normal pressure at King Abdulaziz University, Jeddah, Kingdom of Saudi Arabia.

.

2.3.5 ***MAGNETIC***

Magnetic moments of complexes were measured by the Gouy method using $Hg[Co(SCN)_4]$ as a calebrant with a correction involving Pascal's constant[80,81] applied for diamagnetism at Aston University, Birmingham, United Kingdom.

2.3.6 ***Mass spectra***

Mass spectra were run for free ligands at 70 eV on a RAM-6L Hitachi Perkin-Elmer single-focusing mass spectrometer using direct probe insertion for the samples. The ionization source used a T-2p model at Cairo University, Cairo, Egypt.

2.4 THERMAL ANALYSIS

The thermal analysis studies were carried out on a TG 30 and DSC 30 Mettler system thermobalance with α-alumina as a standard. Thermogravimetry (TG) and differential scanning calorimetry (DSC) curves were obtained at a heating rate of 10° C min^{-1} in static air. In all cases the 50 - 600° C temperature range was studied. The use of heating rates of some samples for the application of non-isothermal kinetic study was 5, 10, 15, and 20° C $min.^{-1}$ at Omm Al-Qora University, Makah, Kingdom of Saudi Arabia.

2.5-CALCINATION OF SAMPLES

Samples of some prepared complexes were inserted into an electrical oven at room temperature which was raised to the desired value and maintained for 10 minutes before the sample was removed and cooled in a desiccator to room temperature. Table 2.3 shows the temperature of calcinations for complexes under investigation.

Table 2.2

Calcination temperature.

Complex	Temperature(°C)						
$Co(PA)_2.2.5H_2O$	90	120	140	310	390		
$Co(NA)_2.4.0H_2O$	50	75	250	380	500	580	
$Co(IA)_2.4.0H_2O$	50	100	150	350	400	450	
$Ni(PA)_2 4.0H_2O$	75	125	160	300	380	500	
$Ni(NA)_2 4.0H_2O$	80	115	160	215	340	390	430
$Ni(IA)_2.3.5H_2O$	80	125	170	310	375	420	

2.6- ELECTRONIC SCANNING MICROSCOPE

The changes in morphology and texture of some of the complexes and their calcination products were undertaken using the Jeol 300 Scanning Electron Microscope at King Abdulaziz University, Jeddah, Kingdom of Saudi Arabia.

2.7-ELECTRICAL CONDUCTIVITY MEASUREMENT

2.7.1 DC MEASUREMENT

The electrical measurements were carried out on prepared hydrous compounds by monitoring currents as a function of temperature at a fixed voltage.

Samples were prepared in the form of discs with a diameter of 13 mm and a thickness of range of 0.06-0.1 mm. A micrometer accurately measured the disc thickness. These discs were formed by compressing powder in a hydraulic press set with an applied force of 10 tons[82-84].

All samples were coated with silver paint through masks to ensure a sharply defined edge to electrodes[85]. The discs were then stored in a desiccator for several days to keep discs dry before being tested.

The sample holder shown in Fig. 2.1 consists of two parallel plates of brass 1.1 cm in diameter, the lower being supported with a light pressure spring[86]. Teflon is used to isolate the two electrodes from each other.

The circuit used for measurement of electrical conductivity is represented in Fig. 2.2. The essential current measuring device was a D.C., Operational Amplifier joined to a Current Meter, and a high impedance voltmeter for measuring potential drop across the sample. In high resistance

circuits the use of coaxial cable, metal shielding, and common ground loop eliminated electronic noise[87].

The sample and its holder were heated in an ultra-thermostat set at a predetermined temperature. An ultra-thermostat set consisting of heating wire was made of Ni-Cr with a resistance of 0.07657 kΩ, which was bonded around the outer surface of the Pyrex tube up and down to avoid the electromagnetic field[88]. An electric unit carefully controlled the heating. This unit is the Thyristor AC regulator (supplied by YKOYAMA ELECTRIC Co., LTD. JAPAN, type SB-10). A calibrated copper constantat as thermocouple PCT 103 that connected with digital (supplied by JENWAY, PWA 1) was used to measure the temperatures on the samples as shown in Fig. 2.3.

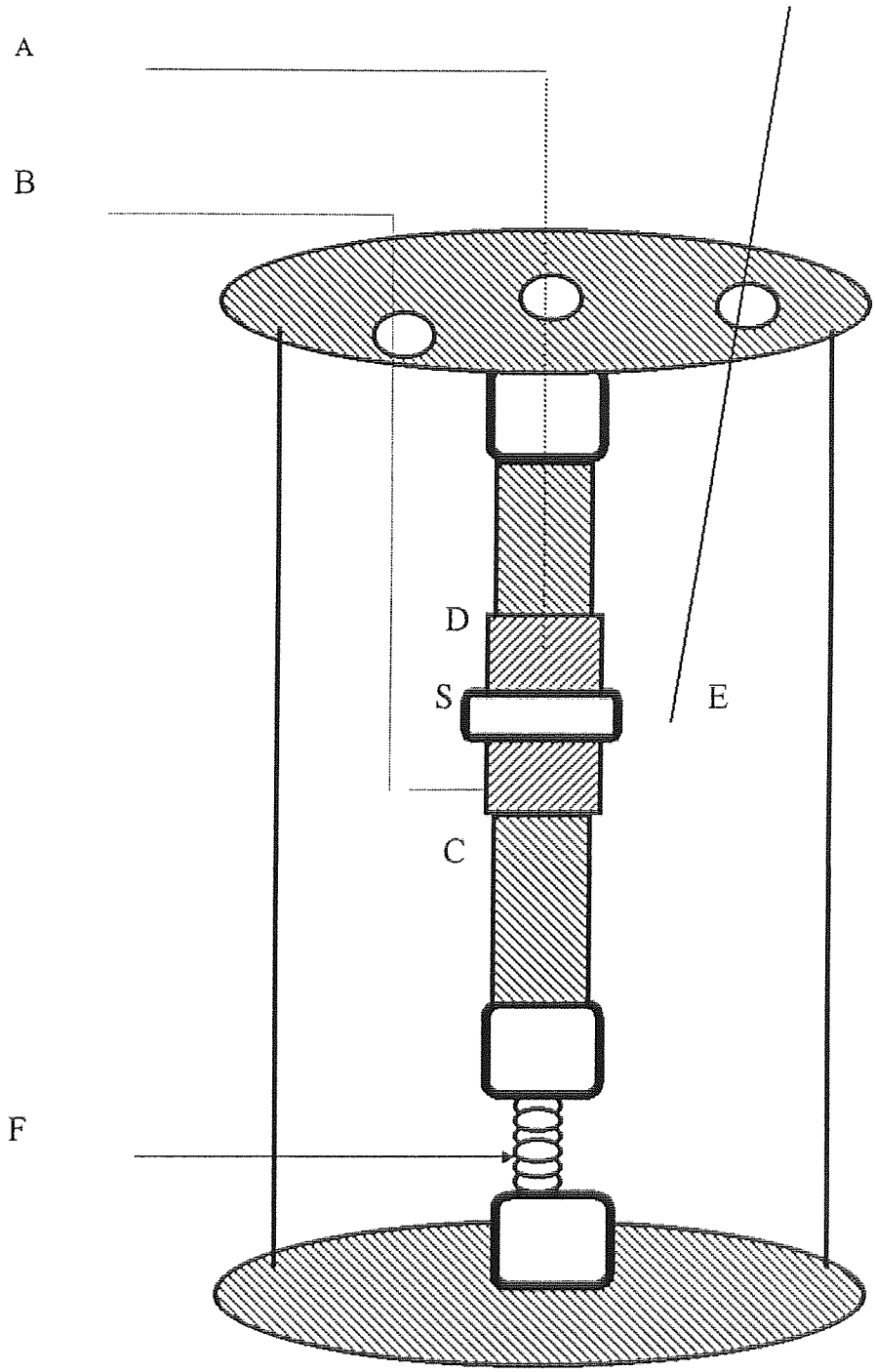

Fig. 2.1: Sample holder used for electrical conductivity measurement

A, B: lead wire. D, C: electrodes. E: thermocouple

F: light pressure spring. S: sample

: brass : Teflon

: brass : Teflon

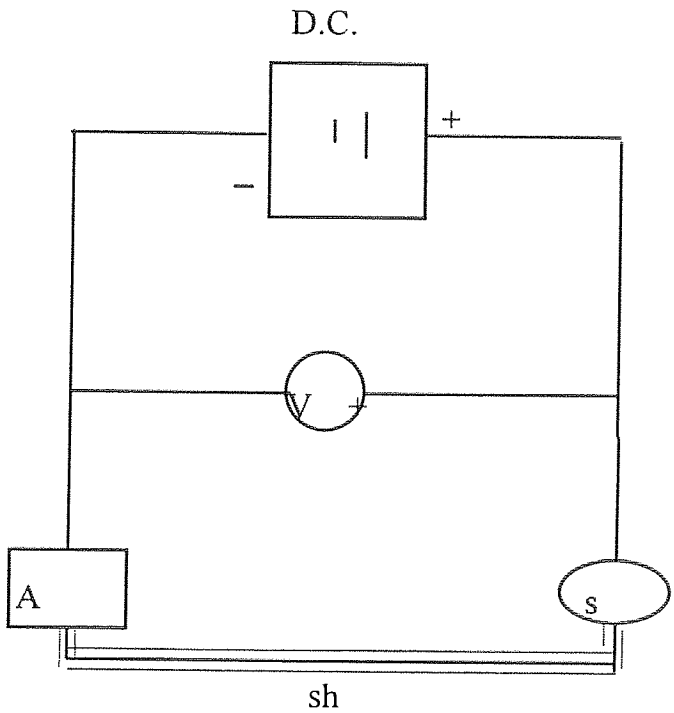

Fig 2.2: The circuit used for electrical conductivity measurements

D.C.: Power supply

S: Sample

Sh: Metallic shield

A: D.C. Current Meter

V: D.C. Voltmeter

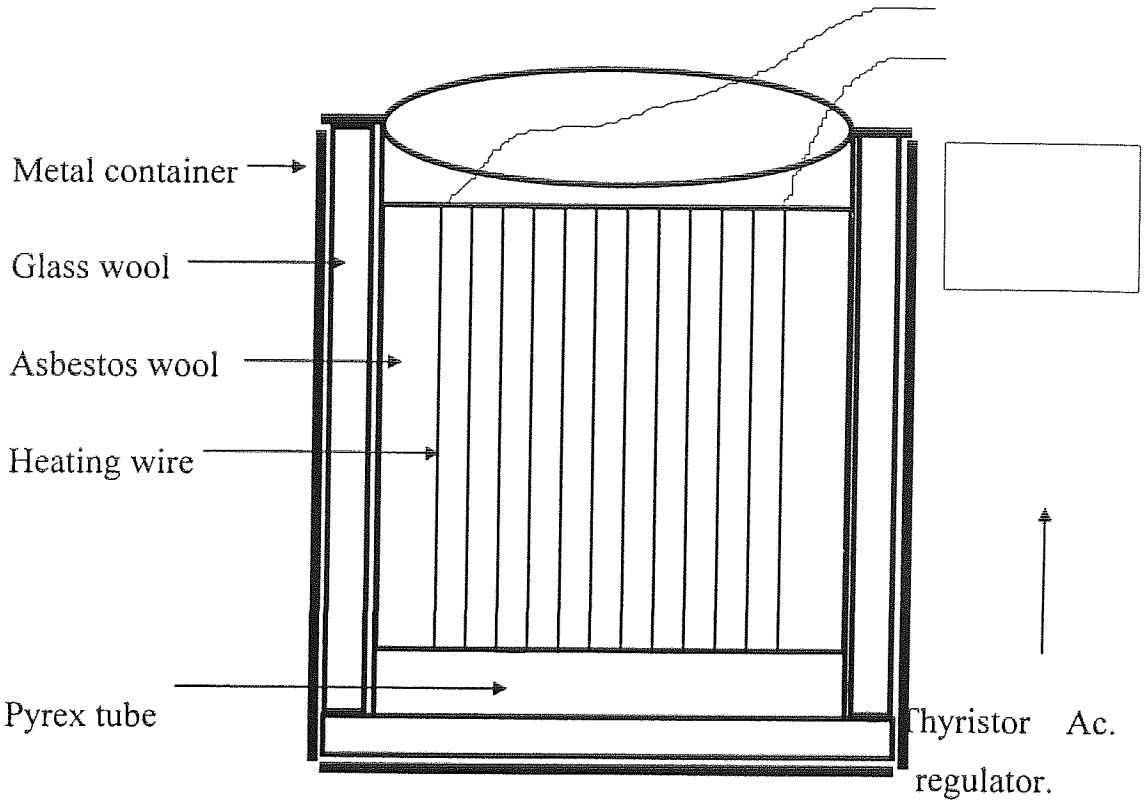

Fig 2.3: An ultra-thermostat set.

2.7.2 AC MEASUREMENT

AC conductivity, dielectric constant, and dielectric loss for some prepared samples were measured in a frequency range from 26 kHz to 13 kHz using a Hewlett Packard 4192A impedance analyser. The voltage was fixed at 0.2V throughout the experiments, since there is neither oxidation nor reduction of ions at this low voltage in the temperature range 20 –80 °C at University of Jordan, Amman, Jordan.

CHAPTER 3

RESUT AND DISCUSSION (I)

FREE LIGANDS (PYRIDINE MONO CARBOXYLIC ACID)

CHAPTER 3

PYRIDINE MONOCARBOXYLIC ACIDS STUDY

3.1 PREFACE

The ligands used in this investigation are isomers of pyridine monocarboxylic acids. Fig. 3.1 shows the isomers, picolinic acid (HPA), nicotinic acid (HNA) and isonicotinic acid (HIA). The difference between the isomers is the position of the carboxylic group.

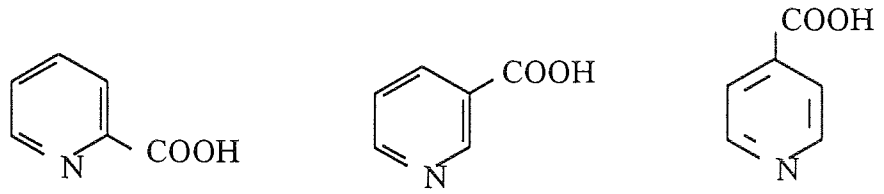

2-pyridinecarboxylic acid (Picolinic acid, (HPA)) 3-pyridinecarboxylic acid (Nicotinic acid, (HNA)) 4-pyridinecarboxylic acid (Isonicotinic acid, (HIA)

Fig (3.1): Isomers of pyridine carboxylic acids

3.2-CHEMICAL ANALYSIS OF PYRIDINE CARBOXYLIC ACIDS

3.2.1- Carbon, Nitrogen and Hydrogen Analysis

The percentages of carbon, nitrogen, and hydrogen were calculated theoretically and determined experimentally for the free ligands (picolinic acid, nicotinic acid and isonicotinic acid). Table 3.1 shows the comparison between the expected and the experimental values.

3.2.2-Infrared Spectra (4000 - 200 cm^{-1})

The mode of the bonding of ligands was examined by IR-spectra. The wavenumbers of IR absorption bands for the free pyridine monocarboxylic acid are shown in Fig. 3.2 and Table 3.2. The IR spectra of free pyridine carboxylic acids show bands at about 1700 and 1442 cm^{-1} (Table 3.1), which correspond

to the carboxylic group. The band at 1700 cm^{-1} was assigned to the (C-O) vibration, while that of 1442 cm^{-1} was assigned to the (C=O) vibration. There was a band in the range of 1610 - 1518 cm^{-1} due to the ring vibration of the aromatic ring.

Table (3.1)

Carbon, Nitrogen and Hydrogen analysis for free pyridine carboxylic acids

Compounds	Calculated %			Experimental		
	C	N	H	C	N	H
Picolinic acid	58.5	11.4	4.09	58.4	9.25	4.25
Nicotinic acid	58.5	11.4	4.09	58.4	11.1	4.17
Isonicotinic acid	58.5	11.4	4.09	58.2	11.1	4.02

Table (3.2)

Infrared Spectra (4000 - 200 cm^{-1}) for free pyridine carboxylic acids.[74]

Comps.	νO-H (H2O)	ν (COOH)	ν (COO^-)	Ring Vibration	ν (C=O)	ν M-O	ν M-N
HPA	--	1700(s)	--	1590(s)-1518(s)	1442(s)	--	--
HNA	--	1795(s)	--	1580(s)-1480(s)	1410(s)	--	--
HIA	--	1708(s)	--	1610(s)-1558(s)	1558(s)	--	--

Key: br., broad; s, strong; m, medium; w, weak and Comps., Compounds

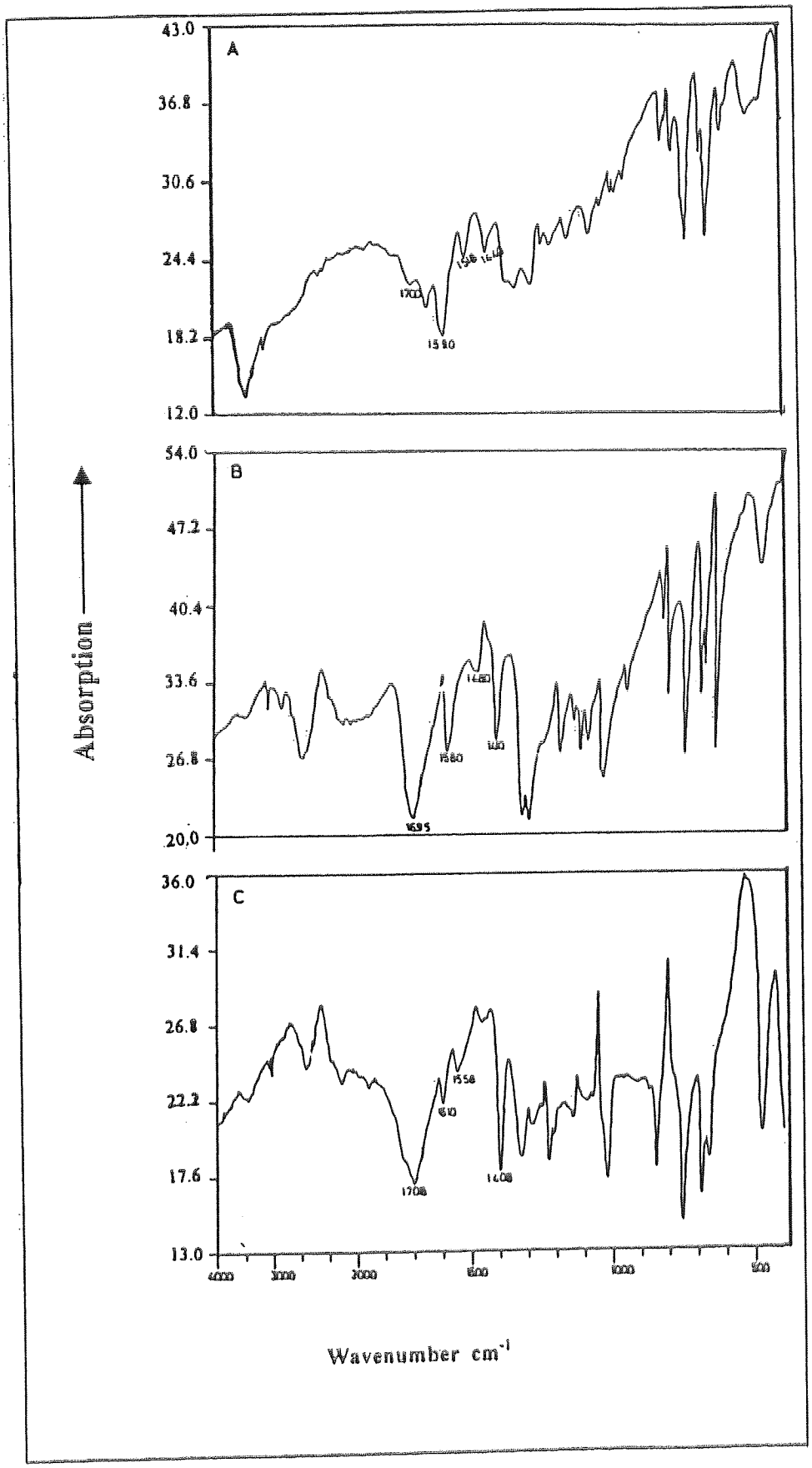

Fig. (3.2): IR Spectra of free ligands, A for HPA, B for HNA and C for HIA

3.2.3-X-Ray Diffraction Patterns

The X-ray diffraction data, angle of incidence or reflectance (2θ), interplanar distance between two planes (d-sp.), intensity (I°) and relative intensity (I/I°) obtained in the present investigation for free ligands are summarised in Table 3.3 and are graphically represented in Fig. 3.2 which shows the x-ray lines (I/ I° against 2θ) of the free ligands (HPA, HIA, HNA). Excel program-V.5.0 (IBM compatible computer) was used to calculate the values of interplanar distance between two planes (d-sp) at each angle of incidence (2θ) on the basis of Bragg's law (equation 3.1)[89]. The same program was used to calculate the values of intensity (I/ I°) which were plotted against the incidence angle (2θ).

$$2d \sin \theta = n \lambda \qquad (3.1)$$

$$d = n \lambda / 2 \sin \theta \qquad (3.2)$$

Where θ is the glancing angle between the incident beam and the reflecting plane, d is the interplanar distance between two planes, λ is the wavelength of x-ray, and n is a positive integer order.

The correlation of d-sp and θ calculated here are, as expected, in agreement with the general tabulation by Switzer et al.,[90]. The values for interplanar distances, d-sp, are summarised in Appendix 1, and they show the necessary relationship between d-sp and θ.

In Appendix 1, the values of the interplanar distance between two planes, d-sp., decrease with increasing angles of incidence. Comparison of the x-ray pattern of the free ligands (Fig. 3.3) shows that the patterns are not similar. It is obviously clear from Fig. 3.3 and Table 3.3 that the maximum relative intensity (I/I°) for the ligands HPA and HIA is at values incidence angles (2θ) 17.3 and 16.3 respectively. However, the corresponding value for

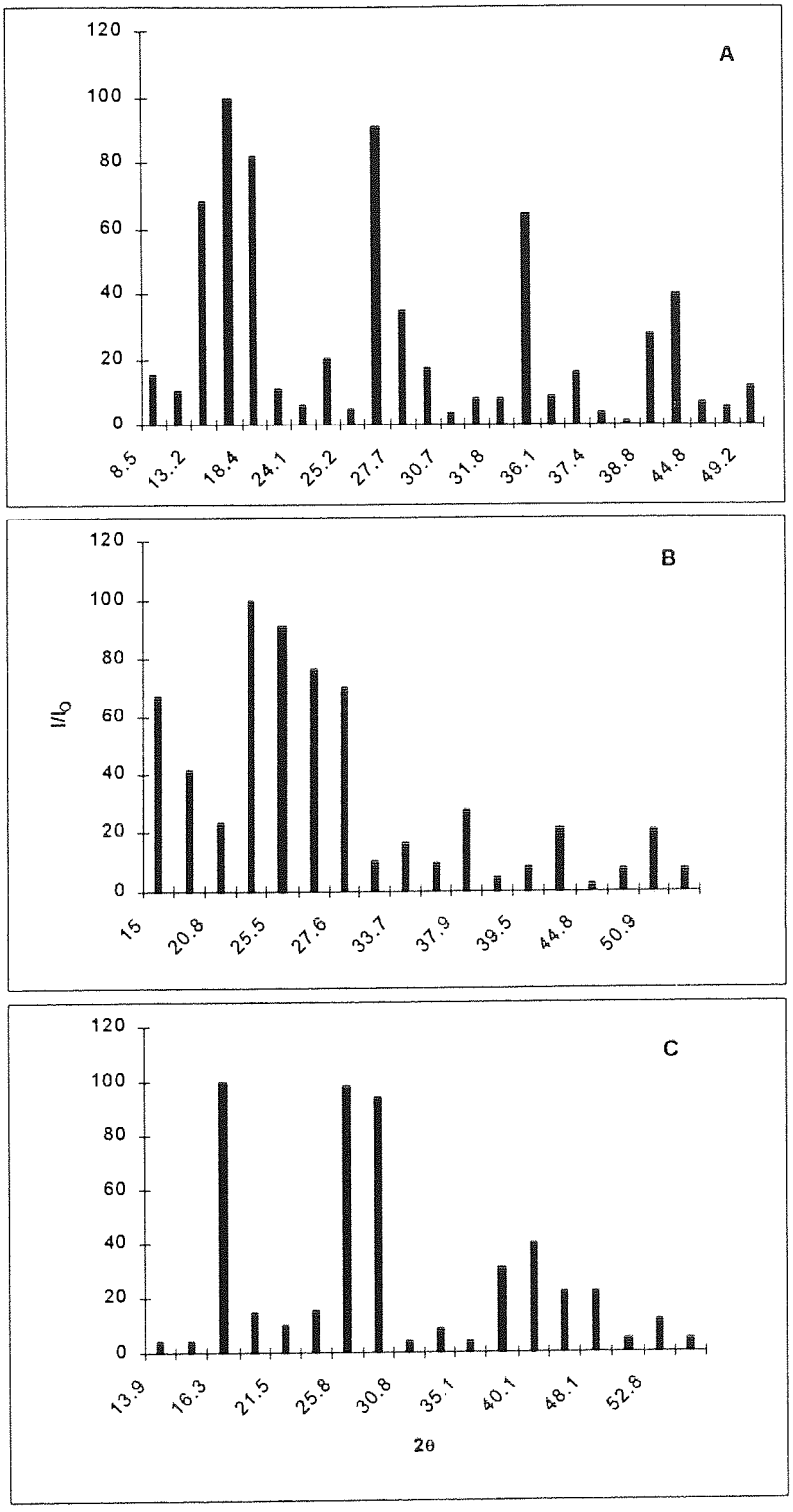

Fig.(3.3): X-ray lines (I/I_o against 2θ) for free ligands; A : HPA, B : HNA, C : HIA.

The ligand HNA is 24.4. The free ligands are crystalline solids with low symmetry and large unit cells; they are characterised by the diversity of their structures [91].

Table 3.3: The maximum value of I/ I∘ at 2θ for free ligands.

Compounds	2θ	I
HPA	17.3	89
HNA	24.4	85.8
HIA	16.3	89

3.2.4-Mass spectral studies

The mass spectra were recorded for free ligands HPA, HNA, and HIA. The most prominent mass spectral peaks of the compounds studied are given in Table 3.4, and a general schematic representation including the main fragmentation is given in bar-graph form in Fig. 3.4-3.6. The most intense peaks of the mass spectra of pyridine mono carboxylic acids are those due to pyridine and its daughter fragments. These fragments are formed through decarboxylation of pyridine mono carboxylic acids.

The fragmentation of carboxylic acids may be written according to the following equation: [92].

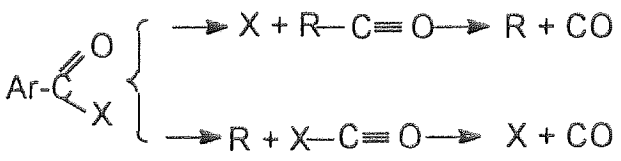

where X= OH, OAr, NH2, NHAr, NarAr.

Table 3.4

The most relevant mass spectral peaks of mono pyridine carboxylic acids.

Ligand	M/(RI)[a]
Picolinic acid (HPA)	50(35), 51(82), 52(100), 53(12), 78(47), 79(99), 123(0.7).
Nicotinic acid (HNA)	50(14), 51(18), 54(16), 55(96), 56(29), 57(100), 60(90), 61(21) 67(17), 68(18), 69(53), 70(18), 71(33), 73(77), 77(12), 81(15), 83(26), 84(17), 85(21), 87(14), 95(11), 96(10), 97(19), 98(18), 99(13), 101(10), 105(11), 106(10), 111(11), 112(10), 115(11), 123(19).
Isonicotinic acid (HIA)	50(46), 51(100), 52(52), 53(12), 55(16), 57(14), 67(19), 73(12), 76(18), 77(32), 78(34), 79(49), 82(10), 83(22), 91(11), 93(13.7), 94(12), 105(22), 106(17), 123(74).

[a]: Relative intensity.

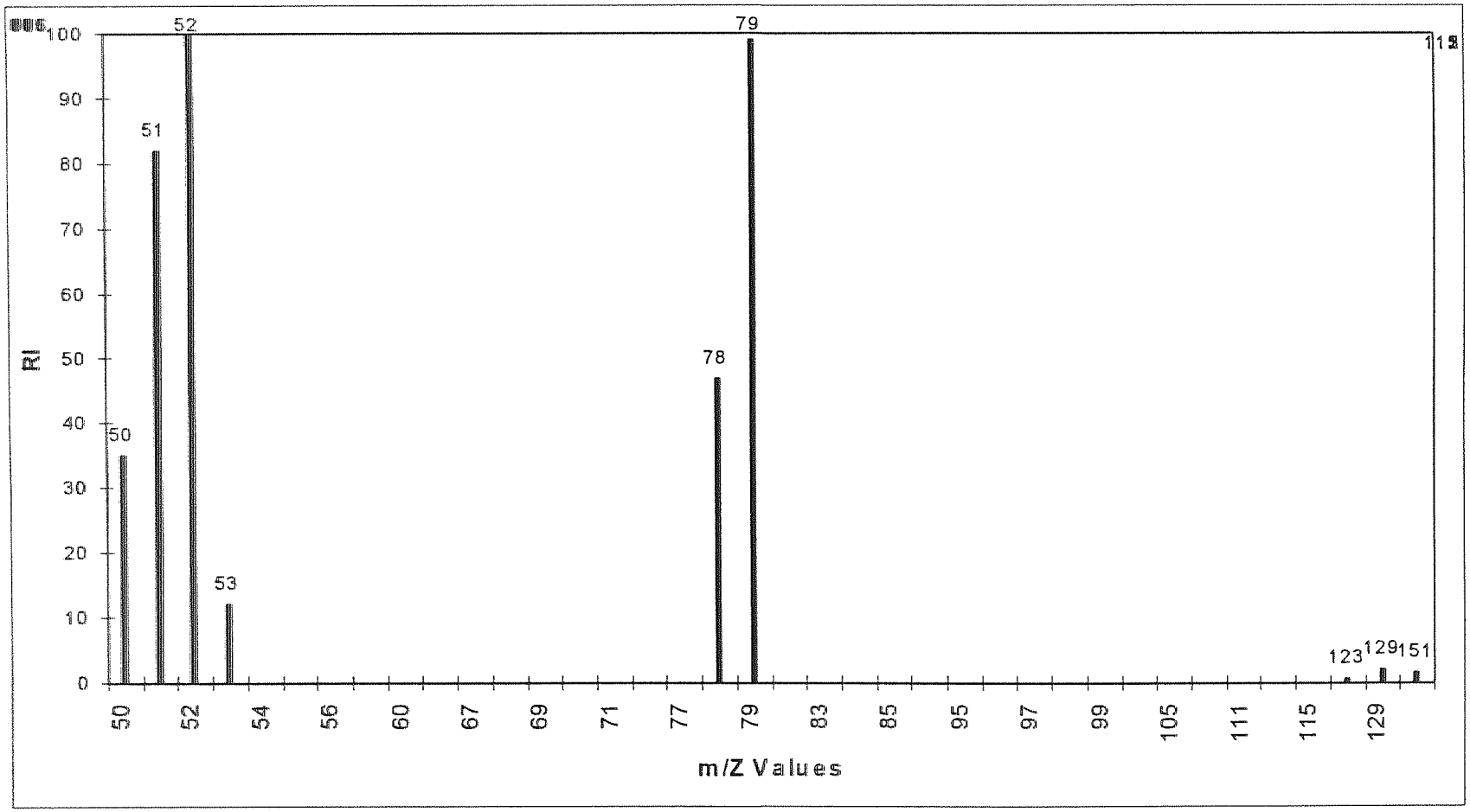

Fig. 3.4 : Schematic representation of the general fragmentation pattern of picolinic acid.

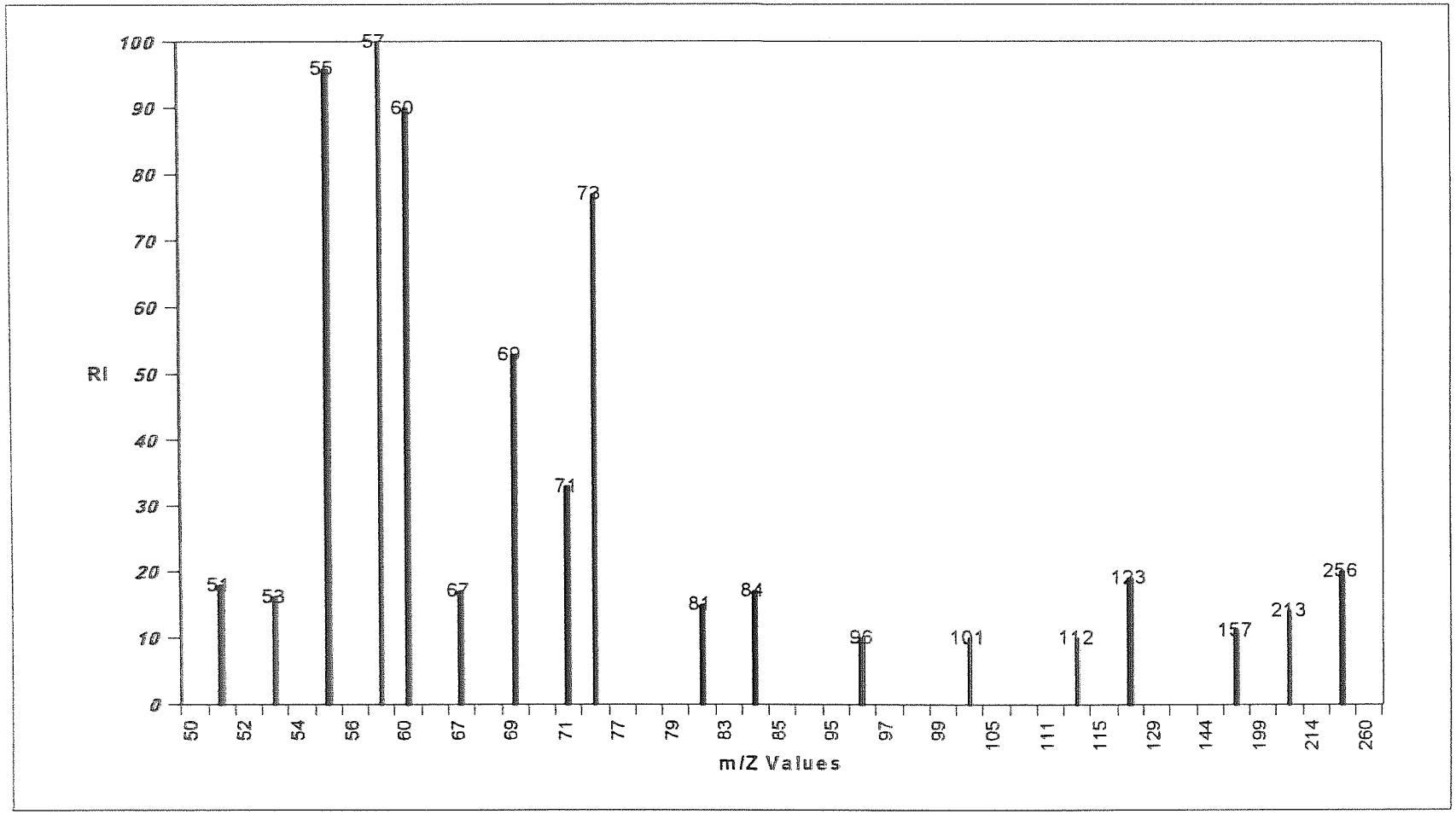

Fig. 3.5 : Schematic representation of the general fragmentation pattern of nicotinic acid.

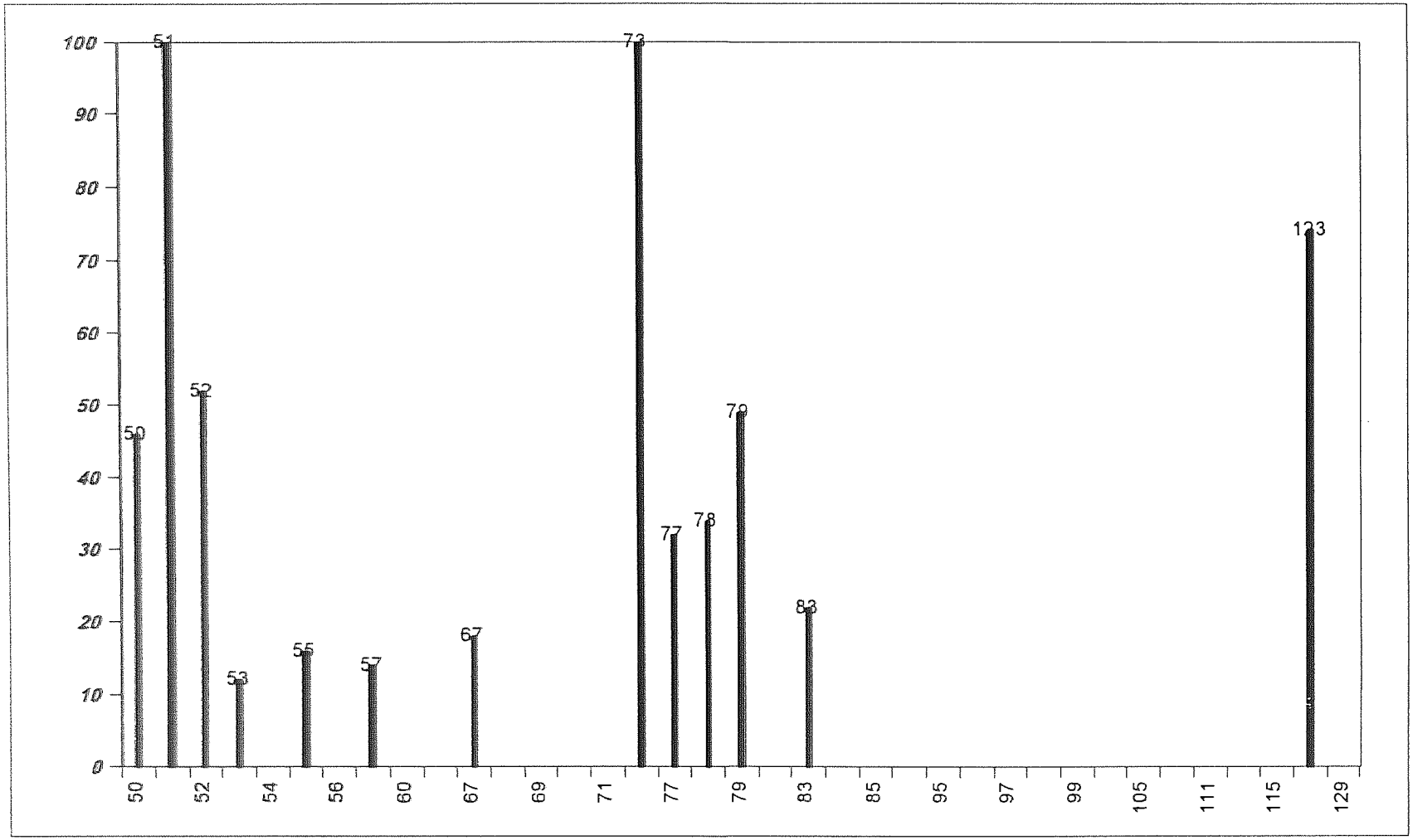

Fig. 3.6 : Schematic representation of the general fragmentation pattern of isonicotinic acid.

3. 3 THERMAL ANALYSIS OF FREE LIGANDS

In this study, the conditions chosen to obtain thermal analysis data are comparable with those of Allan et al[74]. The thermal analysis curves, thermogravimetry (TG), differential thermogravimetry (DTG) and differential scanning calorimetry (DSC), of the free ligands (HPA, HNA and HIA) under study are depicted in Figs. 3.7-3.12. TG and DTA were scanned with a heating rate of 10 °C min^{-1}, while DSC was scanned at different heating rates (5, 10, 15 and 20°C min^{-1}). In all cases the decomposition process was carried out in a dynamic air atmosphere in the temperature range 50-600 °C.

From the TG curve the percentage loss in mass is recorded and the temperature of maximum rate is recorded from the DTG. From the DSC curve the peak temperatures for both endo- and exo- peaks, and the enthalpy changes for the various decomposition steps were obtained. The results are listed in Table 3.5.

There are remarkable differences between our results and the results reported by Allan et. al.[74] on thermal analysis of the pyridine carboxylic acids. Allan et. al. mentioned that the DTA curve for picolinic acid showed an endothermic peak at 138°C due to fusion and an exothermic peak at 415°C due to decomposition. However, in the present study, our result of the DSC curve showed an endothermic peak at 149°C due to fusion, an endothermic peak at 219°C due to decomposition, and an exothermic peak at 415°C which may be due to oxidation of residual carbon in the sample. For nicotinic acid Allan et. al. found that the endothermic peak was at 237°C due to fusion, and the exothermic peak was at 397°C due to decomposition. However, our result showed an endothermic peak at 246°C due to fusion, an endothermic peak at 292°C due to decomposition, and an exothermic peak at 360°C which may be due to oxidation of residual carbon in the sample. For isonicotinic acid Allan et. al. found that the endothermic peak was at 320°C due to fusion, and the

exothermic peak was at 382°C due to decomposition. However, our result showed an endothermic peak at 312°C corresponding to sublimation.

Although the endothermic peaks, which appeared at 219 and 292° C for picolinic acid and nicotinic acid respectively, are quite large in our DSC curve, they appeared small in the DTA curve reported by Allan et.al. and were disregarded.

3. 3.1 THERMAL BEHAVIOR OF PICOLINIC ACID (HPA)

The TG-DTG traces (Fig. 3.8) for picolinic acid (HPA) show no weight loss in the temperature range 50-102°C. This suggests that the picolinic acid is thermally stable in the range 50-102°C. Its pyrolytic decomposition begins at 102°C and is finished at 338.5°C with total elimination of the sample. From 103 °C to 294°C a rapid mass loss of 96.47% was observed. From the DTG traces it was clear that the maximum rate of decomposition occurs at 194° C, followed by a gradual mass loss of 3.53 % which occurs in the temperature range of 220 - 550° C. The DSC trace (Fig. 3.9) for picolinic acid (HPA) shows an endothermic peak at 149°C corresponding to the melting (m.p.139-142°C). The enthalpy of fusion is 23.17kJ mol^{-1}. The endothermic peak observed at 219°C in the DSC traces is then attributed to the decomposition of picolinic acid to carbon dioxide and pyridine, followed by the evaporation of pyridine. The value for decomposition and evaporation enthalpy is 27.01 kJ mol^{-1}. The endothermic peak was at 219°C corresponding to the main decomposition stage of 96.47%, while the exothermic peak at 415°C corresponding to mass loss of 3.53 % with enthalpy change is 2.66 kJ mol^{-1}. Comparing the TG, DTG, and DSC, it is clear that the fusion, evaporation, and decomposition stages in TG and DTG are a combination of two consecutive processes in the DSC.

3. 3.2 THERMAL BEHAVIOR OF NICOTINIC ACID (HNA)

The TG-DTG traces (Fig. 3.10) for nicotinic acid (HNA) show no weight loss in the temperature range 50-139°C. Its pyrolytic decomposition starts at 139°C and finishes at 413°C with total elimination of the sample. The TG curve shows no loss up to (139°C). From 140 °C to 274°C a rapid mass loss was observed of 93.43%. The evaporation of products followed the decarboxylation. From the DTG traces the maximum rate of decomposition occurs at 244°C, followed by a gradual mass loss of 6.57% in the temperature range 249 to 550°C. The DSC traces in Fig. 3.11 show three endothermic peaks. The first endothermic peak at 206°C, with an enthalpy change of 0.15kJ mol^{-1}, is attributed to an isomerization or phase transition since there is no loss in mass at that temperature. The second endothermic peak at 246°C corresponds to fusion (m. p.234-237); the value for the fusion enthalpy is 22.89 kJ mol^{-1}. The third endothermic peak at 292°C corresponds to the main decomposition stage of nicotinic acid (93.43%), during which it converts to pyridine and carbon dioxide and is followed by the evaporation of pyridine with an enthalpy change of 44.45 kJ mol^{-1}. An exothermic peak at 360°C was observed corresponding to a gradual mass loss of 6.57 % with an enthalpy change of 2.66kJ mol^{-1}. Comparing the TG, DTG, and DSC data, it is clear that the main stage seen in TG and TDG is a combination of two consecutive processes shown separately in the DSC.

3. 3.3 THERMAL BEHAVIOR ISONICOTINIC ACID (HIA)

The TG - DTG traces (Fig. 3.12) for isonicotinic acid (HIA) show that it is thermally stable in the temperature range 50-207°C. Its pyrolytic decomposition starts at 207 °C and finishes at 282 °C with a total elimination of the sample. The TG curve showed no loss in mass up to 207 °C. From 207 °C to 274°C a rapid mass loss was observed (90.33%). From the DTG curve, however, it is clear that this stage has its maximum rate of decomposition at 272°C. From 274 to 550°C gradual mass losses occurred of 6.57 %. The DSC

curve (Fig. 3.13) shows only one endothermic peak at 312°C corresponding to sublimation (sublimes 310-315°C) and decomposition to pyridine and carbon dioxide. The enthalpy of sublimation is 138.45 kJ mol^{-1}.

It is clear from the DSC curves (Figs. 3.8, 3.10, and 3.12) that the recorded peak temperature depends on the heating rate, when the heating rate increases the peak temperature becomes higher.

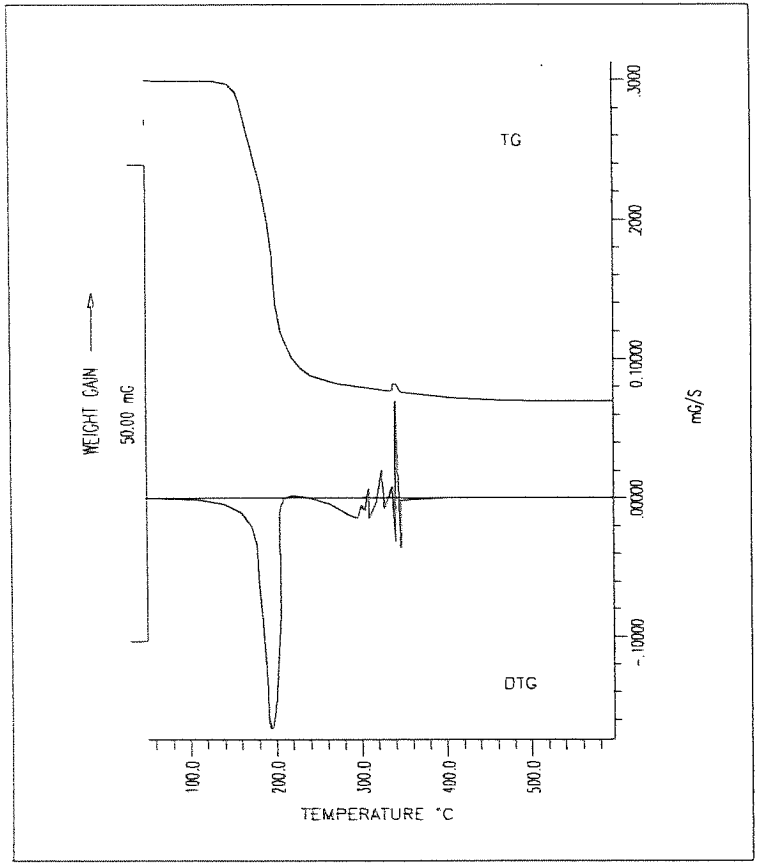

Fig. (3.7): TG/DTG curves of picolinic acid, sample weight 36.231 mg at 10°C min^{-1} in air.

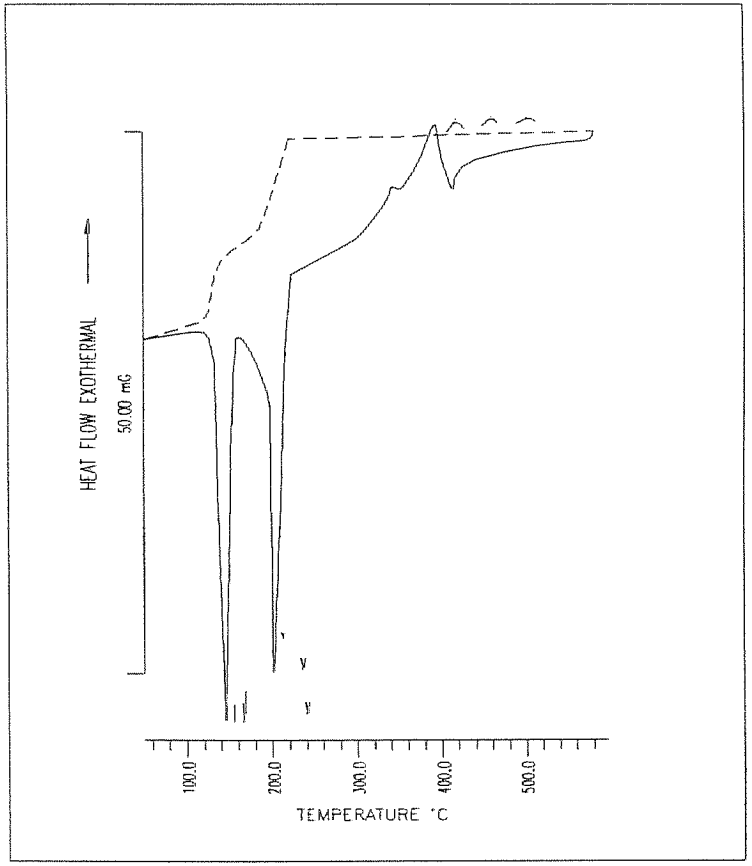

Fig. (3.8) : DSC curve of picolinic acid, sample weight 38.1 mg , at 5°C min^{-1} in air. (.), (..) and (...) at 10, 15 and 20°C min^{-1} respectively.

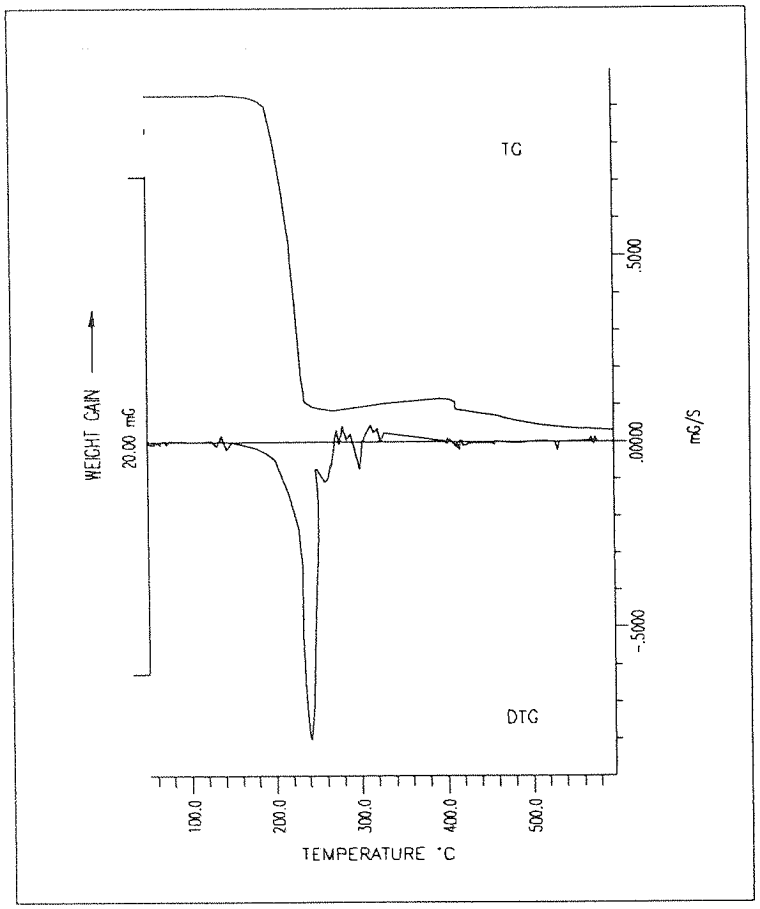

Fig. (3.9) : TG/DTG curves of nicotinic acid, sample weight 17.534 mg at 10°C min^{-1} in air.

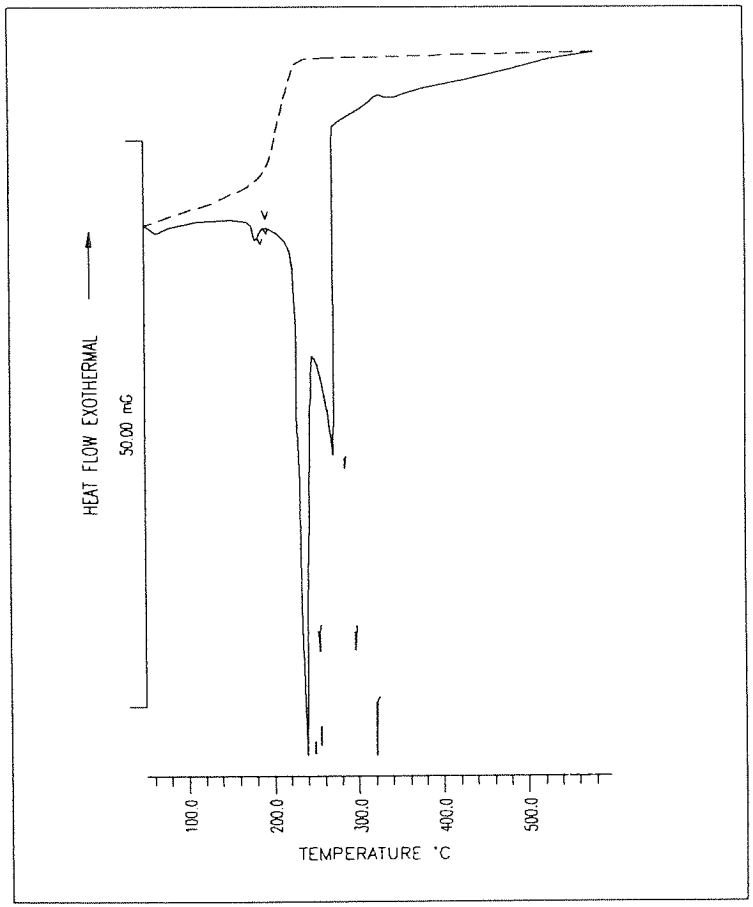

Fig .(3.10) : DSC curve of nicotinic acid, sample weight 18.00 mg , at 5°C min^{-1} in air. (.), (..) and (...) at 10, 15 and 20°C min^{-1} respectively.

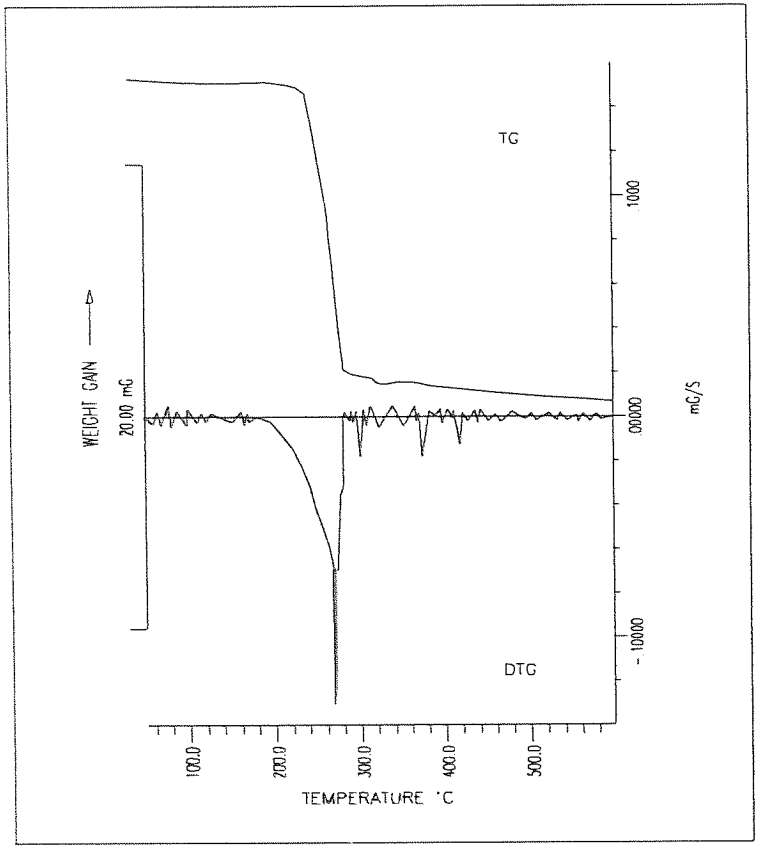

Fig. (3.11) : TG/DTG curves of isonicotinic acid, sample weight 20.530 mg at 10°C min^{-1} in air.

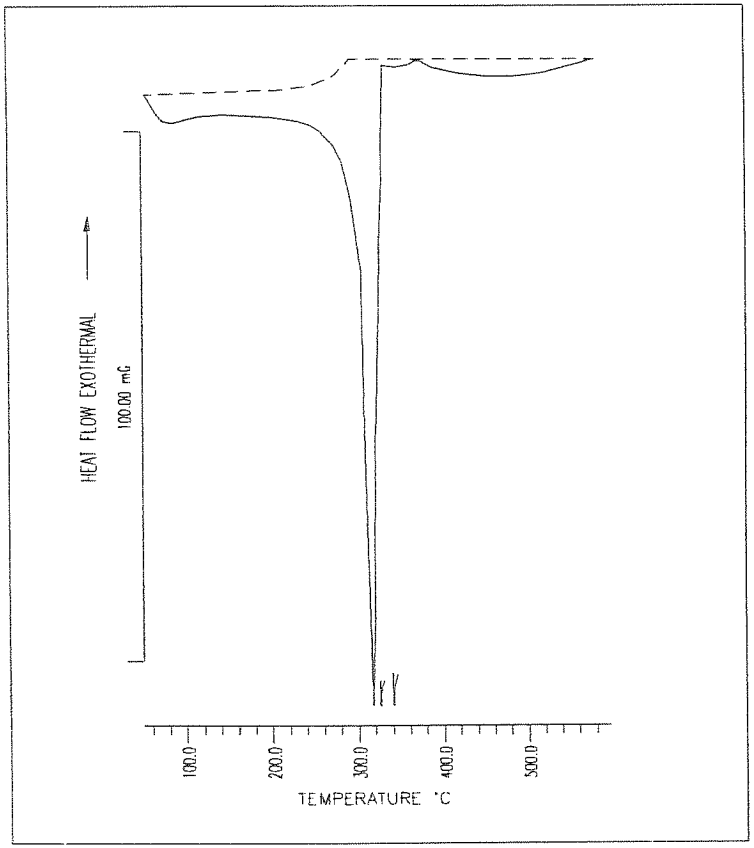

Fig .(3.12) : DSC curve of isonicotinic acid, sample weight 18.10 mg , at 5°C min^{-1} in air. (.), (..) and (...) at 10, 15 and 20°C min^{-1} respectively.

Table 3.5: Decomposition process of each acid.

Process	Stage	Temperature Range °C	Mass Loss %	$DTG_{(max.)}$	TT	Peak Temperature (°C) / (dT/dt)				ΔH kJ mol^{-1}			
						5	10	15	20	5	10	15	20
$HPA_{(s)} \rightarrow HPA_{(s)}$	1	50 - 102	0.0										
$HPA_{(s)} \rightarrow HPA_{(l)}$	2	103 - 221	89.7	194	Endo	142	149	187	163	12.13	23.17	23.18	22.05
$HPA_{(l)} \rightarrow$ pyridine $+CO_2$					Endo	200	219	231	231	31.66	42.07	49.59	40.51
Pyridine $+O_2 \rightarrow$ pyridone or pyridine N-oxide	3	221 - 339	10.3		Exo	387	415			2.98	2.66		
$HNA_{(s)} \rightarrow HNA_{(s)}$	1	50 - 140	0.0		Endo	179	206	189	193	0.88	1.06	1.21	1.17
$HNA \rightarrow HNA_{(l)}$	2	140 - 249	93.43	244	Endo	239	246	252	256	23.53	33.25	18.26	26.21
$HNA_{(l)} \rightarrow$ pyridine $+CO_2$					Endo	272	292	302	319	26.47	44.45	36.12	50.02
Pyridine $+O_2 \rightarrow$ pyridone or pyridine N-oxide	3	249 - 413	6.57		Exo	330	360	345	440				
$HIA_{(s)} \rightarrow HIA_{(g)}$	1	207 – 282	93.43	272	Endo	294	312	326	337	101.81	138.45	107.94	132.76
$HIA_{(g)} \rightarrow$ pyridine $+CO_2$													
Pyridine $+O_2 \rightarrow$ pyridone or pyridine N-oxide	2	282 - 550	3.57		Exo	305	385	390	415				

TT: Thermal nature of Transformation.

3.4-KINETIC STUDIES FOR FREE LIGANDS

All of the experimental data were calculated by using a computer program written in Fortran 77. The program was designed and constructed to be applicable to the kinetic data analysis of the decomposition of the compounds under investigation. This program was used to choose the reaction model that obtained best fit of data in order to calculate the kinetic parameters. Fig. 3.13 shows the flow-chart for the computer program used for this kinetic analysis of non-isothermal differential scanning calorimetry data. Analyses of data, obtained either for a single heating rate or several different heating rates, were performed using the various available kinetic model $g(\alpha)$ functions[93] listed in Table 3.6.

The data can be fed by hand or from a data file and the results can be printed, plotted, and saved. The results of the calculation allow the ability to choose the kinetic mechanism which best fits the data and give the highest correlation coefficient and the lowest standard deviation. The program also calculates the activation energy (E) and the frequency factor (A) from the slope and intercept of the linear fit line. The output file can be opened from the Microsoft Excel program which offers the many advantages of using a spreadsheet. Thus, it can provide a neat format of data and results.

In order to check the computer program, a set of data published by Leo Reich was used[94]. The chosen reaction model and kinetic parameters obtained using our program were identical with the results published.

The kinetic analysis of the nonisothermal decomposition is considered here in view of the integral methods: The Kissinger method[45], the Ozawa method[27], the Coats-Redfern method[39], modified Coats-Redfern[42], the Doyle method[35], the Madhusudanan et. al. method[43] and the Diefallah composite method[46]. In all cases, the comparison of fit to the various models was made for α values in the range $0.05 < \alpha < 0.95$; where α is the degree of conversion.

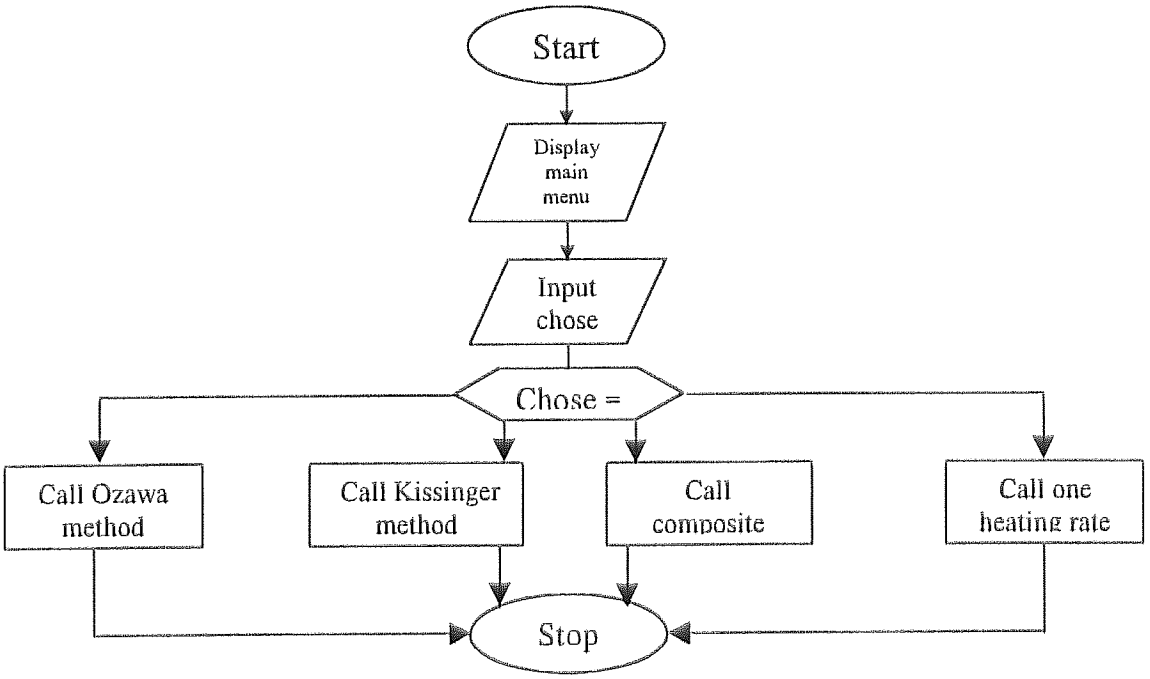

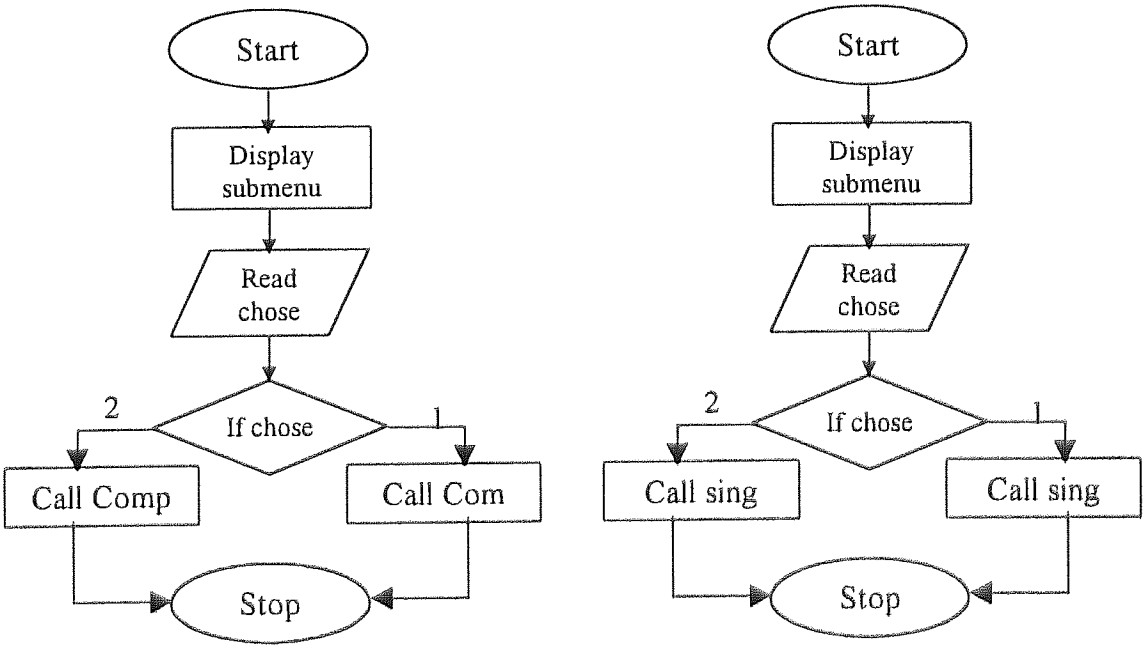

Fig. (3.13): Flow-chart of the computer program for the kinetic analysis of non-isothermal deferential scanning calorimetry data, according to the one heating rate and composite methods.

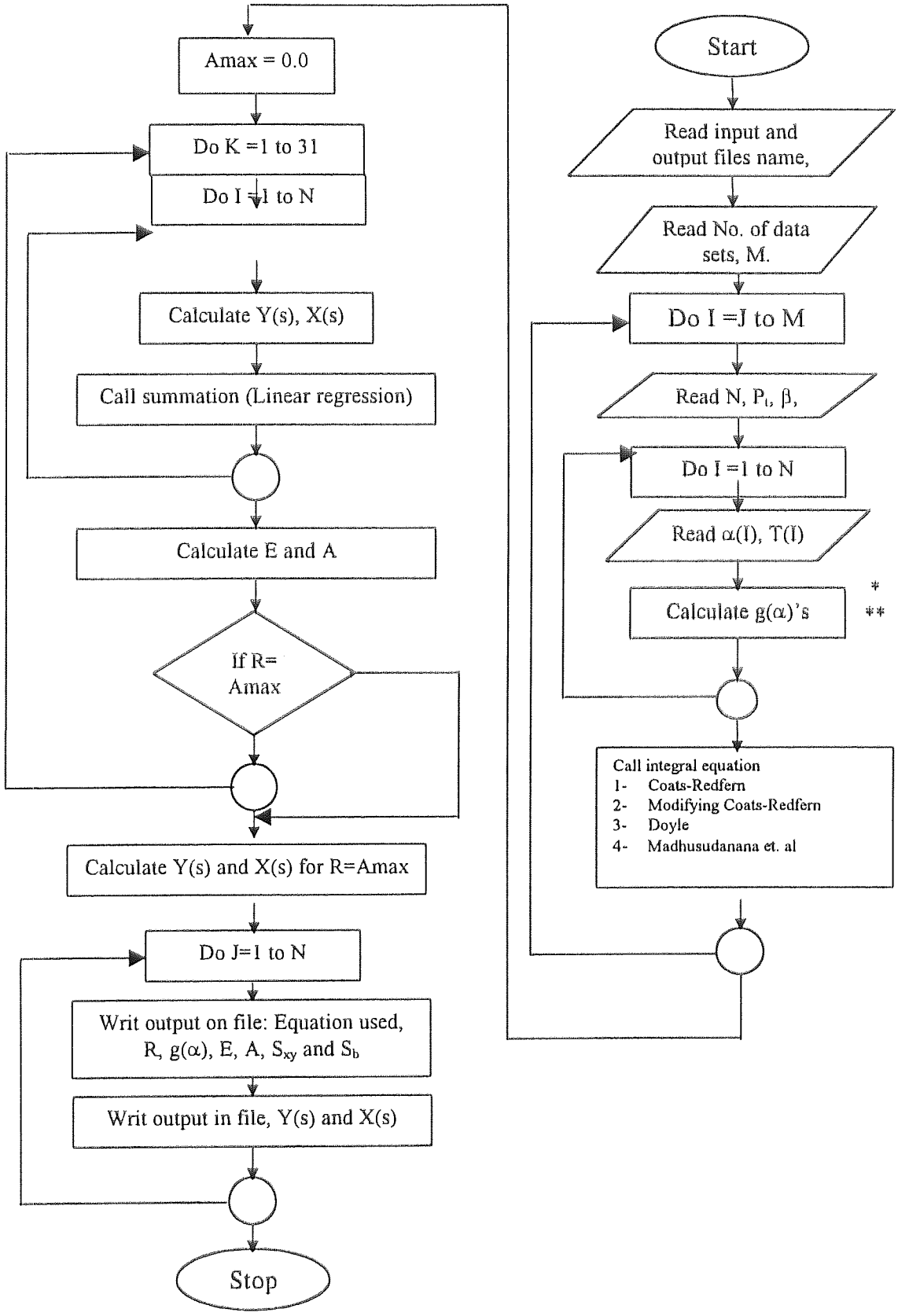

Continue Fig. (3.13):

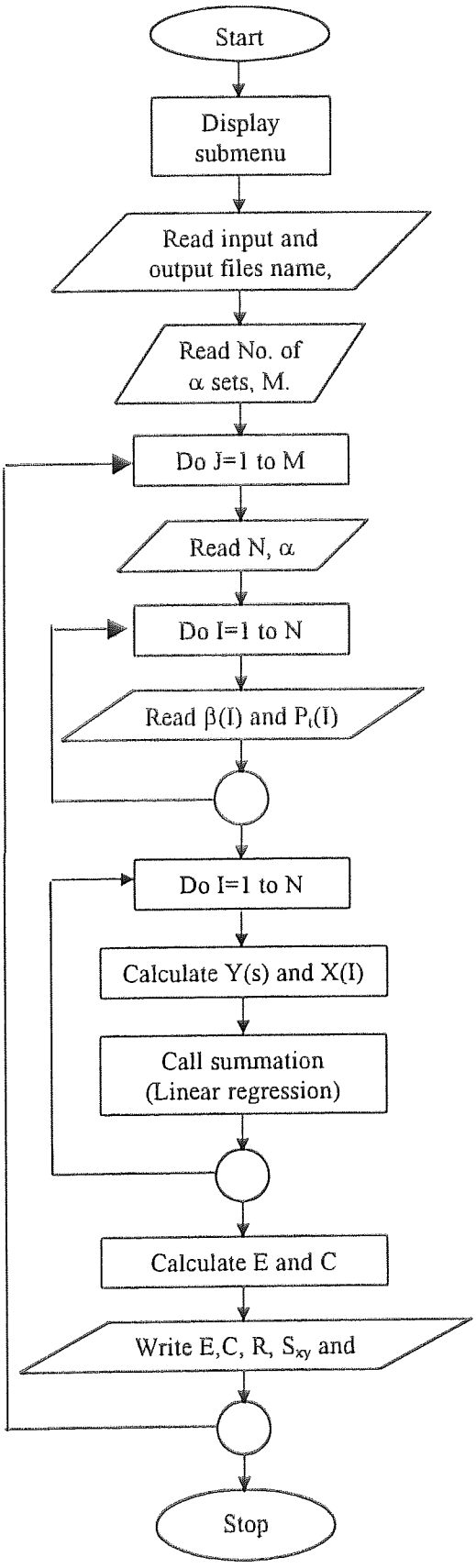

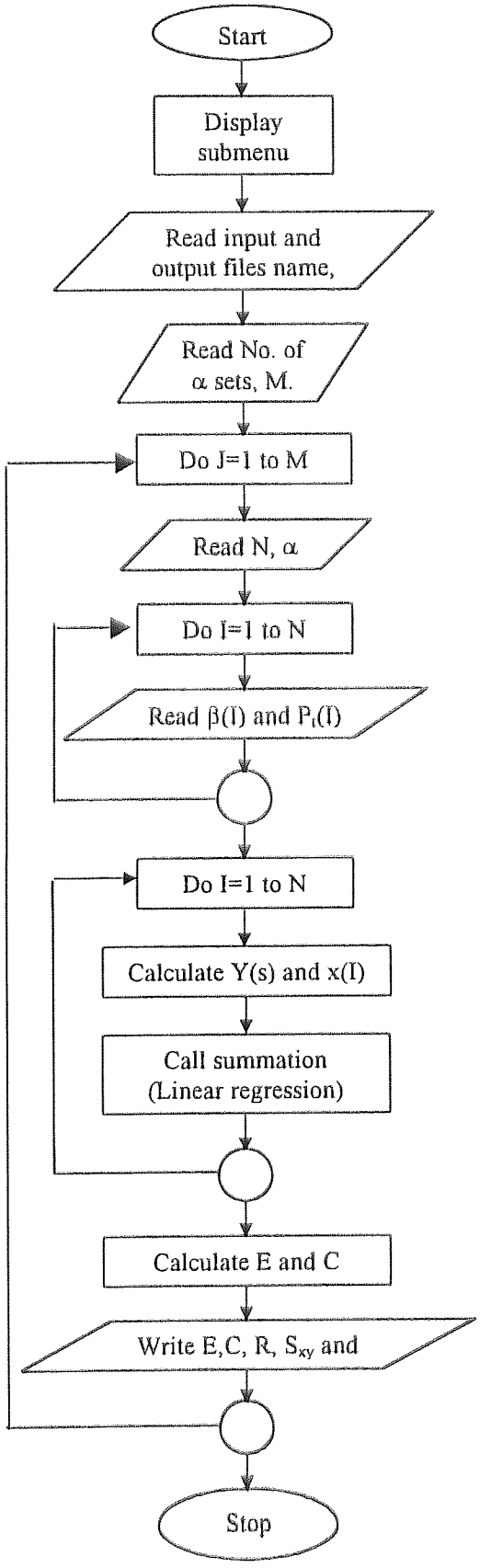

Continue Fig. (3.13)

Table (3.6)

The common forms of g (α) and f (α) proposed in the literature[93].

Function group	Symbol	Mechanism	G(a)	F(a)
Accelerated	P1	Power law	$\alpha^{1/4}$	$4\alpha^{3/4}$
			$\alpha^{2/3}$	$3\alpha^{2/3}$
			$\alpha^{1/2}$	$2\alpha^{1/2}$
			α	1
	E1	Exponential law	$\ln\alpha$	α
S-shaped α– t curve	A1.5	Avrami-Erofeev	$[-\ln(1-\alpha)]^{2/3}$	$3/2(1-\alpha)[-\ln(1-\alpha)]^{1/3}$
	A2	Avrami-Erofeev	$[-\ln(1-\alpha)]^{1/2}$	$2(1-\alpha)[-\ln(1-\alpha)]^{1/2}$
	A3	Avrami-Erofeev	$[-\ln(1-\alpha)]^{1/3}$	$3(1-\alpha)[-\ln(1-\alpha)]^{2/3}$
	A4	Avrami-Erofeev	$[-\ln(1-\alpha)]^{1/4}$	$4(1-\alpha)[-\ln(1-\alpha)]^{3/4}$
	B1	Prout-Topokins	$\ln[\alpha/(1-\alpha)]^{1/4}$	$\alpha(1-\alpha)]$
			$[-\ln(1-\alpha)]^{2}$	$\frac{1}{2}(1-\alpha)[-\ln(1-\alpha)]^{-1}$
			$[-\ln(1-\alpha)]^{3}$	$1/3(1-\alpha)[-\ln(1-\alpha)]^{-2}$
			$[-\ln(1-\alpha)]^{4}$	$\frac{1}{4}(1-\alpha)[-\ln(1-\alpha)]^{-3}$
Decelerated α– t curve	R2	Abstract surface	$1-(1-\alpha)^{1/2}$	$2(1-\alpha)^{1/2}$
	R3		$1-(1-\alpha)^{1/3}$	$3(1-\alpha)^{2/3}$
	D1	1-D diffusion	α^{2}	$\frac{1}{2}\alpha-1$
	D2	2-D diffusion	$(1-\alpha)\ln(1-\alpha)+\alpha$	$-[\ln(1-\alpha)]^{-1}$
	D3	3-D diffusion	$[1-(1-\alpha)^{1/3}]^{2}$	$3/2[1-(1-\alpha)^{1/3}]^{-1}(1-)^{2/3}$
	D4	Ginstling - Brouns	$(1-2\alpha/3)-(1-\alpha)^{2/3}$	$3/2[1-(1-\alpha)^{1/3}]^{-1}$
	F1	First order	$-\ln(1-\alpha)$	$1-\alpha$
	F2	Second order	$1/(1-\alpha)$	$(1-\alpha)^{2}$
	F3	Third order	$[1/(1-\alpha)]^{2}$	$\frac{1}{2}(1-\alpha)^{3}$
			$1-(1-\alpha)^{1/4}$	$4(1-\alpha)^{3/4}$
			$(1-\alpha)^{-1/2}$	$\frac{1}{2}(1-\alpha)^{-2/3}$
			$[(1-\alpha)^{-1/3}-1]^{2}$	$3/2(1-\alpha)^{4/3}[(1-\alpha)^{-1/3}]^{-1}$
			$[1-(1-\alpha)^{1/3}]^{1/2}$	$6[1-(1-\alpha)^{1/3}]^{1/2}(1-\alpha)^{2/3}$
			$[1-(1-\alpha)^{1/2}]^{1/2}$	$4\{(1-\alpha)[1-(1-\alpha)]^{1/2}\}^{1/2}$
			$1-(1-\alpha)^{2}$	$\frac{1}{2}(1-\alpha)^{-1}$
			$1-(1-\alpha)^{3}$	$1/3(1-\alpha)^{-2}$
			$1-(1-\alpha)^{4}$	$\frac{1}{4}(1-\alpha)^{-3}$

The kinetic analysis of the non-isothermal decomposition is applied to the decomposition step of free ligands which is suggested to be decarboxylation followed by evaporation of the products.

Figure 3.14 and Appendix 3 show the results of typical weight changes of the differential scanning calorimetry (DSC) observed under non-isothermal conditions for samples (picolinic, nicotinic, and isonicotinic acids) studied at different heating rates of 5, 10, 15, and 20 ° C min^{-1} in air atmosphere. Analysis of the data was performed in two stages:

(a) In the first stage, data for each specific heating rate (5,10,15 and 20 °C min^{-1}) was separately treated using the approximate integral equations previously mentioned. Tables 3.7, 3.9, and 3.11 show the kinetic parameters and regression results for each of the available models. These were computed according to the different heating rates method for the thermal decomposition of picolinic, nicotinic, and isonicotinic acids, respectively.

The calculation of activation parameters (E and A) using different approximate integral equations gave rise to almost identical values and best fits of experimental data with the same reaction model except Doyle's equation, which differed a little. On the other hand, calculations for different heating rates led to large variations with the different reaction models (See Tables 3.7, 3.9, and 3.11.

(b) In the second stage the composite approach of data was used according to the g (α) functions listed in Table 3.6. A computer program was used to do the calculation and the results showed that the best fit obtained was for the (A_2 model) random nucleation model for picolinic acid (Table 3.8), the (A3 model) random nucleation model for nicotinic acid (Table 3.10), and the Pl model for isonicotinic acid (Tables 3.12). The composite method of analysis involved superposition of all nonisothermal data on one master curve, and led to the same reaction model and to similar values of activation parameters using different approximate integral equations (Coats-Redfern, modified

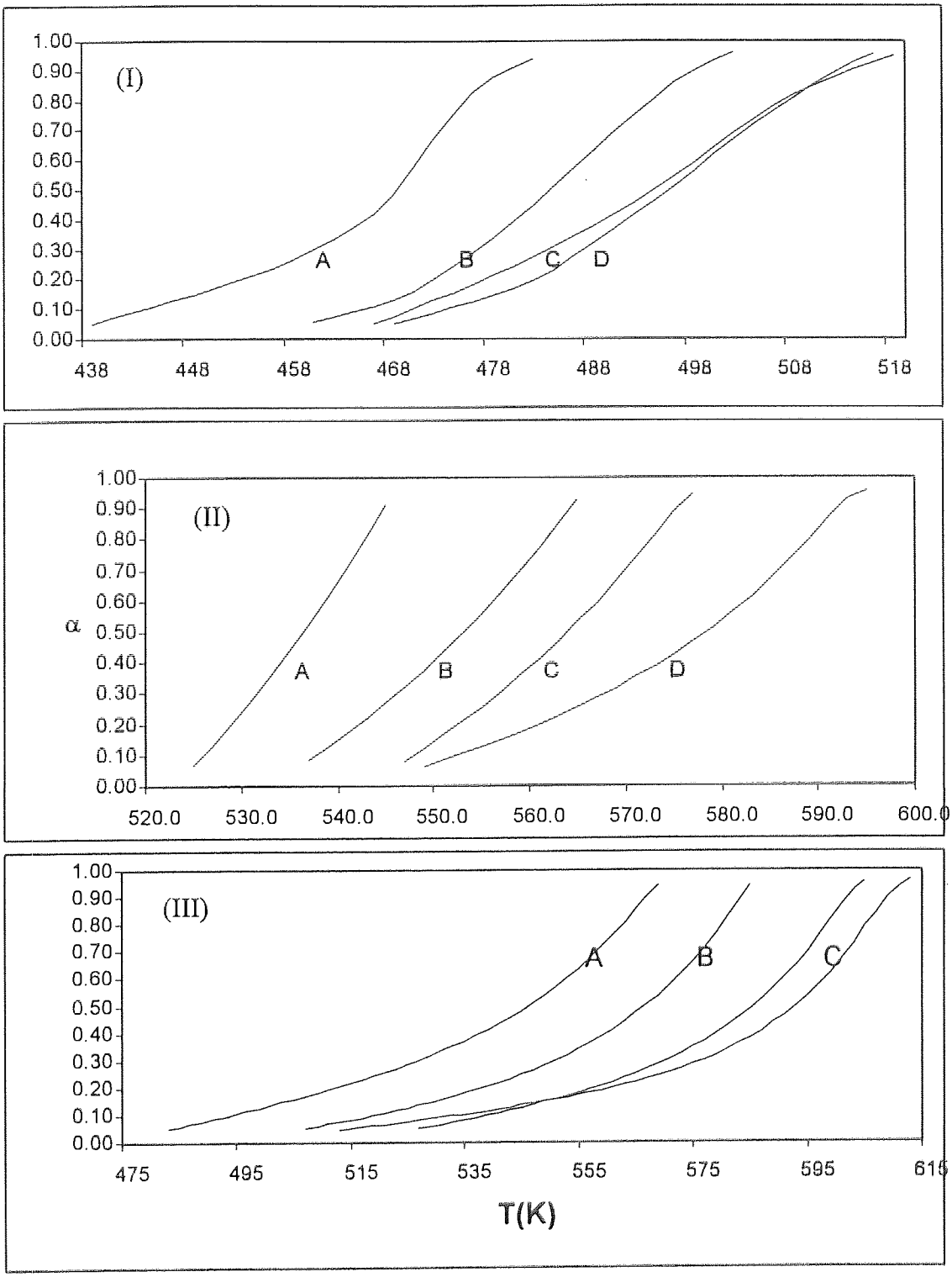

Fig. (3.14): Dynamic measurements for pyridine carboxylic acids thermal decomposition heating rate (A) 5, (B) 10, (C) 15 and (D) 20 ° C min^{-1}; (I) picolinic acid, (II) nicotinic acid and (III) isonicotinic acid.

Coats-Redfern), different approximate integral equations (Coats-Redfern, modified Coats-Redfern, Doyle, and Madhusudanan et. al.). Tables 3.8, 3.10 and 3.12 indicate the thermal decomposition of picolinic acid, nicotinic acid, and isonicotinic acid, respectively.

Typical results are shown in Figs. 3.15, 3.18, and 3.21: (a) for the composite analysis based on Doyle's equation, (b) for composite analysis based on the Madhusudanan et. al. equation, and (c) for the composite analysis based on the Coats-Redfern and modified Coats-Redfern equations. Figs. 3.15, 3.18, and 3.21 (c) show that curves obtained, based on either the Coats-Redfern or the modified Coats-Redfern equations, are identical.

Figs. 3.16, 3.19, and 3.22 show typical results for the Kissinger method while Figs. 3.17,3.20, and 3.23 show typical results for the Ozawa method.

Using the reaction model predicted according to the composite method of analysis and doing the calculation using data obtained at different heating rates gave average values for the activation parameters reaction model similar to those obtained using either of the composite methods, Ozawa and Kissinger (Table 3.7).

In the Ozawa method, the values of E vary much with α, which would imply that the reaction mechanism varies with the fraction reacted (Table 3.7), an unlikely result that would only be acceptable if all other alternatives failed.

The advantages of the Kissinger method are that it is not necessary to know the reaction mechanism to calculate the kinetic parameters, and one needs only to locate the peak maximum temperature for the calculation. The main disadvantage of this method is that it is dependent on the accuracy of the peak position which may be difficult to find in real reactions[31].

All pyridine carboxylic acids do fall in the same mechanism group, namely the Avrami-Erofeev. The physical meaning of this mechanism is that

impingement and coalescence of developed nuclei occurs with ingestion of undeveloped nucleation sites. The integral equation form of the Avrami-Erofeev mechanism is[95]:

$$g(\alpha) = [-\ln(1-\alpha)]^{1/n}$$

where n = 1.5, 2, 3 and 4 for the A1.5, A2, A3 and A4 mechanisms respectively. According to the deduction process of this equation, $n = \lambda + \beta$, where β is the number of steps involved in nucleus formation and λ is the number of dimensions in which the nuclei grow. Most frequently, β equals 0, which corresponds to instantaneous nucleation.

Table (3.7): Kinetic parameters and regression results, for assuming all models of thermal decomposition of picolinic acid at different heating rates.

Equation	β(°Cmin^{-1}	R	M	E(kJmol^{-1})	LnA(min^{-1})	S_{xy}	S_b
Coats-Redfern	5	0.9967	D4	244.99	5.92E+01	1.57E-01	5.25E+02
Modified Coats-Red	5	0.9967	D4	244.99	5.92E+01	1.57E-01	5.25E+02
Doyle's	5	0.9969	D4	240.25	5.82E+01	6.84E-02	2.28E+02
Madusudana et.al.	5	0.9967	D4	245.29	4.60E+01	1.57E-01	5.25E+02
Coats-Redfern	10	0.9992	F1	173.59	4.26E+01	4.87E-02	1.90E+02
Modified Coats-Red	10	0.9992	F1	173.59	4.25E+01	4.87E-02	1.90E+02
Doyle's	10	0.9993	A2	86.34	2.07E+01	1.05E-02	4.08E+01
Madusudana et.al.	10	0.9992	F1	173.91	2.93E+01	4.87E-02	1.90E+02
Coats-Redfern	15	0.9983	F1	156.28	3.76E+01	6.76E-02	2.27E+02
Modified Coats-Red	15	0.9983	F1	156.28	3.76E+01	6.76E-02	2.27E+02
Doyle's	15	0.9985	A1.	104.27	2.49E+01	1.94E-02	6.52E+01
Madusudana et.al.	15	0.9983	F1	156.6	2.44E+01	6.75E-02	2.27E+02
Coats-Redfern	20	0.9928	F1	134.8	3.27E+01	1.31E-01	3.91E+02
Modified Coats-Red	20	0.9928	F1	134.8	3.26E+01	1.31E-01	3.91E+02
Doyle's	20	0.9937	F1	135.97	3.30E+01	5.64E-02	1.69E+02
Madusudana et.al.	20	0.9928	F1	135.12	1.95E+01	1.31E-01	3.91E+02

b: Heating rate.
R: Correlation coefficient.
M: Model reaction.
E: Activation energy.
A: Frequency
S_{xy}: Standard derivation
S_b: Standard derivation of slop

Table (3.8): Kinetic and regression results of the thermal decomposition of picolinic acid for different heating rates and composite methods, assuming the A2 model was chosen by the composite method.

Method	Equation	β(° C min^{-1})	R	M	E(kJ mol^{-1})	LnA(min^{-1})	S_{xy}	S_b
Composite	Coats-Redfern		0.97564	A2	72.12	1.94E+01	1.64E-01	2.00E+02
	Modified Coats-Redfern		0.97564	A2	72.12	1.93E+01	1.64E-01	2.00E+02
	Doyle's		0.98009	A2	76.17	1.83E+01	7.13E-02	8.70E+01
	Madusudana et.al.		0.97585	A2	72.44	6.14E+00	1.64E-01	2.00E+02
Singel	Coats-Redfern	5	0.99208	A2	66.93	1.55E+01	6.67E-02	2.22E+02
	Coats-Redfern	10	0.99907	A2	82.79	1.96E+01	2.47E-02	9.61E+01
	Coats-Redfern	15	0.9981	A2	74.05	1.72E+01	3.41E-02	1.15E+02
	Coats-Redfern	20	0.99176	A2	63.31	1.48E+01	6.57E-02	1.97E+02
	Average		0.9952525		71.77	1.68E+01	4.78E-02	1.58E+02
	Modified Coats-Redfern	5	0.99208	A2	66.93	1.53E+01	6.67E-02	2.22E+02
	Modified Coats-Redfern	10	0.99907	A2	82.79	1.95E+01	2.47E-02	9.61E+01
	Modified Coats-Redfern	15	0.9981	A2	74.05	1.71E+01	3.41E-02	1.15E+02
	Modified Coats-Redfern	20	0.99176	A2	63.31	1.47E+01	6.57E-02	1.97E+02
	Average		0.9952525		71.77	1.67E+01	4.78E-02	1.58E+02
	Doyle's	5	0.99351	A2	70.92	1.69E+01	2.92E-02	9.73E+01
	Doyle's	10	0.99926	A2	86.34	2.07E+01	1.05E-02	4.08E+01
	Doyle's	15	0.99851	A2	78.2	1.86E+01	1.45E-02	4.89E+01
	Doyle's	20	0.99366	A2	67.98	1.65E+01	2.82E-02	8.45E+01
	Average		0.996235		75.86	1.82E+01	2.06E-02	6.79E+01
	Madusudana et.al.	5	0.99215	A2	67.23	2.23E+00	6.67E-02	2.22E+02
	Madusudana et.al.	10	0.99908	A2	83.11	6.34E+00	2.46E-02	9.60E+01
	Madusudana et.al.	15	0.99811	A2	74.37	3.99E+00	3.41E-02	1.15E+02
	Madusudana et.al.	20	0.99185	A2	63.63	1.59E+00	6.56E-02	1.97E+02
	Average		0.9952975		72.085	3.54E+00	4.78E-02	1.58E+02
	Ozawa α =	0.1	0.935		68.31		0.113613	1.01E+03
		0.3	0.946		83.28		0.103971	1.11E+03
		0.5	0.969		72.05		0.079262	7.16E+02
		0.7	0.978		78.88		0.066846	6.55E+02
		0.9	0.989		75.11		0.048227	4.45E+02
	Average		0.96871625		74.9625		7.66E-02	6.82E+02
	Kissinger		0.976		71.37		0.143898	1.35E+03

b: Heating rate.
R: Correlation coefficient.
M: Model reaction.
E: Activation energy.
A: Frequency
S_{xy}: Standard derivation
S_b: Standard derivation of slop

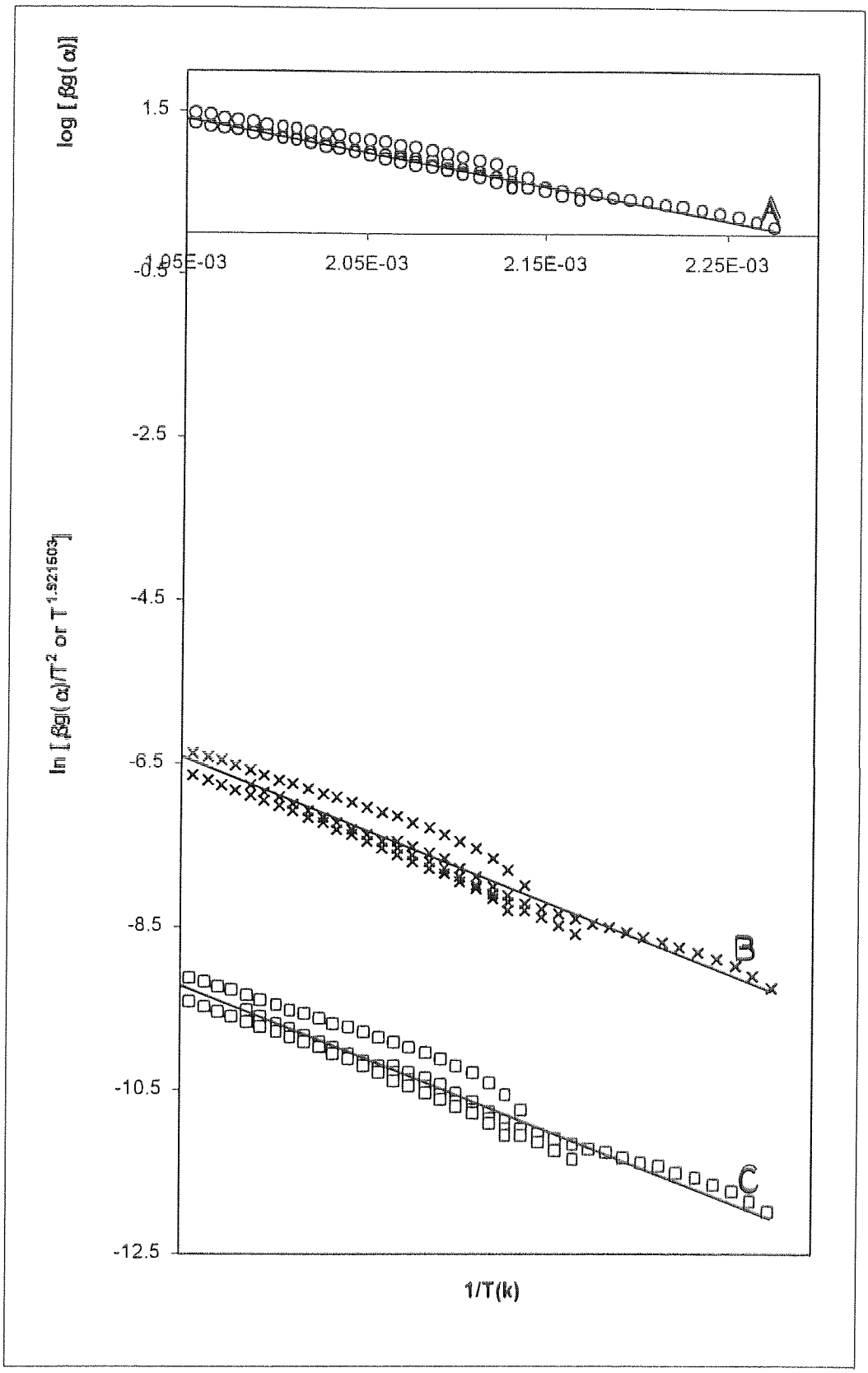

Fig. (3.15): Composite analysis of the dynamic decomposition of picolinic acid, based on (A) Doyle equation, (B) Madhusudanan-Krisshnan-Ninan, and (C) Coats-Redfern and modified Coats-Redfern, assuming the A3 model.

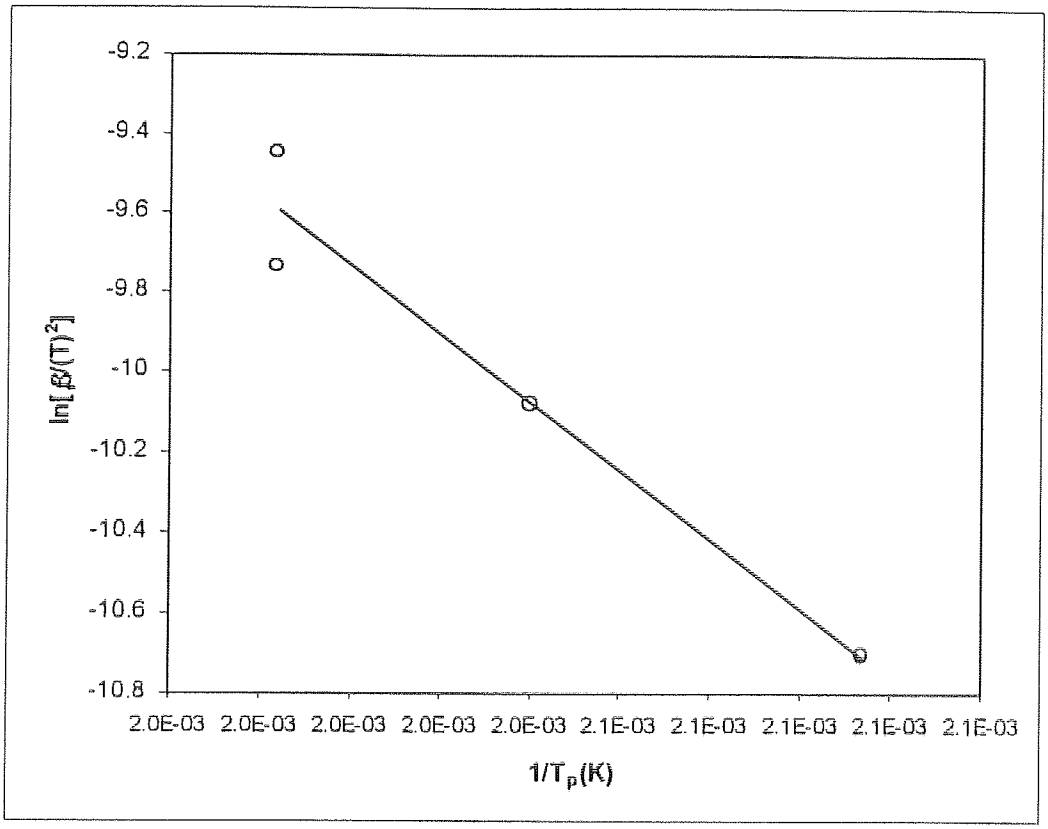

Fig. (3.16): Regression analysis of the dynamic thermal decomposition of picolinic acid, based on the Kissinger method.

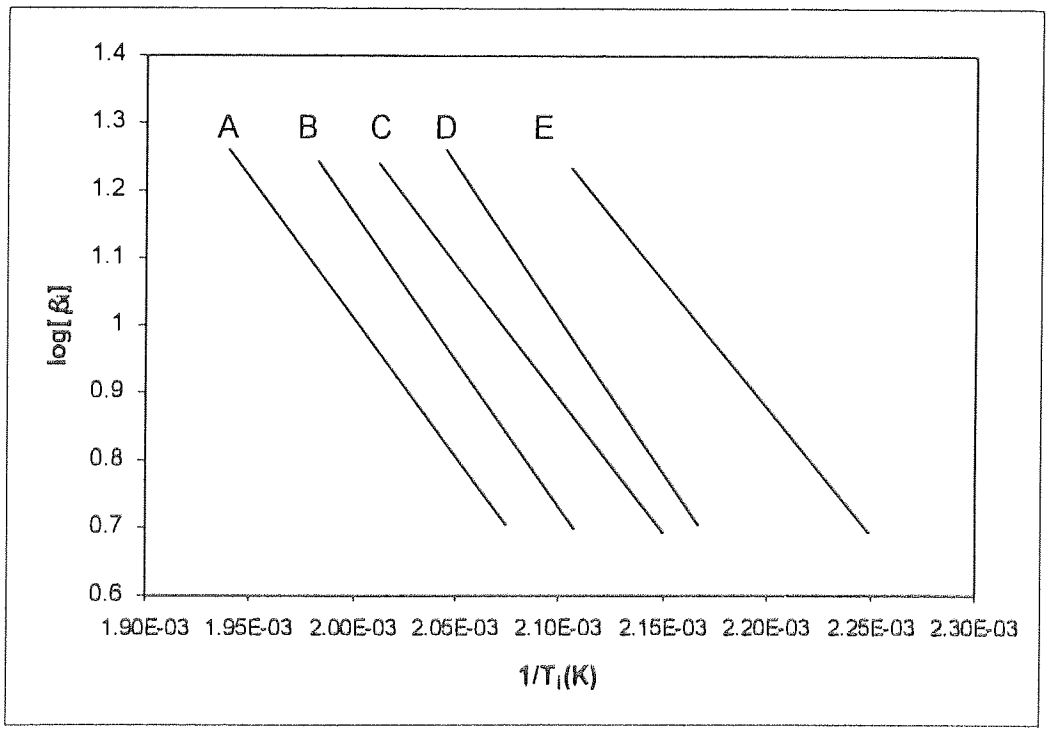

Fig. (3.17): Regression analysis of the dynamic thermal decomposition of picolinic acid, based on the Ozawa method. (A) a=0.9, (B) a=0.7, (C) a=0.5, (D) a=0.3, (E) a=0.1.

Table (3.9): Kinetic parameters and regression results, assuming all models of thermal decomposition of nicotinic acid at different heating rates.

Equation	β(° C min^{-1})	R	M	E($kJmol^{-1}$)	LnA(min^{-1})	S_{xy}	S_b
Coats-Redfern	5	0.98798	F1	376.87	8.39E+01	1.73E-01	2.36E+03
Modified Coats-Redfern	5	0.98798	F1	376.87	8.38E+01	1.73E-01	2.36E+03
Doyle's	5	0.98853	A1.5	244.56	5.40E+01	5.01E-02	6.84E+02
Madusudana et.al.	5	0.98801	F1	377.22	7.06E+01	1.73E-01	2.36E+03
Coats-Redfern	10	0.9948	F1	269.2	5.83E+01	1.01E-01	9.19E+02
Modified Coats-Redfern	10	0.9948	F1	269.2	5.82E+01	1.01E-01	9.19E+02
Doyle's	10	0.99515	A3	88.23	1.84E+01	1.47E-02	1.33E+02
Madusudana et.al.	10	0.99482	F1	269.56	4.50E+01	1.01E-01	9.19E+02
Coats-Redfern	15	0.99532	F1	272.73	5.83E+01	9.94E-02	8.51E+02
Modified Coats-Redfern	15	0.99532	F1	272.73	5.82E+01	9.94E-02	8.51E+02
Doyle's	15	0.99564	A4	67.06	1.40E+01	1.08E-02	9.23E+01
Madusudana et.al.	15	0.99534	F1	273.09	4.50E+01	9.94E-02	8.51E+02
Coats-Redfern	20	0.99645	D4	362.67	7.33E+01	1.63E-01	7.86E+02
Modified Coats-Redfern	20	0.99645	D4	362.67	7.33E+01	1.63E-01	7.86E+02
Doyle's	20	0.99664	D4	353.92	7.20E+01	7.07E-02	3.41E+02
Madusudana et.al.	20	0.99646	D4	363.05	6.00E+01	1.63E-01	7.85E+02

B: Heating rate.
R: Correlation coefficient.
M: Model reaction.
E: Activation energy.
A: Frequency
S_{xy}: Standard derivation
S_b: Standard derivation of slop

Table (3.10): Kinetic and regression results of the thermal decomposition of nicotinic acid for different heating rates and composite methods, assuming the A3 model was chosen by the composite method.

Method	Equation	β(° C min^{-1})	R	M	E(kJmol^{-1})	LnA(min^{-1})	S_{xy}	S_b
Composite	Coats-Redfern		0.98094	A3	79.13	1.86E+01	1.04E-01	2.36E+02
	Modified Coats-Redfern		0.98094	A3	79.13	1.85E+01	1.04E-01	2.36E+02
	Doyle's		0.98492	A3	84.08	1.75E+01	4.47E-02	1.01E+02
	Madusudana et.al.		0.98112	A3	79.49	5.40E+00	1.04E-01	2.36E+02
Singel	Coats-Redfern	5	0.98676	A3	119.69	2.54E+01	5.78E-02	7.89E+02
	Coats-Redfern	10	0.994	A3	83.63	1.71E+01	3.39E-02	3.07E+02
	Coats-Redfern	15	0.99459	A3	84.68	1.73E+01	3.32E-02	2.84E+02
	Coats-Redfern	20	0.99409	A3	59.59	1.16E+01	3.46E-02	1.67E+02
	Average	12.5	0.99236		86.8975	1.79E+01	3.99E-02	3.87E+02
	Modified Coats-Redfern	5	0.98676	A3	119.69	2.53E+01	5.78E-02	7.89E+02
	Modified Coats-Redfern	10	0.994	A3	83.63	1.69E+01	3.39E-02	3.07E+02
	Modified Coats-Redfern	15	0.99459	A3	84.68	1.72E+01	3.32E-02	2.84E+02
	Modified Coats-Redfern	20	0.99409	A3	59.59	1.15E+01	3.46E-02	1.67E+02
	Average	12.5	0.99236		86.8975	1.77E+01	3.99E-02	3.87E+02
	Doyle's	5	0.98853	A3	122.28	2.60E+01	2.51E-02	3.42E+02
	Doyle's	10	0.99515	A3	88.23	1.84E+01	1.47E-02	1.33E+02
	Doyle's	15	0.99564	A3	89.41	1.87E+01	1.44E-02	1.23E+02
	Doyle's	20	0.99557	A3	65.71	1.36E+01	1.51E-02	7.27E+01
	Average	12.5	0.9937225		91.4075	1.92E+01	1.73E-02	1.66E+02
	Madusudana et.al.	5	0.98684	A3	120.04	1.22E+01	5.78E-02	7.89E+02
	Madusudana et.al.	10	0.99405	A3	83.99	3.83E+00	3.39E-02	3.07E+02
	Madusudana et.al.	15	0.99464	A3	85.05	4.08E+00	3.32E-02	2.84E+02
	Madusudana et.al.	20	0.99417	A3	59.97	*********	3.46E-02	1.67E+02
	Average	12.5	0.992425		87.2625	6.70E+00	3.99E-02	3.87E+02
	Ozawa α =	0.1	0.997		115.24		2.46E-02	3.46E+02
		0.3	0.991		91.89		4.29E-02	4.83E+02
		0.5	0.989		83.44		4.79E-02	4.91E+02
		0.7	0.988		79.28		4.96E-02	4.83E+02
		0.9	0.984		75.38		5.64E-02	5.25E+02
	Average	0.5	0.9898		89.046		4.43E-02	465.4
	Kissinger		0.988		73.01		1.00E-01	9.62E+02

B: Heating rate.
R: Correlation coefficient.
M: Model reaction.
E: Activation energy.
A: Frequency
S_{xy}: Standard derivation
S_b: Standard derivation of slop

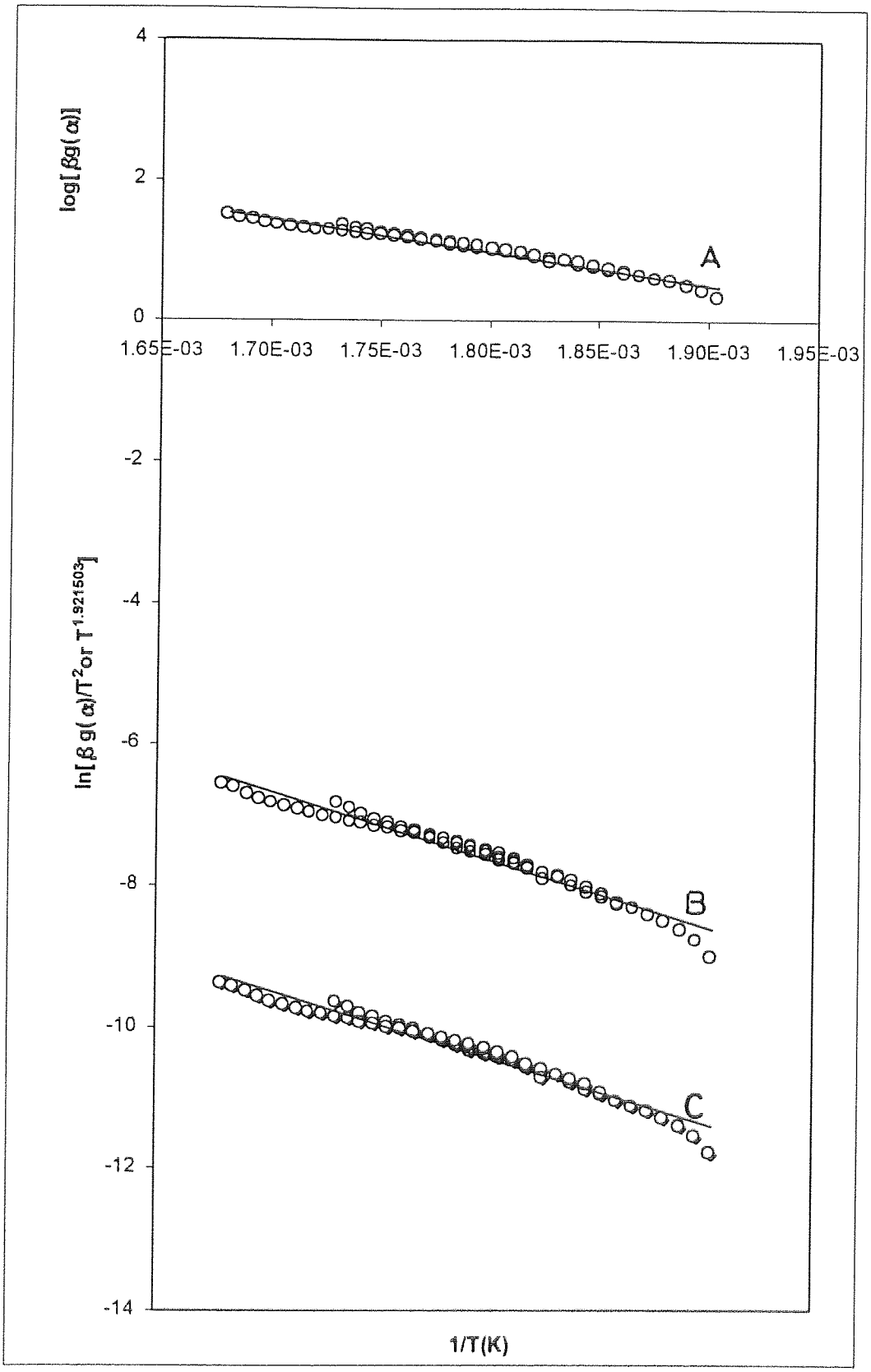

Fig. (3.18): Composite analysis of the dynamic decomposition of nicotinic acid, based on (A) Doyle equation, (B) Madhusudanan-Krisshnan-Ninan, and (C) Coats-Redfern and modified Coats-Redfern, assuming the A3 model.

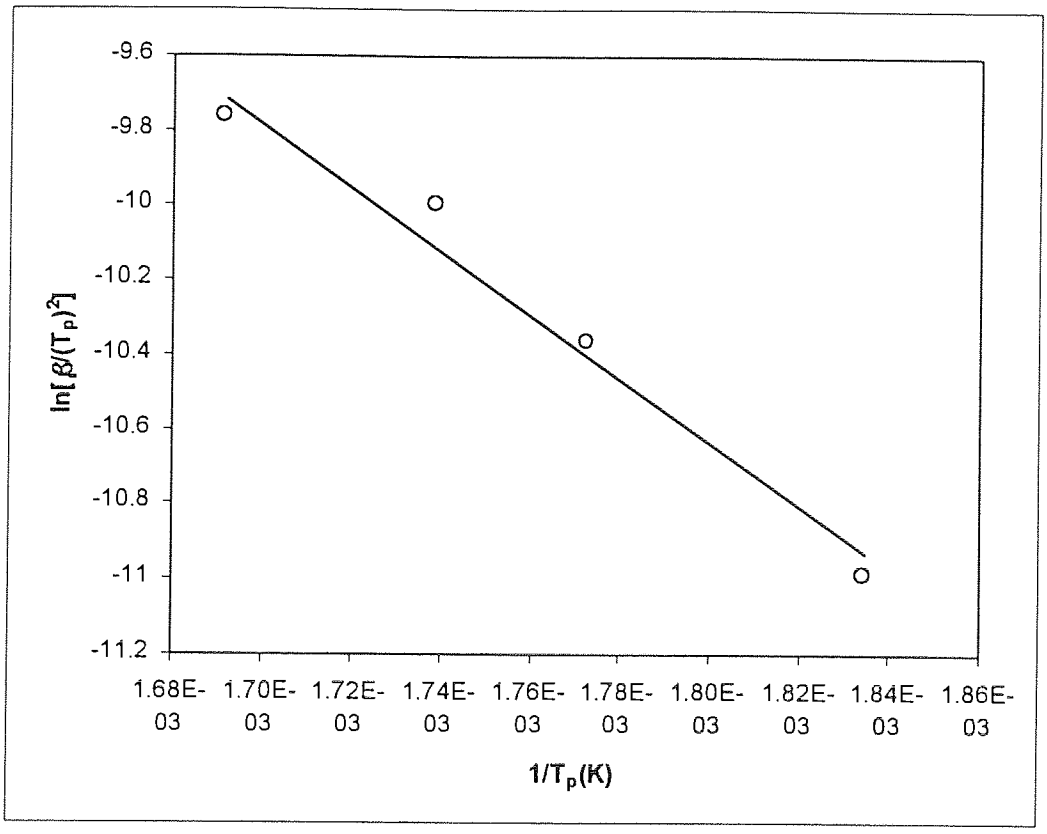

Fig. (3.19): Regression analysis of the dynamic thermal decomposition of nicotinic acid, based on the Kissinger method.

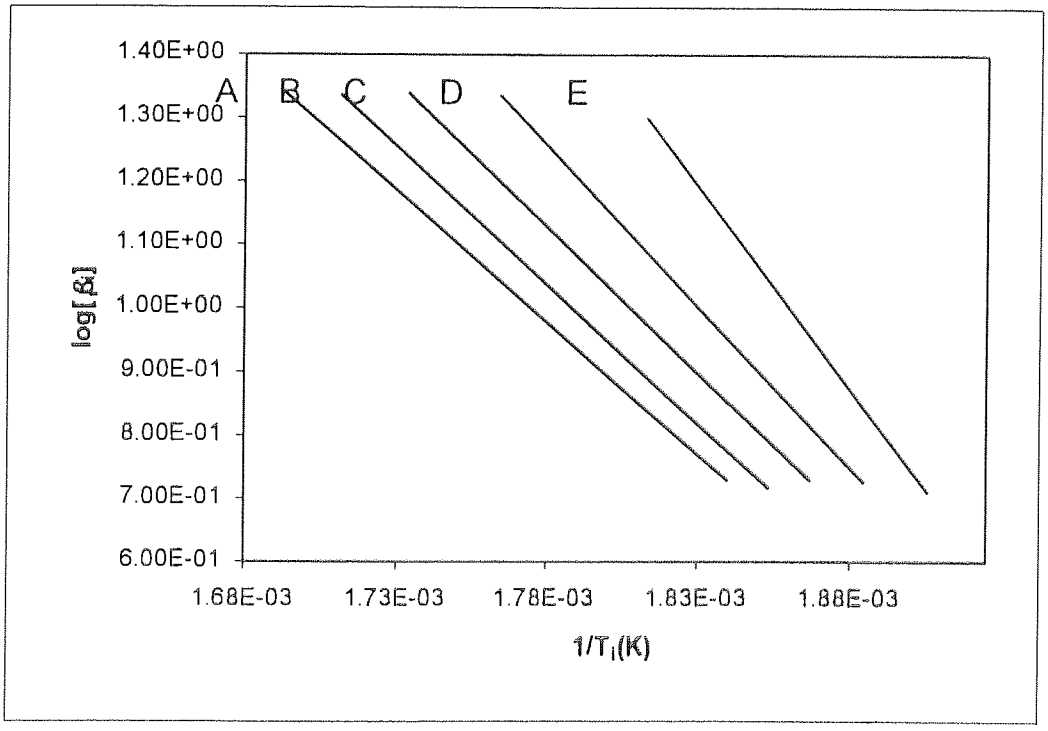

Fig. (3.20): Regression analysis of the dynamic thermal decomposition of nicotinic acid, based on the Ozawa method. (A) a=0.9, (B) a=0.7, (C) a=0.5, (D) a=0.3, (E) a=0.1.

Table (3.11): Kinetic parameters and regression results, assuming all models of thermal decomposition of isonicotinic acid at different heating rates.

Equation	β(° C min^{-1})	R	M	E($kJmol^{-1}$)	LnA(min^{-1})	S_{xy}	S_b
Coats-Redfern	5	0.99523	D2	145.06	2.90E+01	1.61E-01	2.64E+02
Modified Coats-Redfern	5	0.99523	D2	145.06	2.89E+01	1.61E-01	2.64E+02
Doyle's	5	0.99579	D2	146.23	2.93E+01	6.98E-02	1.14E+02
Madusudana et.al.	5	0.99526	D2	145.41	1.58E+01	1.61E-01	2.64E+02
Coats-Redfern	10	0.9985	D1	164.97	3.33E+01	8.69E-02	1.77E+02
Modified Coats-Redfern	10	0.9985	D1	164.97	3.32E+01	8.69E-02	1.77E+02
Doyle's	10	0.99867	P1	27.58	5.46E+00	6.25E-03	1.27E+01
Madusudana et.al.	10	0.9985	D1	165.32	2.00E+01	8.68E-02	1.77E+02
Coats-Redfern	15	0.99849	D1	182.15	3.61E+01	8.96E-02	1.96E+02
Modified Coats-Redfern	15	0.99849	D1	182.15	3.60E+01	8.96E-02	1.96E+02
Doyle's	15	0.99864	P1	22.77	4.87E+00	4.84E-03	1.06E+01
Madusudana et.al.	15	0.99849	D1	182.52	2.28E+01	8.96E-02	1.96E+02
Coats-Redfern	20	0.99549	D1	141.43	2.74E+01	1.54E-01	2.31E+02
Modified Coats-Redfern	20	0.99549	D1	141.43	2.73E+01	1.54E-01	2.31E+02
Doyle's	20	0.99594	P1	17.92	4.30E+00	8.48E-03	1.27E+01
Madusudana et.al.	20	0.99551	D1	141.8	1.41E+01	1.55E-01	2.32E+02

b: Heating rate.
R: Correlation coefficient.
M: Model reaction.
E: Activation energy.
A: Frequency
S_{xy}: Standard derivation
S_b: Standard derivation of slop

Table (3.12): Kinetic and regression results of the thermal decomposition of isonicotinic acid for different heating rates and composite method, assuming the A4 model was chosen by the composite method.

Method	Equation	β(° C min^{-1})	R	M	E(kJmol^{-1})	LnA(min^{-1})	S_{xy}	S_b
Composite	Coats-Redfern		0.98361	A4	67.73	1.48E+01	1.51E-01	1.14E+02
	Modified Coats-Redfern		0.98361	A4	67.73	1.47E+01	1.51E-01	1.14E+02
	Doyle's		0.987	A4	73.05	1.41E+01	6.63E-02	4.97E+01
	Madusudana et.al.		0.98377	A4	68.09	1.62E+00	1.51E-01	1.14E+02
Singel	Coats-Redfern	5	0.99271	A4	62.71	1.12E+01	8.65E-02	1.41E+02
	Coats-Redfern	10	0.9983	A4	77.96	1.48E+01	4.37E-02	8.89E+01
	Coats-Redfern	15	0.9983	A4	86.38	1.64E+01	4.50E-02	9.84E+01
	Coats-Redfern	20	0.99496	A4	66.06	1.21E+01	7.63E-02	1.14E+02
	Average	12.5	0.906068		73.2775	1.36E+01	6.29E-02	1.11E+02
	Modified Coats-Redfern	5	0.99271	A4	62.71	1.11E+01	8.65E-02	1.41E+02
	Modified Coats-Redfern	10	0.9983	A4	77.96	1.46E+01	4.37E-02	8.89E+01
	Modified Coats-Redfern	15	0.9983	A4	86.38	1.63E+01	4.50E-02	9.84E+01
	Modified Coats-Redfern	20	0.99496	A4	66.06	1.19E+01	7.63E-02	1.14E+02
	Average	12.5	0.906068		73.2775	1.35E+01	6.29E-02	1.11E+02
	Doyle's	5	0.99455	A4	67.92	1.30E+01	3.69E-02	6.03E+01
	Doyle's	10	0.99867	A4	82.74	1.62E+01	1.87E-02	3.81E+01
	Doyle's	15	0.99864	A4	91.07	1.77E+01	1.94E-02	4.23E+01
	Doyle's	20	0.99594	A4	71.68	1.39E+01	3.39E-02	5.09E+01
	Average	12.5	0.90665		78.3525	1.52E+01	2.72E-02	4.79E+01
	Madusudana et.al.	5	0.9928	A4	63.05	*******	8.64E-02	1.41E+02
	Madusudana et.al.	10	0.99831	A4	78.31	1.53E+00	4.37E-02	8.89E+01
	Madusudana et.al.	15	0.99831	A4	86.75	3.16E+00	4.50E-02	9.84E+01
	Madusudana et.al.	20	0.99501	A4	66.42	*********	7.64E-02	1.14E+02
	Average	12.5	0.996108		73.6325	2.35E+00	6.29E-02	1.11E+02
	Ozawa α =	0.1	0.968		57.9		0.08062	5.86E+02
		0.3	0.997		65.93		0.02431	1.95E+02
		0.5	0.995		74.56		0.03145	2.86E+02
		0.7	0.903		42.74		0.07737	7.91E+02
		0.9	0.992		83.02		0.04076	4.14E+02
	Average	0.5	0.971		64.83		5.09E-02	4.55E+02
	Kissinger		0.999		82.43		0.03276	3.49E+02

b: Heating rate.
R: Correlation coefficient.
M: Model reaction.
E: Activation energy.
A: Frequency
S_{xy}: Standard derivation
S_b: Standard derivation of slop

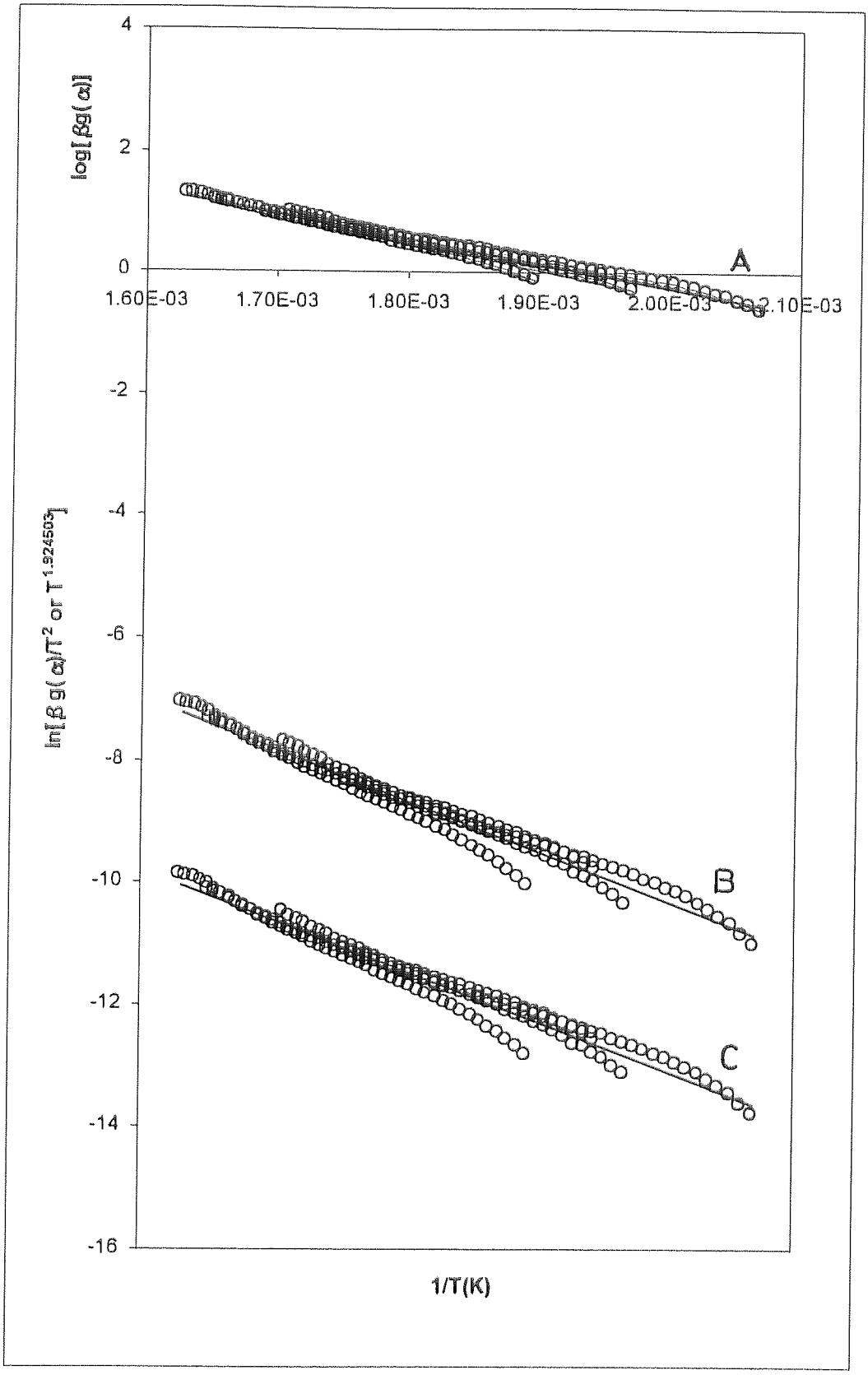

Fig (3.21): Composite analysis of the dynamic decomposition of isonicotinic acid, based on (A) Doyle equation, (B) Madhusudanan-Krisshnan-Ninan, and (C) Coats-Redfern and modified Coats-Redfern, assuming the A4 model.

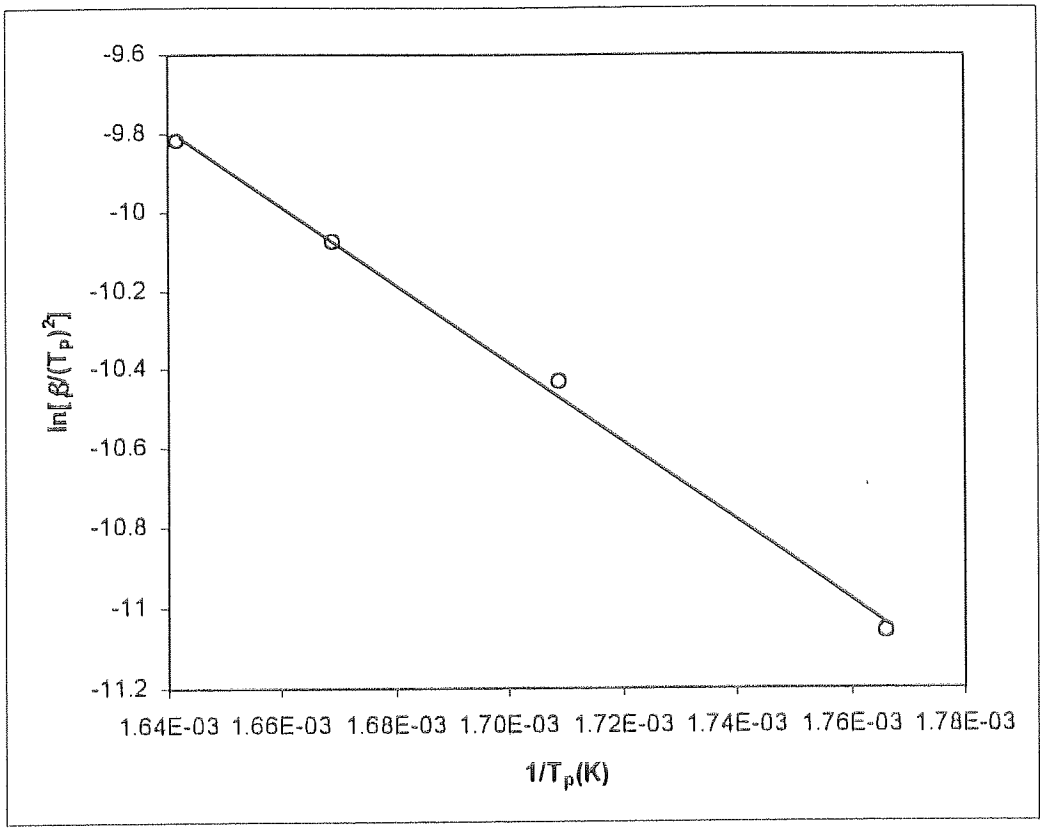

Fig (3.22): Regression analysis of the dynamic thermal decomposition of isonicotinic acid, based on the Kissinger method.

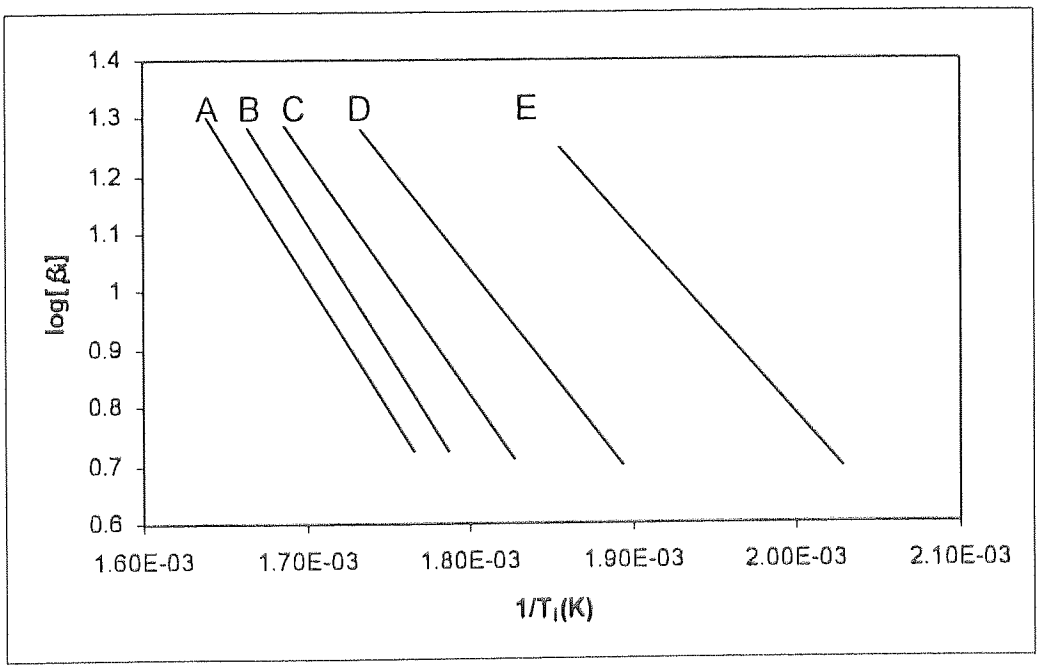

Fig (3.23): Regression analysis of the dynamic thermal decomposition of isonicotinic acid, based on the Ozawa method. (A) a=0.9, (B) a=0.7, (C) a=0.5, (D) a=0.3, (E) a=0.1.

CHAPTER 4

RESULTS AND DISCUSSION (II)

COMPLEXES STUDIES

RESULTS (II)

IDENTIFICATION OF PREPARED COMPOUNDS

4.1 PREFACE

The coordination compounds are formed as solids that have the colors typical of complexes of the metal ions of Co(II), Ni(II) and Cu(II) with N- and O- donor ligands. They form with the following stiochiometry: $ML_2.X(H_2O)$, where **M** is the metal ion, **L** ligand (picolinate (PA), nicotinate (NA) or isonicotinate (IA) and **X** is the number of water molecules.

4.2 CHEMICAL ANALYSIS OF PREPARED COMPLEXES

4.2.1 ANALYSIS

The analytical result for the metals, carbon, hydrogen, and nitrogen of prepared complexes are given in Table 4.1. In general, the elemental analyses are in good agreement with acceptable formulae that can be proposed for all the compounds:

$Co(PA)_2.2.5H_2O$, $Co(NA)_2.4H_2O$, $Co(IA)_2.4H_2O$, $Ni(PA)_2.4H_2O$
$Ni(NA)_24H_2O$, $Ni(IA)_2.3.5H_2O$, $Cu(PA)_2$, $Cu(NA)_2$ $Cu(IA)_2.4.5H_2O$

The number of molecules of water of hydration in these formulae is consistent with the results of predictions from the TG data.

Table 4.1

Elemental analysis of complexes

Compounds	% (Theory)				% (Experimental)			
	Metal	Carbon	Nitrogen	Hydrogen	Metal	Carbon	Nitrogen	Hydrogen
$Co(PA)_2$ $2.5(H_2O)$	16.93	41.38	8.05	3.77	16.92	41.91	7.41	3.48
$Co(NA)_2$ 4 (H_2O)	15.71	38.40	7.47	4.3	15.00	33.91	6.59	4.33
$Co(IA)_2$ 4 (H_2O)	15.71	38.40	7.47	4.30	15.70	36.24	6.56	4.45
$Ni(PA)_2$ 4 (H_2O)	15.66	38.42	7.47	4.30	15.26	35.42	6.47	4.16
$Ni(NA)_2$ 4 (H_2O)	15.66	38.42	7.47	4.30	15.26	35.30	6.49	4.30
$Ni(IA)_2$ $3.5(H_2O)$	16.03	39.36	7.65	4.13	15.97	37.49	6.98	4.37
$Cu(PA)_2$	20.66	46.81	9.11	2.62	20.00	46.24	8.50	2.70
$Cu(NA)_2$	20.66	46.81	9.11	2.62	20.01	46.60	8.05	2.60
$Cu(IA)_2$ $4.5(H_2O)$	16.35	37.05	7.21	4.41	16.40	37.50	6.91	3.94

(PA): Picolinate, (NA): Nicotinate and (IA): Isonicotinate.

4.2.2 Infrared Spectra (4000 – 200 cm^{-1})

The mode of bonding of the ligands to Co(II), Ni(II), or Cu(II) was examined by the IR-spectra for complexes. The wavenumbers of IR absorption bands for the free pyridine monocarboxylic acids (picolinic acid (HPA), nicotinic acid (HNA), and isonicotinic acid (HIA)) and its complexes are shown in Tables 4.2-4.4 with the descriptions and assignments of the relevant wavenumbers. The mode of bonding of the complexes are shown in Figs.4.1-4.9.

A comparison of the main bands in infrared spectra of the hydrated metal complexes with those of the free pyridine carboxylic acids (see Table 3.2 in the preceding chapter) shows that the spectra are similar in the 2000-650 cm^{-1} region.

The IR spectra of all the complexes, except for $Cu(PA)_2$ and $Cu(NA)_2$, have strong broad bands in the range of 3600-2550 cm^{-1}, ν(OH), indicating the presence of water molecules which are not coordinated to the metal ion. The presence of these bands suggests that the water molecules are present as water of crystallization. The presence of coordinated water in cobalt, nickel, and copper complexes with picolinate, nicotinate, and isonicotinate is confirmed by the bands present in the range 331-438 cm^{-1} (Tables 4.2-4.4) which have been assigned to the M-OH vibration. W. Brzyska and A. Krol [81] have reported that the water present can interact with other species in three different ways. It can interact with the anion in the space lattice attached by a hydrogen bond (loss at 313-328 K), or it may H- bond to an inner sphere water molecule (loss at 423 K). Finally, it may be present as coordinated water strongly bonded to the metal ion, (lost at the highest temperature simultaneously with the decomposition of organic ligand). In the IR spectrum of complexes, a broad band is observed in the 3600-2500 cm^{-1} region. This indicates the presence of hydrogen bonding in the complex [94].

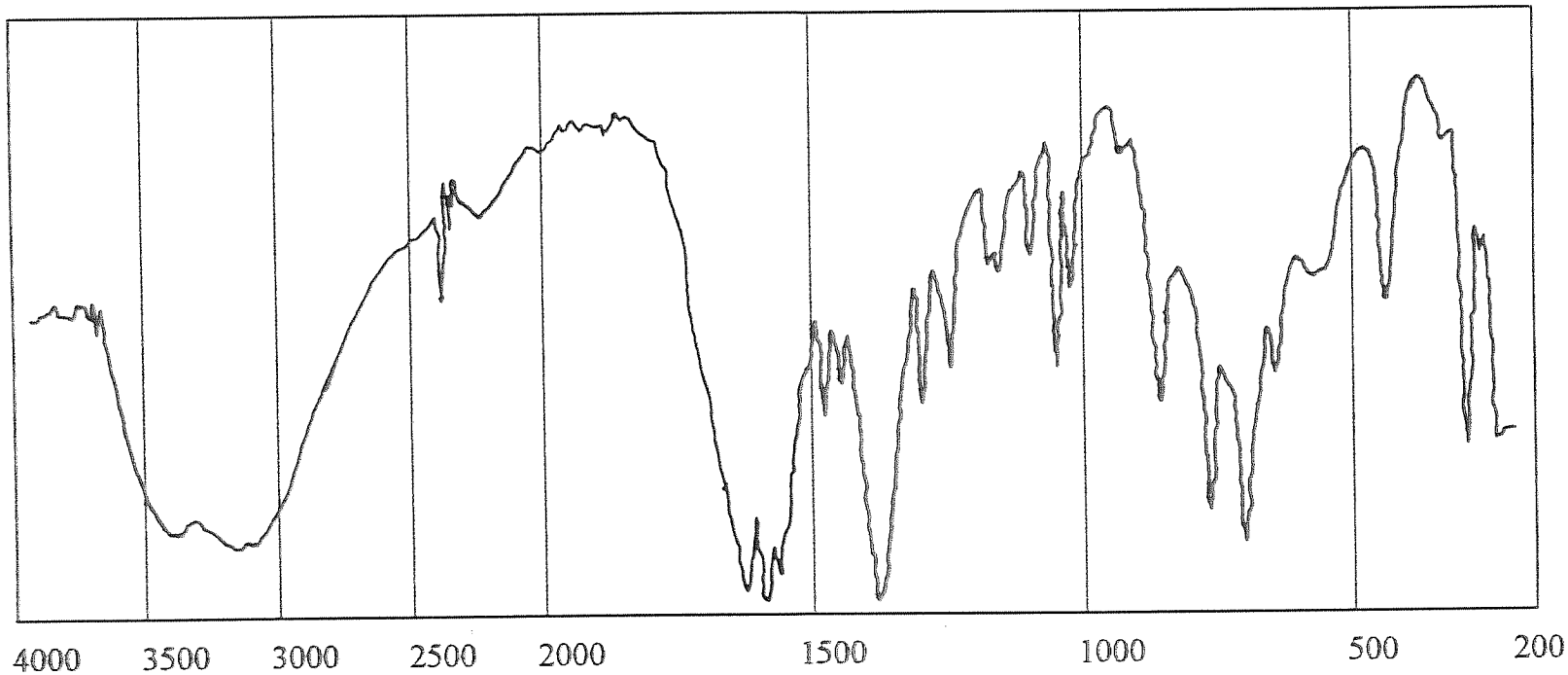

Fig. (4.1): IR Spectra of cobalt(II) picolinate.

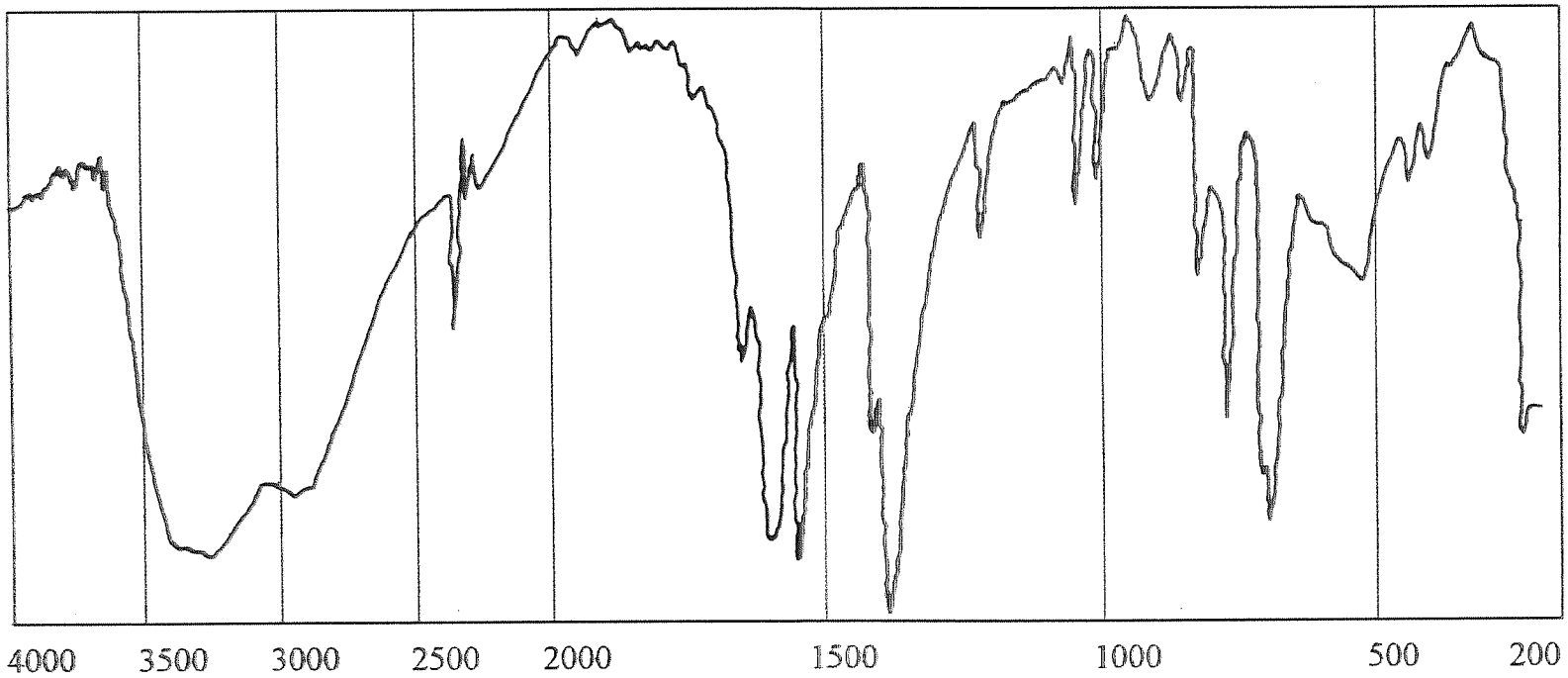

Fig. (4.2): IR Spectra of cobalt(II) nicotinate

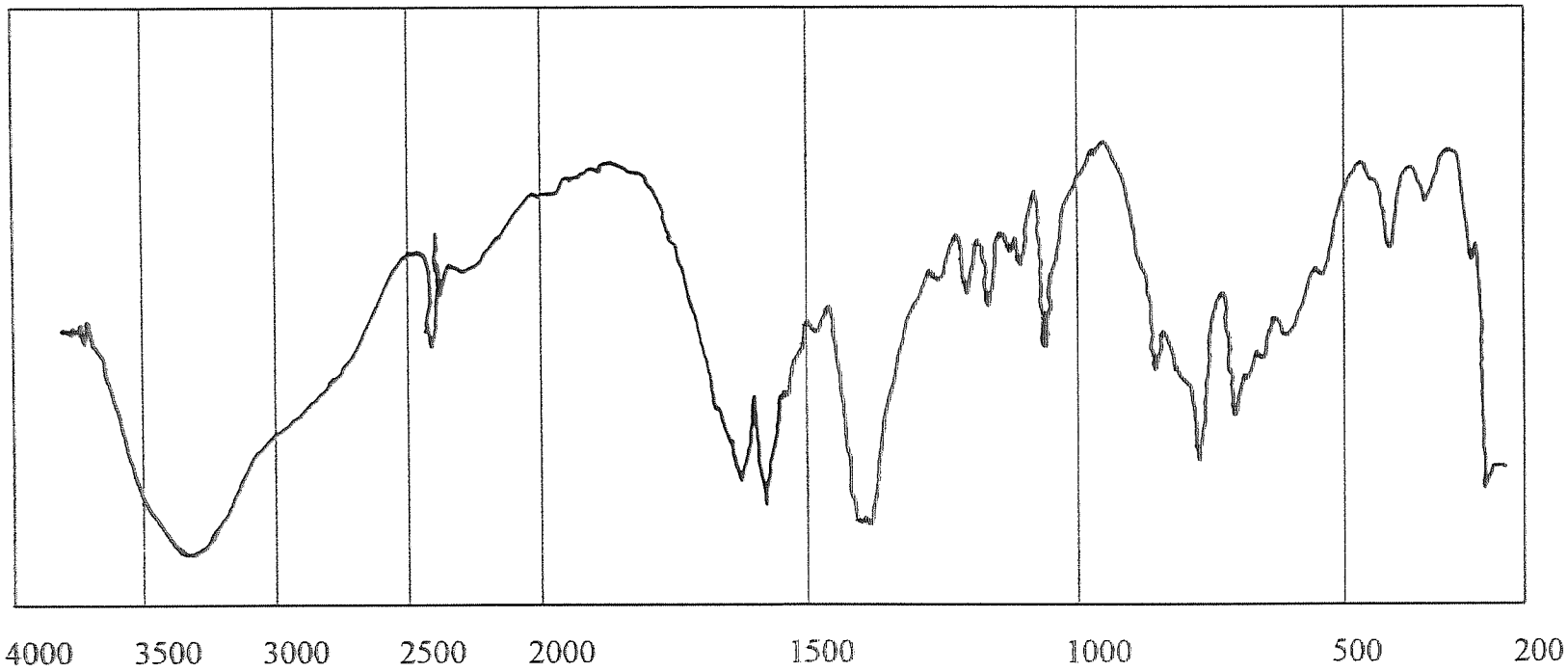

Fig. (4.3): IR Spectra of cobalt(II) isonicotinate

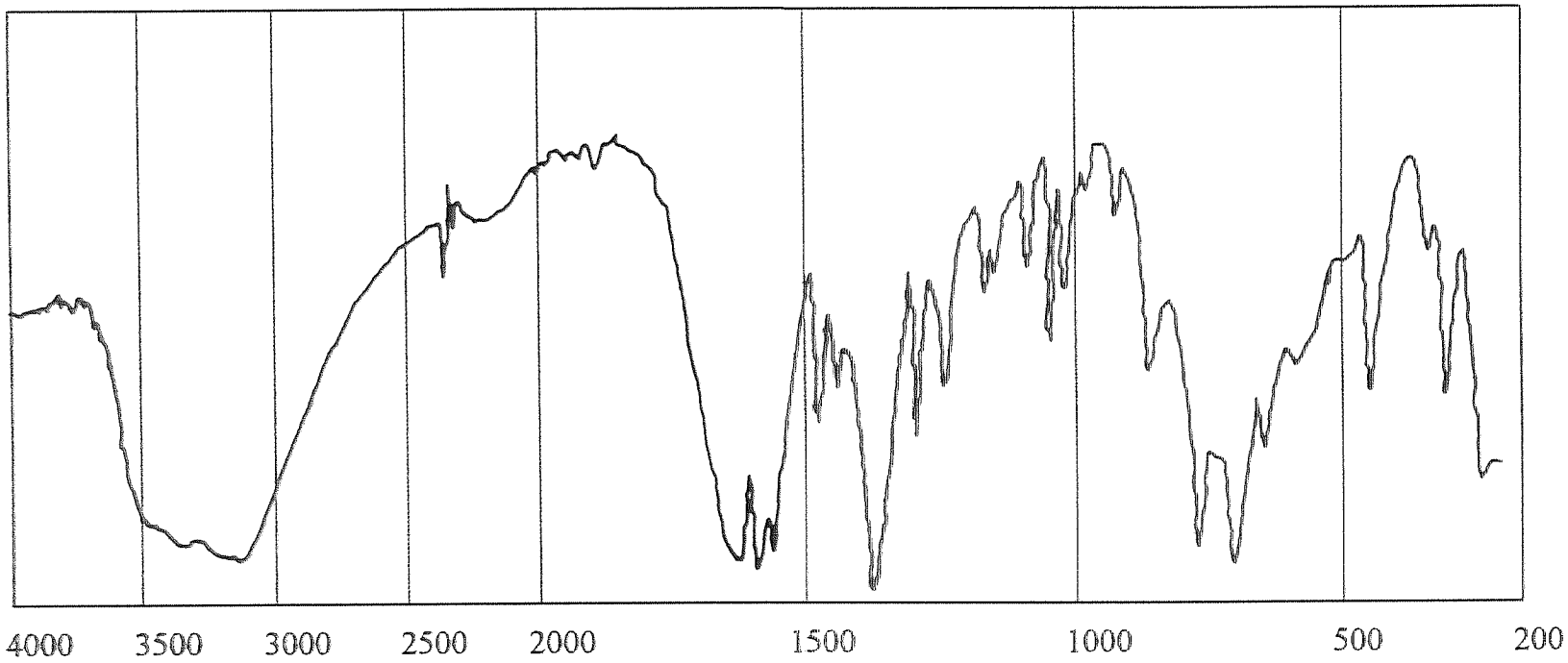

Fig. (4.4): IR Spectra of nickel(II) picolinate.

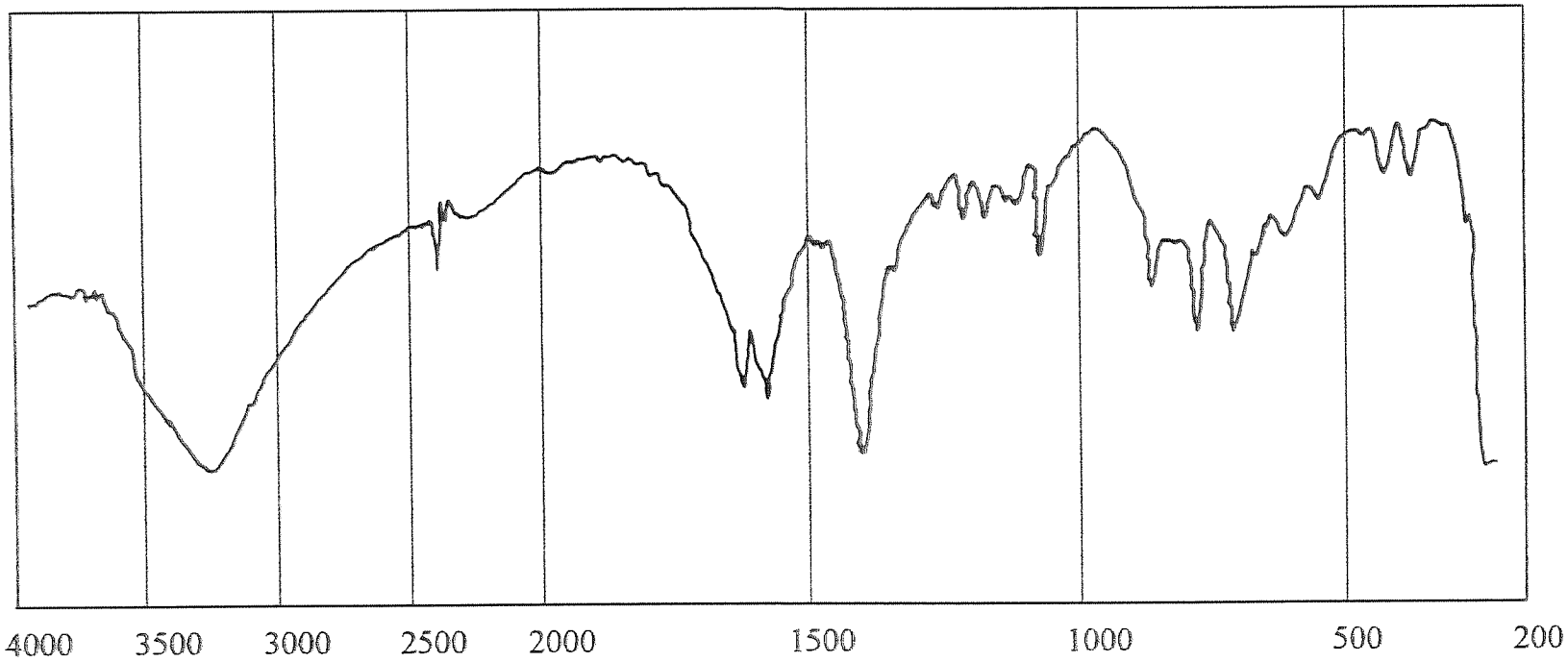

Fig. (4.5): IR Spectra of nickel(II) nicotinate

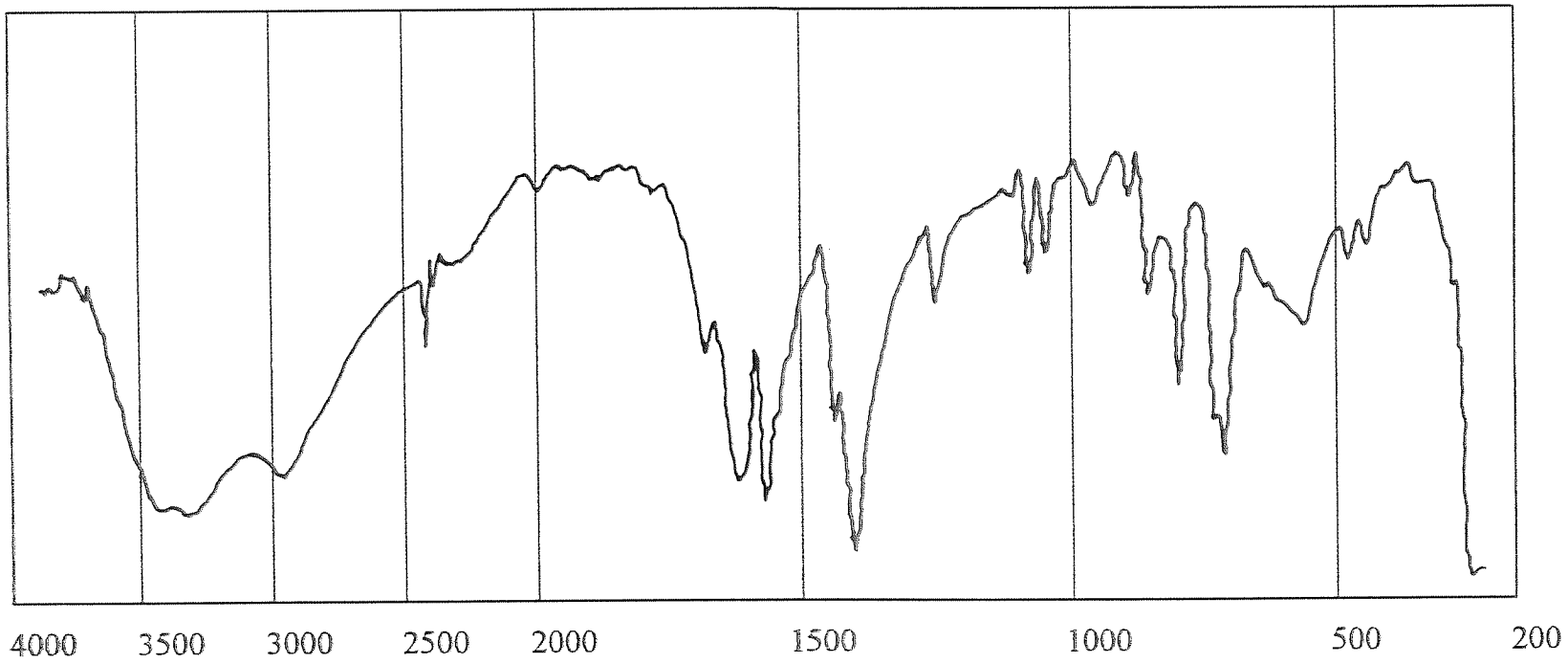

Fig. (4.6): IR Spectra of nickel(II) isonicotinate

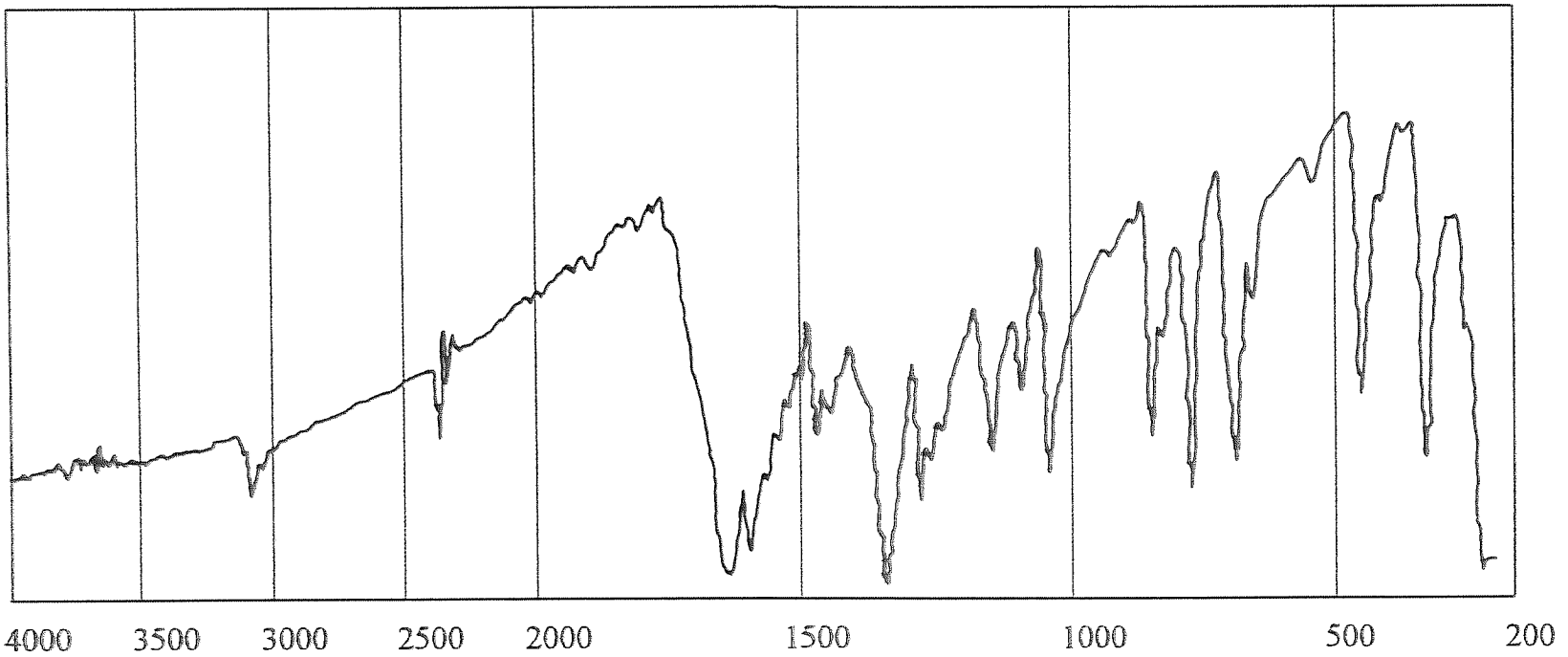

Fig. (4.7): IR Spectra of copper(II) picolinate.

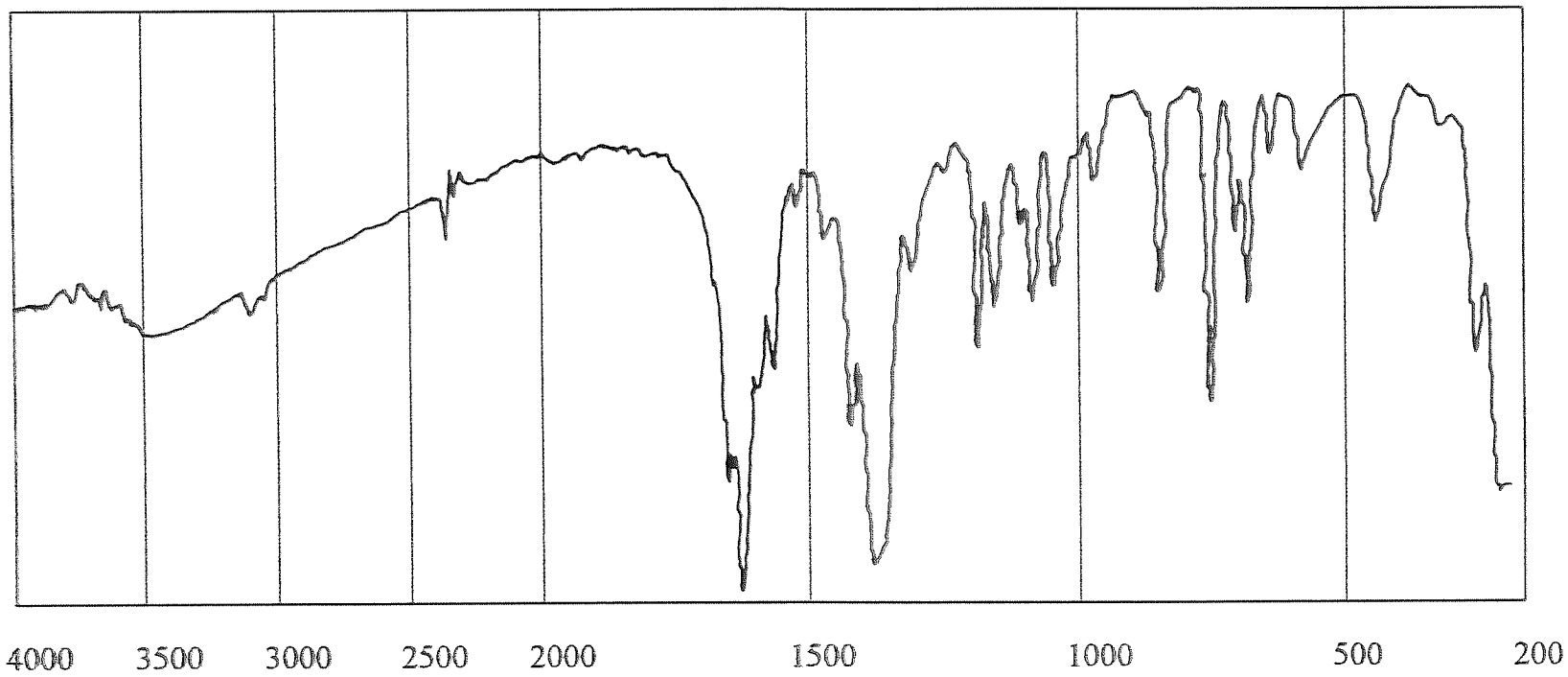

Fig. (4.8): IR Spectra of copper(II) nicotinate

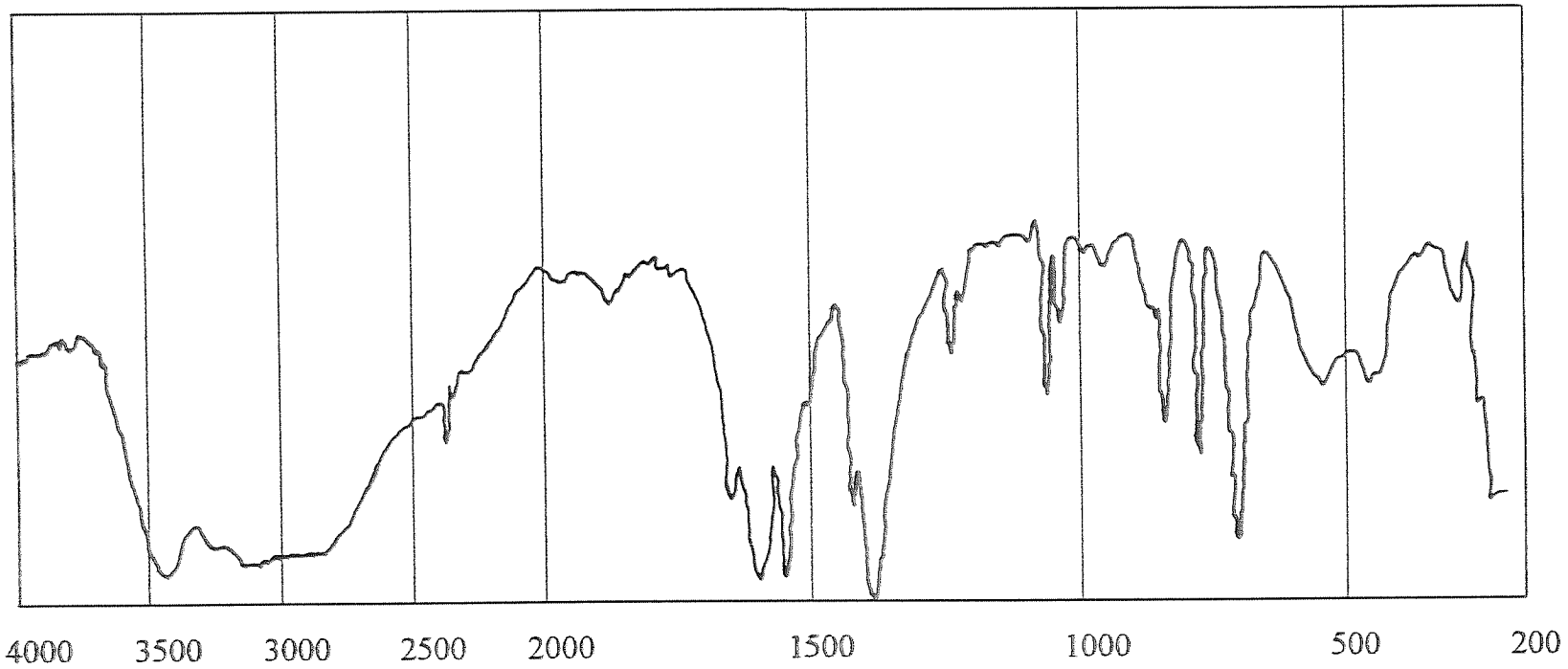

Fig. (4.9): IR Spectra of copper(II) isonicotinate

TABLE (4.2)

Infrared Spectra (4000 - 200 cm^{-1}) for Co, Ni, and Cu picolinate.

Compounds	νO-H (H2O)	ν(COOH)	ν(COO^-)	Ring vibration	ν(C=O)	νM-N	ν(M-OH_2)	ν(M-O)
Picolinic acid, (PA)		1700(s)		1590-(w) 1518(w)	1442			
$Co(PA)_2$2.5H2O	3600-2500(br, m)		1625(w)	1589-(w) 1530(w)	1446(w)	290(s)	330(w)	440(s)
$Ni(PA)_2$4.0H2O	2700-2500(br, m)		1636(w)	1597(w)-1530(w)	1447(w)	305(s)	342(w)	448(s)
$Cu(PA)_2$	-		1644(w)	1604(w)-1530(w)	1448(w)	335(s)	-	457(s)

Key: br, broad; s, strong; m, medium; w, weak

TABLE (4.3):

Infrared Spectra (4000 - 200 cm^{-1}) for Co, Ni, and Cu nicotinat.

Compounds	νO-H (H2O)	ν(COOH)	ν(COO^-)	Ring vibration	ν(C=O)	νM-N	ν(M-OH_2)	ν(M-O)
Nicotinic acid, (NA)		1695		1580-1480	1410			
$Co(NA)_2 4.0H_2O$	3600-2500(br, m)		1660(w)	1599-(w) 1511((w)	1471(w)	233(s)	422(s)	456(s)
$Ni(NA)_2 4.0H_2O$	2700-2500(br, m)		1618(w)	1570(w)-1511(w)	1462(w)	261(s)	412(w)	452(s)
$Cu(NA)_2$	-		1602(w)	1572(w)-1529(w)	1428(w)	266(s)	-	450(s)

Key: br, broad; s, strong; m, medium; w, weak

TABLE (4.4):

Infrared Spectra (4000 - 200 cm^{-1}) for Co, Ni, and Cu isonicotinat.

Compounds	νO-H (H2O)	ν(COOH)	ν(COO^-)	Ring vibration	ν(C=O)	νM-N	ν(M-OH_2)	ν(M-O)
Isonicotinic acid, (IA)		1708		1590-1518	1408(s)			
$Co(IA)_2 4.0H_2O$	3600-2500(br, m)		1650(w)	1595-(w) 1530(w)	1471(w)	261(W)	-	412(W)
$Ni(IA)_2 3.5H_2O$	2700-2500(br, m)		1661(w)	1598(w)-1530(w)	1423(w)	261(W)	-	459(W)
$Cu(IA)_2 4.5H_2O$	3600-2500(br, m)		1652(w)	1603(w)-1510(w)	1423(w)	250 (W)	-	460(W)

Key: br, broad; s, strong; m, medium; w, weak

The IR spectra of free pyridine monocarboxylic acids show bands at about 1700 and 1442 cm^{-1} (Tables 4.2-4.4) which correspond to the carboxylic group.

The band at about 1700 cm^{-1} was assigned to the (C-OOH) vibration, while that at 1442 cm^{-1} was assigned to the (C=O) vibration. The band at about 1700 cm^{-1}, which was assigned to the ν(COOH) vibration, was absent in the IR spectra of the complexes, due to the formation of COO^- group which bonds to metal [74]. The ν(C-O) band in the IR spectra of cobalt, nickel, and copper complexes with picolinic, nicotinic, or isonicotinic acids showed a marked shift to lower frequency, due to the stretching vibration of the carboxylate group linked to the metal[77]. This suggests that the oxygen of the carboxylic group is then coordinated to the metal atom. Also, peak in the far infrared confirms the previous suggestions. The bands observed in the range 430-440 cm^{-1} which have been assigned to the M-O vibration in complexes of cobalt, nickel, or copper complexes with nicotinic acid was not observed. The fact that little change was observed in the wavenumbers of the ν(C=O) vibration of the carboxylate group for picolinate and nicotinate coordinated to cobalt, nickel, or copper (Tables 4.2-4.3) suggests that bonding is not taking place between the oxygen atom of the C=O group and metal atom, whereas the greater change of the ν(C=O) vibration of the carboxylate group for isonicotinate coordinated to cobalt, nickel, or copper (Table 4.4) suggests that bonding is taking place between the oxygen atom of the C=O group and metal ion.

Comparing the IR spectra for the free ligands and that of its complexes, shows that the bands due to the aromatic ring vibrations shift to higher energy on complex formation. This would suggest that the aromatic ring is coordinated to the metal ion through the ring nitrogen atom [74]. Also, the bands which were observed in the range 235-335 cm^{-1} in the far infrared and assigned to M-N confirm the co-ordination between the nitrogen atom and the metal ion.

4.2.3 X-ray Diffraction Patterns

The X-ray diffraction data, diffraction angle (2θ), interplant distance between two planes (d-sp), intensity (I°), and relative intensity (I/I°), were obtained in the present investigation for the series of the complexes prepared (Co, Ni, and Cu with picolinic, nicotinic, and isonicotinic acid). These results are summarised in Table 4.5 and Appendix 2 and are graphically represented in Figs. 4.1-4.4, which show the X-ray lines I/I° against 2θ.

The data were obtained as explained in Chapter 3 from Bragg's law[89]. The calculated (Appendix 2) values of d-spacing are in agreement with those values obtained by Switzer et al., 1948[90]

Comparison of the x-ray patterns with those of free ligands (Fig 3.2) shows that the patterns are not similar. Also, comparisons between Figs 4.10-4.12 show that the x-ray patterns for metals complexes (Co, Ni, and Cu) have different patterns, as with those of the free ligands. Figs. 3.2 and 4.10-4.12.0 , and Tables 4.5 and Appendix 2 shows that the maximum relative intensity ($I/I_{\circ}$) for both the free ligand and prepared compounds had different values of incidence angle (2θ). The data are summarised in Table 4.5.

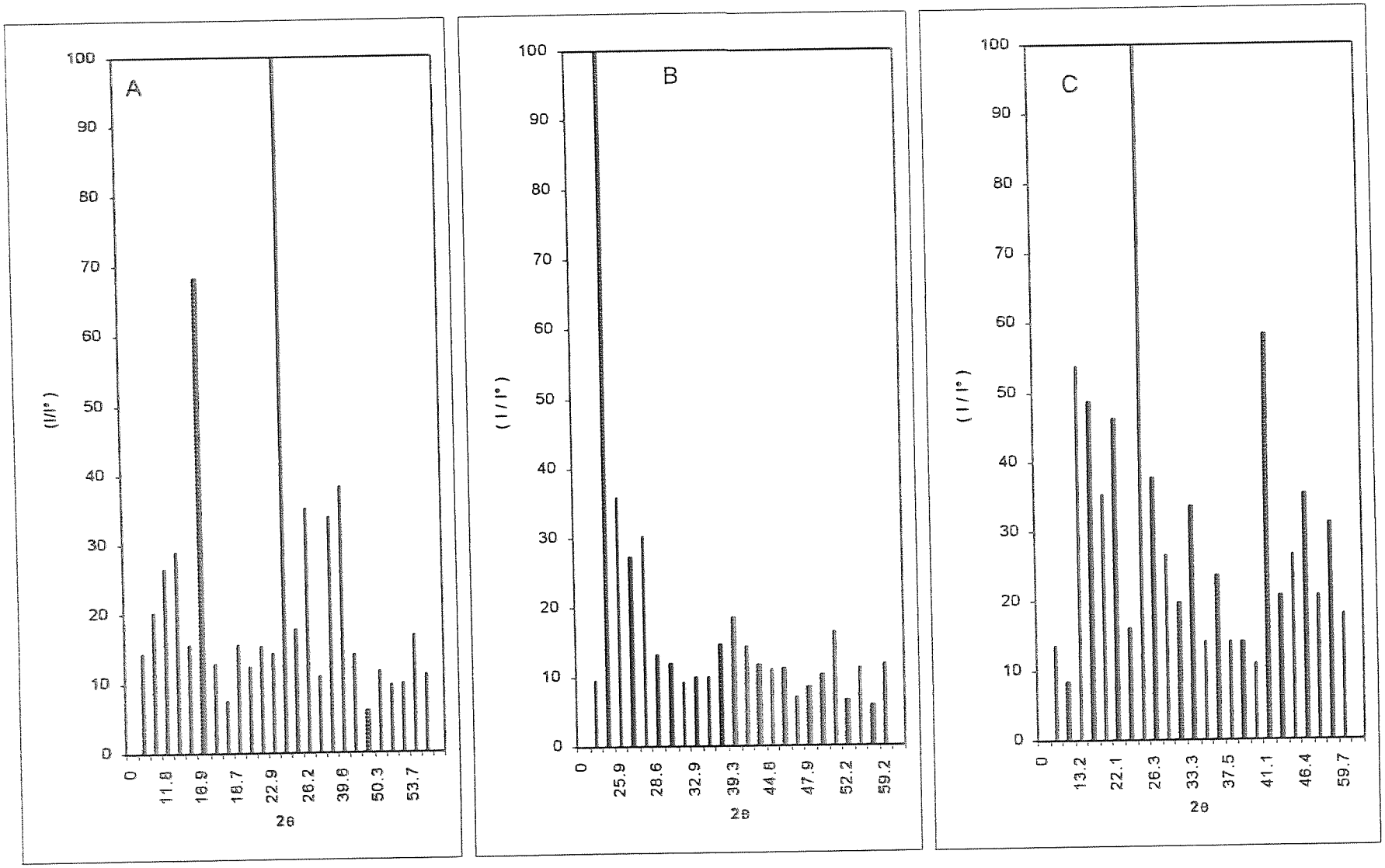

Fig.4.10:X-ray lines (I/I°) against 2θ for cobalt(II) picolinate(A), cobalt(II) nicotinate(B), and cobalt(II) isonicotinate(C) .

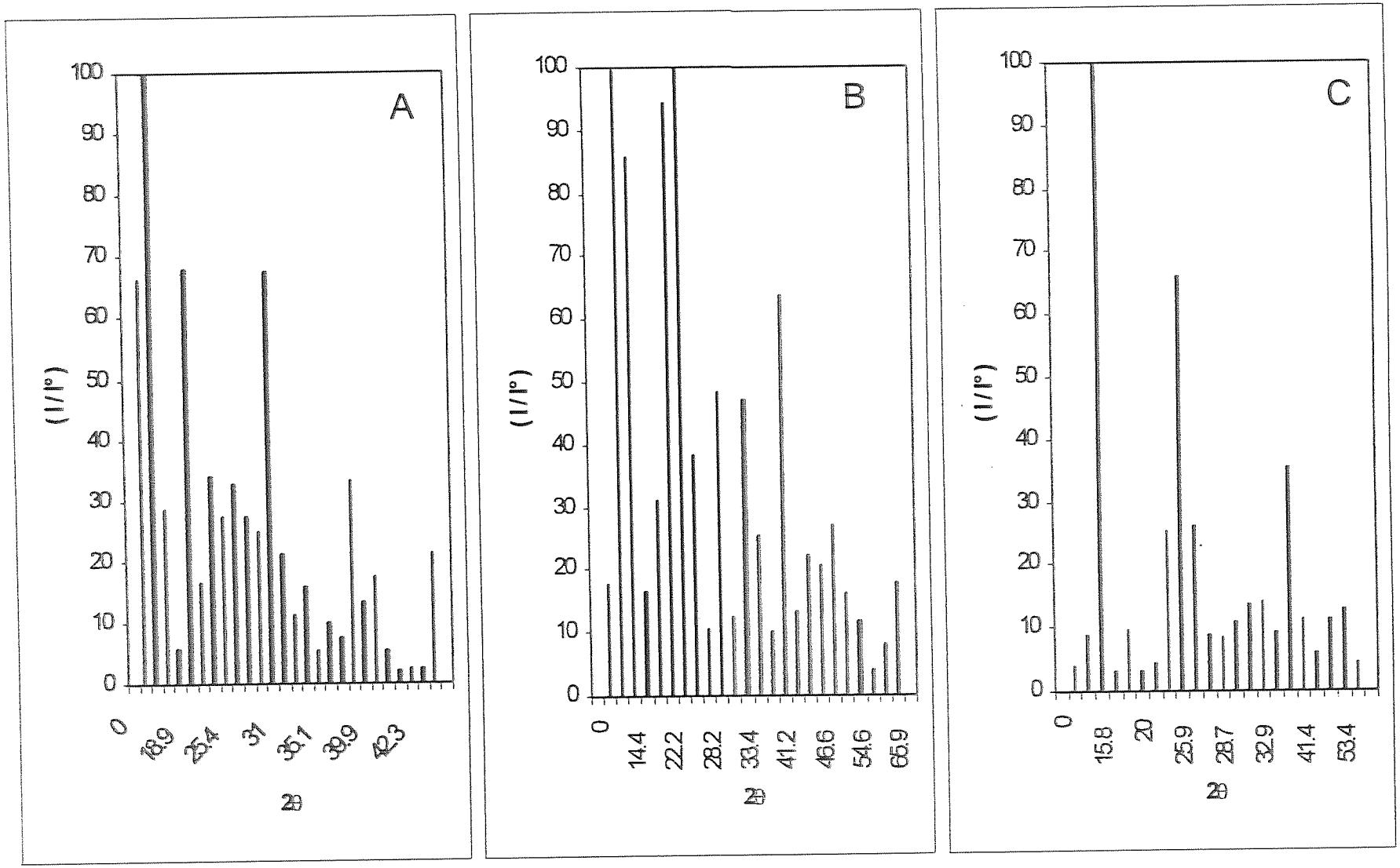

Fig.4.11: X-ray lines (I/I°) against 2θ for nickel(II) picolinate(A), nickel(II) nicotinate(B), and nickel (II) isonicotinate(C)

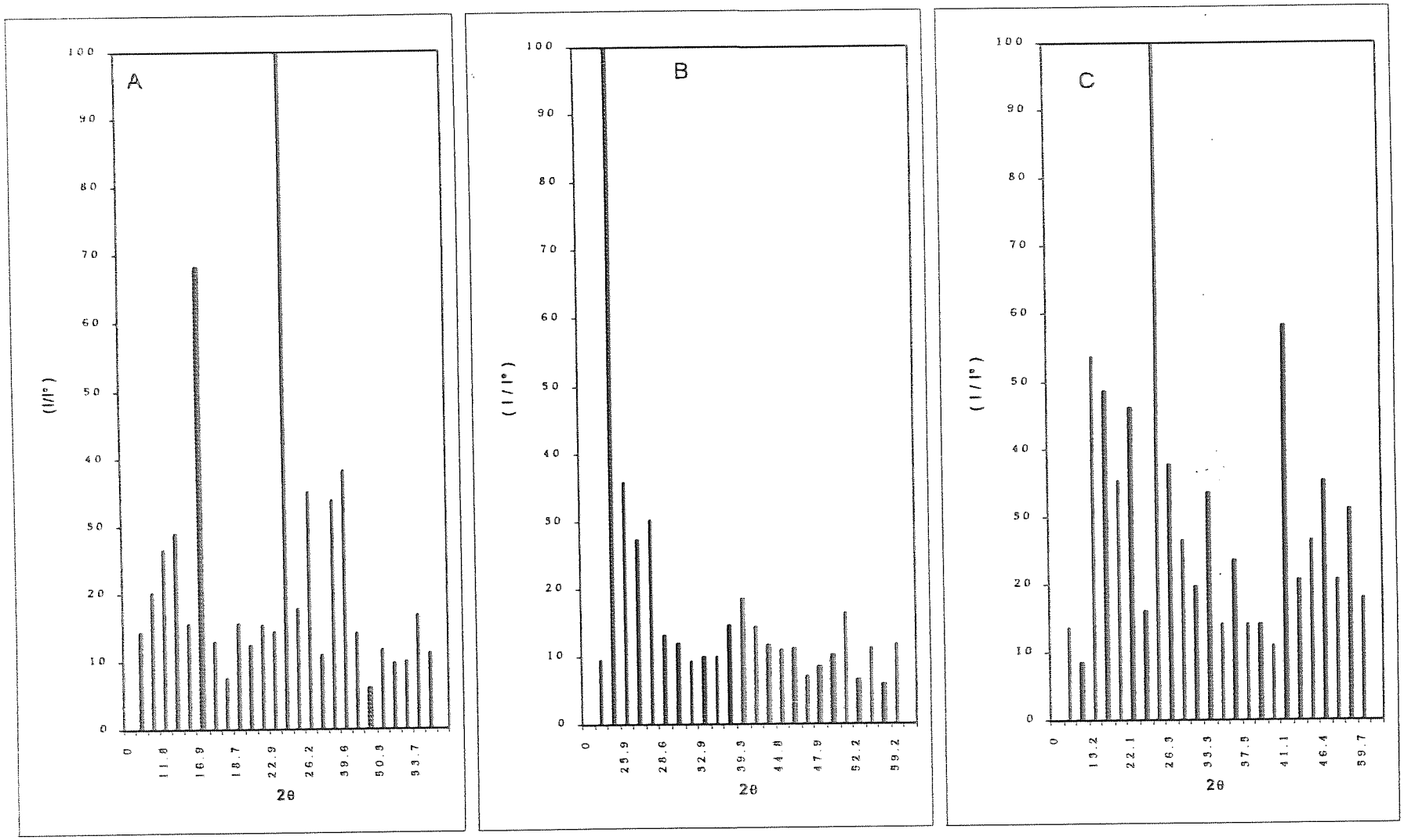

Fig.4.12: X-ray lines (I/I°) against 2θ for copper(II) picolinate(A), copper (II) nicotinate(B), and copper (II) isonicotinate(C).

Table 4.5

2θ values for XRD lines with maximum intensity for free ligands, and prepared complexes for cobalt, nickel, and copper.

Compound	2θ	I
Picolinic acid (PA)	17.3	89
Nicotinic acid (NA)	24.4	85.8
Isonicotinic acid (IA)	16.3	89
$Co(PA)_2 2.5H_2O$	24.3	24.9
$Co(NA)_2 3H_2O$	15.6	30.2
$Co(IA)_2 4H_2O$	25.5	19.9
$Ni(PA)_2 4H_2O$	11.8	90
$Ni(NA)_2 4H_2O$	25.5	53.6
$Ni(IA)_2 3.5H_2O$	15.8	86.4
$Cu(PA)_2 4H_2O$	88.1	11.7
$Cu(NA)_2 4H_2O$	83.4	24.3
$Cu(IA)_2 4H_2O$	90	15.3

4.2.4 Electronic Spectra and Magnetic moments

Magnetic susceptibility measurements were made by the Gouy method using $Hg[Co(SCN)_4]$ as a calibrate. The complexes were studied at room temperature, and the magnetic moment of the metal ion contained in the compound was obtained according to the Curie-Weiss equation.

$$\mu = 2.84(\chi_M^{Corr} \cdot T(K))^{1/2} \quad (5) \qquad 4.1$$

Diamagnetic corrections were applied using the atomic diamagnetic susceptibilities tabulated by Figgis and Lewis [96].

By the Gouy method, the volume of the cylindrical tube(v) was 0.82465 cm^{-3}, the weight of standard was 1.03553 gm, and the force exerted by the field on the quantity of standard (F) was equal to 0.12963 gm. The molar susceptibility of the standard is given by the equation:

$$\chi_m = M\left[\frac{kv + F\beta}{w}\right] \qquad 4.2$$

where M is the molecular weight, β is a constant, and k is the volume susceptibility of air ($k=2.910^{-8}$).

Since the susceptibility of standard is known, β can be determined for the experimental conditions, and is equal to 0.000131304. The same equation can then be applied to determine the values of χ_m for the samples under investigation. The experimental data obtained are listed in Table 4.6.

The visible spectra are dominated by the highest energy transitions for complexes. The d-d bands in the electronic reflectance spectra and magnetic moments of the compounds are listed in Table 4.7.

The position of the bands in the spectra and the magnetic moments of the cobalt complexes indicate that the cobalt ion is six co-ordinate in an octahedral environment[97,98]. In the octahedral field, the ground state $^4T_1$ is orbitally degenerate, and this results in an orbital angular momentum contribution to the magnetic moment. This comes from the fact that the $^4T_1$ and

$^4T_2$ states are split into four states, one of which in each state has the same symmetry as the $^4A_{2g}$ ground state. Thus, these levels mix, and there is a sharing of properties with the result that a certain amount of orbital angular momentum is introduced into the ground state and, hence, there is an orbital contribution to the magnetic moment. The magnetic moment then lies between the spin only value ($\mu = [4S(S+1)]^{1/2} = 3.88$ BM) and the spin-orbital value ($\mu = [4S(S+1)] + L(L+1)]^{1/2} = 5.2$ BM). The value for magnetic moments of compounds $Co(PA)_2$ $2.5(H_2O)$ and $Co(NA)_2 4.0(H_2O)$ are between the experimental values which normally lie in the range of 4.7 – 5.2 BM for the cobalt(II) in an octahedral environment. Meanwhile the value for magnetic moments of compound $Co(IA)_2$ $4.0(H_2O)$ is higher than the experimental value. This suggests an orbital that is greater than that normally observed for cobalt (II) in an octahedral environment[8].

The position of the bands in the spectra and the magnetic moments of the nickel complexes indicate that the nickel ion is in an octahedral environment[6,98-99]. The three spin allowed transition from $^3A_{2g}$ to $^3T_{2g}$, $^3T_{1g}$ and $^3T_{1g}(p)$ generally fall within the ranges 7000 - 13000, 11000 – 20000, and 19000 – 27000 cm^{-1} respectively, in a regular octahedral environment for nickel ion[102]. The magnetic moment then lies between the spin only value ($\mu = [4S(S+1)]^{1/2} = 2.83$ BM) and the spin-orbital value ($\mu = [4S(S+1)] + L(L+1)]^{1/2} = 4.47$ BM) with the actual value of L depending on the strength of the crystal field). The value for magnetic moment of compound $Ni(PA)_2 4.0(H_2O)$ lies between the experimental values which normally lie in the range of 2.8 – 4.0 BM for the nickel (II) in an octahedral environment. Meanwhile, the values for magnetic moments of compounds $Ni(NA)_2 4.0(H_2O)$ and $Ni(IA)_2 3.5(H_2O)$ are higher than the experimental values. This suggests an orbital that is greater than that normally observed for nickel (II) in an octahedral environment[6].

Because of the relatively low symmetry of the environment in which the Cu^{2+} ion is characteristically found, detailed interpretation of the spectra and magnetic properties are somewhat complicated. Virtually all complexes and

compounds are blue or green[1]. In the compound $Cu(PA)_2$, the band at 17253 cm^{-1} would suggest that the copper compound has a tetragonal structure[98]. In the compounds $Cu(NA)_2$ and $Cu(IA)_2$ $4.5H_2O$, the copper complex has a single broad band in its electronic spectrum between 10000 and 15000 cm^{-1}, suggesting that copper atoms are in an octahedral environment[96]. The magnetic moment for copper compounds ≈ 3 BM is equal to the spin orbital value and higher than spin only of 1.78 BM, and shows the absence of a copper-copper magnetic interaction[100].

Table 4.6

The values of experimental data and the susceptibility for the complexes

Compounds	W4	W5	χ_m
$Co(PA)_2$ $2.5(H_2O)$	12.38019	12.45050	0.01113
$Co(NA)_2$ $4(H_2O)$	12.44771	12.5277	0.01066
$Co(IA)_2$ $4H_2O)$	12.41652	12.4964	0.01208
$Ni(PA)_2$ $4(H_2O)$	12.4885	12.53224	0.00632
$Ni(NA)_2$ $4(H_2O)$	12.39874	12.4356	0.00694
$Ni(IA)_2$ $3.5(H_2O)$	12.40495	12.4435	0.00688
$Cu(PA)_2$	12.43838	12.46235	0.00395
$Cu(NA)_2$	12.46100	14.48750	0.00391
$Cu(IA)_2$ $4.5(H_2O)$	12.55755	12.5815	0.00370

W4: is the weight of tube filled to mark with powdered complex, field off.

W5: is the weight of tube filled to mark with powdered complex, field on.

Table 4.7

Electronic spectra.

Compound	Colour	Band position (cm^{-1})	d-d transition
$Co(PA)_2$ $2.5(H_2O)$	Pink	14917	$^4T_{1g}(F) \rightarrow {}^4A_{2g}(F)$
$Co(NA)_2$ $4(H_2O)$	Pink	14917 20425	$^4T_{1g}(F) \rightarrow {}^4A_{2g}(F)$ $^4T_{1g}(F) \rightarrow {}^4T_{1g}(P)$
$Co(IA)_2$ $4H_2O)$	Pink	14620 20425	$^4T_{1g}(F) \rightarrow {}^4A_{g}(F)$ $^4T_{1g}(F) \rightarrow {}^4T_{1g}(P$
$Ni(PA)_2$ $4(H_2O)$	Light Blue	22163	$^3A_{2g}(F) \rightarrow {}^3T_{1g}(p)$
$Ni(NA)_2$ $4(H_2O)$	Turquoise	21259	$^3A_{2g}(F) \rightarrow {}^3T_{1g}(p)$
$Ni(IA)_2$ $3.5(H_2O)$	Turquoise	21259	$^3A_{2g}(F) \rightarrow {}^3T_{1g}(p)$
$Cu(PA)_2$	Violet	17053	$^2B_1 \rightarrow {}^2A_1$
$Cu(NA)_2$	Deep blue	13441	$^2E_g(D) \rightarrow {}^2T_{2g}(D)$
$Cu(IA)_2$ $4.5(H_2O)$	Blue	16005	$^2E_g(D) \rightarrow {}^2T_{2g}(D)$

4.3 THERMAL DECOMPOSITION OF COMPLEXES

Thermogravimetry is very useful for studying the thermal decomposition of solid substances involving both simple compounds and complexes. In the present investigation picolinic acid, nicotinic acid, isonicotinic acid, (see chapter 3) and their cobalt, nickel, and copper complexes were subjected to thermal analysis.

In this study the conditions chosen to obtain thermal analysis data are comparable with those of Allan[74]. Allan[74] studied the thermal analysis of pyridine carboxylic acid complexes with Zn(II). However, no detailed studies of transition metal complexes with isomers of pyridine carboxylic acids were carried out. In the present study preparation of picolinic, nicotinic, and isonicotinic acids with transition metal ions were performed and their thermal behaviours were studied using TG, DTG, and DSC techniques. The results of the thermogravimetry (TG), differential thermogravimetry (DTG), and differential scanning calorimetry (DSC) for the prepared complexes at a heating rate 10°C min^{-1} are given in Figs. 4.13-4.30 and Tables 4.8-4.9. Data for the dehydration and decomposition processes of each complex are given in Tables 4.8-4.9. The temperature ranges and percentage losses of the decomposition are also given in Tables 4.8-4.9, as are the temperatures of the greatest rate of decomposition (DTG_{max}), the theoretical percentage mass losses, and the DSC data.

4.3.1 TG-DTG and DSC behaviour of $[Co(PA)_2 2.5H_2O]$

The TG-DTG and DSC traces for the cobalt picolinate hydrate $[Co(PA)_2 2.5H_2O]$, are shown in Figs. 4.13 and 4.14 respectively. The TG trace shows that dehydration, in which all 2.5 water molecules are removed, proceeds in three steps in the ranges 76.5-103°C (Found 5.08%; Calculated 5.18%), 103-129.5°C (Found 5.22%; Calculated 5.18%) and 129.5-146.5 °C (Found 2.70%; Calculated 2.59%). The DTG trace only shows two separate

dehydration steps in the temperature ranges 76.5-103 °C (Found 5.08%; Calculated 5.18%) and 103-146.5 °C (Found 7.92%; Calculated 7.77%). It is clear that the second peak in the DTG trace is the combination of two consecutive processes seen in the TG trace. Between 140 and 327°C no changes are detailed by TG, DTG, or DSC investigations. The anhydrous complex $Co(PA)_2$ is thermally stable over this temperature range. From 327 to 403°C rapid mass loss is observed, corresponding overall to the total loss of organic ligand; and the residual weights are in good agreement with the values required for CoO formation (Found 61.21%; Calculated 61.21%). See Tables 4.8 and 4.9. The DTG trace shows there are two overlapping peaks in this temperature range.

The DSC trace of $[Co(PA)_2 2.5H_2O]$ shows three peaks; the first two are endothermic and the third one is exothermic. The first endothermic peak is observed at 132.3 °C and its enthalpy change (ΔH) of 121 kJ mol^{-1}, is due to remove one of molecule of water. The second endothermic peak at 167.9°C, with an enthalpy change (ΔH) of 67 kJ mol^{-1} corresponds to the removal of 1.5 H_2O. The exothermic peak with a shoulder is observed at 447.5° C with an enthalpy change of -1809 kJ mol^{-1}, due to oxidation and loss of the organic ligands. The shoulder on the exothermic peak probably indicates that the decomposition of the anhydrous complex proceeds in at least two stages[22]. In the first stage loss of one ligand occurs (Found 36.35%; Calculated 35.06%) in the temperature range 327-379°C. In the second stage another molecule of ligand is lost and decarboxylated to form pyridine and carbon dioxide. The decomposition steps may be summarised as follows:

$$Co(PA)_2 2.5H_2O \longrightarrow Co(PA)_2 1.5H_2O$$

$$Co(PA)_2 1.5H_2O \longrightarrow Co(PA)_2$$

$$Co(PA)_2 \longrightarrow Co(PA) + PA$$

$$Co(PA) \longrightarrow CoO$$

4.3.2 TG-DTG and DSC behaviour of $[Co(NA)_2 4H_2O]$

The TG-DTG and DSC curves for the cobalt nicotinate hydrate $[Co(NA)_2 4.H_2O]$ are shown in Figs. 4.15 and 4.16 respectively. The TG trace shows that dehydration in which all four water molecules are removed proceeds in three steps in the ranges 111-121°C (Found 4.59%; Calculated 4.80%), 128-135°C (Found 3.72%; Calculated 4.80%) and 135-141°C (Found 10.40%; Calculated 9.61%). The TG trace shows a small protrusion in the temperature range 141- 353°C. This suggests that an anhydrous is not thermally stable over this temperature range. The anhydrous complex Co(NA)2 is decomposition starts at 353.5° C and completes at 389.5 with loss of organic ligand (Found 59.77%; Calculated 61.21%), and residual weights are in a good agreement with the values required for CoO (Table 4.8 and 4.9). The DTG trace shows two peaks; the first one is due to the dehydration process, and the second one corresponds to the main decomposition of the complex.

The DSC trace of $[Co(NA)_2 4.H_2O]$ shows four peaks (Fig.4.16). The first one is endothermic and the last three are exothermic. First, an endothermic peak is observed at 150.5° C with an enthalpy change (ΔH) of 230 kJ mol^{-1} and is due to the dehydration process. The exothermic peaks are observed at 241.1, 401.1, and 452.8°C with enthalpy changes of -13, -380, and −1030 kJ mol^{-1} respectively. The first exothermic peak is due to instability of the complex, while the last two peaks overlapped. The consecutively exothermic peaks allow us to suggest that there is more than one intermediate compound present through the decomposition process in forming CoO. The decomposition scheme is:

$$Co(NA)_2\,4H_2O \longrightarrow Co(NA)_2 3H_2O$$
$$Co(NA)_2 3H_2O \longrightarrow Co(NA)_2\,2H_2O$$
$$Co(NA)_2\,2H_2O \longrightarrow Co(NA)_2$$
$$Co(NA)_2 \longrightarrow CoO$$

4.3.3 TG-DTG and DSC behaviour of $[Co(IA)_2 4H_2O]$

The TG-DTG and DSC curves of cobalt isonicotinate hydrate $[Co(IA)_2\ 4H_2O]$ are shown in Figs. 4.17 and 4.18 respectively. The TG and DTG traces show that the four water molecules are removed at one point in the temperature range 81-167.5°C. The observed weight loss for this process compares favourably with the theoretical value (Found 19.64%; Calculated 19.22%; peak temperature at 133.5°C) as shown in Tables 4.8 and 4.9. TG and DTG traces show that the anhydrous complex is thermally stable over the temperature range 167.5-382°C. The complex, and, then, decomposition starts at 382°C and is completed at 402°C with loss of the organic ligand (Found 59.34%; Calculated 60.65%). The residual weights are in good agreement with the values required of CoO (Found 21.02%; Calculated 19.98%) as given in Tables 4.8 and 4.9.

The DSC trace of $[Co(IA)_2 4H_2O]$shows three peaks; the first one is endothermic and the last two are exothermic. First, an endothermic peak is observed in the DSC trace at 169.1°C, and its enthalpy change (ΔH) is 305 kJ mol^{-1} due to the dehydration process. The exothermic peaks are observed at 410.1 and 487.9°C with an enthalpy change of -237 and -11865 kJ mol^{-1} respectively. The consecutive exothermic peaks allow us to suggest that more than one intermediate compound is present through the decomposition process to form CoO. The decomposition scheme is:

$$Co(IA)_2\ 4H_2O \longrightarrow Co(IA)_2$$

$$Co(IA)_2 \longrightarrow CoO$$

4.3.4 TG-DTG and DSC behaviour of $[Ni(PA)_2 4H_2O]$

The TG-DTG and DSC traces of nickel picolinate hydrate $[Ni(PA)_2\ 4H_2O]$ are shown in Figs. 4.19 and 4.20. By comparing Figs.4.13 and 4.19 it is clear that the decomposition behaviour trends of $[Co(PA)_2 2.5H_2O]$ and $[Ni(PA)_2\ 4H_2O]$ are identical. TG and DTG traces show that the four water

molecules are also removed at two steps in the temperature range 52.5-109.5°C (Found 9.56%; Calculated 9.61%) and 109.5-191.5°C (Found 9.37%; Calculated 9.61%). The TG trace shows also that the anhydrous complex is thermally stable over the temperature range 191.5-309 °C. From 309.5 °C to 425.5°C, rapid mass loss was observed (Found 60.76 %; Calculated 60.82%), corresponding to the loss of organic ligand where residual weights are in good agreement with the values required for NiO (Tables 4.8 and 4.9).

The DSC trace shows three peaks; the first two peaks are endothermic, and the last one is exothermic. The same observation is noted in the DSC curve of $[Co(PA)_2 2.5H_2O]$. First, an endothermic peak is observed in the DSC trace at 112.8°C, and its enthalpy change (ΔH) is 81 kJ mol^{-1} due to the dehydration process of two water molecules; while the second is an endothermic peak at 203.7°C with an enthalpy change, ΔH, 100 kJ mol^{-1}, corresponding to the loss of the remaining two water molecules. The exothermic peak is observed at 480.6°C with an enthalpy change of (ΔH) -787 kJ mol^{-1} due to the loss of organic ligand and the formation of nickel oxide. The decomposition scheme is:

$$Ni(PA)_2\,4H_2O \longrightarrow Ni(PA)_2 2H_2O$$
$$Ni(PA)_2\,2H_2O \longrightarrow Ni(PA)_2$$
$$Ni(PA)_2 \longrightarrow NiO$$

4.3.5 TG-DTG and DSC behaviour of $[Ni(NA)_2 4H_2O]$

The TG-DTG and DSC traces on nickel nicotinate hydrate $[Ni(NA)_2 4H_2O]$ are shown in Figs. 4.21 and 4.22. The TG and DTG traces show that the four water molecules are removed at one step (Found 19.77%; Calculated 19.12%) in the temperature range 96.0-161.5 °C. The TG curve shows that the anhydrous complex is stable over the temperature range 161.5-341°C. The decomposition of anhydrous complex starts at 341°C and completes at 390°C with a loss of organic ligand (Found 59.46 %; Calculated

60.84) where residual weights are in good agreement with the value required for NiO (Found 20.77 %; Calculated 19.97 %). See Tables 4.8 and 4.9. The DTG trace shows only two main peaks corresponding to dehydration and decomposition respectively.

The DSC traces show three peaks; the first one is endothermic, and the last two peaks are exothermic. The endothermic peak with a shoulder is observed in the DSC trace at 192.6°C, and its enthalpy change (ΔH) is 280 kJ mol^{-1} due to dehydration of water molecules. The exothermic peaks are observed at 416.4 and 500.6°C with an enthalpy change (ΔH) is -306 and -1023 kJ mol^{-1} due to loss of ligand and formation of nickel oxide. The decomposition scheme is:

$$Ni(NA)_2\,4H_2O \longrightarrow Ni(NA)_2 2H_2O$$
$$Ni(NA)_2\,2H_2O \longrightarrow Ni(NA)_2$$
$$Ni(NA)_2 \longrightarrow NiO$$

4.3.6 TG-DTG and DSC behaviour of $[Ni(IA)_2 3.5H_2O]$

The TG-DTG and DSC traces of nickel isonicotinate hydrate $[Ni(IA)_2\ 3.5H_2O]$ are shown in Figs. 4.23 and 4.24. The TG curve shows that the water molecules are removed at two points. The first step (Found 5.19 %; Calculated 4.93 %) is in the temperature range 106.5-139.5°C, and the second step (Found 12.06%; Calculated 12.31 %) is in the temperature range 139.5-167.0°C. The TG-DTG trace shows that the anhydrous complex is stable over the temperature range 167-276°C. The decomposition starts at 246.5°C and is completed at 356°C with a loss of organic ligand where the residual weights (Found 61.07 %; Calculated 62.32 %) are in good agreement with values required for NiO (Found 21.07 %; Calculated 20.41 %). See Tables 4.8 and 4.9.

The DSC curve showed three peaks; the first one is endothermic and the remaining peaks are exothermic. The endothermic peak is observed in the DSC

trace at 190.3°C, and its enthalpy change (ΔH) is 216 kJ mol^{-1} due to the dehydration of water molecules. The exothermic peaks are observed at 372.3 and 485.3°C with an enthalpy change (ΔH) of -78 and -1146 kJ mol^{-1} corresponding to the loss of ligand and formation of NiO. The decomposition scheme is:

$$Ni(IA)_2\,3.5H_2O \longrightarrow Ni(IA)_2 2.5H_2O$$
$$Ni(IA)_2\,2.5H_2O \longrightarrow Ni(IA)_2$$
$$Ni(IA)_2 \longrightarrow NiO$$

4.3.7 TG-DTG and DSC behaviour of $[Cu(PA)_2]$

The TG-DTG and DSC traces of copper picolinate anhydrate $[Cu(PA)_2]$ are shown in Figs. 4.25 and 4.26. The TG-DTG trace shows that the anhydrous complex is stable over the temperature range 50-264.5°C. At 264.5°C a fast weight loss is observed and completed at 323.5°C with a loss of organic ligand (Found 74.90%; Calculated 74.12%) where the residual weight is in good agreement with values required for CuO (Found 25.10 %; Calculated 25.86%).See Tables 4.8 and 4.9.

The DSC curve shows two peaks: The first one is endothermic at 335°C with an enthalpy change (ΔH) of 82 kJ mol^{-1}, and the second peak is exothermic at 446.3°C with enthalpy change (ΔH) of -1524 kJ mol^{-1} corresponding to the loss of ligand and the formation of CuO. The decomposition scheme is:

$$Cu(PA)_2 \longrightarrow CuO$$

4.3.8 TG-DTG and DSC behaviour of $[Cu(NA)_2]$

The TG-DTG and DSC traces of copper nicotinate anhydrate $[Cu(NA)_2]$ are shown in Fig. 4.17 and 4.28. TG-DTG curve shows that the anhydrous complex is stable over the temperature range 50-243.5°C. At 243.5°C a fast weight loss is observed and completed at 266°C with a loss of organic ligand

(Found 75.11%; Calculated 74.12%) where the residual weight is in good agreement with values required for CuO (Found 24.89%; Calculated 25.86 %). See Tables 4.8 and 4.9.

The DSC trace shows two peaks. The first one is endothermic at 291.3°C with enthalpy change (ΔH) is 61 kJ mol^{-1}. The second peak in DSC trace is exothermic at 458°C and with an enthalpy change (ΔH) of -965 kJ mol^{-1}. The endothermic and exothermic peaks correspond to the loss of ligand and formation of CuO. The decomposition scheme is:

$$Cu(NA)_2 \longrightarrow CuO$$

4.3.9 TG-DTG and DSC behaviour of $[Cu(IA)_2 4.5H_2O]$

The TG-DTG and DSC traces of copper isonicotinate anhydrate $[Cu(IA)_2 4.5H_2O]$ are shown in Fig. 4.29 and 4.30. The TG and DTG traces show that the water molecules are removed at one point (Found 20.46%; Calculated 20.86%) in the temperature range 53-169.5 °C. The TG-DTG traces shows that the anhydrous complex is stable over the temperature range 169.5-198°C. It is decomposed in the temperature range 189-377.5°C with a loss of organic ligand (Found 64.49; Calculated 62.79%) where the residual weight is in good agreement with values required for Cu (Found 15.32%; Calculated 16.35%). See Tables 4.8 and 4.9.

The DSC curve shows three endothermic peaks. The first one is at 134.1°C with an enthalpy change (ΔH) of 252 kJ mol^{-1} due to the dehydration process. The second peak in the DSC trace is at 295°C with an enthalpy change (ΔH) of 79 kJ mol^{-1}. The third peak is at 356.6°C with an enthalpy change (ΔH) of 221 kJ mol^{-1}. The last two endothermic peaks correspond to the loss of ligand and formation of Cu. The decomposition scheme is:

$$Cu(IA)_2 4.5H_2O \longrightarrow Cu(IA)_2$$

$$Cu(IA)_2 \longrightarrow Cu$$

4.3.10 Thermal summary:

The dehydration processes are endothermic processes. Water loss occurs in two temperature ranges, 50-100 and 100-160°C. Brzyska and Krol [101] have reported that the water molecules within such crystalline solids may be bonded in three different ways. They may interact with anion (loss at 40-55°C) in the space lattice; they may be attached by hydrogen bonding to an anion or to an inner-sphere water molecule (loss at 76-103 °C, Dehydration I); or they may occur as directly coordinated water, which is strongly bonded to the metal ion (loss at 103-146.5 °C, Dehydration II). Comparing the DTG temperature of the first and second steps of the dehydration, it is possible to suggest that the water of crystallisation molecules are more strongly bonded with the anion in the Ni(II) complexes than in the complexes of Co(II) and Cu(II). All the complexes form an anhydrous compound on heating. The further decomposition of all the anhydrous complexes is strongly exothermic, except for $(Cu(IA)_2]$ which is endothermic. The greater magnitudes of the enthalpy changes for these exothermic peaks indicate that the ignition of the decomposition products occurs in addition to the formation of the metal oxide. The intermediate products of decomposition were not identified. During heating, the complexes of Co(II), Ni(II) and Cu(II) decompose directly to the oxides (CoO, NiO and CuO) without forming free metal as an intermediate. This is confirmed by the absence of weight gain in the TG curves at higher temperatures for Co, Ni and Cu complexes. Comparing the start temperatures of decomposition (Table 4.8) The stability of complexes decreases with increasing atomic number Z of the metal in the order Co>Ni>Cu[5,101]. Also, the temperature of the oxide formation increases in the order CuO< NiO< CoO with decreasing atomic number of the metal[101].

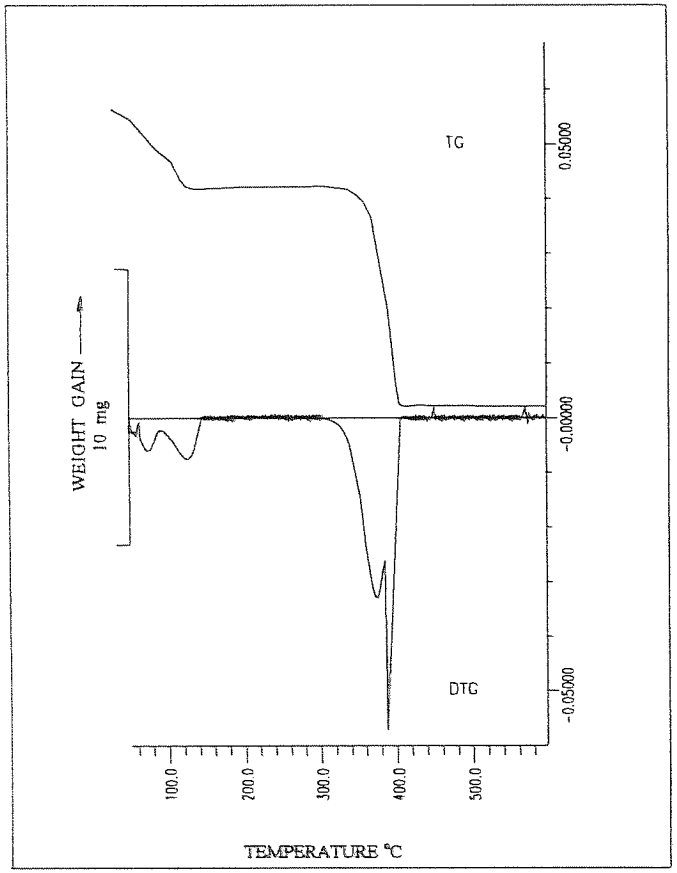

Fig. (4.13): TG and DTG curve of cobalt picolinate. Heating rate 10°C min^{-1}.

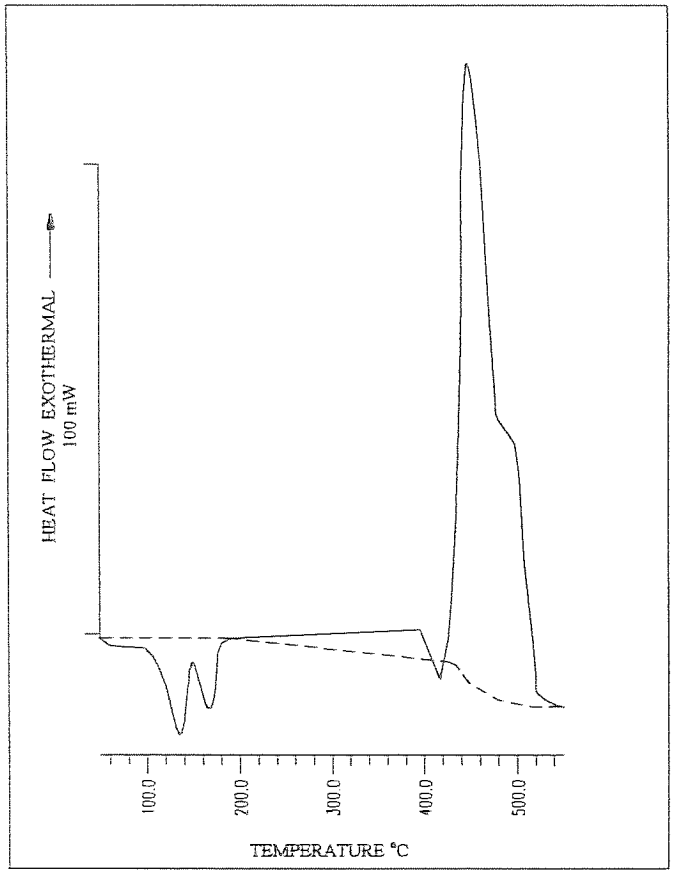

Fig. (4.14): DSC curve of cobalt picolinate. Heating rate 10°C min^{-1}.

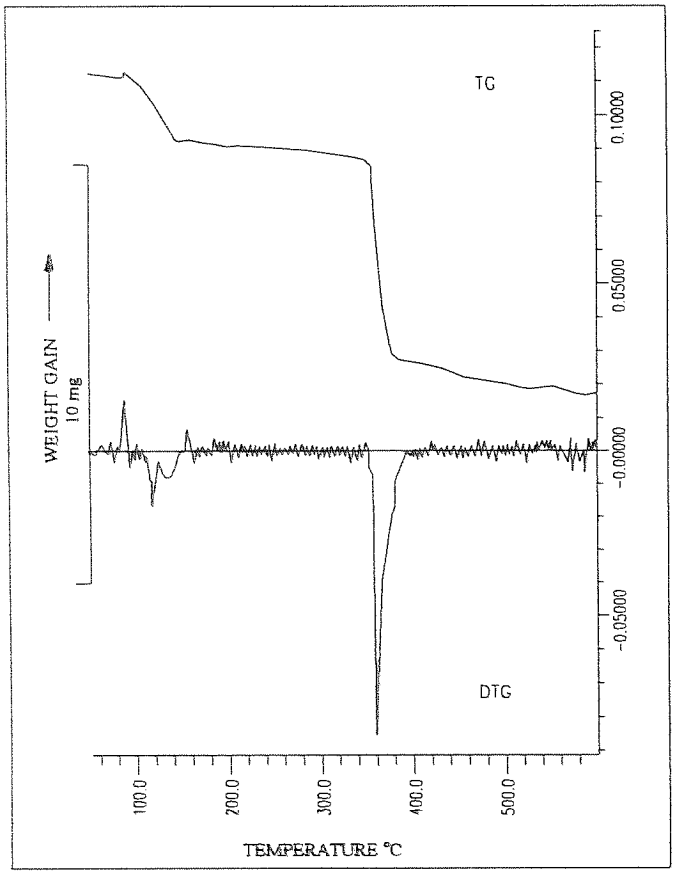

Fig. (4.15): TG and DTG curve of cobalt nicotinate. Heating rate 10°C min^{-1}.

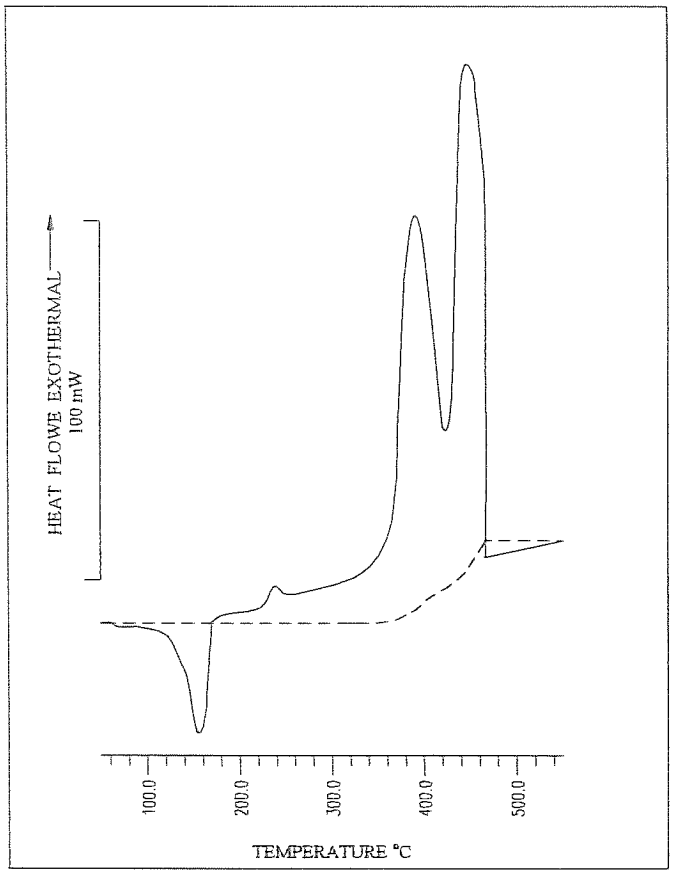

Fig. (4.16): DSC curve of cobalt nicotinate. Heating rate 10°C min^{-1}.

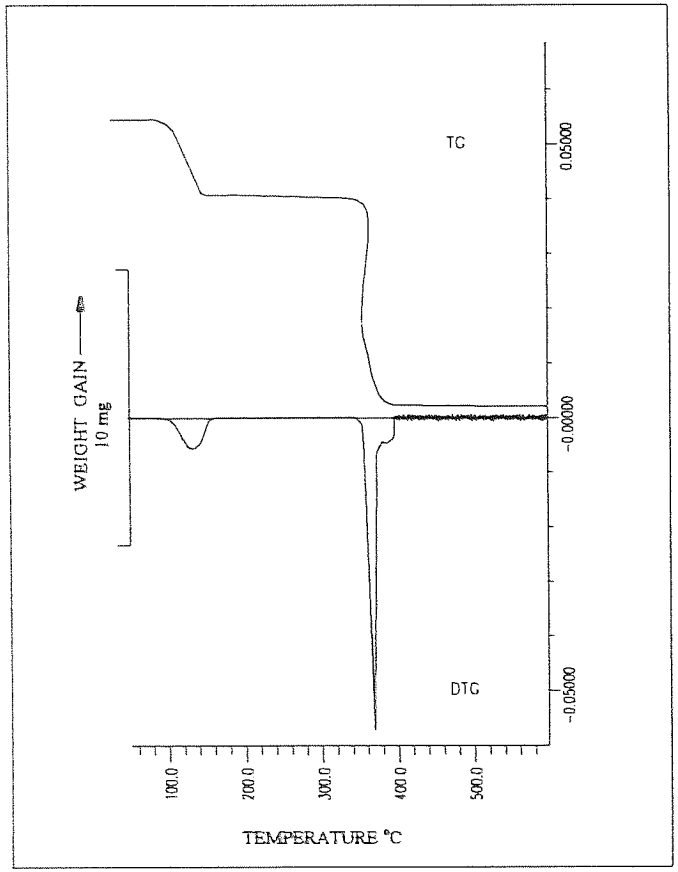

Fig. (4.17): TG and DTG curve of cobalt isonicotinate. Heating rate 10°C min^{-1}.

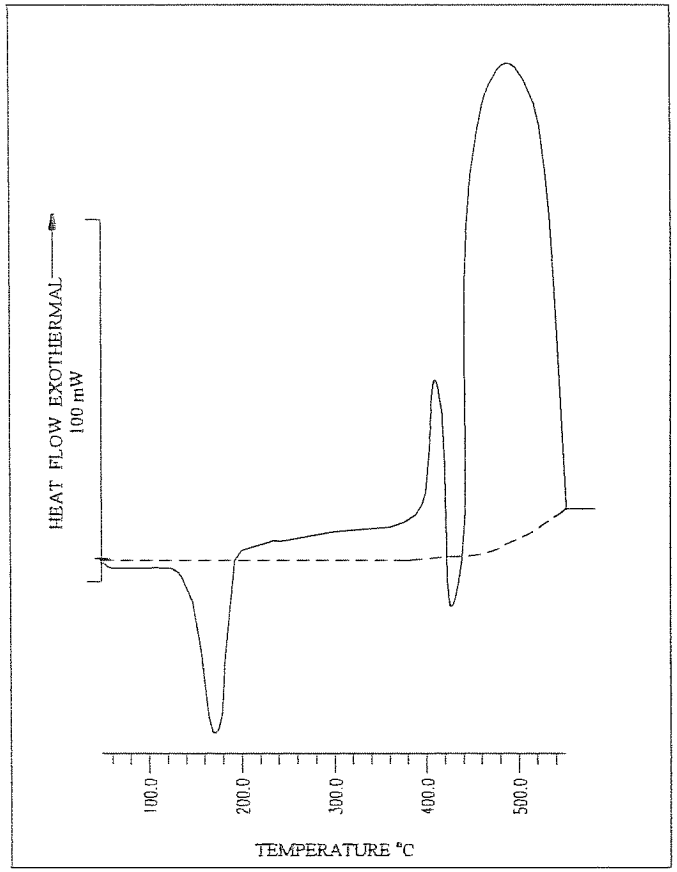

Fig. (4.18): DSC curve of cobalt isonicotinate. Heating rate 10°C min^{-1}.

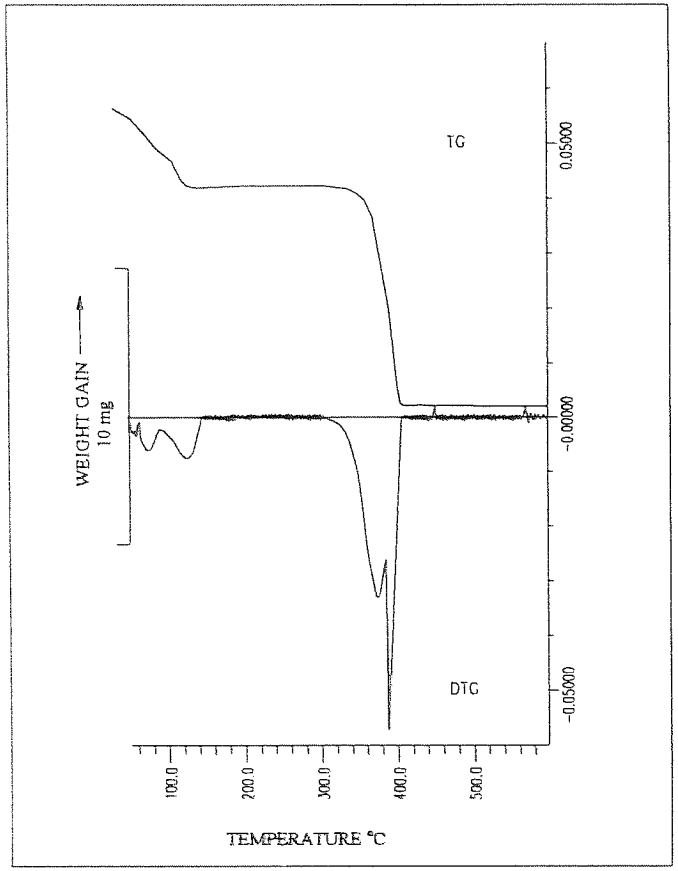

Fig. (4.19): TG and DTG curve of nickel picolinate. Heating rate 10°C min^{-1}.

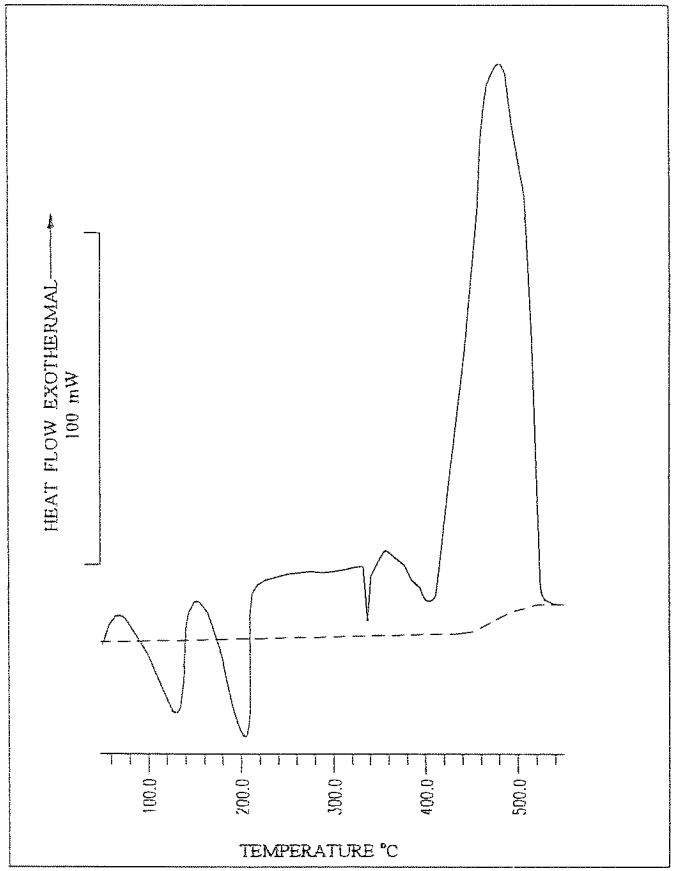

Fig. (4.20): DSC curve of nickel picolinate. Heating rate 10°C min^{-1}.

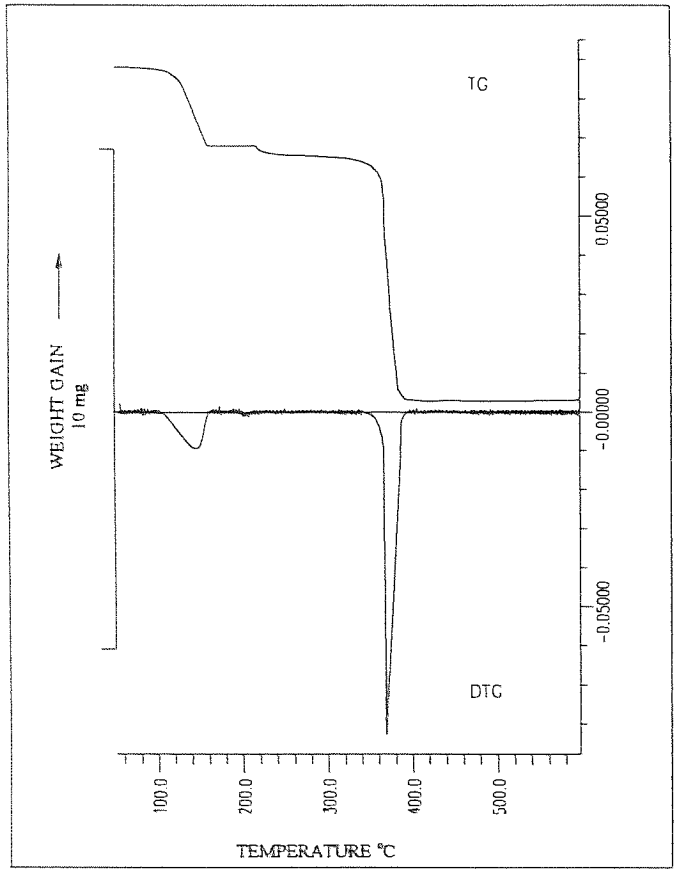

Fig. (4.21): TG and DTG curve of nickel nicotinate. Heating rate 10°C min^{-1}.

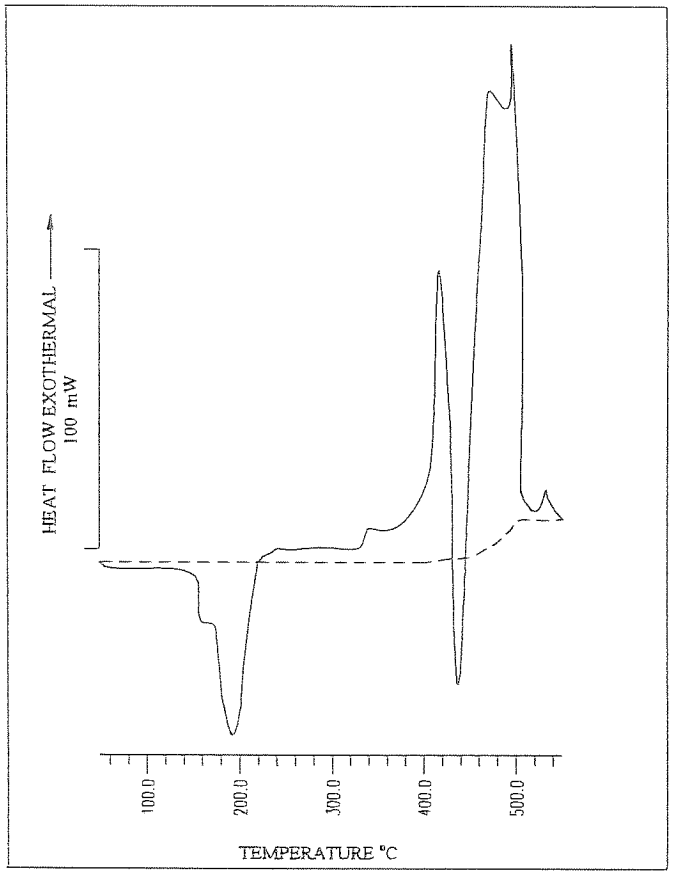

Fig. (4.22): DSC curve of nickel nicotinate. Heating rate 10°C min^{-1}.

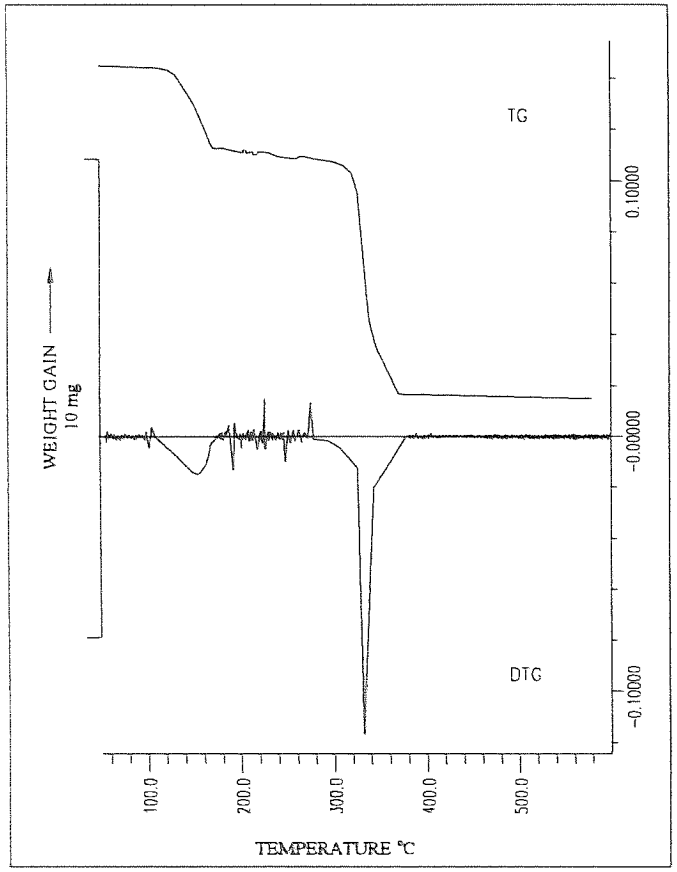

Fig. (4.23): TG and DTG curve of nickel isonicotinate. Heating rate 10°C min^{-1}.

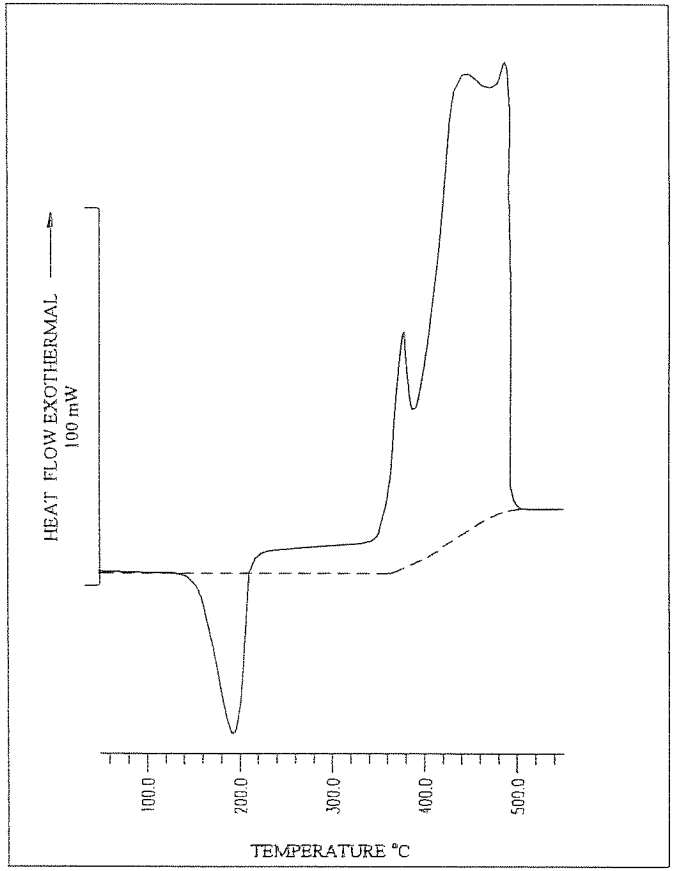

Fig. (4.24): DSC curve of nickel isonicotinate. Heating rate 10°C min^{-1}.

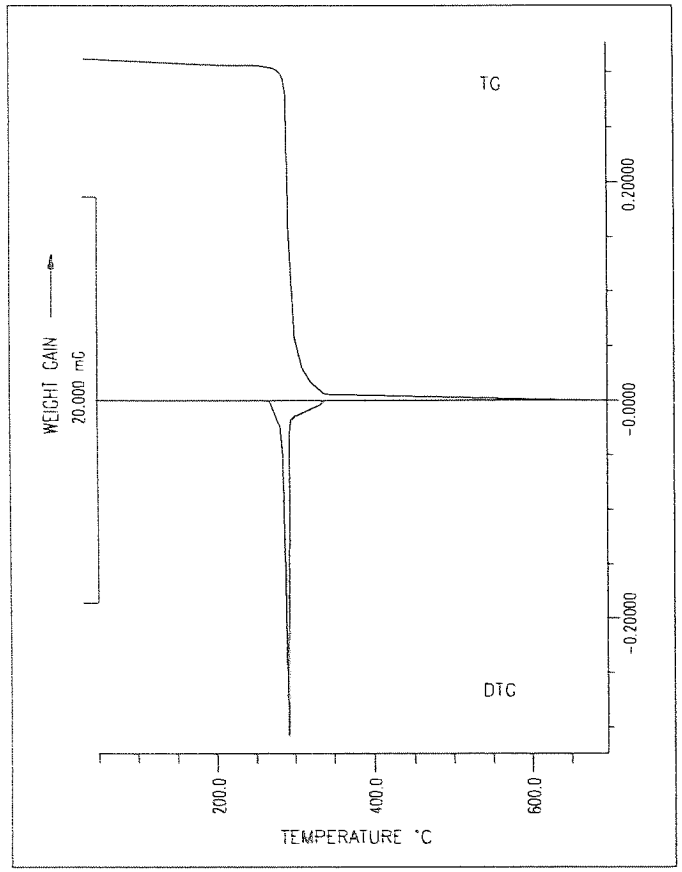

Fig. (4.25): TG and DTG curve of copper picolinate. Heating rate 10°C min^{-1}.

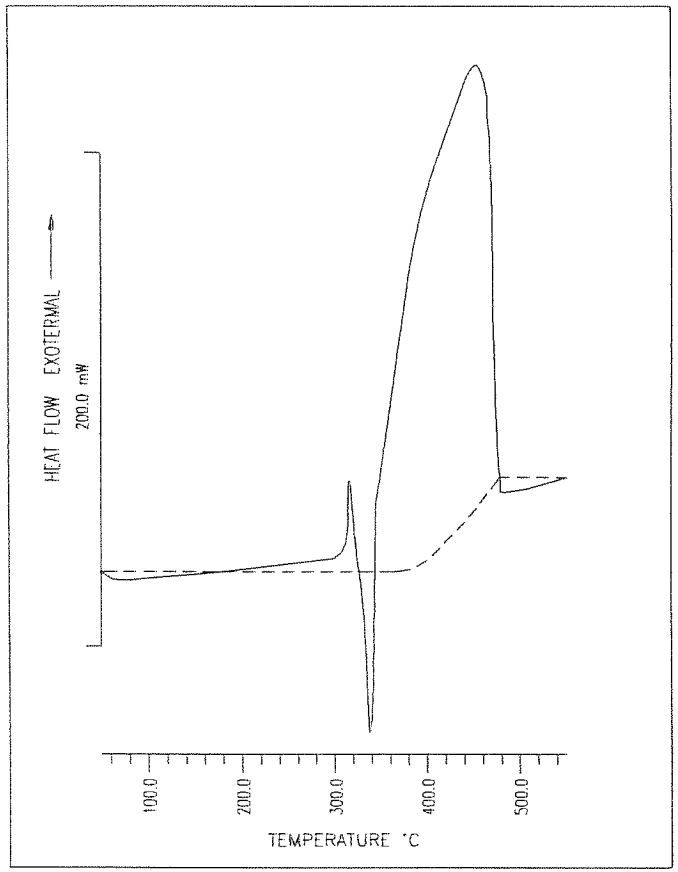

Fig. (4.26): DSC curve of copper picolinate. Heating rate 10°C min^{-1}.

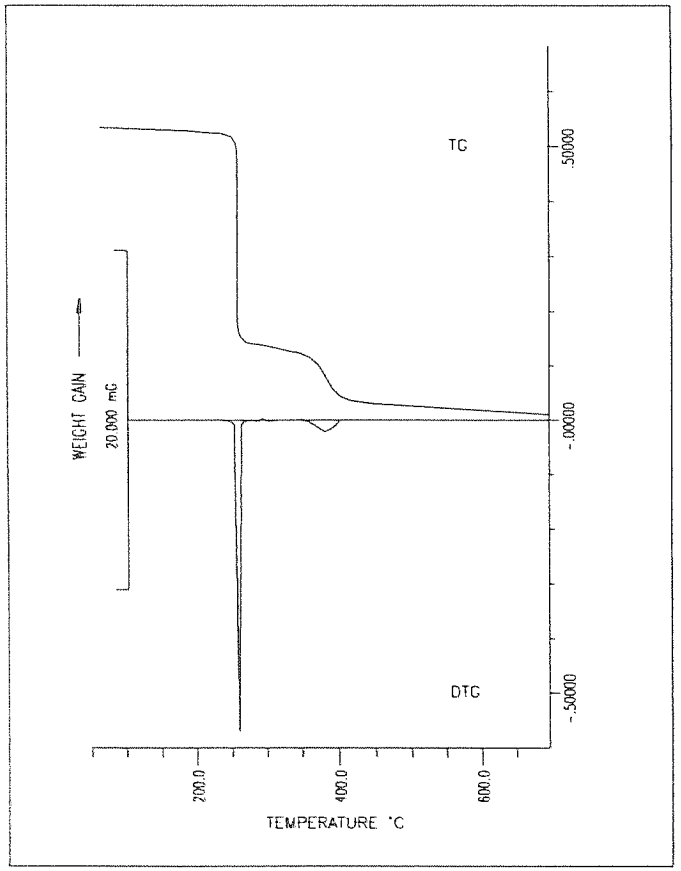

Fig. (4.27): TG and DTG curve of copper nicotinate. Heating rate 10°C min^{-1}.

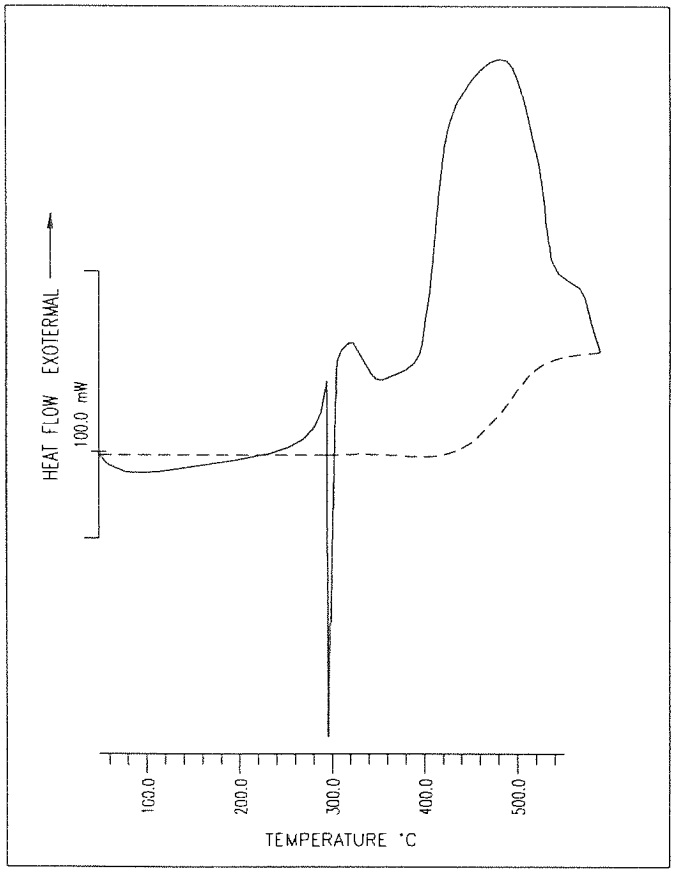

Fig. (4.28): DSC curve of copper nicotinate. Heating rate 10°C min^{-1}.

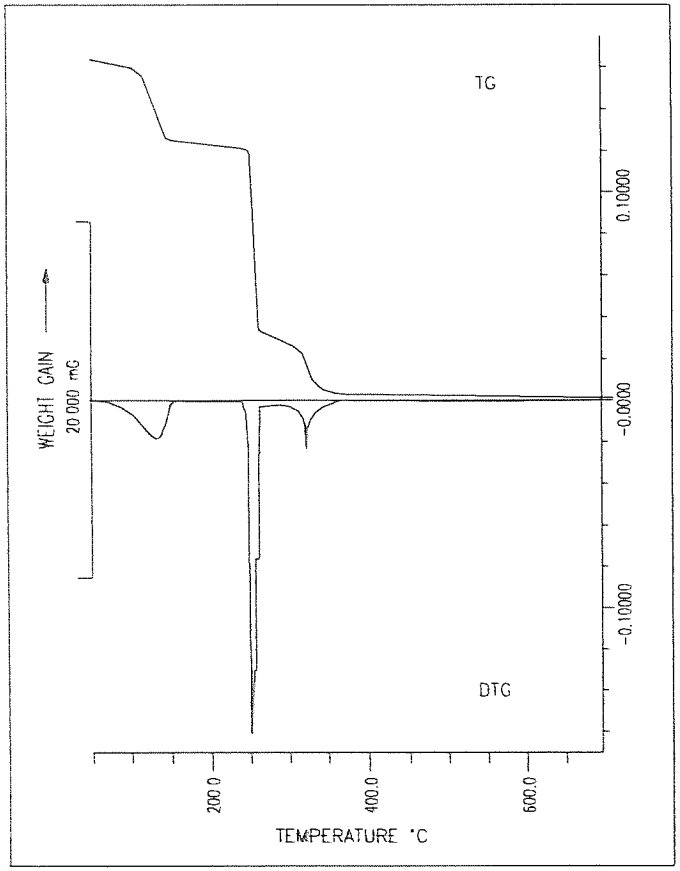

Fig. (4.29): TG and DTG curve of copper isonicotinate. Heating rate 10°C min^{-1}.

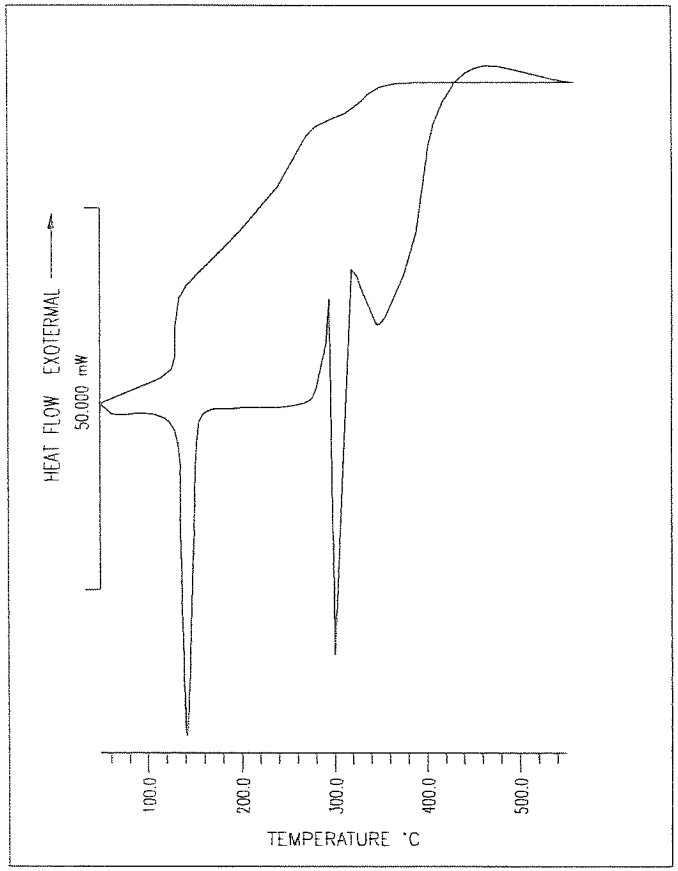

Fig. (4.30): DSC curve of copper isonicotinate. Heating rate 10°C min^{-1}.

Table 4.8
Dehydration processes of metal complexes.

Dehydration process	TG					DTG	DSC			
	Step	Temperature Range(°C)	Peak T(°C)	Mass loss % Theory	Mass loss % Found	DTG (Max) °C	TT	Temperature Range(°C)	Peak T(°C)	ΔH kJ mol^{-1}
$Co(PA)_2 2.5H_2O \rightarrow Co(PA)_2 1.5H_2O$	1	076.5-103.0	90.0	5.18	5.08	090.0	Endo	090.0-150.0	132.3	121
$Co(PA)_2 1.5H_2O \rightarrow Co(PA)_{20}.5H_2O$	2	103.0-129.5	127.0	5.18	5.22	125.0	Endo	150.0-190.0	167.9	67
$Co(PA)_2 0.5H_2O \rightarrow Co(PA)_2$	3	129.5-146.5	132.5	2.58	2.70					
$Co(NA)_2 4.0H_2O \rightarrow Co(NA)_2$	1	111.0-121.0	117.5	4.80	4.59	115.0	Endo	110.0-180.0	150.0	230
$Co(NA)_2 3.0H_2O \rightarrow Co(NA)_2 2H_2O$	2	128.0-135.0	133.0	4.80	3.72	148.0				
$Co(NA)_2 2H_2O \rightarrow Co(NA)_2$	3	135.0-141.0	137.5	9.61	10.40					
$Co(IA)_2 4.0H_2O \rightarrow Co(IA)_2$	1	81.0-167.5	133.5	19.22	19.64	150.0	Endo	120.0-200.0	169.5	305
$Ni(PA)_2 4.0H_2O \rightarrow Ni(PA)_2 2.0H_2O$	1	52.5-109.5	92.5	9.61	9.56	95.0	Endo	60.0-150.0	130.7	81
$Ni(PA)_2 2.0H_2O \rightarrow Ni(PA)_2$	2	109.5-191.5	156.0	9.61	9.37	160.0	Endo	160.0-240.0	203.7	100
$Ni(NA)_2 4.0H_2O \rightarrow Ni(NA)_2 0.5H_2O$	1	96.0-149.5	145.5	19.12	19.77	150.0	Endo	120.0-220.0	192.6	280
$Ni(IA)_2 3.5H_2O \rightarrow Ni(IA)_2 2.5H_2O$	1	106.5-139.5	136.5	4.93	5.19	155.0	Endo	140.0-220.0	190.3	216
$Ni(IA)_2 2.5H_2O \rightarrow Ni(IA)_2$	2	139.5-167.0	163.5	12.31	12.06					
$Cu(PA)2 \rightarrow Cu(PA)_2$	1		-	-	-	-	-	-	-	-
$Cu(NA)_2 \rightarrow Cu(NA)_2$	1		-	-	-	-	-	-	-	-
$Cu(IA)_2 4.5H_2O \rightarrow Cu(IA)_2$	1	53.0-169.0	136.0	20.86	20.46	130	Endo	100.0-170.0	134	252
$Zn(PA)_2 4H_2O$[74] $\rightarrow Zn(PA)_2$	1			18.89	18.68		Endo		114	282
$Zn(NA)_2 4H_2O$[74] $\rightarrow Zn(NA)_2$	1			18.89	19.76		Endo		93	214
$Zn(IA)_2 0.5H_2O$[74] $\rightarrow Zn(IA)_2$	1			2.82	2.62		Endo		104	55

TT: Thermal nature of temperature.

Table 4.9
Decomposition process of metal complexes.

Decomposition process	TG			DTG	DSC			
	Temperature Range (°C)	Residue % Theory	Residue % Found	DTG (Max) °C	TT	Temperature Range (°C)	Peak T(°C)	ΔH kJ mol^{-1}
Co(PA) → CoO	327.0-403.0	21.53	23.97	380	Exo	420.052.0	447.5	-1809
$Co(NA)_2$ → CoO	353.5-389.5	19.98	24.66	360	Exo Exo	370.0-420.0 425.0-470.0	401.1 452.8	-380 -1030
$Co(IA)_2$ → CoO	338.5-402.0	19.98	21.02	390	Exo Exo	360.0-425.0 425.0-524.0	410.0 478.9	-237 -1865
$Ni(PA)_2$ → NiO	309.0-425.5	19.97	19.85	360 385	Exo	410.0-540.0	480.6	-787
$Ni(NA)_2$ → NiO	341.0-390.0	19.97	20.77	370	Exo Exo	340.0-440.0 440.0-520.0	416.4 500.4	-306 -1023
$Ni(IA)_2$ → NiO	276.5-368.0	20.41	21.07	330.0	Exo Exo	340.0-390.0 390.0-510.0	372.3 485.3	-78 -1146
$Cu(PA)_2$ → CuO	264.5-323.0	25.86	25.10	295.0	Endo Exo	330.0-350.0 250.0-480.0	335.0 446.3	82 -1524
$Cu(NA)_2$ → CuO	243.5-266.0	25.86	24.89	260.0	Endo Exo	290.0-310.0 360.0-550	291.3 458.0	61 -965
$Cu(NA)_2$ → Cu	198.0-377.5	16.35	15.32	250.0	Endo Endo	290.0-320.0 320.0-400.0	295.0 356.6	79 221
$Zn(PA)_2$[74] ZnO	312.0-530.0	21.31	22.52		Exo			
$Zn(NA)_2$[74] ZnO	210.0-502.0	21.31	20.93		Exo			
$Zn(IA)_2$[74] ZnO	350.0-470.0				Exo			

TT: Thermal nature of temperature.

4.4 Proposed structure

Because the compounds are isolated as small crystallites rather than single crystal, no complete structural determination using X-ray crystallography could be carried out. The electronic spectra and magnetic data enable one to predict a likely sterochemistry of the metal complexes [102]. The coordination of metal ions to the oxygen or the nitrogen atom of donor molecules can be deduced by a study of IR spectra of their complexes [103]. The stoichiometries of the metal complexes show that the maximum number of ligand molecules present in any compound is two. The ligands (picolinate, nicotinate, and isonicotinate) have two coordinating atoms, nitrogen atom of the aromatic ring and oxygen atom of the carboxylic group, but only in the case where the carboxylate group is at position 2 on the pyridine ring can chelation occur. For the 3-and 4- substituted rings use of both donor atoms would require the bridging of two metal ions.

In the compounds consisting of cobalt, nickel or copper ion and picolinate, $M(PA)_2x(H_2O)$, the picolinate acts as a chelating ligand by coordinating to the metal ion through both the nitrogen atom of the aromatic ring and an oxygen atom of the carboxylate group. In the cobalt and nickel complexes two of the water molecules give a six-coordinate environment for the metal ion. Any remaining water molecule is involved in hydrogen bonding, which exists between molecules in the crystal lattice Fig 4.31. For the copper complex, a tetragonal environment is proposed, Fig.4.32. The presence of the coordinated and uncoordinated water in the compound is again evident from the bands recorded in the IR spectrum.

In the compounds $Co(NA)_2$ $4H_2O$ and $Ni(NA)_2$ $4H_2O$ the cobalt or nickel atom is bonded to the nitrogen atoms of two nicotinate groups, but not their carboxylate groups, and the completion of the six-coordination is achieved by bonding to the oxygen atoms of four water molecule as shown in Fig. 4.33.

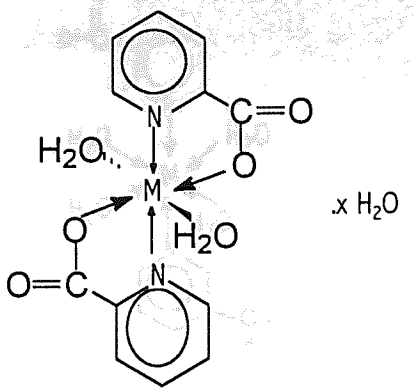

Fig. (4.31) Proposed structure of picolinate coordinated to cobalt or nickel; M = Co or Ni; x= 0.5 for Co or 2 for nickel

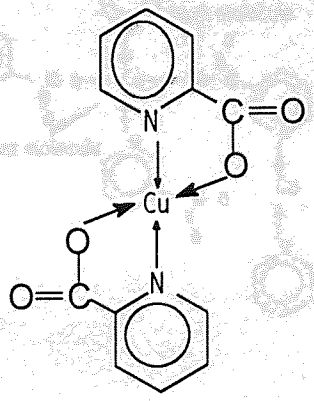

Fig. (4.32) Proposed structure of picolinate coordinated to copper.

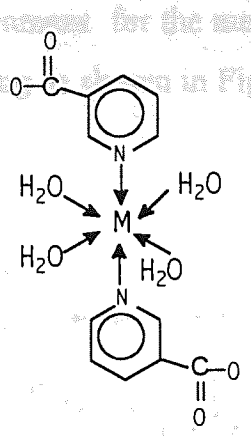

Fig.(4.33): Proposed structure of nicotinate coordinated to cobalt.

In the compound $Cu(NA)_2$ the copper atom is bonded to two nitrogen atoms of two nicotinate groups and is given its six-coordinate environment by four oxygen atoms in adjacent molecules as shown in Fig. 4.34.

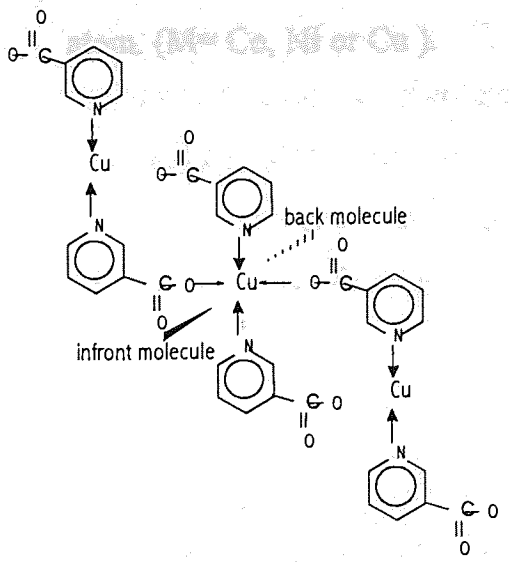

Fig.(4.34): Proposed structure of nicotinate coordinated to copper.

In the complexes formed of Co, Ni or Cu and isonicotinate, a nitrogen atom and an oxygen atom of the carboxylic group of each isonicotinate bonded to two different metal atoms to give a chain-like structure. It is further suggested that each metal atom is bonded to oxygen atoms in adjacent layers to give the six-coordinate environment for the metal atom. The water molecules are attached by hydrogen bonding as shown in Fig. 4.35.

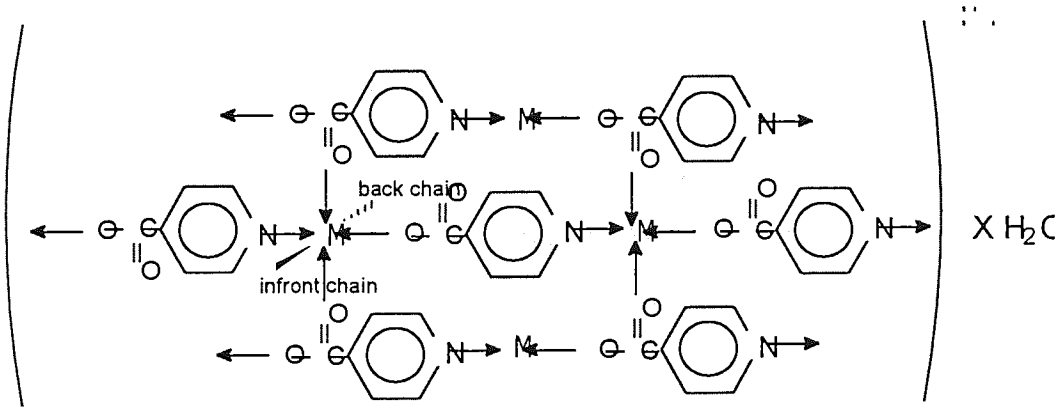

Fig.(4.35): Proposed structure of isonicotinate coordinated to metal atom. (M= Co, Ni or Cu).

4.5 ELECTRON MICROSCOPIC EXAMINATION

Scanning electron photomicrographs were taken for parent complexes and their calcination products (Table2.2) at different temperatures to correlate the morphological change accompanying the decomposition of complexes with the corresponding texture. Each sample was calcined for about10 minutes at the specified temperature. The scanning electronic micrographes are illustrated in Figs. 4.36-4.41. The results showed that the particle shape and size changed throughout the decomposition.

4.5.1 SEM for $[Co(PA)_2 2.5H_2O]$

At room temperature the scanning electronic micrographs (Fig. 4.36a) showed crystallites of needle shape for the parent material $[Co(PA)_2 2.5H_2O]$. At 500°C complete decomposition to CoO takes place, and there is growth of particles with change in crystal structure giving particles of irregular shapes (Fig. 4.36b).

4.5.2 SEM for $[Co(NA)_2 4H_2O]$

SE micrographs (Fig. 4.37a) of the parent material $[Co(NA)_2 4H_2O]$ at room temperature show rounded particles and regularly-shaped crystals of the same size. A micrograph of a sample calcined at 250°C (Fig. 4.37b) had dehydration showing superficial roughening and rounding of crystal edges. The decomposition of $[Co(NA)_2 4H_2O]$ at 380 °C produced a large number of small granules (Fig. 4.37c). The ES micrograph of a sample calcined at 500°C shows a gelatinous appearance (Fig. 4.37d) due to absorption of moisture from the atmosphere.

4.5.3 SEM for $[Co(IA)_2 4H_2O]$

At room temperature the SE micrograph of the parent compound $[Co(IA)_2 4H_2O]$ showed amorphous shape of the polymer compound (Fig.4.38a). At 150 °C, the decomposition yielded crystals of a cubic shape (Fig. 4.38b). The increasing temperature caused degradation that produce CoO (Fig. 4.38c).

4.5.4 SEM for $[Ni(PA)_2 4H_2O]$

SE micrograph at room temperature showed crystals of a large size (Fig4.39a) which lost water in the electron beam of the electronic microscope. At 250 °C dehydration took place with the coalescing of particles (Fig.4.39b). At 500 °C decomposition to NiO occurred with the formation of crystals relatively large in size (Fig. 4.39c).

4.5.5 SEM for $[Ni(NA)_2 4H_2O]$

By comparing the SE micrographs for $[Co(NA)_2 4H_2O]$ and $[Ni(NA)_2 4H_2O]$ it is clear that they are identical in the behavior towered calcination temperatures as shown in Figs. 4.37 and Figs. 4.40. Figure 4.40a shows that the parent material $[Ni(NA)_2 4H_2O]$ at room temperature has rounded particles and regularly-shaped crystals of the same size (Fig. 4.40a). A micrograph of the sample calcined at 215°C (Fig. 4.40b) which had dehydration shows superficially roughened crystal edges (Fig. 4.40c). The decomposition of $[Ni(NA)_2 4H_2O]$ at 390 °C produced a large number of small granules (Fig. 4.40d).

4.5.6 SEM for $[Ni(IA)_2 3.5H_2O]$

At room temperature the SE micrograph of the parent compound $[Ni(IA)_2 3.5H_2O]$ showed an amorphous shape of the polymer compound (Fig. 4.41a). At 170°C, the decomposition yielded crystals of a cubic shape (Fig. 4.41b). The increasing temperature caused degradation to produce NiO (Fig.4.41c).

a

b

Fig (4.36): Scanning electronic micrographs of cobalt picolinate complex.

(a): Parent compound at room temperature. (b): Sample calcined at 500 °C.

a

b

c

d

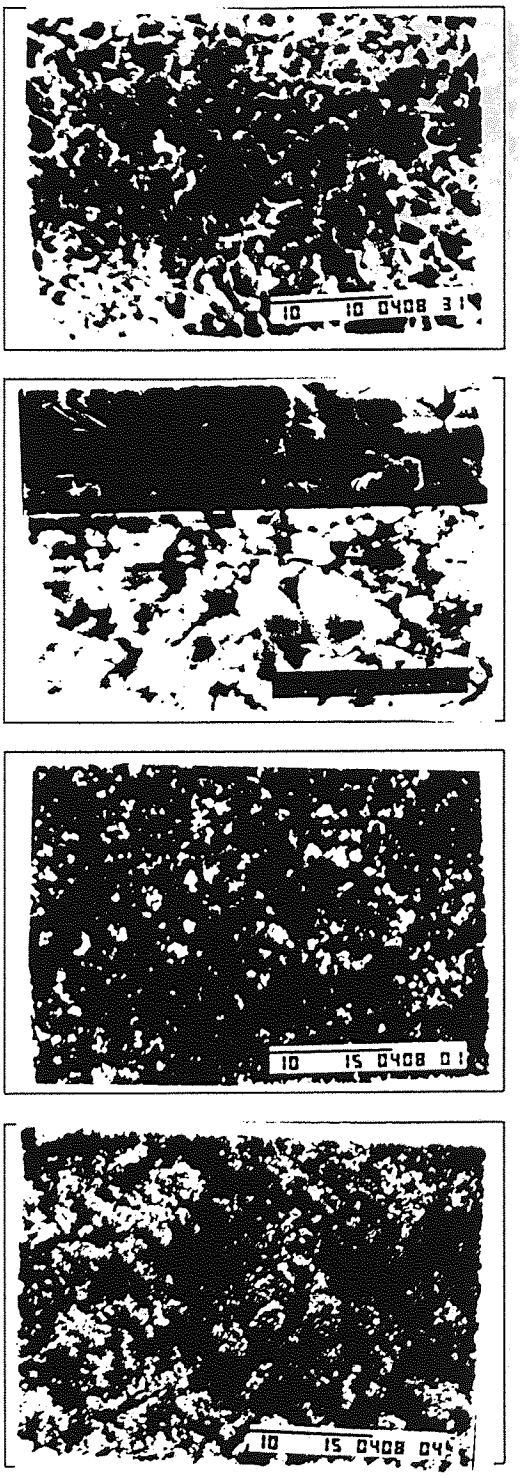

Fig (4.37): Scanning electronic micrographs of cobalt nicotinate complex.

(a): Parent compound at room temperature. (b): Sample calcined at 250 °C.

(c): Sample calcined at 380 °C. (d): Sample calcined at 500 °C.

a

b

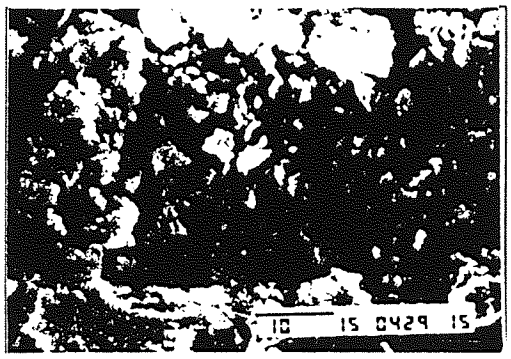

c

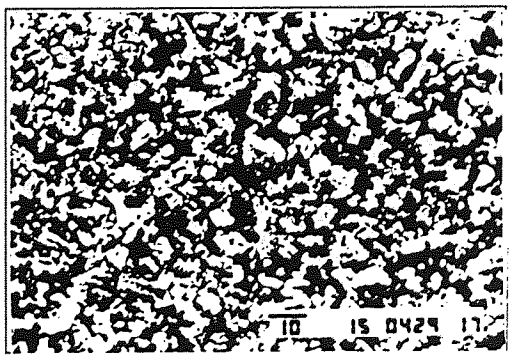

Fig (4.38): Scanning electronic micrographs of cobalt isonicotinate complex.

(a): Parent compound at room temperature. (b): Sample calcined at 150 °C.

(c): Sample calcined at 450 °C.

a

b

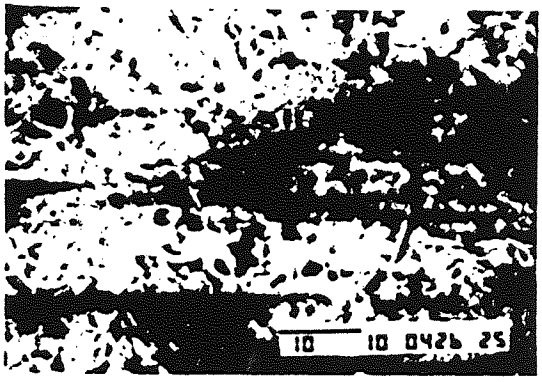

c

Fig (4.39): Scanning electronic micrographs of nickel picolinate complex.

(a): Parent compound at room temperature. (b): Sample calcined at 250 °C.

(c): Sample calcined at 500 °C

a

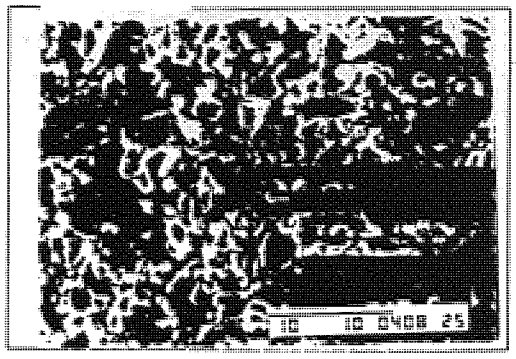

b

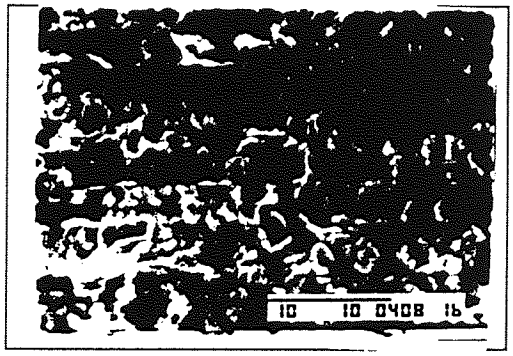

c

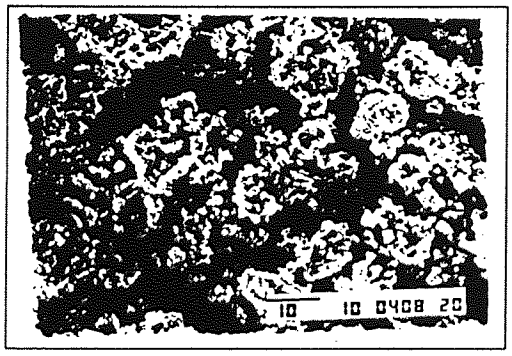

d

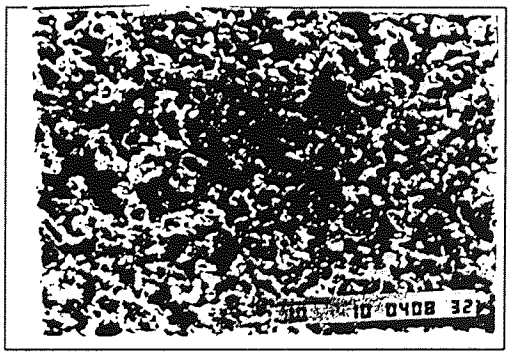

Fig (4.40): Scanning electronic micrographs of nickel nicotinate complex.

(a): Parent compound at room temperature. (b): Sample calcined at 215 °C.

(c): Sample calcined at 390 °C. (d): Sample calcined at 430 °C.

a

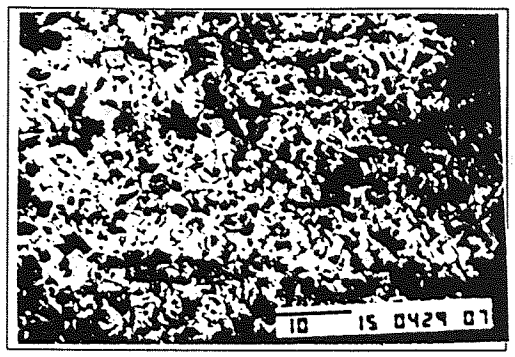

b

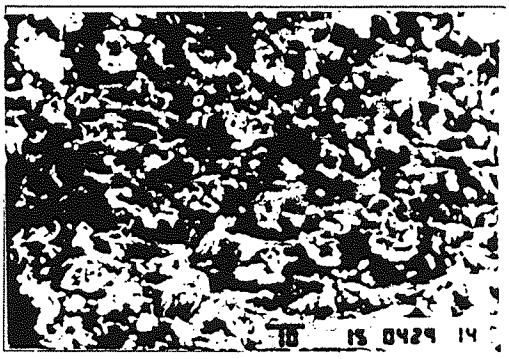

c

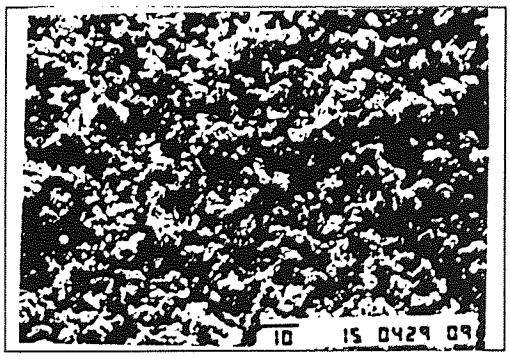

Fig (4.41): Scanning electronic micrographs of nickel isonicotinate complex.

(a): Parent compound at room temperature. (b): Sample calcined at 170 °C.

(c): Sample calcined at 310 °C.

4.6 KINETIC STUDIES

4.6.1 Kinetic analysis of non-isothermal data

In chapter 3 the kinetics of the thermal decomposition of free ligands were studied using dynamic thermogravimetric techniques. Kinetic analysis of dynamic data were made using different integral methods involving a single heating rate, a composite method, and the Ozawa and Kissinger methods. The single and composite methods were based on Coats-Redfern[41], modified Coats-Redfern[45], Doyle[40] and Madhusudanan et.al equations[46]. The kinetic analysis for complexes under investigation was made using single and composite methods only. In the composite method of analysis the results obtained (not only at different heating rates, but also with different α values) are superimposed on one master curve[46]. The correlation coefficient r and standard derivations are used to test linearity. The nearer r approaches unity, and the smaller S_{xy} and S_b are, the better the linearity[93]. The best interfacial reaction mechanism can be found, and the activation energy can be calculated[40]. Also, all calculations were made using the computer program discussed in chapter 3.

The non-isothermal kinetic parameters (activation energy (E) and pre-exponential factor (A)) were determined for the dehydration and the decomposition stages of the complexes under investigation (cobalt picolinate, cobalt nicotinate, cobalt isonicotinate, nickel picolinate, nickel nicotinate, and nickel isonicotinat) using data obtained from the DSC curves measured at different heating rates. Analysis was made according to single and composite methods using the $g(\alpha)$ function listed in Table 3.6. All DSC measurements were carried out in air atmosphere at different heating rates of 5, 10,15 and 20 °C min^{-1}.

Figs. 4.42, 4.44, 4.46, 4.48, 4.50, and 4.52 show the typical weight changes of thermal decomposition under nonisothermal measurements for cobalt picolinate complex $[Co(PA)_2 2.5H_2O]$, cobalt nicotinate complex $[Co(NA)_2 4H_2O]$, cobalt isonicotinate complex $[Co(IA)_2 4H_2O]$, nickel

picolinate complex [$Ni(PA)_2 4H_2O$], nickel nicotinate complex [$Ni(NA)_2 4H_2O$], and nickel isonicotinate complex [$Ni(NA)_2 4H_2O$] respectively for dehydration and decomposition processes.

It has been stated that reliable kinetic parameters for the dehydration process are obtained by minimizing the influence of water vapor[104]. The present study was carried out under a dynamic atmosphere, and the influence of the water vapor was at a minimum.

The results showed that the best fit is obtained, for random nucleation models, using the method of composite analysis based on equations according to Coats-Redfern[41], modified Coats-Redfern[45], Doyle[40] and Madhusudanan et.al[46]. The results agree with the results obtained by others[51]. The data are plotted in Figs. 4.43, 4.45, 4.47, 4.49, 4.51 and 4.53. Tables 4.10 - 4.15 list the result of activation parameters and thermodynamic parameters obtained under dynamic condition calculated to the single and composite methods using the different approximate integral equations.

It is clear from Tables 4.10-4.15 that the best fits for the correlation coefficients (r) were in the range 0.9788-0.9954. The highest value of the correlation coefficient is obtained with Doyle's equation. The other equations give a good linear curve with high correlation coefficients, though they are not as high as that for Doyle's equation.

4.6.2 Calculation of activation parameters:

Also, Tables 4.10-4.15 show that the values of activation parameters obtained by Doyle's equation are the highest among the values obtained by other equations (Coats-Redfern, modified Coats-Redfern, and Madhusudanan et.al) either involving single and composite methods. The average values for activation parameters obtained using a single heating rate are higher than the average values obtained by the composite method.

The decomposition stages with positive[29] values of $\Delta S^{\#}$ indicate that the activated complex has a less ordered structure compared to the reactant, and that reaction, in these cases, may be described as " faster than normal ". The stages having negative entropy of activation indicate that the activated complex has a more ordered structure than the reactant, and the reaction is " slower than normal ". The variation of activation energy is paralleled by a similar trend regarding the entropy of activation.

It was noted from DTG and DSC studies that in the cobalt picolinate complex $[Co(PA)_2 4H_2O]$ and nickel picolinate complex $[Ni(PA)_2 4H_2O]$, the dehydration processes were carried out into two stages, while carried out in one stage for the remaining complexes. Tables 4.10-4.15 show that the activation energy for the first stage lies in the range 23-30 kJ mol^{-1}, whereas for the second stage the activation energy is in the range 46-70 kJ mol^{-1}. In addition, for compounds dehydrated in one stage, the activation energy is in range 41-57 kJ mol^{-1}. The water[77] in crystalline hydrate may be considered either as crystal water or as coordinated water. The binding strength of these molecules in the crystal lattice is different and, hence, different dehydration temperatures and kinetic parameters result. The water eliminated at 150°C and below can be considered as crystal water, whereas water eliminated at 200°C and above indicates its coordination by metal atom. Water molecules eliminated at intermediate temperatures can be coordinatively linked as water, as well as crystal water. In the compounds dehydrated in two stages, the energy of activation and the dehydration temperature found for two dehydration stages suggest that the first group of water molecules are present in the crystal as lattice molecules, but the second group is present as coordinated water molecules to the metal atom. As for compounds dehydrated in one stage, the water molecules are present also as coordination molecules.

The DTG and DSC curves include that anhydrous salts of cobalt picolinate, nickel picolinate, and nickel isonicotinate which decompose in one

stage (exothermic effect), and also cobalt nicotinate, nickel nicotinate, and cobalt isonicotinate which decompose in two stages (exothermic effect).

The kinetics of the different stages of the decomposition reaction of the anhydrous salt were also investigated under nonisothermal conditions.

From Tables 4.10-4.15 it can be seen that both E and A calculated for dehydration and decomposition are dependent on heating rates, and the kinetic parameters are not appreciably affected by heating rate. The minor variations are rather irregular.

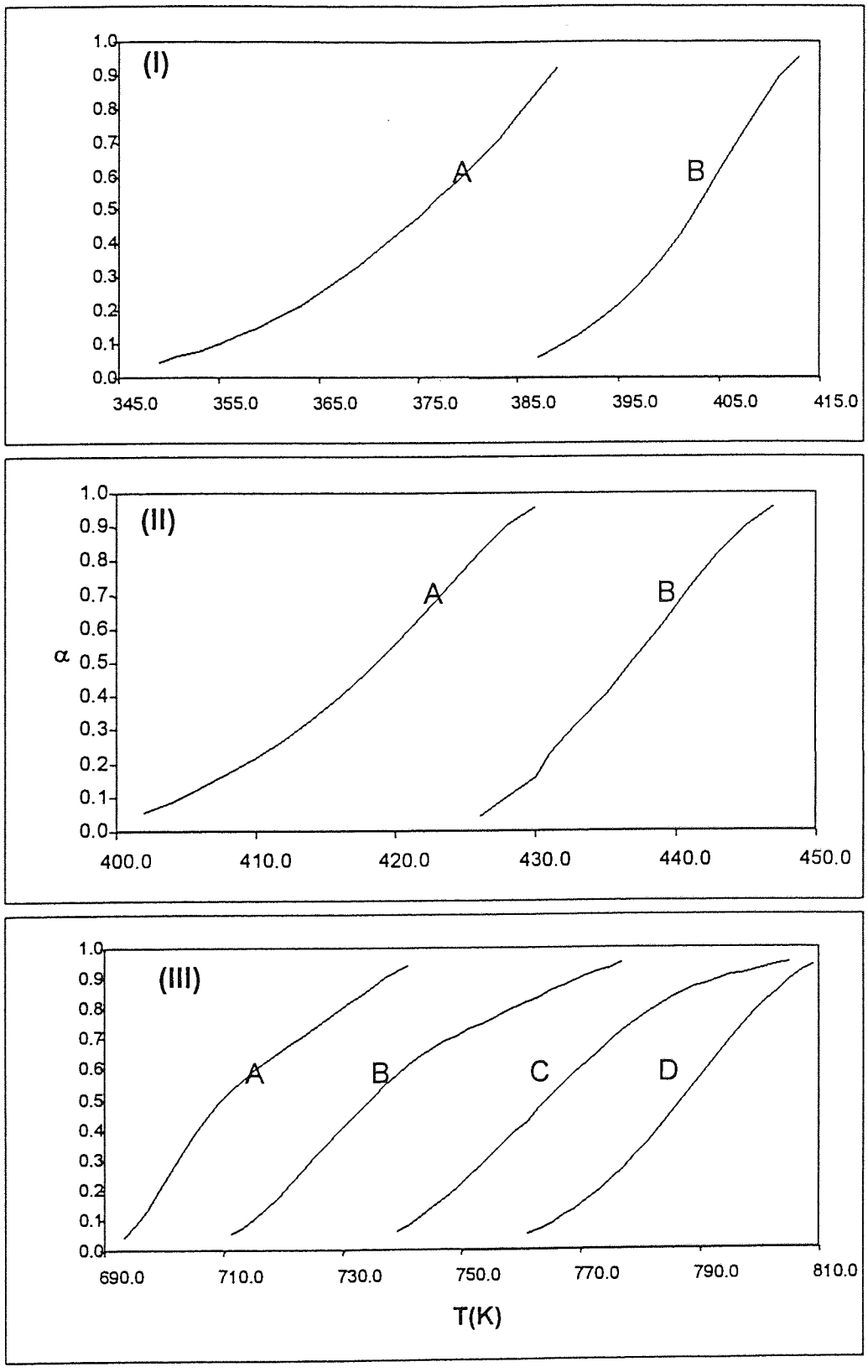

Fig.(4.42): Dynamic measurements for cobalt (II) picolinate thermal decomposition. Heating rate: curve A, 5°C min^{-1}; B, 10°C min^{-1}; C, 15°C min^{-1}; D, 20°C min^{-1}. Diagrams [(I) and (II)] for the dehydration and diagram (III) for decomposition.

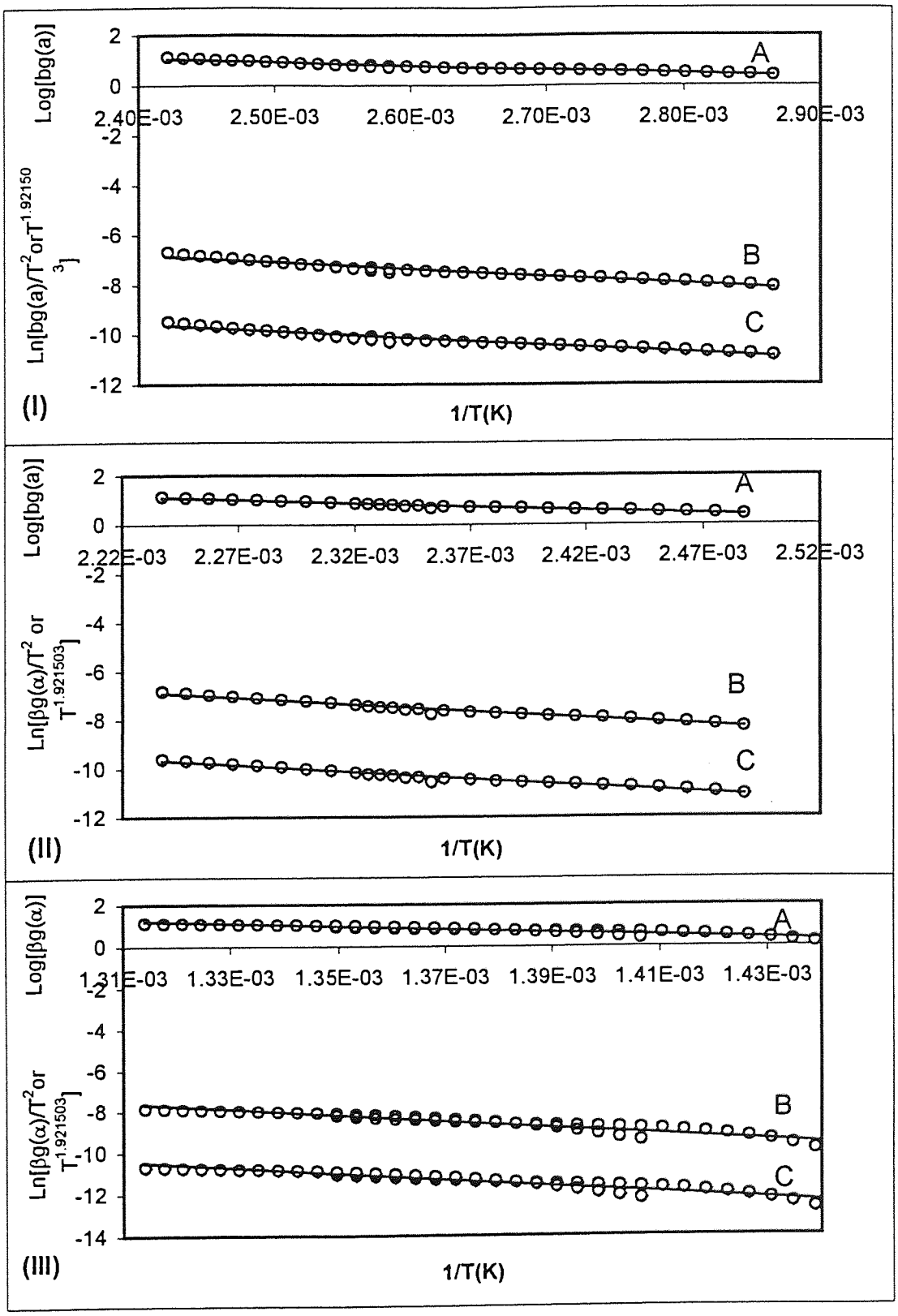

Fig.(4.43): Composite analysis of dynamic DSC data of dehydration [(I) and (II)] and decomposition(III) of cobalt picolinate based on (A) Doyle's equation, (B) Madhusudanan et.al. equation, and (C) Coast-Redfern and modified Coast-Redfern equations.

Table (4.10): Kinetic parameters, thermodynamic parameters and regression results for thermal decomposition of cobalt (II) picolinate involving single heating rate and composite methods based on integral equations.

Method	Step	Equation	β	R	M	E(kJ mol^{-1})	LnA(min^{-1})	S_{xy}	S_b	$\Delta S^{\#}$	$\Delta G^{\#}$
Composite	1	Coats-Redfern		0.97885	A4	23.25	7.38E+00	7.75E-02	1.02E+02		
		Modified Coats-Redfern		0.97885	A4	23.25	7.01E+00	7.75E-02	1.02E+02		
		Doyle's		0.98616	A4	28.11	8.21E+00	3.44E-02	4.52E+01		
		Madusudana et.al.		0.97925	A4	23.5	-6.03E+00	7.75E-02	1.02E+02		
Single		Coats-Redfern	5	0.99672	A4	19.81	4.23E+00	1.81E-02	4.44E+01	-213	111
			10	0.99911	A4	40.96	1.11E+01	1.13E-02	6.01E+01	-155	107
		Average		0.997915		30.385	7.665	0.0147	52.25	-184	109
		Modified Coats-Redfern	5	0.99672	A4	19.81	3.78E+00	1.81E-02	4.44E+01	-217	112
			10	0.99911	A4	40.96	1.10E+01	1.13E-02	6.01E+01	-157	108
		Average		0.997915		30.385	7.39	0.0147	52.25	-187	110
		Doyle's	5	0.99815	A4	24.66	7.16E+00	7.74E-03	1.89E+01	-188	105
			10	0.99935	A4	45.27	1.32E+01	4.90E-03	2.60E+01	-139	104
		Average		0.99875		34.965	10.18	0.00632	22.45	-163.5	104.5
		Madusudana et.al.	5	0.9968	A4	20.05		1.81E-02	4.43E+01	-325	159
			10	0.99912	A4	41.22		1.13E-02	6.00E+01	-266	155
		Average		0.99796		30.635		0.0147	52.15	-295.5	157
Composite	2	Coats-Redfern		0.98785	A4	46.74	1.37E+01	6.50E-02	1.77E+02		
		Modified Coats-Redfern		0.98785	A4	46.74	1.35E+01	6.50E-02	1.77E+02		
		Doyle's		0.99061	A4	51.14	1.36E+01	2.85E-02	7.75E+01		
		Madusudana et.al.		0.98798	A4	47.01	3.70E-01	6.50E-02	1.77E+02		
Single		Coats-Redfern	5	0.99614	A4	40.99	9.96E+00	2.33E-02	1.20E+02	-167	127
			10	0.98864	A4	62.84	1.64E+01	4.57E-02	3.63E+02	-113	121
		Average		0.99239		51.915		0.0345	241.5	-140	124
		Modified Coats-Redfern	5	0.99614	A4	40.99	9.73E+00	2.33E-02	1.20E+02	-169	128
			10	0.98864	A4	62.84	1.63E+01	4.57E-02	3.63E+02	-114	122
		Average		0.99239		51.915		0.0345	241.5	-141.5	125

Continue Table (4.10):

Method	Step	Equation	β	R	M	E(kJmol^{-1})	LnA(min^{-1})	S_{xy}	S_b	ΔS#	ΔG#
		Doyle's	5	0.99721	A4	45.56	1.20E+01	1.01E-02	5.20E+01	-150	123
			10	0.99091	A4	66.65	1.78E+01	1.98E-02	1.57E+02	-102	119
		Average		0.99406		56.105		0.01495	104.5	-126	121
		Madusudana et.al.	5	0.9962	A4	41.27	********	2.33E-02	1.20E+02	-277	184
			10	0.98874	A4	63.13	3.14E+00	4.57E-02	3.63E+02	-223	178
		Average		0.99247		52.2	3.14	0.0345	241.5	-250	181
Composite	3	Coats-Redfern		0.95182	A2	124.85	2.09E+01	1.64E-01	6.91E+02		
		Modified Coats-Redfern		0.95182	A2	124.85	2.08E+01	1.64E-01	6.91E+02		
		Doyle's		0.95963	A2	130.21	2.01E+01	7.10E-02	2.99E+02		
		Madusudana et.al.		0.95217	A2	125.32	7.68E+00	1.64E-01	6.91E+02		
Single		Coats-Redfern	5	0.93249	A2	133.18	2.04E+01	1.82E-01	1.29E+03	-78	167
			10	0.94624	A2	103.69	1.45E+01	1.56E-01	7.54E+02	-127	158
			15	0.96748	A2	119.35	1.64E+01	1.28E-01	6.63E+02	-111	167
			20	0.99295	A2	193.07	2.76E+01	6.77E-02	5.78E+02	-18	201
		Average		0.95979		137.3225	19.725	0.13343	821.25	-83.5	173.25
		Modified Coats-Redfern	5	0.93249	A2	133.18	2.03E+01	1.82E-01	1.29E+03	-78	167
			10	0.94624	A2	103.69	1.45E+01	1.56E-01	7.54E+02	-127	158
			15	0.96748	A2	119.35	1.64E+01	1.28E-01	6.63E+02	-111	167
			20	0.99295	A2	193.07	2.76E+01	6.77E-02	5.78E+02	-18	201
		Average		0.95979		137.3225	19.7	0.13343	821.25	-83.5	173.25
		Doyle's	5	0.9424	A2	137.98	2.14E+01	7.88E-02	5.61E+02	-70	168
			10	0.95668	A2	110.36	1.61E+01	6.75E-02	3.26E+02	-114	159
			15	0.97348	A2	125.69	1.78E+01	5.51E-02	2.87E+02	-100	168
			20	0.99386	A2	196	2.81E+01	2.93E-02	2.50E+02	-14	202
		Average		0.966605		142.5075	20.85	0.05768	356	-74.5	174.25
		Madusudana et.al.	5	0.93292	A2	133.65	7.21E+00	1.82E-01	1.29E+03	-188	214
			10	0.94671	A2	104.18	1.35E+00	1.56E-01	7.54E+02	-237	205
			15	0.96775	A2	119.85	3.25E+00	1.28E-01	6.63E+02	-221	214
			20	0.99299	A2	193.58	1.44E+01	6.77E-02	5.78E+02	-128	248
		Average		0.960093		137.815	6.5525	0.13343	821.25	-193.5	220.25

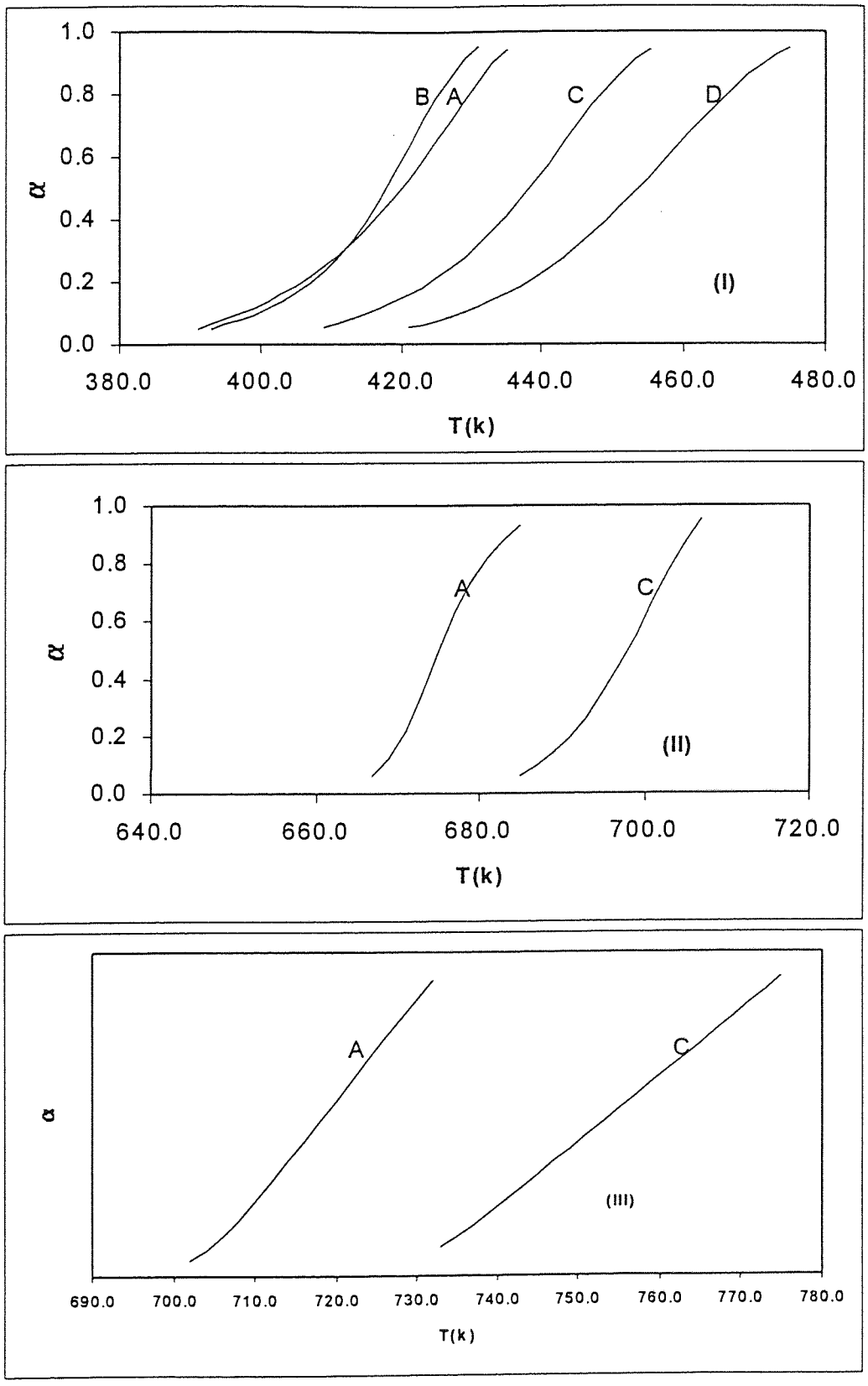

Fig.(4.44): Dynamic measurements for cobalt (II) nicotinat thermal decomposition. Heating rate: curve A, 5°C min^{-1}; B, 10°C min^{-1}; C, 15°C min^{-1}; D, 20°C min^{-1}. Diagram (I) dehydration diagrams [(II) and (III)] decomposition.

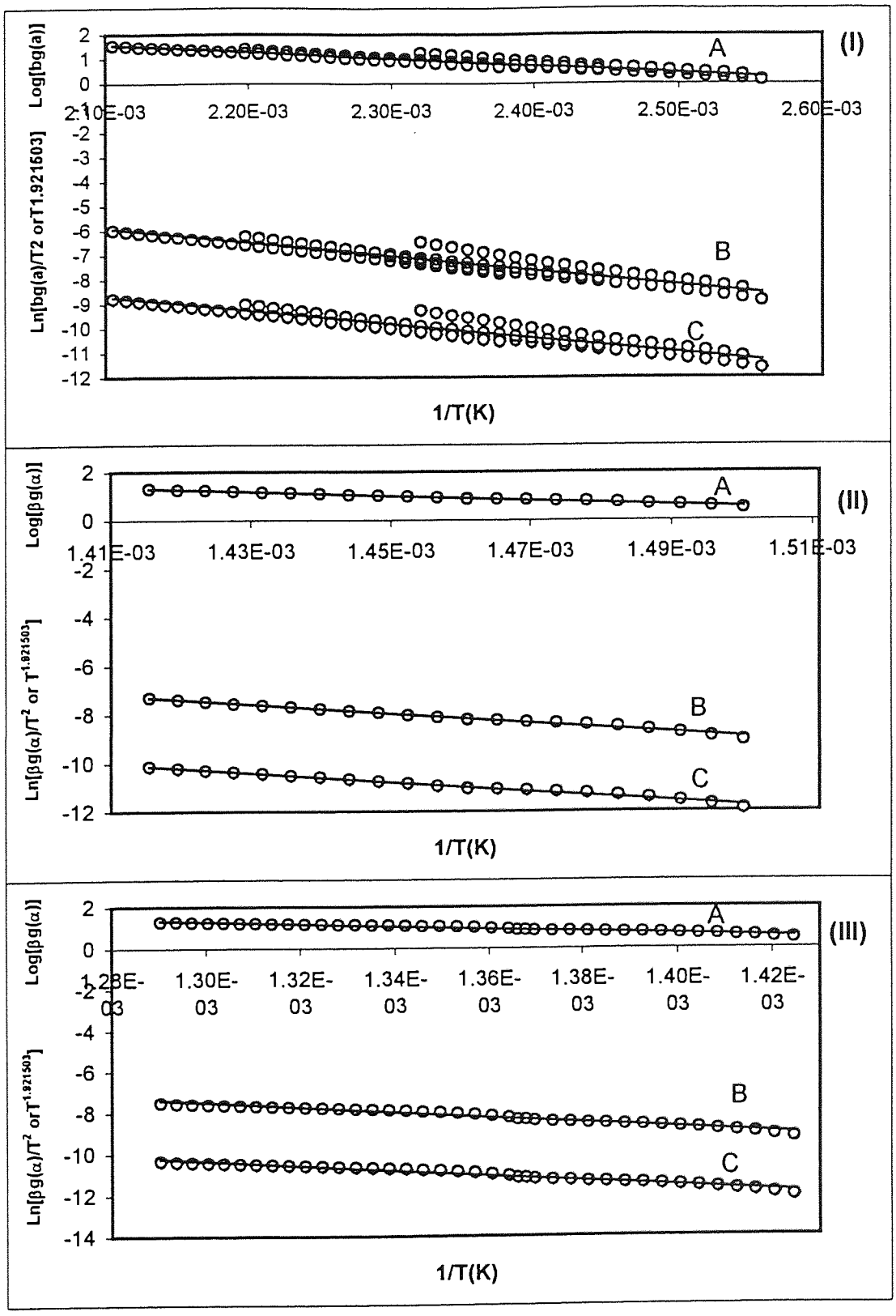

Fig. (4.45): Composite analysis of dynamic DSC data of dehydration (I) and decomposition [(II), (III) and (IIII)] of cobalt nicotinate based on (A) Doyle's equation, (B) Madhusudanan et. al. equation (C) Coast-Redfern and modified Coast-redfern equations.

Table (4.11): Kinetic parameters, thermodynamic parameters and regression results for thermal decomposition of cobalt(II) nicotinate involving single heating rate and composite methods based on integral equations.

Method	Step	Equation	β	R	M	E(kJ mol^{-1})	LnA(min^{-1})	S_{xy}	S_b	$\Delta S^{\#}$	$\Delta G^{\#}$
Composite	1	Coats-Redfern		0.93967	A2	47.05	1.45E+01	2.33E-01	2.14E+02		
		Modified Coats-Redfern		0.93967	A2	47.05	1.44E+01	2.33E-01	2.14E+02		
		Doyle's		0.95366	A2	51.53	1.39E+01	1.01E-01	9.26E+01		
		Madusudana et.al.		0.94032	A2	47.33	1.29E+00	2.33E-01	2.14E+02		
Single		Coats-Redfern	6	0.99843	A2	54.1	1.40E+01	2.98E-02	7.97E+01	-131	111
			10	0.99814	A2	68.31	1.89E+01	3.60E-02	1.18E+02	-91	107
			15	0.99965	A2	57.56	1.51E+01	1.42E-02	3.91E+01	-122	110
			20	0.99976	A2	53.74	1.37E+01	1.18E-02	2.77E+01	-134	111
		Average		0.998995		58.4275	15.425	0.02295	66.125	-119.5	109.75
		Modified Coats-Redfern	6	0.99843	A2	54.1	1.38E+01	2.98E-02	7.97E+01	-133	111
			10	0.99814	A2	68.31	1.87E+01	3.60E-02	1.18E+02	-92	108
			15	0.99965	A2	57.56	1.50E+01	1.42E-02	3.91E+01	-123	110
			20	0.99976	A2	53.74	1.36E+01	1.18E-02	2.77E+01	-135	112
		Average		0.998995		58.4275	15.275	0.02295	66.125	-120.75	110.25
		Doyle's	6	0.99873	A2	57.97	1.56E+01	1.31E-02	3.51E+01	-119	109
			10	0.9984	A2	71.46	2.00E+01	1.59E-02	5.24E+01	-81	106
			15	0.9997	A2	61.55	1.67E+01	6.46E-03	1.77E+01	-109	108
			20	0.99985	A2	58.17	1.55E+01	4.69E-03	1.10E+01	-119	109
		Average		0.99917		62.2875	16.95	0.01004	29.05	-107	108
		Madusudana et.al.	6	0.99844	A2	54.37	7.16E-01	2.98E-02	7.98E+01	-242	158
			10	0.99815	A2	68.58	5.62E+00	3.60E-02	1.18E+02	-201	155
			15	0.99965	A2	57.84	1.90E+00	1.43E-02	3.91E+01	-232	157
			20	0.99977	A2	54.03	4.93E-01	1.18E-02	2.76E+01	-244	158
		Average		0.999003		58.705	2.18225	0.02298	66.125	-229.75	157

Continue Table (4.11):

Method	Step	Equation	β	R	M	E(kJ mol^{-1})	LnA(min^{-1})	S_{xy}	S_b	$\Delta S^{\#}$	$\Delta G^{\#}$
Composite	2	Coats-Redfern		0.9947	A4	159.07	2.92E+01	5.21E-02	4.42E+02		
		Modified Coats-Redfern		0.9947	A4	159.07	2.91E+01	5.21E-02	4.42E+02		
		Doyle's		0.9954	A4	162.13	2.74E+01	2.26E-02	1.92E+02		
		Madusudana et.al.		0.9947	A4	159.52	1.59E+01	5.21E-02	4.42E+02		
Single		Coats-Redfern	6	0.97486	A4	180.54	3.08E+01	6.98E-02	1.75E+03	5	178
			15	0.99888	A4	161.85	2.73E+01	1.44E-02	2.91E+02	-24	178
		Average		0.98687	A4	171.195	29.05	0.0421	1020.5	-9.5	178
		Modified Coats-Redfern	6	0.97486	A4	180.54	3.07E+01	6.98E-02	1.75E+03	4	178
			15	0.99888	A4	161.85	2.73E+01	1.44E-02	2.91E+02	-25	179
		Average		0.98687	A4	171.195	29	0.0421	1020.5	-10.5	178.5
		Doyle's	6	0.97767	A4	182.37	3.11E+01	3.03E-02	7.61E+02	7	178
			15	0.99903	A4	164.91	2.79E+01	6.22E-03	1.26E+02	-20	178
		Average		0.98835	A4	173.64	29.5	0.01826	443.5	-6.5	178
		Madusudana et.al.	6	0.97498	A4	180.98	1.76E+01	6.98E-02	1.75E+03	-106	252
			15	0.99889	A4	162.3	1.41E+01	1.44E-02	2.91E+02	-134	253
		Average		0.986935	A4	171.64	15.85	0.0421	1020.5	-120	252.5
Composite	3	Coats-Redfern		0.98645	A4	100.73	1.73E+01	8.08E-02	3.31E+02		
		Modified Coats-Redfern		0.98645	A4	100.73	1.72E+01	8.08E-02	3.31E+02		
		Doyle's		0.98937	A4	107.45	1.65E+01	3.48E-02	1.43E+02		
		Madusudana et.al.		0.98659	A4	101.21	4.07E+00	8.07E-02	3.31E+02		
Single			6	0.97924	A4	116.39	1.76E+01	5.56E-02	7.74E+02	-102	160
			15	0.9803	A4	75.3	1.06E+01	4.47E-02	3.98E+02	-160	144
		Average		0.97977	A4	95.845	14.1	0.05015	586	-131	152
			6	0.97924	A4	116.39	1.75E+01	5.56E-02	7.74E+02	-102	160
			15	0.9803	A4	75.3	1.05E+01	4.47E-02	3.98E+02	-161	144
		Average		0.97977	A4	95.845	14	0.05015	586	-131.5	152

Continue Table (4.11):

Method	Step	Equation	β	R	M	E(kJ mol^{-1})	LnA(min^{-1})	S_{xy}	S_b	$\Delta S^{\#}$	$\Delta G^{\#}$
			6	0.98291	A4	122.02	1.89E+01	2.41E-02	3.36E+02	-91	161
			15	0.98555	A4	83.51	1.27E+01	1.93E-02	1.72E+02	-142	144
		Average		0.98423	A4	102.765	15.8	0.0217	254	-116.5	152.5
			6	0.9794	A4	116.86	4.41E+00	5.56E-02	7.74E+02	-211	207
			15	0.98056	A4	75.79	********	4.47E-02	3.98E+02	-270	191
		Average		0.97998	A4	96.325	4.41	0.05015	586	-240.5	199

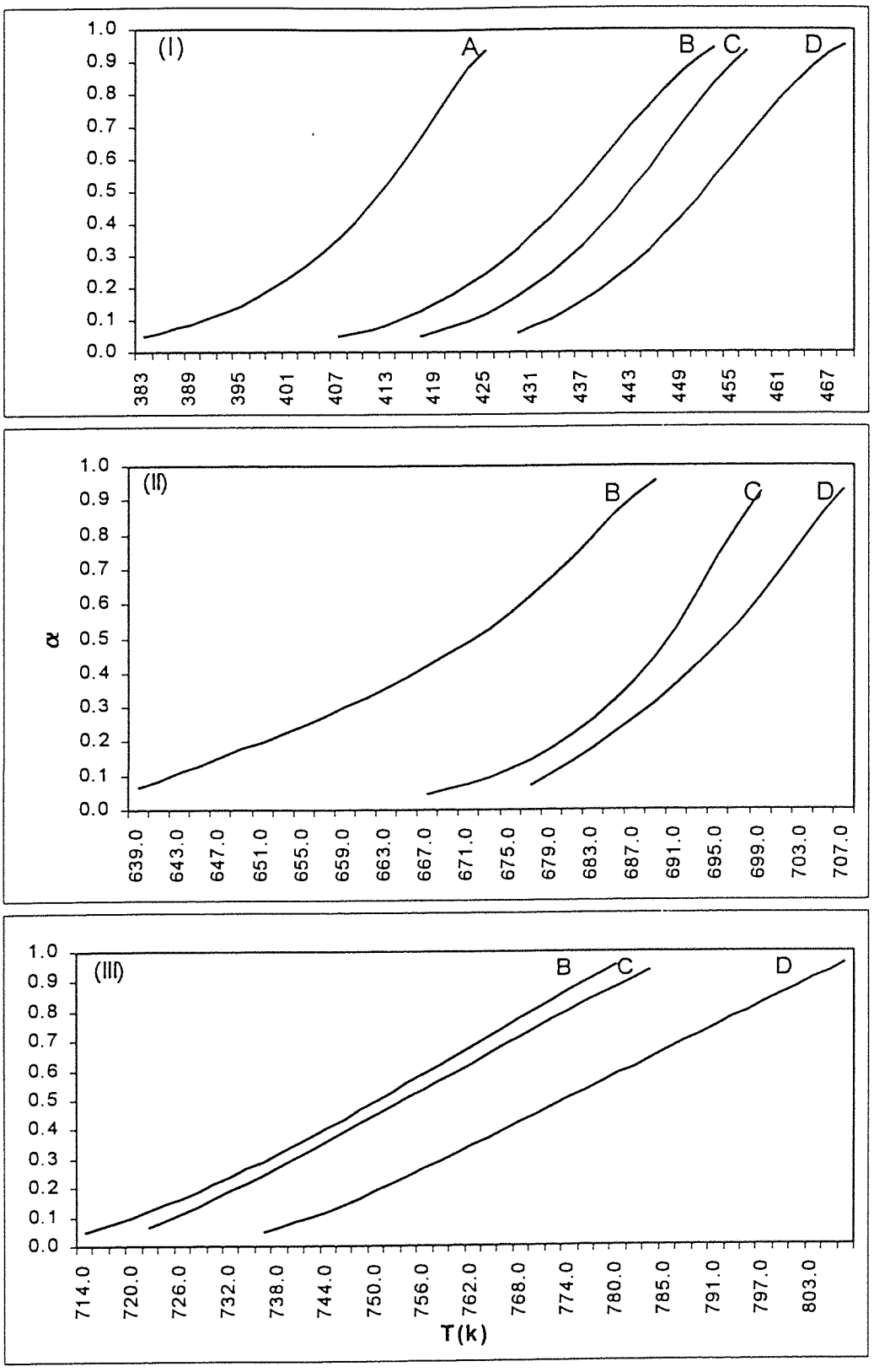

Fig.(4.46): Dynamic measurement for cobalt (II) isonicotinate thermal decomposition. Heating rate: A, 5°Cmin^{-1}; B, 10°Cmin^{-1}; C, 15°Cmin^{-1}, D 20°Cmin^{-1}. Diagram (I) dehydration, diagrams [(II) and (III)] decomposition.

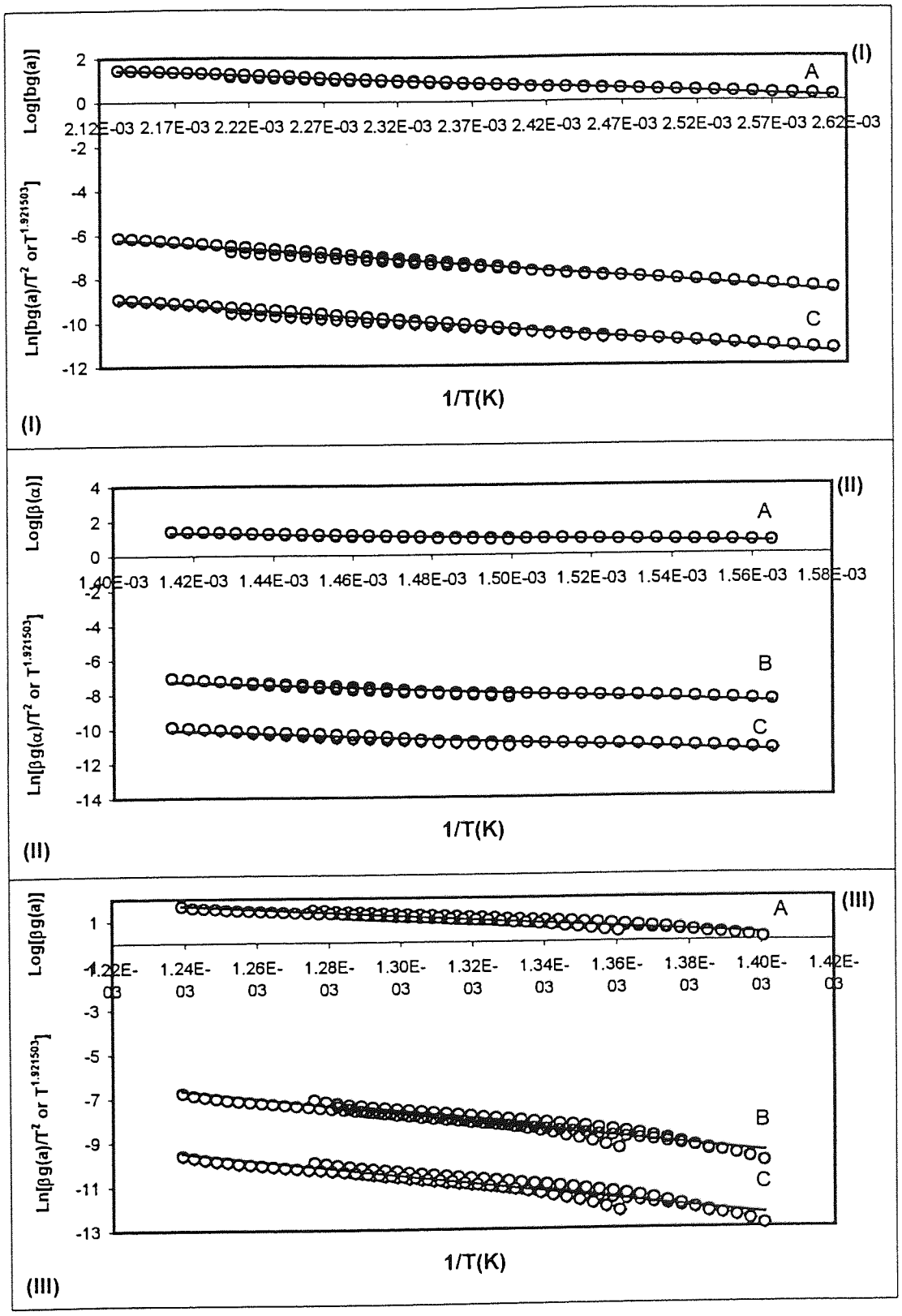

Fig.(4.47): Composite analysis of dynamic DSC data of dehydration (I) and decomoisition [(II) and (III)] of cobalt isonicotinate based on (A) Doyle's equation, (B) Madhusudanan et. al. equation, and (C) Coast-Redfern and modified Coast-Redfern equations.

Table (4.12): Kinetic parameters, thermodynamic parameters and regression results for thermal decomposition of cobalt(II) isonicotinate involving single heating rate and composite methods based on integral equations.

Method	Step	Equation	β	R	M	E(kJ mol^{-1})	LnA(min^{-1})	S_{xy}	S_b	$\Delta S^{\#}$	$\Delta G^{\#}$
Composite	1	Coats-Redfern		0.9888	A3	41.83	1.29E+01	8.81E-02	8.19E+01		
		Modified Coats-Redfern		0.9888	A3	41.83	1.27E+01	8.81E-02	8.19E+01		
		Doyle's		0.99149	A3	46.49	1.25E+01	3.89E-02	3.62E+01		
		Madusudana et.al.		0.98893	A3	42.1	-3.74E-01	8.82E-02	8.19E+01		
Single		Coats-Redfern	5	0.99744	A3	34.95	8.24E+00	2.46E-02	6.74E+01	-179	110
			10	0.99955	A3	37.37	8.95E+00	1.06E-02	2.88E+01	-173	110
			15	0.99972	A3	44.11	1.11E+01	8.45E-03	2.90E+01	-155	109
			20	0.99798	A3	45.3	1.15E+01	2.20E-02	7.96E+01	-152	109
		Average		0.998673		40.4325	9.9475	0.01641	51.2	-164.75	109.5
		Modified Coats-Redfern	5	0.99744	A3	34.95	8.01E+00	2.46E-02	6.74E+01	-181	111
			10	0.99955	A3	37.37	8.75E+00	1.06E-02	2.88E+01	-175	111
			15	0.99972	A3	44.11	1.10E+01	8.45E-03	2.90E+01	-157	110
			20	0.99798	A3	45.3	1.13E+01	2.20E-02	7.96E+01	-1534	110
		Average		0.998673		40.4325	9.765	0.01641	51.2	-511.75	110.5
		Doyle's	5	0.99809	A3	39.62	1.05E+01	1.10E-02	3.01E+01	-160	107
			10	0.99971	A3	42.33	1.13E+01	4.42E-03	1.20E+01	-154	107
			15	0.9998	A3	48.85	1.32E+01	3.60E-03	1.24E+01	-138	107
			20	0.99858	A3	50.17	1.35E+01	9.29E-03	3.37E+01	-135	107
		Average		0.999045		45.2425	12.125	0.00708	22.05	-146.75	107
		Madusudana et.al.	5	0.99747	A3	35.22	********	2.46E-02	6.74E+01	-290	157
			10	0.99956	A3	37.65	********	1.06E-02	2.88E+01	-284	157
			15	0.99972	A3	44.39	********	8.44E-03	2.90E+01	-266	156
			20	0.99801	A3	45.59	********	2.19E-02	7.96E+01	-263	156
		Average		0.99869		40.7125	#DIV/0!	0.01639	51.2	-275.75	156.5

Continue Table (4.12):

Method	Step	Equation	β	R	M	E(kJmol^{-1})	LnA(min^{-1})	S_{xy}	S_b	$\Delta S^{\#}$	$\Delta G^{\#}$
Composite	2	Coats-Redfern		0.94452	A4	70.55	1.38E+01	1.14E-01	3.91E+02		
		Modified Coats-Redfern		0.94452	A4	70.55	1.36E+01	1.14E-01	3.91E+02		
		Doyle's		0.95738	A4	77.72	1.31E+01	4.98E-02	1.71E+02		
		Madusudana et.al.		0.94513	A4	70.99	4.89E-01	1.14E-01	3.91E+02		
Single		Coats-Redfern	10	0.99018	A4	50.06	7.15E+00	3.01E-02	1.74E+02	-192	181
			15	0.99741	A4	103.89	1.72E+01	2.01E-02	2.33E+02	-109	178
			20	0.99541	A4	97.06	1.61E+01	2.31E-02	3.00E+02	-118	178
		Average		0.994333		83.67	13.483333	0.02443	235.6667	-139.667	179
		Modified Coats-Redfern	10	0.99018	A4	50.06	6.89E+00	3.01E-02	1.74E+02	-195	183
			15	0.99741	A4	103.89	1.71E+01	2.01E-02	2.33E+02	-110	179
			20	0.99541	A4	97.06	1.60E+01	2.31E-02	3.00E+02	-119	178
		Average		0.994333		83.67	13.33	0.02443	235.6667	-141.333	180
		Doyle's	10	0.99334	A4	58.09	9.66E+00	1.31E-02	7.55E+01	-172	175
			15	0.99786	A4	109.59	1.86E+01	8.82E-03	1.02E+02	-98	176
			20	0.99635	A4	103.24	1.76E+01	1.00E-02	1.30E+02	-106	175
		Average		0.99585		90.306667	15.286667	0.01064	102.5	-125.333	175.333
		Madusudana et.al.	10	0.99034	A4	50.49	********	3.01E-02	1.74E+02	-303	257
			15	0.99743	A4	104.34	3.98E+00	2.02E-02	2.33E+02	-218	254
			20	0.99546	A4	97.51	2.85E+00	2.31E-02	3.00E+02	-228	253
		Average		0.99441		84.113333	3.415	0.02447	235.6667	-249.667	254.667
Composite	3	Coats-Redfern		0.96557	A1.5	146.41	2.49E+01	1.87E-01	4.72E+02		
		Modified Coats-Redfern		0.96557	A1.5	146.41	2.48E+01	1.87E-01	4.72E+02		
		Doyle's		0.97072	A1.5	151.21	2.31E+01	8.11E-02	2.05E+02		
		Madusudana et.al.		0.9658	A1.5	146.9	1.16E+01	1.87E-01	4.72E+02		

Continue Table (4.12):

Method	Step	Equation	β	R	M	E(kJ mol^{-1})	LnA(min^{-1})	S_{xy}	S_b	$\Delta S^{\#}$	$\Delta G^{\#}$
Single		Coats-Redfern	10	0.98986	A1.5	157.69	2.40E+01	9.88E-02	4.81E+02	-53	194
			15	0.98469	A1.5	153.42	2.35E+01	1.10E-01	5.96E+02	-56	192
			20	0.9849	A1.5	152.41	2.30E+01	1.19E-01	5.45E+02	-60	194
		Average		0.986483		154.50667	23.5	0.10927	540.6667	-56.33	193.333
		Modified Coats-Redfern	10	0.98986	A1.5	157.69	2.39E+01	9.88E-02	4.81E+02	-53	19
			15	0.98469	A1.5	153.42	2.34E+01	1.10E-01	5.96E+02	-56	192
			20	0.9849	A1.5	152.41	2.29E+01	1.19E-01	5.45E+02	-61	194
		Average		0.986483		154.50667	23.4	0.10927	540.6667	-56.67	135
		Doyle's	10	0.99135	A1.5	161.76	2.47E+01	4.27E-02	2.08E+02	-46	193
			15	0.98697	A1.5	157.79	2.44E+01	4.76E-02	2.58E+02	-49	192
			20	0.98723	A1.5	157.11	2.39E+01	5.15E-02	2.35E+02	-53	194
		Average		0.988517		158.88667	24.333333	0.04727	233.6667	-49.33	193
		Madusudana et.al.	10	0.98993	A1.5	158.18	1.07E+01	9.88E-02	4.81E+02	-163	269
			15	0.98479	A1.5	153.91	1.03E+01	1.10E-01	5.96E+02	-166	267
			20	0.98501	A1.5	152.92	9.77E+00	1.19E-01	5.44E+02	-171	269
		Average		0.986577		155.00333	10.256667	0.10927	540.3333	-166.667	268.333

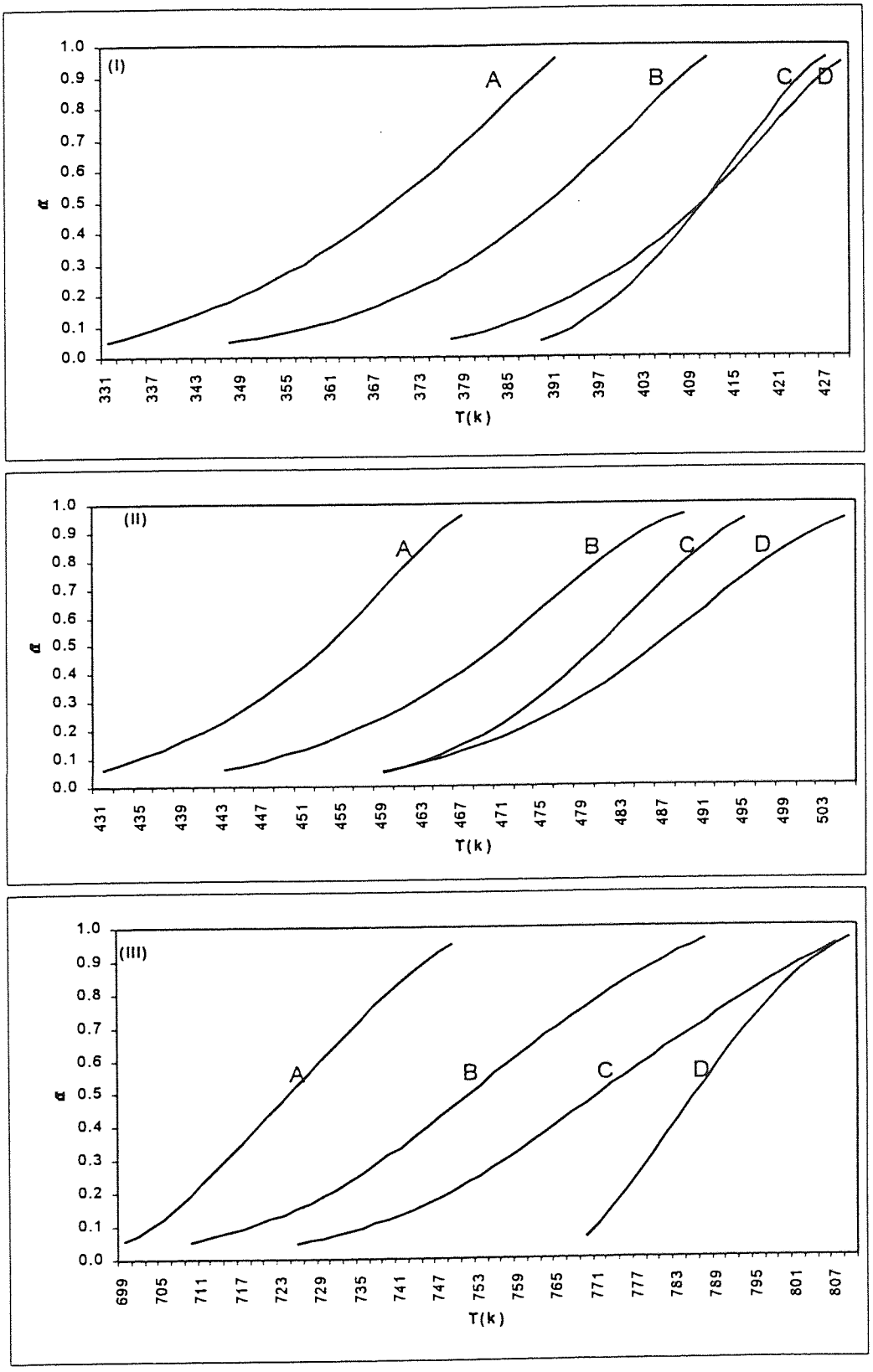

Fig. (4.48): Dynamic DSC data for nickel (II) picolinate thermal decomposition. Heating rate: curve a, 5°C min^{-1}; B 10°Cmin^{-1}; C 15°Cmin^{-1};D 20°Cmin^{-1}. Diagrams [(I) and (II)] dehydration and diagram (III) decomposition.

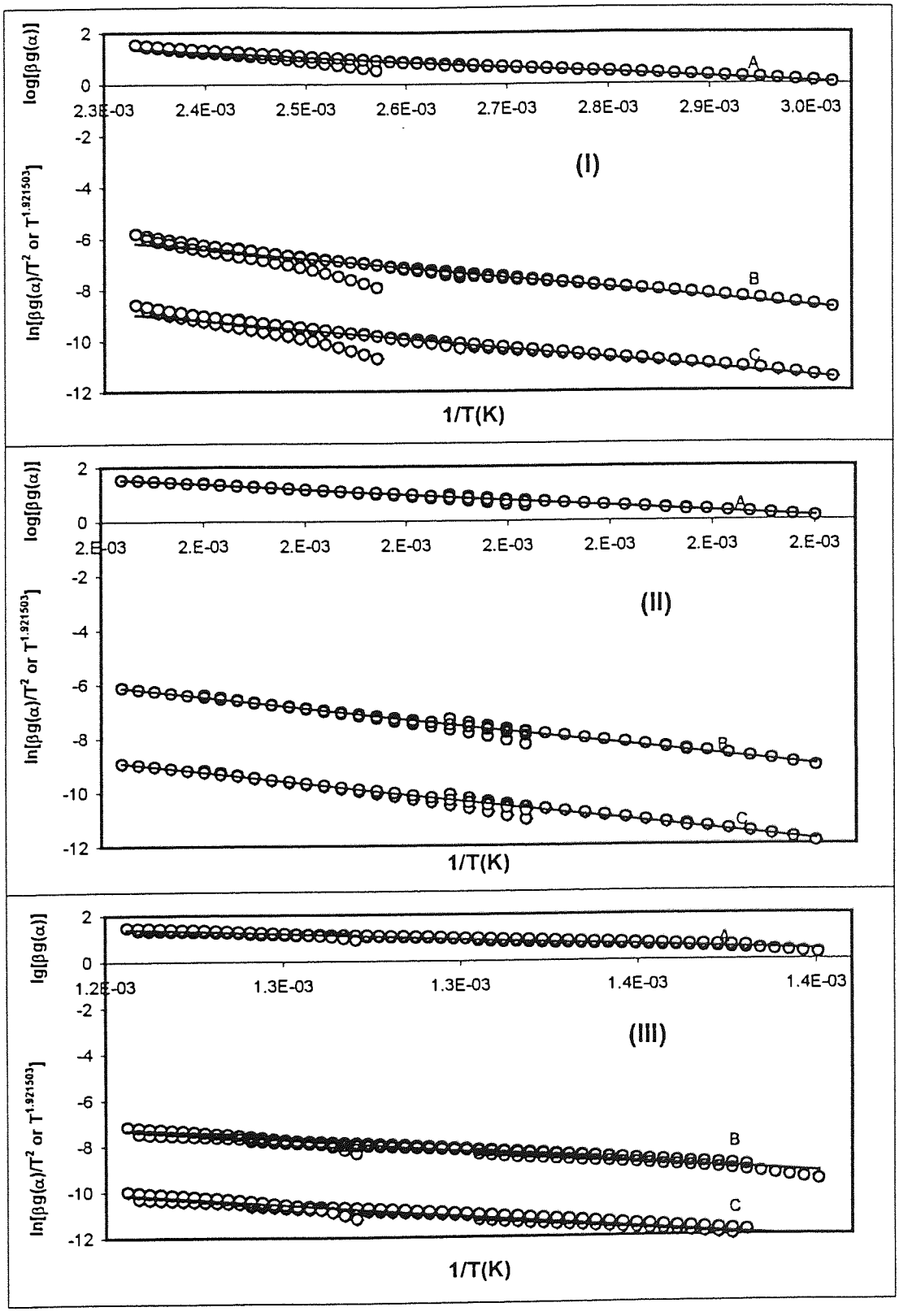

Fig.(4.49): Composite analysis of the dynamic DSC data for nickel(II) picolinate complexe based on (A) Doyle's equation, (B) Madhusudanan et.al. and (C) coats-Redfern and modified Coats-Redfern. Diagram(I) dehdration and diagrams [(II) and (III)] decomposition.

Table (4.13): Kinetic parameters, thermodynamic parameters and regression results for thermal decomposition of nickel(II) picolinate involving single heating rate and composite methods based on integral equations.

Method	Step	Equation	β	R	M	E(kJ mol^{-1})	LnA(min^{-1})	S_{xy}	S_b	$\Delta S^{\#}$	$\Delta G^{\#}$
Composite	1	Coats-Redfern		0.95661	A2	30.12	1.03E+01	1.93E-01	1.06E+02		
		Modified Coats-Redfern		0.95661	A2	30.12	1.00E+01	1.93E-01	1.06E+02		
		Doyle's		0.96911	A2	34.63	1.03E+01	8.48E-02	4.64E+01		
		Madusudana et.al.		0.95724	A2	30.37	-3.02E+00	1.93E-01	1.06E+02		
Single		Coats-Redfern	5	0.99574	A2	27.22	6.86E+00	4.33E-02	5.63E+01	-190	101
			10	0.99699	A2	30.39	8.03E+00	3.91E-02	5.10E+01	-180	100
			15	0.9961	A2	65.31	1.87E+01	5.09E-02	1.64E+02	-92	101
			20	0.99872	A2	41.96	1.18E+01	2.56E-02	5.12E+01	-149	99
		Average		0.996888		41.22	11.3475	0.03973	80.625	-152.75	100.25
		Modified Coats-Redfern	5	0.99574	A2	27.22	6.59E+00	4.33E-02	5.63E+01	-192	101
			10	0.99699	A2	30.39	7.80E+00	3.91E-02	5.10E+01	-182	101
			15	0.9961	A2	65.31	1.86E+01	5.09E-02	1.64E+02	-93	101
			20	0.99872	A2	41.96	1.16E+01	2.56E-02	5.12E+01	-150	100
		Average		0.996888		41.22	11.1475	0.03973	80.625	-154.25	100.75
		Doyle's	5	0.99712	A2	31.57	9.36E+00	1.88E-02	2.45E+01	-169	97
			10	0.99773	A2	34.87	1.04E+01	1.78E-02	2.32E+01	-160	97
			15	0.99687	A2	68.55	1.99E+01	2.18E-02	7.04E+01	-82	100
			20	0.999	A2	46.26	1.38E+01	1.14E-02	2.27E+01	-132	97
		Average		0.99768		45.3125	13.365	0.01745	35.2	-135.75	97.75
		Madusudana et.al.	5	0.99581	A2	27.45	********	4.33E-02	5.63E+01	-301	143
			10	0.99703	A2	30.64	********	3.92E-02	5.11E+01	-291	143
			15	0.99614	A2	65.57	5.43E+00	5.09E-02	1.64E+02	-201	143
			20	0.99873	A2	42.23	********	2.56E-02	5.12E+01	-259	142
		Average		0.996928		41.4725	5.43	0.03975	80.65	-263	142.75

Continue Table (4.13):

Method	Step	Equation	β	R	M	E(kJ mol^{-1})	LnA(min^{-1})	S_{xy}	S_b	$\Delta S^{\#}$	$\Delta G^{\#}$
Composite	2	Coats-Redfern		0.99091	A2	70.53	1.95E+01	9.43E-02	1.26E+02		
		Modified Coats-Redfern		0.99091	A2	70.53	1.94E+01	9.43E-02	1.26E+02		
		Doyle's		0.99255	A2	74.45	1.84E+01	4.11E-02	5.48E+01		
		Madusudana et.al.		0.99098	A2	70.83	6.26E+00	9.43E-02	1.26E+02		
Single		Coats-Redfern	5	0.99825	A2	77.86	1.91E+01	3.19E-02	1.35E+02	-89.54	119
			10	0.99919	A2	67.8	1.63E+01	2.19E-02	7.00E+01	-113.17	120
			15	0.99836	A2	94.79	2.33E+01	3.33E-02	1.58E+02	-54.83	120
			20	0.99901	A2	72.97	1.77E+01	2.43E-02	8.31E+01	-101.73	120
		Average		0.998703		78.355	19.1	0.02785	111.525	-89.8175	119.75
		Modified Coats-Redfern	5	0.99825	A2	77.86	1.90E+01	3.19E-02	1.35E+02	-90.4	120
			10	0.99919	A2	67.8	1.62E+01	2.19E-02	7.00E+01	-114.17	120
			15	0.99836	A2	94.79	2.32E+01	3.33E-02	1.58E+02	-55.53	120
			20	0.99901	A2	72.97	1.75E+01	2.43E-02	8.31E+01	-102.65	120
		Average		0.998703		78.355	18.975	0.02785	111.525	-90.6875	120
		Doyle's	5	0.99853	A2	81.13	2.02E+01	1.39E-02	5.87E+01	-80.32	118
			10	0.99935	A2	71.83	1.77E+01	9.53E-03	3.05E+01	-101.31	119
			15	0.99864	A2	97.67	2.42E+01	1.43E-02	6.79E+01	-47.62	119
			20	0.99924	A2	77.01	1.90E+01	1.03E-02	3.51E+01	-90.42	119
		Average		0.99894		81.91	20.275	0.01201	48.05	-79.9175	118.75
		Madusudana et.al.	5	0.99826	A2	78.15	5.89E+00	3.19E-02	1.35E+02	-199.59	170
			10	0.9992	A2	68.1	3.04E+00	2.19E-02	7.00E+01	-223.24	171
			15	0.99838	A2	95.1	1.01E+01	3.33E-02	1.58E+02	-164.81	171
			20	0.99903	A2	73.29	4.43E+00	2.43E-02	8.30E+01	-211.75	171
		Average		0.998718		78.66	5.865	0.02785	111.5	-199.848	170.75

Continue Table (4.13):

Method	Step	Equation	β	R	M	E(kJ mol^{-1})	LnA(min^{-1})	S_{xy}	S_b	$\Delta S^{\#}$	$\Delta G^{\#}$
Composite	3	Coats-Redfern		0.97429	A3	83.28	1.40E+01	1.20E-01	2.06E+02		
		Modified Coats-Redfern		0.97429	A3	83.28	1.39E+01	1.20E-01	2.06E+02		
		Doyle's		0.98049	A3	91.12	1.35E+01	5.22E-02	8.90E+01		
		Madusudana et.al.		0.97458	A3	83.78	8.23E-01	1.20E-01	2.06E+02		
Single		Coats-Redfern	5	0.98347	A3	94.39	1.34E+01	6.23E-02	4.27E+02	-137.41	158
			10	0.99594	A3	65.3	8.44E+00	3.01E-02	1.15E+02	-178.33	147
			15	0.99437	A3	65.09	8.49E+00	3.54E-02	1.32E+02	-177.94	147
			20	0.97498	A3	138.8	2.05E+01	7.79E-02	8.73E+02	-78.21	175
		Average		0.98719		90.895	12.7075	0.05143	386.75	-142.973	156.75
		Modified Coats-Redfern	5	0.98347	A3	94.39	1.33E+01	6.23E-02	4.27E+02	-138.12	158.01
			10	0.99594	A3	65.3	8.32E+00	3.01E-02	1.15E+02	-179.37	148
			15	0.99437	A3	65.09	8.37E+00	3.54E-02	1.32E+02	-178.98	148
			20	0.97498	A3	138.8	2.04E+01	7.79E-02	8.73E+02	-78.68	175
		Average		0.98719		90.895	12.5975	0.05143	386.75	-143.788	157.253
		Doyle's	5	0.98707	A3	101.2	1.50E+01	2.69E-02	1.84E+02	-123.52	158
			10	0.99728	A3	73.9	1.08E+01	1.27E-02	4.86E+01	-158.56	147
			15	0.99624	A3	73.99	1.09E+01	1.50E-02	5.59E+01	-157.77	147
		Average		0.985655		88.205882	12.085176	0.05771	286.0588	-144.127	155.539
		Madusudana et.al.	5	0.98363	A3	94.86	1.73E-01	6.23E-02	4.27E+02	-247.11	209
			10	0.99601	A3	65.79	********	3.01E-02	1.15E+02	-288.08	199
			15	0.99446	A3	65.59	********	3.54E-02	1.32E+02	-287.67	198
			20	0.97516	A3	139.31	7.30E+00	7.79E-02	8.73E+02	-187.88	226
		Average		0.987315		91.3875	3.7365	0.05143	386.75	-252.685	208

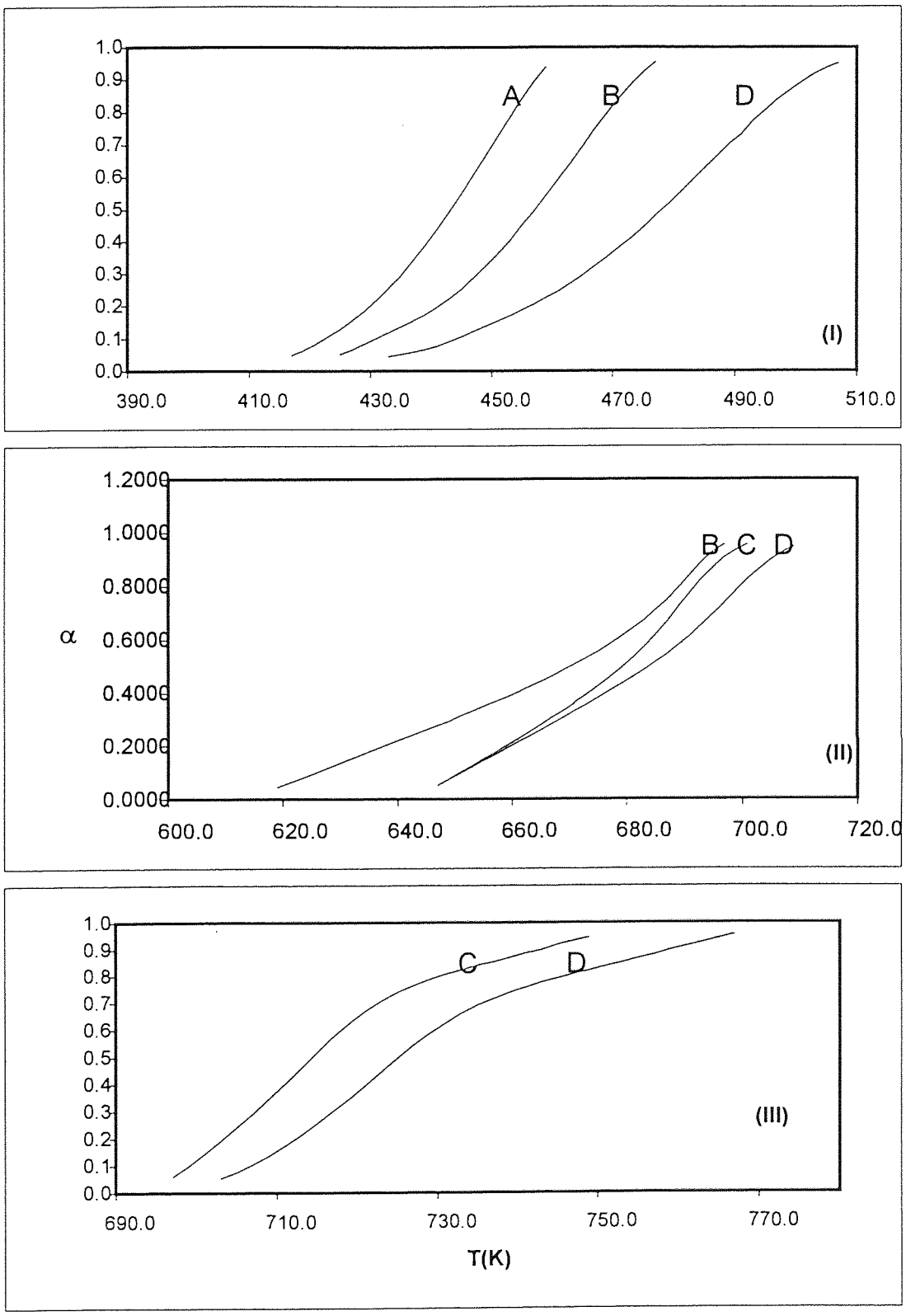

Fig. (4.50): Dynamic DSC data for nickel(II) nicotinate thermal decomposition. Heating rate: curve a, 5°C min^{-1}; B 10°C min^{-1}; C 15°C min^{-1}; D 20°C min^{-1}. Diagram (I) dehydration and diagrams [(II) and (III) decomposition.

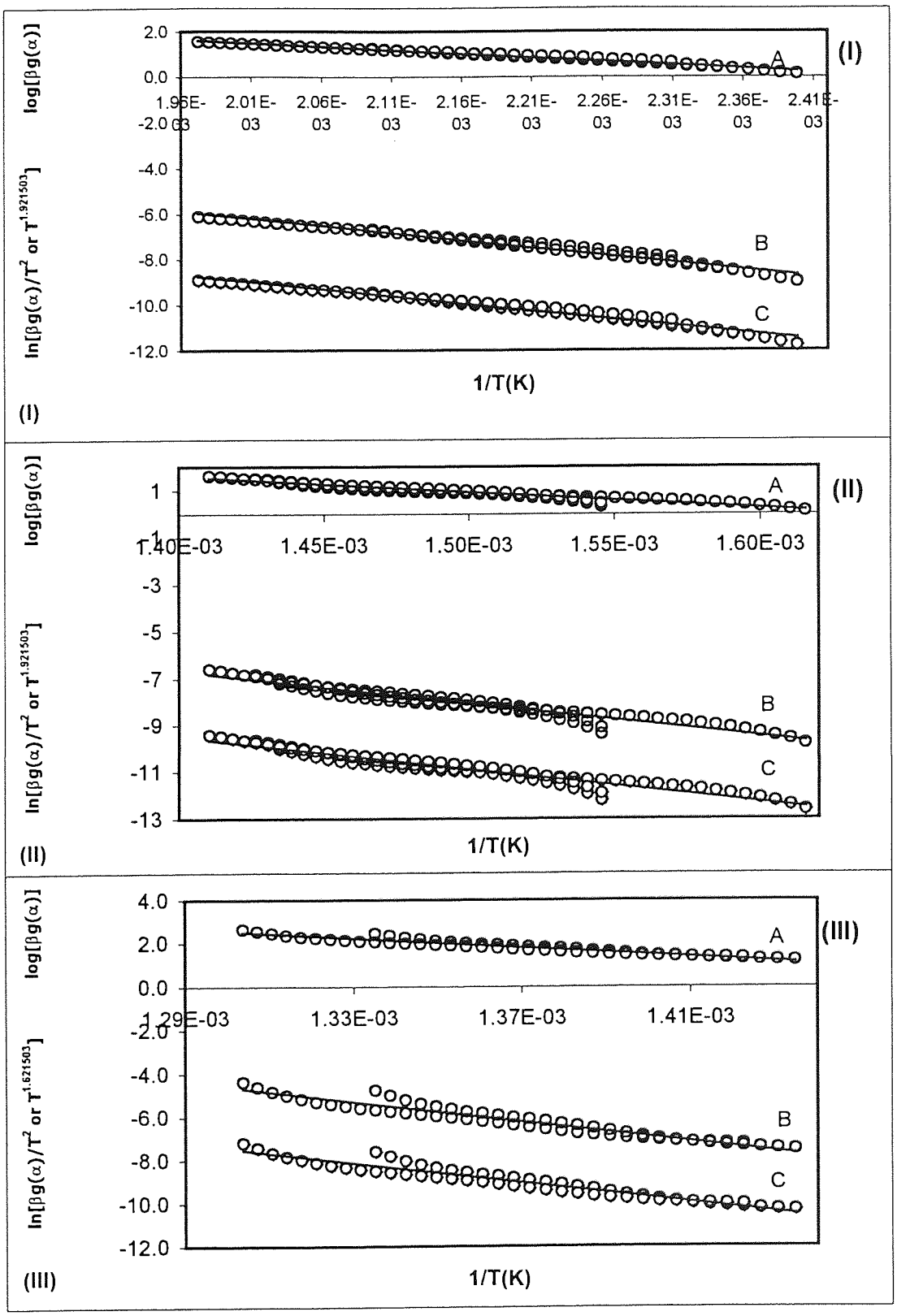

Fig.(4.51): Composite analysis of the dynamic DSC data for nickel(II) nicotinate complex based on (A) Doyle's equation, (B) Madhusudanan et.al. and (C) coats-Redfern and modified Coats-Redfern. Diagram(I) dehydration and diagrams [(II) and(III)] decomposition.

Table (4.14): Kinetic parameters, thermodynamic parameters and regression results for thermal decomposition of nickel(II) picolinate involving single heating rate and composite methods based on integral equations.

Method	Step	Equation	β	R	M	E(kJ mol^{-1})	LnA(min^{-1})	S_{xy}	S_b	$\Delta S^{\#}$	$\Delta G^{\#}$
Composite	1	Coats-Redfern		0.98735	A2	52.41	1.51E+01	1.09E-01	1.10E+02		
		Modified Coats-Redfern		0.98735	A2	52.41	1.50E+01	1.09E-01	1.10E+02		
		Doyle's		0.99064	A2	57.09	1.44E+01	4.63E-02	4.69E+01		
		Madusudana et.al.		0.98751	A2	52.71	1.88E+00	1.08E-01	1.10E+02		
Single		Coats-Redfern	6	0.9979	A2	65.09	1.62E+01	3.53E-02	1.14E+02	-113.93	116
			10	0.99862	A2	54.82	1.32E+01	2.77E-02	6.94E+01	-138.24	117
			20	0.9989	A2	42.71	9.96E+00	2.48E-02	4.03E+01	-165.55	117
		Average		0.998473		54.206667	13.12	0.02927	74.56667	-139.24	116.667
		Modified Coats-Redfern	6	0.9979	A2	65.09	1.60E+01	3.53E-02	1.14E+02	-114.95	117
			10	0.99862	A2	54.82	1.31E+01	2.77E-02	6.94E+01	-139.46	118
			20	0.9989	A2	42.71	9.77E+00	2.48E-02	4.03E+01	-167.15	118
		Average		0.998473		54.206667	12.956667	0.02927	74.56667	-140.52	117.667
		Doyle's	6	0.99834	A2	68.81	1.76E+01	1.52E-02	4.88E+01	-102.42	115
			10	0.99893	A2	59.25	1.50E+01	1.20E-02	3.02E+01	-123.78	115
			20	0.99927	A2	48.02	1.22E+01	1.03E-02	1.68E+01	-146.98	114
		Average		0.998847		58.693333	14.933333	0.0125	31.93333	-124.393	114.667
		Madusudana et.al.	6	0.99792	A2	65.37	2.93E+00	3.53E-02	1.14E+02	-224.03	166
			10	0.99863	A2	55.11	********	2.77E-02	6.94E+01	-248.41	167
			20	0.99891	A2	43.02	********	2.47E-02	4.02E+01	-275.89	167
		Average		0.998487		54.5	2.93	0.02923	74.53333	-249.443	166.667

Continue Table (4.14):

Method	Step	Equation	β	R	M	E(kJmol^{-1})	LnA(min^{-1})	S_{xy}	S_b	$\Delta S^{\#}$	$\Delta G^{\#}$
Composite	2	Coats-Redfern		0.96801	A1.5	115.28	2.22E+01	1.79E-01	3.63E+02		
		Modified Coats-Redfern		0.96801	A1.5	115.28	2.21E+01	1.79E-01	3.63E+02		
		Doyle's		0.97301	A1.5	120.12	2.06E+01	7.81E-02	1.58E+02		
		Madusudana et.al.		0.96823	A1.5	115.71	8.93E+00	1.79E-01	3.63E+02		
Single		Coats-Redfern	10	0.98397	A1.5	93.44	1.53E+01	1.12E-01	3.30E+02	-124.28	178
			15	0.99174	A1.5	155.57	2.69E+01	8.94E-02	4.74E+02	-28.02	1745
			20	0.98829	A1.5	129.63	2.23E+01	1.00E-01	4.39E+02	-66.69	175
		Average		0.988		126.21333	21.5	0.10047	414.3333	-72.9967	699.333
		Modified Coats-Redfern	10	0.98397	A1.5	93.44	1.52E+01	1.12E-01	3.30E+02	-125.36	179
			15	0.99174	A1.5	155.57	2.68E+01	8.94E-02	4.74E+02	-28.65	175
			20	0.98829	A1.5	129.63	2.22E+01	1.00E-01	4.39E+02	-67.45	176
		Average		0.988		126.21333	21.4	0.10047	414.3333	-73.82	176.667
		Doyle's	10	0.98714	A1.5	99.24	1.68E+01	4.84E-02	1.43E+02	-112.13	176
			15	0.99283	A1.5	158.59	2.75E+01	3.88E-02	2.06E+02	-23.14	175
			20	0.99011	A1.5	133.98	2.32E+01	4.33E-02	1.90E+02	-58.93	174
		Average		0.990027		130.60333	22.5	0.0435	179.6667	-64.7333	175
		Madusudana et.al.	10	0.98412	A1.5	93.87	2.09E+00	1.12E-01	3.30E+02	-234.41	254
			15	0.99179	A1.5	156.01	1.37E+01	8.94E-02	4.74E+02	-138.03	250
			20	0.98837	A1.5	130.07	9.03E+00	1.00E-01	4.39E+02	-176.71	251
		Average		0.988093		126.65	8.2733333	0.10047	414.3333	-183.05	251.667

Continue Table (4.14):

	Step	Equation	β	R	M	E(kJ mol^{-1})	LnA(min^{-1})	S_{xy}	S_b	$\Delta S^{\#}$	$\Delta G^{\#}$
Composite	3	Coats-Redfern		0.96673	F2	187.51	3.48E+01	2.11E-01	7.83E+02		
		Modified Coats-Redfern		0.96673	F2	187.51	3.47E+01	2.11E-01	7.83E+02		
		Doyle's		0.97045	F2	189.85	3.23E+01	9.17E-02	3.40E+02		
		Madusudana et.al.		0.96689	F2	187.98	2.15E+01	2.11E-01	7.83E+02		
Single		Coats-Redfern	15	0.99085	F2	220.59	3.77E+01	1.12E-01	7.23E+02	62	176
			20	0.98292	F2	186.9	3.17E+01	1.53E-01	7.56E+02	11	179
		Average		0.986885		203.745	34.7	0.1325	739.5	36.5	177.5
		Modified Coats-Redfern	15	0.99085	F2	220.59	3.77E+01	1.12E-01	7.23E+02	61	177
			20	0.98292	F2	186.9	3.16E+01	1.53E-01	7.56E+02	11	179
		Average		0.986885		203.745	34.65	0.1325	739.5	36	178
			15	0.99171	F2	221.19	3.78E+01	4.88E-02	3.15E+02	62	176
			20	0.9848	F2	189.34	3.21E+01	6.68E-02	3.29E+02	15	179
		Average		0.988255		205.265	34.95	0.0578	322	38.5	177.5
		Madusudana et.al.	15	0.99089	F2	221.06	2.45E+01	1.12E-01	7.23E+02	-49	256
			20	0.983	F2	187.38	1.85E+01	1.53E-01	7.56E+02	-99	258
		Average		0.986945		204.22	21.5	0.1325	739.5	-74	257

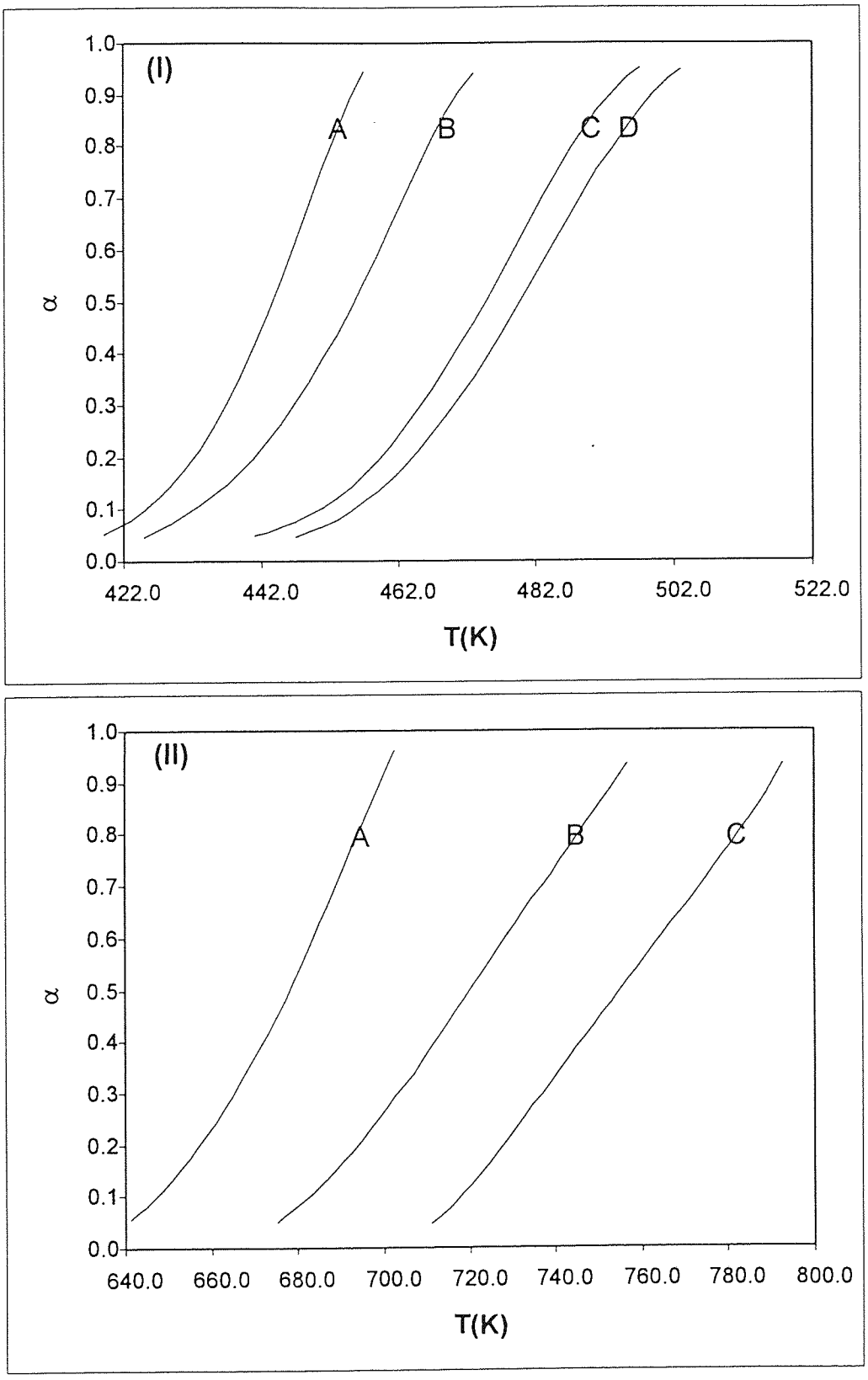

Fig.(4.52): Dynamic measurements for nickel(II) isonicotinate thermal decomposition. Heating rate: curve A, 5°C min^{-1}; B, 10°C min^{-1}; C, 15°C min^{-1}; D, 20°C min^{-1}. Diagram (I) dehydration and diagram (II) decomposition.

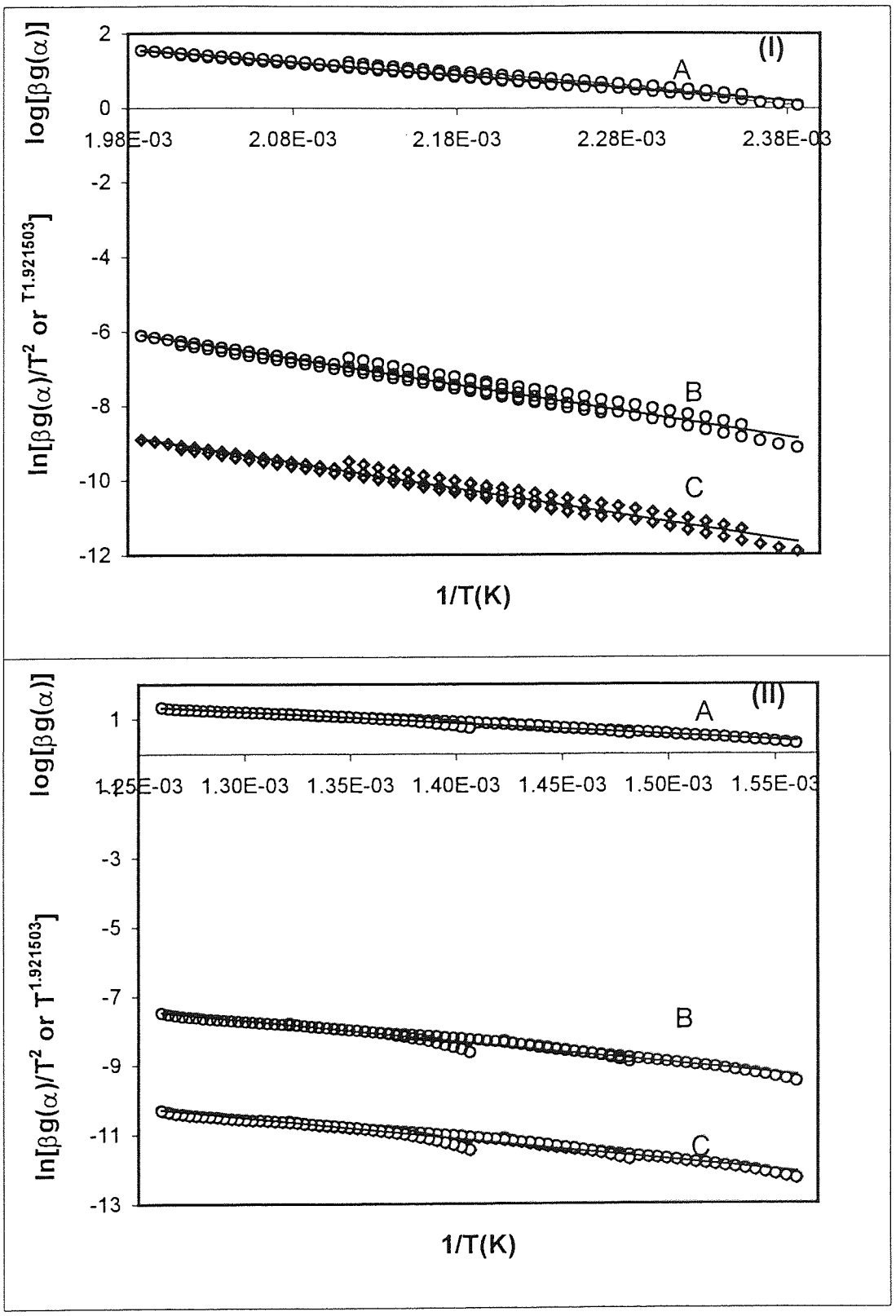

Fig. (4.53): Composite analysis of dynamic DSC data of nickel(II) isonicotinate complex based on (A) Doyle's equationm (B) Madhusudanan et. al. equation, and (C) Coast-Redfern and modified Coast-Redfern equation. Diagram (I) dehydration and diagram (II) decomposition.

Table (4.15): Kinetic parameters, thermodynamic parameters and regression results for thermal decomposition of nickel(II) isonicotinate involving single heating rate and composite methods based on integral equations.

Method	Step	Equation	β	R	M	E(kJ mol^{-1})	LnA(min^{-1})	S_{xy}	S_b	$\Delta S^{\#}$	$\Delta G^{\#}$
Composite	1	Coats-Redfern		0.9818	A2	57.96	1.65E+01	1.36E-01	1.34E+02		
		Modified Coats-Redfern		0.9818	A2	57.96	1.64E+01	1.36E-01	1.34E+02		
		Doyle's		0.9858	A2	62.38	1.56E+01	5.86E-02	5.80E+01		
		Madusudana et.al.		0.9820	A2	58.26	3.28E+00	1.36E-01	1.34E+02		
Single		Coats-Redfern	6	0.9979	A2	65.09	1.62E+01	3.53E-02	1.14E+02	-114	116
			10	0.99862	A2	54.82	1.32E+01	2.77E-02	6.94E+01	-138	117
			20	0.9989	A2	42.71	9.96E+00	2.48E-02	4.03E+01	-166	117
		Average		0.998473		54.206667	13.12	0.02927	74.56667	-139.333	116.667
		Modified Coats-Redfern	6	0.9979	A2	65.09	1.60E+01	3.53E-02	1.14E+02	-115	117
			10	0.99862	A2	54.82	1.31E+01	2.77E-02	6.94E+01	-140	118
			20	0.9989	A2	42.71	9.77E+00	2.48E-02	4.03E+01	-167	118
		Average		0.998473		54.206667	12.956667	0.02927	74.56667	-140.667	117.667
		Doyle's	6	0.99834	A2	68.81	1.76E+01	1.52E-02	4.88E+01	-102	115
			10	0.99893	A2	59.25	1.50E+01	1.20E-02	3.02E+01	-124	115
			20	0.99927	A2	48.02	1.22E+01	1.03E-02	1.68E+01	-147	114
		Average		0.998847		58.693333	14.933333	0.0125	31.93333	-124.333	114.667
		Madusudana et.al.	6	0.99792	A2	65.37	2.93E+00	3.53E-02	1.14E+02	-224	166
			10	0.99863	A2	55.11	********	2.77E-02	6.94E+01	-248	166.97
			20	0.99891	A2	43.02	********	2.47E-02	4.02E+01	-275.89	167
		Average		0.998487		54.5	2.93	0.02923	74.53333	-249.297	166.657

Continue Table (4.15):

Method	Step	Equation	β	R	M	E(kJ mol^{-1})	LnA(min^{-1})	S_{xy}	S_b	$\Delta S^{\#}$	$\Delta G^{\#}$
Composite	2	Coats-Redfern		0.96801	A3	115.28	2.22E+01	1.79E-01	3.63E+02		
		Modified Coats-Redfern		0.96801	A3	115.28	2.21E+01	1.79E-01	3.63E+02		
		Doyle's		0.97301	A3	120.12	2.06E+01	7.81E-02	1.58E+02		
		Madusudana et.al.		0.96823	A3	115.71	8.93E+00	1.79E-01	3.63E+02		
Single		Coats-Redfern	10	0.98397	A2	93.44	1.53E+01	1.12E-01	3.30E+02	-124	178
			15	0.99174	A2	155.57	2.69E+01	8.94E-02	4.74E+02	-28	175
			20	0.98829	A2	129.63	2.23E+01	1.00E-01	4.39E+02	-67	175
		Average		0.988		126.21333	21.5	0.10047	414.3333	-73	176
		Modified Coats-Redfern	10	0.98397	A2	93.44	1.52E+01	1.12E-01	3.30E+02	-125	179
			15	0.99174	A2	155.57	2.68E+01	8.94E-02	4.74E+02	-29	175
			20	0.98829	A2	129.63	2.22E+01	1.00E-01	4.39E+02	-68	176
		Average		0.988		126.21333	21.4	0.10047	414.3333	-74	176.667
		Doyle's	10	0.98714	A2	99.24	1.68E+01	4.84E-02	1.43E+02	-112	176
			15	0.99283	A2	158.59	2.75E+01	3.88E-02	2.06E+02	-23	174
			20	0.99011	A2	133.98	2.32E+01	4.33E-02	1.90E+02	-59	174
		Average		0.990027		130.60333	22.5	0.0435	179.6667	-64.67	174.667
		Madusudana et.al.	10	0.98412	A2	93.87	2.09E+00	1.12E-01	3.30E+02	-234	254
			15	0.99179	A2	156.01	1.37E+01	8.94E-02	4.74E+02	-138	250.28
			20	0.98837	A2	130.07	9.03E+00	1.00E-01	4.39E+02	-177	251
		Average		0.988093		126.65	8.2733333	0.10047	414.3333	-183	251.76

4.7 ELECTRICAL STUDIES

The work presented in this chapter is an attempt to study the effects of the DC and AC electric field on some prepared complexes.

4.7.1 Temperature dependence of DC conductivity

The variation of the electrical conductivity (σ_{dc}) with temperature (T) for samples of hydrated cobalt isonicotinate [$Co(IA)_2 4H_2O$], hydrated nickel isonicotinate [$Ni(IA)_2 3.5H_2O$], and hydrated copper isonicotinate [$Cu(IA)_2 4.5H_2O$] was investigated to obtain comparative information on the conduction process. From Fig. 4.54 it can be seen that at a relatively low temperature range the values of the electrical conductivity of all three samples decrease with an increase in temperature. This attenuated part in $\ln\sigma$ - $10^3/T$ relation may be described by an Arrhenius relation[105]

$$\sigma_{dc} = BT \exp(\Delta\bar{E}/KT) \qquad (4.3)$$

where B is the temperature independent pre-exponential parameter, $\Delta\bar{E}$ is an activation energy term concerning the attenuation in the conduction process, and K is Boltzmann's constant. The values of $\Delta\bar{E}$, which can be calculated by the best fit of equation 4.3, are listed in Table 4.16. For the sample [$Cu(IA)_2$ $4.5H_2O$] the attenuation in the electrical conductivity is extended to a temperature of approximately 80°C. Then it passes through a minimum before rising with further increase in temperature. The activation in σ_{dc} with T may then be described according to the Arrhenius relation as:

$$\sigma_{dc} = \frac{A}{T}\exp^{(-\Delta E/KT)} \qquad (4.4)$$

where ΔE is the activation energy of conduction and A is temperature independent parameter, the value of ΔE, which fits this equation for copper isonicotinate hydrate, is equal 0.68 eV (Table 4.16).

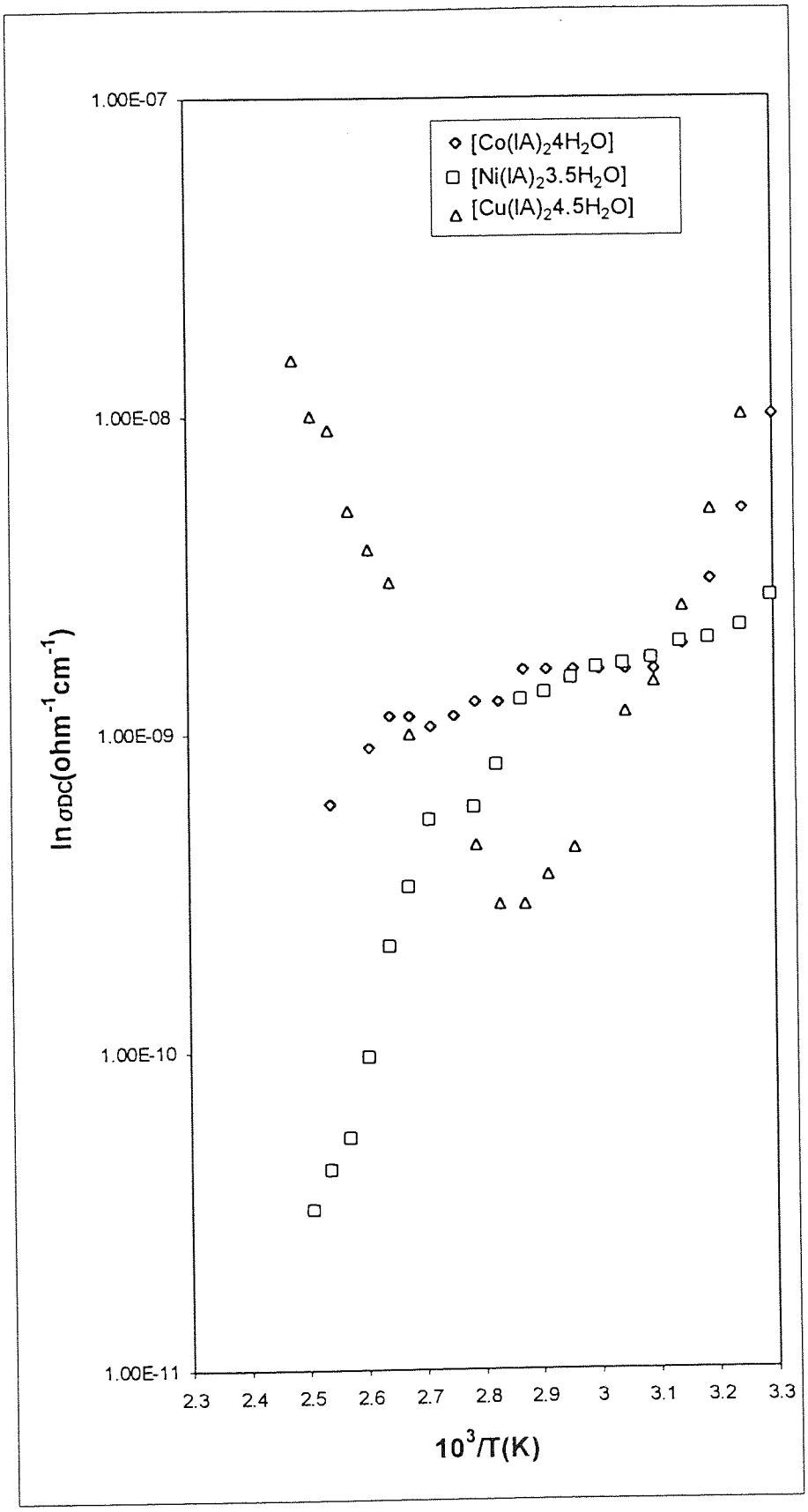

Fig. (4.54): Temperature dependence of electrical conductivity for direct current.

Table 4.16

Activation energy of conduction

Compound	$\Delta\bar{E}$ (eV) (35-50°C)	ΔE(eV) (100-150°C)
$Co(IA)_2\ 4H_2O$	0.67	-
$Ni(IA)_2\ 3.5H_2O$	0.11	-
$Cu(IA)_2\ 4.5H_2O$	1.10	0.68

The attenuation in conductivity with temperature for all investigated samples in the relatively low temperature range may be attributed to hydration of samples. Therefore, the presence of such H_2O molecules results in protonic conduction which contributes remarkably to the conductivity[106]. The increases in temperature lead to dehydration of both absorbed and lattice water at grain boundaries. Chowdhry et al.[107] have attributed the conduction of dehydrated metal oxide materials at relatively low temperatures up to 100°C to protonic conduction. In addition, England et al.[106] have shown that the protonic conduction is strongly dependent on the water content of metal oxides from which the high proton conductivity necessitates a large concentration of mobile protons with high mobility. However, it is separately argued that the absorbed water may reduce the binding energy of protons or attenuate the activation energy of a hopping mechanism for conduction[108]. Therefore, as the temperature is raised, water content decreases which results in the discontinuity of the water chain (the rigid hydrogen bond network becomes weak), which leads to the reduction of proton concentration and protonic jumping between water molecule terminals. This, in turn, leads to the observed attenuation in σ_{dc} with an increase in temperature. Shash and Aly[109] have studied the effect of water content on the electrical conductivity and they concluded that as the water content increases the activation energy decreases.

The thermal analysis for the three samples studied here indicates that the starting temperature for dehydration of the sample of $[Cu(IA)_2\ 4.5H_2O]$ is the lowest of the three. Thus, the water content in this sample disappears early, which causes the appearance of the minimum in the $\ln\sigma$- $10^3/T$ relation and the activation in the electrical conductivity observed (Table 4.8). For the other two samples containing Co and Ni, the attenuation in σ is extended to higher temperatures and, thus, the activation part in $\ln\sigma$-$10^3/T$ relation was not observed in this range of temperature.

4.7.2 Temperature and frequency dependence of AC conductivity:

The AC conductivity (σ_T) of the three samples having the same ligand, isonicotinic, with different metals, Co, Ni, and Cu, was measured against $10^3/T$. Fig 4.55 shows, as a representational figure, the dependence of σ_T on temperature for nickel isonicotinate hydrate, $[Ni(IA)_2\ 3.5H_2O]$. It is noticed that at a relatively high temperature range, as the frequency increases the values of σ_T increases; whereas in the relatively low range of temperature this dependence is weaker. Similar to the DC conductivity dependence on temperature, the value of AC conductivity attenuates with a rise in temperature, and this may be due to the dehydration of these samples.

The dependence of σ_T on the frequency at different fixed temperatures for nickel isonicotinate hydrate is shown in Fig. 4.56. The values of σ_T increase with an increase in frequency obeying the relation $\sigma_T = A\omega^s$, where s is a parameter concerning the type of conduction mechanism, A is a constant, and $\omega = 2\pi f$, where f is the frequency. The values of s have been calculated from the plots of log σ_{ac} vs. log f (calculated experimental values of s) for nickel isonicotinate hydrate Fig. 4.57. These values were found to slowly increase with temperature as shown in Table 4.17.

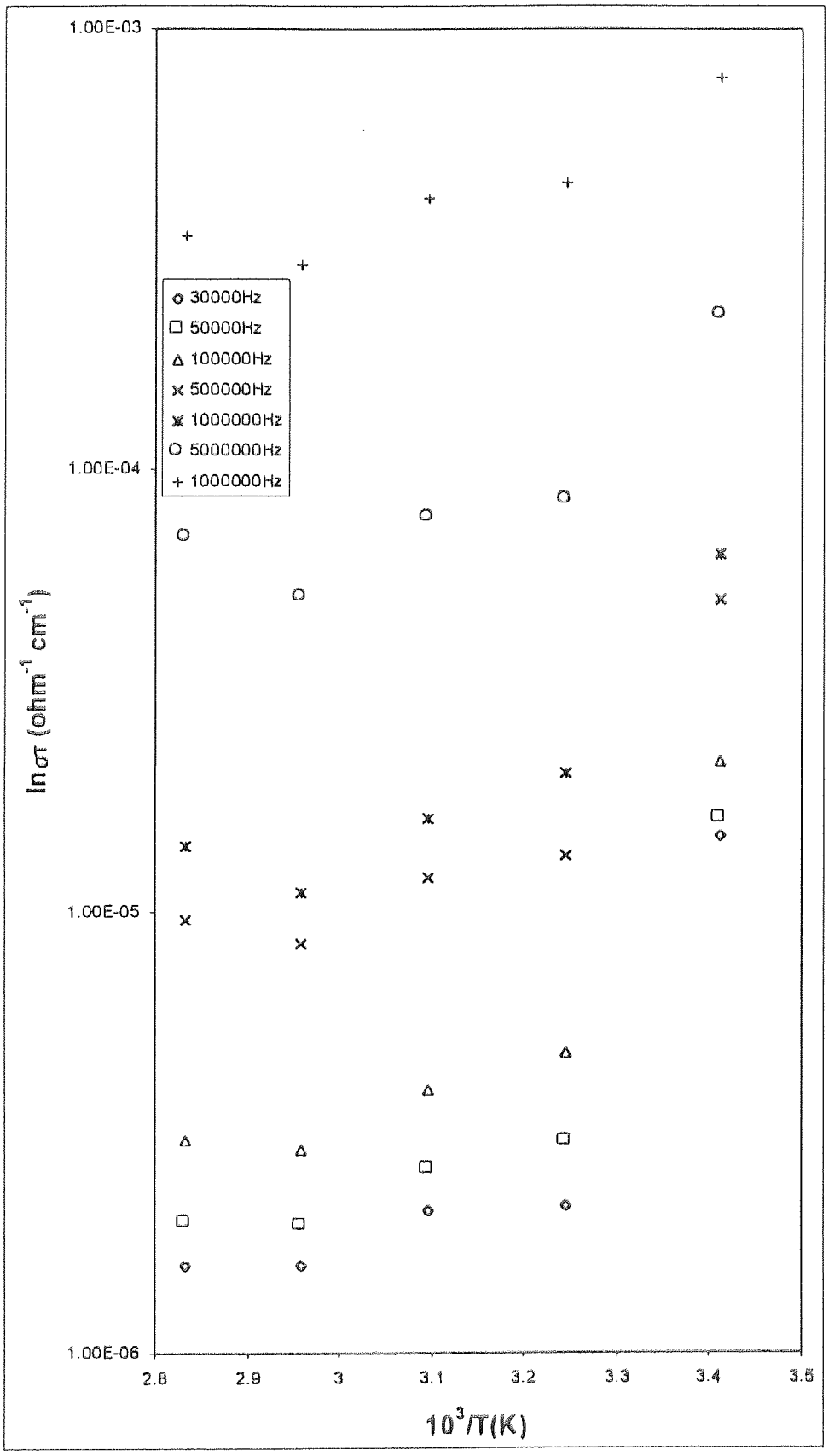

Fig.(4.55): Temperature dependence of electrical conductivity for alternative current.

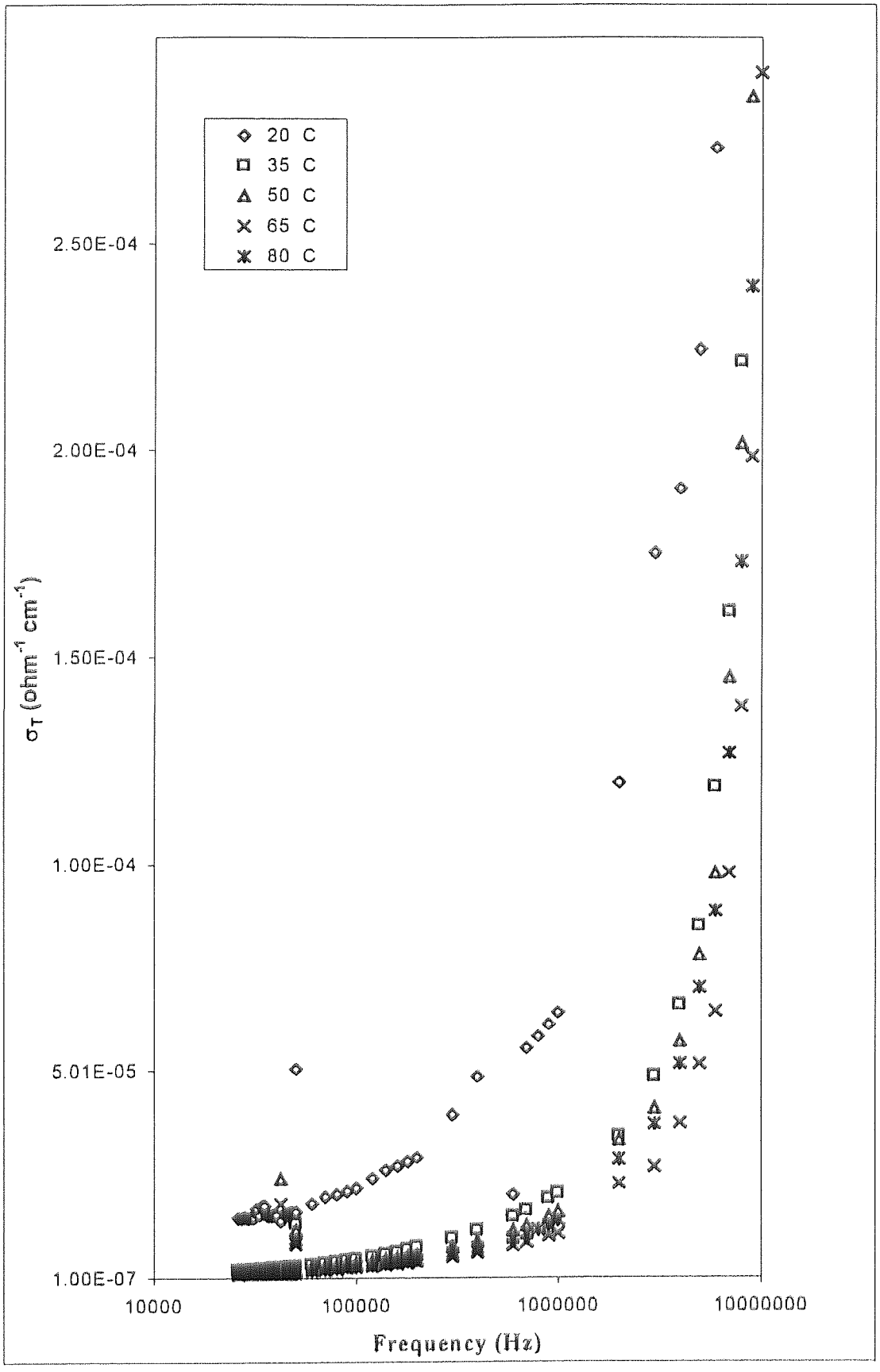

Fig.(4.56): Frequency dependence of electrical conductivity.

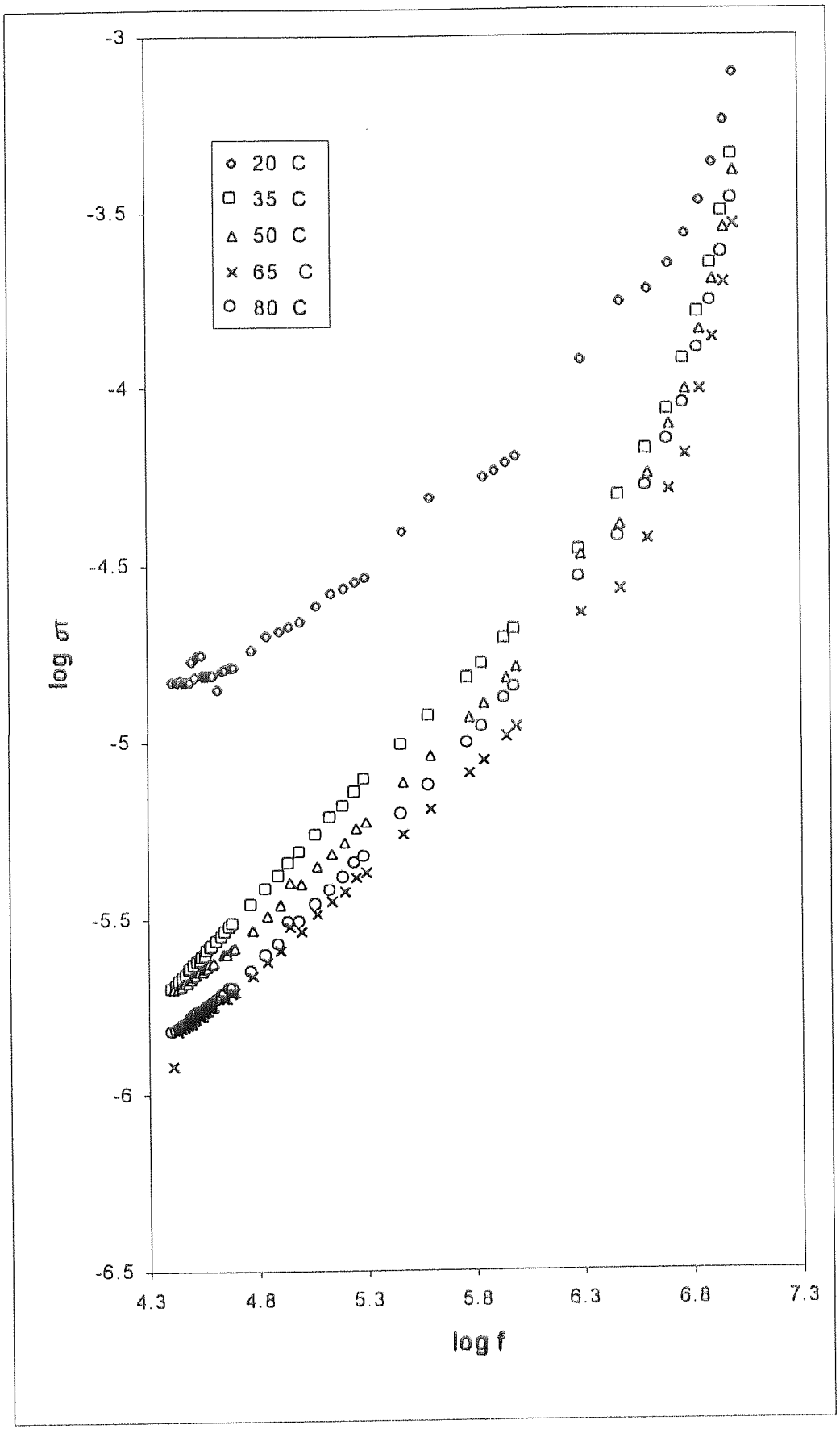

Fig (4.57): log σ_T vs. log f

Table 4.17: The values of s parameter for nickel isonicotinate hydrate $[Ni(IA)_2 3.5H_2O]$.

Temperature	20	35	50	65	85
Parameter s	0.54	0.60	0.61	0.64	0.68

The AC conductivity has been expressed by Pollak[110], according to the relation:

$$\sigma_{AC} = \frac{\pi^3}{96} e^2 kT[N(E_f)^2 \alpha^{-5} \omega (\ln \upsilon_o)/\omega)^4] \quad (4.5)$$

where e is the electron charge, k is Boltzmane constant, T is absolute temperature, $N(E_f)$ is the density of states, α is the electron wave function decay constant, ν_o is the characteristic phonon frequency, and f is the frequency.

The values of $N(E_f)$ can be calculated using the value of AC conductivity in equation 4.5. The values of $N(E_f)$ depend upon the value of α and are almost independent of the value of ν_o. Assuming the value of α =0.5 A^{o-1}, the value $N(E_f)$ has been calculated at fixed frequency equal to $5x10^5$ Hz at different temperatures for nickel isonicotinate hydrate, $[Ni(IA)_2 3.5H_2O]$, as the representative one. The values of $N(E_f)$ are given in Table 4.18. The order of values of $N(E_f)$ is 10^{23} eV^{-1} cm^{-3}. From Table 4.18, it is noticed that the value of $N(E_f)$ decreases as the temperature increases, which conforms to the behavior of DC conductivity against temperature in which an attenuation in σ_{ac} versus temperature has occurred.

The values of both the parameter s and $N(E_f)$ for nickel isonicotinate hydrate $[Ni(IA)_2 3.5H_2O]$ have almost the values for cobalt isonicotinate hydrate $[Co(IA)_2.4H_2O]$ and copper isonicotinate hydrate $[Cu(IA)_2.4.5H_2O]$. This means that the variation of different metals has no effect on either the mechanism nor the values of the mentioned parameters calculated.

Table 4.18: Values of σ_T and $N(E_f)$ at $5x10^5$ Hz at different temperatures for the compound of nickel isonicotinate hydrate,$[Ni(IA)_2 3.5H_2O]$.

Temperature (T°K)	σ_T at $5x10^5$Hz,($sec^{-1}cm^{-1}$)	$N(E_f)$ for A = 0.5(eV^{-1} cm^{-3})
293	$2.25x10^{-4}$	$11.4x10^{23}$
308	$8.51x10^{-5}$	$6.85x10^{23}$
323	$7.81x10^{-5}$	$6.41x10^{23}$
338	$5.61x10^{-5}$	$5.09x10^{23}$
353	$7.02x10^{-5}$	$5.81x10^{23}$

Fig.4.58 illustrates the dependence of dielectric constant ε' on frequency at different constant temperatures for nickel isonicotinate hydrate. The values of ε' decrease with an increase in frequency passing through a minimum value at about $3x10^6$ Hz. Then, it increases at a very high frequency. Also, it is noticed that the values of ε' decrease as the temperature is increased. The compound of nickel isonicotinate hydrate shows the same values and behavior as the other two compounds, cobalt isonicotinate hydrate and copper isonicotinate hydrate. The attenuation in ε' with frequency in a relatively low frequency range may be due to the absence of most polarizing items (molecules and atoms) with increasing frequency. The raising of ε' with the frequency in the very high frequency range is due to the electronic polarization only.

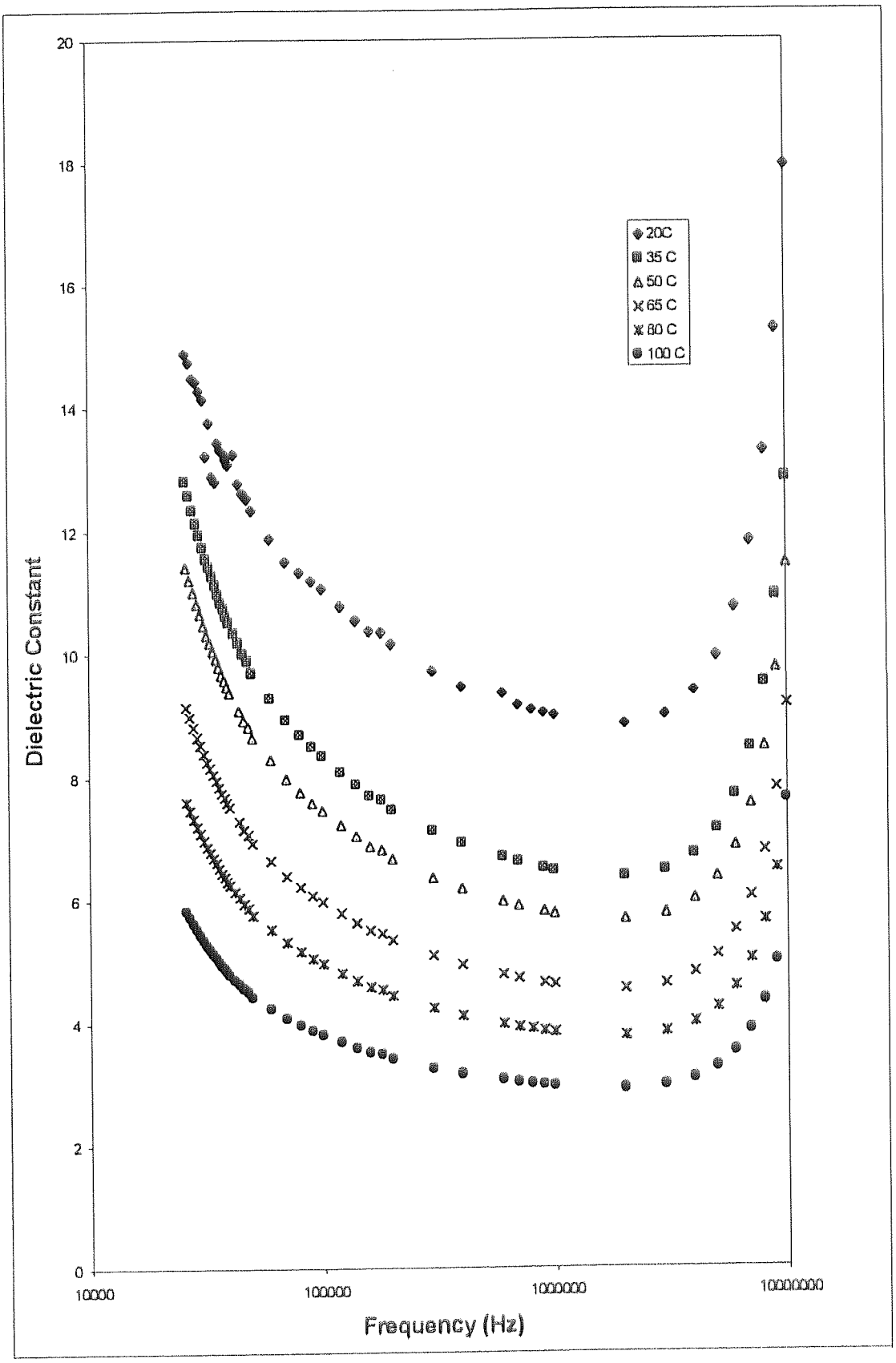

Fig.(4.58):Frequency dependence of dielectric constant.

The dependence of the dielectric loss, ε'' on the frequency, in general, can be discussed according to the following: At a relatively or very low frequency dielectric loss, ε'', attenuates with frequency. This may be due to the appearance of a conduction loss leading to a migration and reordering of atoms over large distances. The applied field in this situation tends to supply the required energy. In a relatively high frequency the values of dielectric loss ε'' increase with the frequency. This may be due to the contribution of ions jumping and conduction loss of ion migration loss, in addition to the electron polarization loss. The atoms in the network can vibrate around their equilibrium positions. Whenever the applied electric field alternates at a frequency near one of the constituent atoms, they are excited to high resonant amplitudes accompanied by high dielectric loss.

Fig.(4.59) illustrates the dependence of the dielectric loss, ε'', on the frequency in a very high range. It is noticed that as the frequency increases the values of ε'' decrease. This may be attributed to the fact that, in the very high frequency range, the ion vibrations are the only source of the dielectric loss. It is not very clear that there is a shift of the loss-peak to higher frequency with the increase in temperature. This is consistent with the Debye model for dielectric relaxation.

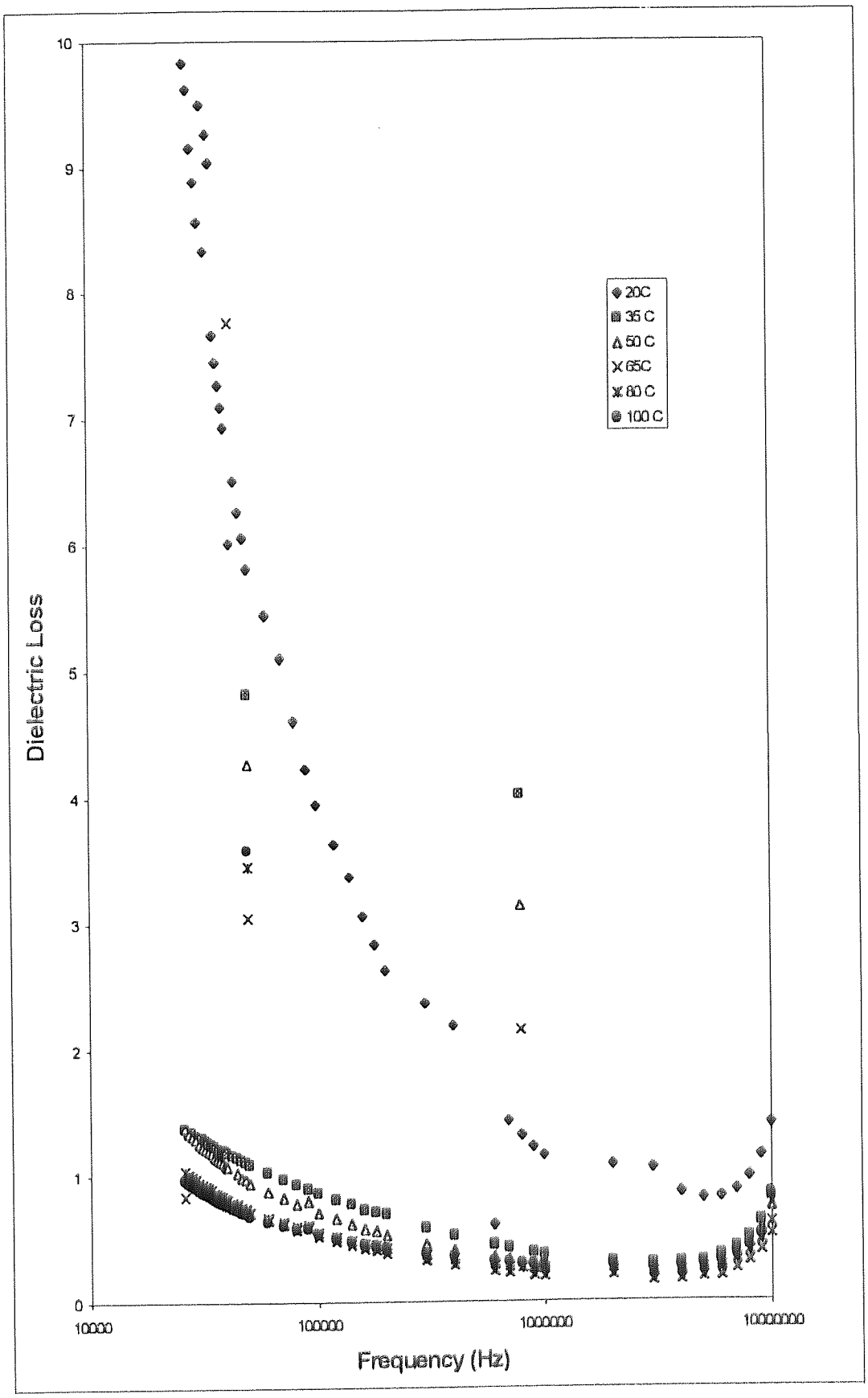

Fig. (4.59): Frequency dependence of dielectric loss.

CHAPTER 5

CONCLUSION

Conclusion

The thermal stabilities of the free ligands differ, such that picolinic acid is thermally stable in the range 50-102°C, nicotinic acid in the range 50-139°C, and isonicotinic acid in the range 50-207°C. From the DTG traces it is clear that the maximum rates of decomposition occur at 193.5°C, 243.5°C, and 271.5°C respectively. The DSC traces for picolinic and nicotinic acids show endothermic peaks due to melting at 149.2°C and 245.5°C. The mechanistic behaviour of all these pyridine carboxylic acids fall into the same mechanistic group, namely the Avrami-Erofeev group, but their fine detail varies. The mechanisms found are A2, A3, and A4 respectively.

The compounds formed between divalent metal ions (Co, Ni and Cu) and these pyridine carboxylic acids in aqueous solution have the following stoichiometries:

$Co(PA)_2.2.5H_2O$, $Co(NA)_2.4H_2O$, $Co(IA)_2.4H_2O$, $Ni(PA)_2.4H_2O$, $Ni(NA)_24H_2O$, $Ni(IA)_2.3.5H_2O$, $Cu(PA)_2$, $Cu(NA)_2$, and $Cu(IA)_2.4.5H_2O$.

In the picolinates, $M(PA)_2xH_2O$, the picolinate acts as a chelating ligand by coordinating to the metal ion through both the nitrogen atom of the aromatic ring and an oxygen atom of the carboxylate group. For cobalt and nickel the metal atom is considered to be in an octahedral environment, while in the anhydrous copper picolinate the copper atom has a tetragonal environment.

In the compounds $Co(NA)_24H_2O$ and $Ni(NA)_24H_2O$ the metal atom is bonded to the nitrogen atoms of two nicotinate group, but not to their carboxylate groups. The completion of six-coordination is achieved by bonding to the oxygen atoms of four water molecules. In the compound $Cu(NA)_2$ the copper atom is bonded to the nitrogen atoms of two nicotinate groups and gains its six-coordinate environment by interacting with four oxygen atoms in adjacent molecules.

In the isonicotinate complexes the nitrogen atom and an oxygen atom of the carboxylic group of each isonicotinate are bonded to different metal atoms to give a chain-like structure. It is further suggested that each metal atom is bonded to oxygen atoms from adjacent layers to give the net six-coordinate environment for the metal atom. The water molecules are attached to the complex by hydrogen bonding.

The dehydration processes of the hydrated complexes are endothermic. Water loss occurs in two temperature ranges, 50-100°C and 100-160°C. Water lost in the lower range is judged to have been attached by hydrogen bonding to an anion or to a coordinated ligand, while water lost at 100-160°C is identified as more strongly bound, ligated water. Comparison of the DTG-determined temperatures of the first two steps of dehydration suggests the water of crystallisation is more strongly bonded to the anions in the Ni(II) complexes than in the complexes of Co(II) and Cu(II). This correlates with the radii of the divalent ions, Ni(II) being smaller than Co(II) and Cu(II). Except for the case of [Cu(IA)2] which is endothermic and decomposes at the lowest temperature, the decomposition of all the anhydrous complexes is strongly exothermic. This, and the recorded weight losses, leads us to conclude that for the copper complex intermediate decomposition products of the organic molecules reduce the copper(II) at a relatively low temperature. The differing observations made for all the other complexes, viz: higher temperatures, exothermicity, and different weight losses, show that they decompose directly to the oxides (CoO, NiO and CuO) without forming free metal at any stage. The absence of any weight gain in the TG curves at higher temperatures for these Co, Ni and Cu complexes confirms that free metal was not formed as an intermediate. The temperatures at which decomposition begins also indicate that the stability of complexes with respect to oxide formation decreases with increasing atomic number Z, Co>Ni>Cu.

A computer program has been developed and used for the kinetic evaluation of non-isothermal DSC data. It makes use of integral methods of kinetic analysis, which are generally preferred because they are more reliable and convenient than the differential methods. This program can also be applied to analyse the reaction kinetics of other thermal analytical techniques, such as TG and DTA curves. This facility offers a simplified and convenient method for rapidly calculating kinetic parameters either for single heating rate experiments, or for sets of data with several different heating rates, and allows the use of any of the recommended kinetic model $g(\alpha)$ functions. The data can be fed by hand or from a data file and the results can be printed, plotted, or saved. Identification of the kinetic mechanism which best fits the data and gives the highest correlation coefficient and the lowest standard deviation can be achieved. The program also calculates the activation energy (E) and the frequency factor (A) from the slope and intercept of the linear regression fit. The output file can be opened from a Microsoft Excel program which offers the many advantages of using a spreadsheet. Thus, it can provide a neat format of data and results.

The use of different methods of kinetic analysis for both isothermal and non-isothermal thermogravimetric data obtained for a compound often give different results. The variations in the calculated activation parameters appear to be both a function of experimental conditions and errors, and of the approximations necessarily made to permit data analysis. This is unsatisfactory and has been addressed here.

The advantages of determining kinetic parameters for solid state reactions by using non-isothermal methods are that considerably fewer data are required; the kinetics can be calculated over an entire temperature range in a continuous manner; a sample undergoes a considerable degree of reaction, often complete reaction, in being raised to the required temperature; and only a single sample is required. By contrast the results obtained by an isothermal method are often

questionable. Thus the work described here has concentrated on non-isothermal studies.

In summary, an integral method for the evaluation of non-isothermal kinetic parameters has been developed. The advantages of the method are: its applicability to any form of $f(\alpha)$ or $g(\alpha)$, and thus its generality; it uses local heating rates; and it uses practically all the range of the values of the degree of conversion. The main disadvantage of the method is the large number of calculations involved, but this can be removed by the using automatic data processing.

In composite methods of analysis, the results obtained not only at a different heating rate but also with different α values are superimposed on one master curve. This is achieved by rewriting the various approximate equations for the integral kinetic analysis of non-isothermal data in such a form that the kinetic function $g(\alpha)$ and the linear heating rate (β) lie on one side of the equation and $\ln(1/T)$ on the other side. The approach we adopted for the development of our composite method is now described.

The kinetics of the non-isothermal decomposition of the compounds under investigation were initially considered in two ways. One is the single-heating rate, and the other is the composite method. In both methods we started by making use of the Coats-Redfern, modified Coats-Redfern, Doyle, and Madhusudanan equations. The analysis of the dynamic data using the Ozawa and Kissinger methods was separately undertaken, and the various sets of results were compared.

For the single heating rate data, each data set was treated using the first list of approximate integral equations. The kinetic parameters (E and A), the quality of fit and the regression results were almost identical, except for Doyle's equation, for which the results differed a little at each heating rate. However, comparison of calculations made for different heating rates showed large variations for each

equation type with different mechanistic models for each rate. It is unlikely that each simple change of heating rate will lead to a change in mechanism. Therefore that approach is seriously flawed.

The composite method of analysis, which involves superposition of all non-isothermal data on one master curve, led to the same reaction model and to similar values of activation parameters for each of the approximate integral equations of Coats-Redfern, modified Coats-Redfern, Doyle, and Madhusudanan. For the first two the curves obtained are indistinguishable.

The use of the reaction model we identified above was then extended to all data and also used with the Ozawa and Kissinger equations. All gave comparable values for the activation parameters. Our approach is internally consistent.

When the results obtained for the separate compounds are considered it is seen from the DTG and DSC studies that in the complexes $[Co(PA)_2 4H_2O]$ and $[Ni(PA)_2 4H_2O]$, the dehydration process occurs in two stages. The activation energy for the first stage lies in the range 23-30 kJ mol-1, and for the second stage is in the range 46-70 kJ mol-1. The remaining complexes proceed in a single step for which the activation energy is in range 41-57 kJ mol-1. The water eliminated at 150°C and below is identified as water of crystallisation, whereas water eliminated at 200°C and above is directly coordinated to the metal atom. Water molecules eliminated at intermediate temperatures might be either. Where two stages are seen both types of water are presumably present and distinct.

The DTG and DSC curves also cover the anhydrous salts of cobalt picolinate, nickel picolinate, and the nickel isonicotinate which decompose in single stages (exothermic effect); and the cobalt nicotinate, nickel nicotinate, and cobalt isonicotinate which decompose in two stages (exothermic effect). From the kinetic studies it can be seen that the values of E and A calculated for dehydration

and decomposition are still very slightly dependent on heating rates, but no pattern to the minor variations could be discerned.

The variation of the electrical conductivity (σ_{dc}) with temperature (T) for samples of [$Co(IA)_2 4H_2O$], [$Ni(IA)_2 3.5H_2O$], and [$Cu(IA)_2 4.5H_2O$] was measured. At a relatively low temperature range the values of the electrical conductivity of all three samples decrease with an increase in temperature. For the sample [$Cu(IA)_2 4.5H_2O$] the attenuation in the electrical conductivity extends to a temperature of approximately 80°C. Then it passes through a minimum before rising with further increases in temperature. The attenuation in conductivity with temperature for all investigated samples in the relatively low temperature range may be attributed to the hydration of the samples. The presence of such H_2O molecules results in protonic conduction which contributes remarkably to the conductivity. The increases in temperature lead to dehydration of both absorbed and lattice water at grain boundaries.

We also note that protonic conduction is strongly dependent on the water content of the sample; a high level of proton conductivity requires both a large concentration of mobile protons and high mobility. It has been argued that absorbed water may reduce the binding energy of protons or attenuate the activation energy of a hopping mechanism for conduction. Therefore, as the temperature is raised and the water content decreases, the hydrogen bonded water network becomes discontinuous, and hence a reduction of proton concentration and of protonic jumping between water molecules occurs. This leads to the observed attenuation in σ_{dc} with an increase in temperature. The thermal analysis for the three samples studied here shows that the sample of [$Cu(IA)_2 4.5H_2O$] has the lowest onset temperature for dehydration. The water content in this sample disappears early, causing the observed minimum in the $\ln\sigma$- $10^3/T$ relation and the activation in the electrical conductivity. For the other two samples containing Co

and Ni, the attenuation in (extends to higher temperatures and so the activation part in lnσ-103/T relation is not observed in this range of temperatures.

The AC conductivity (σ_T) of the three isonicotinate complexes was measured against 10^3/T. For the nickel isonicotinate hydrate, [Ni(IA)$_2$3.5H$_2$O], which is taken as the example here, a strong link between frequency and the values of σ_T is observed at a relatively high temperature, but this relationship is weak in the lower temperature range. As with the DC conductivity dependence on temperature, so also the value of AC conductivity attenuates with a rise in temperature, presumably due to the dehydration of the samples.

The dependence of σ_T on frequency at different fixed temperatures was measured. The values of σ_T increase with an increase in frequency. Values of s (a parameter concerning the type of conduction mechanism) have been calculated from the plots of log σ_T vs. log f. These values were found to slowly increase with temperature. Values of N(Ef), the density of states, were calculated using the value of AC conductivity at a fixed frequency of 5x105 Hz at different temperatures. They approximate to N(Ef) = 10^{23} eV^{-1} cm^{-3}. The value of N(Ef) is shown to decrease as the temperature rises, which conforms to the behaviour of DC conductivity with temperature.

The values of s and N(Ef) for [Co(IA)$_2$.4H$_2$O] and [Cu(IA)$_2$.4.5H$_2$O]. are almost identical to those for [Ni(IA)23.5H2O], implying a common mechanism for all three complexes.

The value of ε' (dielectric constant) decreases with an increase in frequency passing through a minimum value at about 3x10^6 Hz, before increasing at very high frequencies. Also ε' decreases as the temperature is increased. Again the nickel isonicotinate hydrate shows the same values and behaviour as the other two compounds. The attenuation in ε' with frequency in a relatively low frequency

range may be due to the absence of strongly polarizing functional groups, while the later rise of ε' in the very high frequency range is due solely to the electronic polarization.

It is noticed that as the frequency increases the values of ε'', dielectric loss, decrease. This occurs as ion vibration is the only source of the dielectric loss in the very high frequency range. No shift of the loss-peak to higher frequency with the increase in temperature was observed. This is consistent with the Debye model for dielectric relaxation.

Further studies in the immediate area of the research described in this thesis are needed to complete the investigations. These follow-up experiments, which were ruled out here because of a lack of available time should focus on:

1- The confirmation of the nature of the residues of thermal decomposition. Here they are variously identified as Cu metal or as metal oxides. X-ray diffraction studies would offer a straightforward method of investigation.

2- The original aim of these studies, the investigation of the effects of gamma radiation on the complexes, as investigated by their thermal behaviour, activation parameters, reaction models, and electrical conductivities, is still worthy of attention.

3- The effect of particle size on these same properties is also called for.

4- The development of my computer program, for the determination of the kinetic parameters of thermogravimetric data from solid-state reactions, to work under a Windows environment would also be worthwhile.

REFERENCES

References:

1 F. Cotton, F. G. Wilkinson. Advanced Inorganic Chemistry, Interscience publishers, New York. Third edition, (1972).

2 R. Chang, Chemistry, Williams College, Second Edition (1984).

3 J. R. Allan, A. D. Paton, K. Turver, H. J. Bowley, and D. L. Gerrard. Thermal and electrical structure studies on quinxaline xompounds of some first row transition metal ions, Thermochimica Acta, **122**(1987) 403.

4 M. Lalia-Kantouri and M. Hartophylles. Thermal behaviour and kinetic analysis of the thermogravimetric data of some copper(II), nickel(II), and palladium(II) 2-hydroxyaryloximate, Thermochimica Acta, **224**(1993) 203.

5 J. R. Allan, N. D. Baird and A. L. Kassyk. Some first row transition complexes of nicotinamide and nicotinic acid, J. of Thermal Analysis, **16**(1979) 79.

6 J. R. Allan, N. D. Baird and N. D. Baird. The spectral and magnetic properties of some chloro and bromo transition metal complexes of isonicotinic acid, Journal of Coord. Chem., **10**(1980) 171.

7 J. D. Roberts, M. C. Caserio. Basic principles of organic chemistry, W. A. Benjamin, Inc Menlo park, California.third printing, 1965.

8 R.T. Morrison and R. N. Boyd. Organic Chemistry, Allyn and Bacon, INC. Third edition, June 16, 1981.

9 R. K. Bhubon Singh and S. Mitra. Thermal investigation and stereochmical studies of some cyclic ligand complexes of copper(II) and cadmium(II) in the solid state, Thermochimica Acta, **181**(1991) 289.

10 Samiran Mitra, Parimal Kundu, and Rajkumar Bhubon Singh. Thermal investigation and stereochemical studies of some cyclic ligand complexes of nickel(II), copper(II), zinc(II), and cadmium(II) in the solid state, part 1, Thermochimica Acta, **236**(1994) 175.

11 W. K. Musker and M. Sskhawat Hussain. Medium-Ring complexes. III. A comparison of planar pyramidial copper(II) and planar nickel(II) complexes containing seven- and eight- membered- ring diamines, Inorganic Chemistry, **8**, No. 3 (1969) 528.

12 J. R. Allan and J. Dalrymole. The thermal, spectral, and magnetic studies of hippuric acid compounds of cobalt(II), nickel(II), copper(II), and zinc(II) ions, Thermochimica Acta, **185**(1991) 83.

13 J. R. Allan, G. H. W. Milburn and F. Richmond. Thermal, spectral, and magnetic studies of chloro complexes of cobalt, nickel, and copper with 4-(butylamino) benzoic acid, Thermochimica Acta, **177**(1991) 213.

14 P. J. Elving and I. M. Kolthoff. Thermal methods of Analysis. John wiley and Sons, New York, second edition.

15 C. J. Keattch and D. Dollimore. An introduction to thermogravimetry 2nd. Ed., Heyden, London 1975.

16 S. G. Viswanath, S. S. Umare, and M. C. Gupta. Standard polynomial method for derivatives: Application to non-isothermal and isothermal kinertics and computer programming for the Sharp-Wentworth and Freeman-Carrol methods, Thermochimica Acta, **233** (1994) 47.

17 Ching-Jiang Hwang, Jinn-Shing Lee and Ching –Wang Huang. Computerized analysis of single data curved data by a multiple linear regression method for the evaluation of nonisothermal kinetic parameters, Thermochimica Acta, **177**(1991) 253.

18 Jiri Malek and Jode M. Criado. A simple method of kinetic model discrimination. Part 1. Analysis of differential non-isothermal data, Thermochimica Acta, **236**(1994) 187.

19 S. V. Vyazovkiv, A. I. Lesnikovich and V. I. Goryachko. A method of comparing kinetic curves obtained under isothermal and nonisothermal conditions, Thermochimica Acta, **177**(1991) 259.

20 M. A. Mousa and A. M. Summan. Knetic studies on the thermal decomposition of tetrahydrated cobalt(II) methanesulphonate, Thermochimica Acta, **167**(1990) 123.

21 El-H. M. Diefallah, S. N. Basahel and A. A. El-Bellihi. Thermal decomposition of ammonium trioxalatoferrate(III) trihydrate in air, Thermochimica Acta, **290**(1996) 123.

22 El-H. M. Diefallah, A. A. El-Bellihi ,S. N. Basahel and, M. Abed Wahab and Z. A. Omran. Kinetic analysis of thermal decomposition reactions. Part 8. Radiation effects on the thermal decomposition of ammonium oxalate monohydrate, Thermochimica Acta, **230**(1993) 143.

23 C. G. Suresh Mathew and K. N. Ninan. Quantitative correlations of activation parameters and procedural factors-dependence on reaction type, Thermochimica Acta, **184**(1991) 269.

24 Nobuyoshi Koga and Haruhiko Tanaka. Effect of sample mass on the kinetics of thermal decomposition of solid. Part 3. Non-isothermal mass-loss process of molten NH_4NO_3, Thermochimica Acta, **240**(1994) 141.

25 K. K. Aravindakashan and K. Muraleedharan. Kinetics of non-isothermal decomposition of polymeric complexes of *N*, *N'*-bis(dithiocarboxy) piperazine with iron, and cobalt(III), Thermochimica Acta, 159 (1990) 101.

26 Dun Chen, Xiang Gao and David Dollimore. A generalized form of Kissinger equation, Thermochimica Acta, **215** (1993) 109.

27 T. Ozawa. A new method of analyzing thermogravimetric data, Bull. Chem., Sos. Jpn., 38(1965) 1881.

28 David Domllimor. The application of thermal analysis in studying the thermal decomposition of solids, J. Thermal Analysis (1992)

29 Suresh Mahew and C. G. Nair. Thermal decomposition kinetic-part XV. Kinetics and mechanism of thermal decomposition of trtrammine copper(II) sulphste monohydtate. Thermochimica Acta, **144** (1989) 33.

30 J. Sestak and Berggren. On the applicability of the p(x)-function to the determination of reaction kinetics under nonisothermal, Thermochimica Acta, **3**, (1971) 150.

31 V. Satava. Mechanism and kinetics from non-isothermal thermogravimetric traces. Thermochimica Acta, **2** (1971) 423.

32 E. Urbanovicl and E. Segal. An integral method to evaluate the non-isothermal kinetic parameters. Thermochimica Acta, **153** (1989) 257.

33 Dun Chen, Xiang Gao and David Dollimore. The importance of the pre-history of a sample on its thermal behaviour. Part 1, Thermochimica Acta, **215**(1993) 133.

34 E. S. Freeman and B. Carroll. The application of thermoanalytical techniques to reaction kinetics. The thermogravimetry evaluation of the kinetics of the decomposition of calcium oxalate monohydrate. J. Phys. Chem., **62** (1958) 394.

35 C. D. Doyle. Kinetic analysis of thermogravimetric data. J. Appl. Polym. Sci., **5** (1961) 285.

36 Coats, A. W., and J. P. Redfern. Kinetic parameters from thermogravimetric data, Nature, **201** (1964) 68.

37 Turner, R. C., J. Hofman, and D. Chen. Thermogravimetry of the dehydration of $Mg(OH)_2$, Can. J. Chem., **41** (1963) 243.

38 D. W. Van Krevelen, C. van Heerden, J. Huntjens. Physicohemical aspects of the pyrolysis of coal and related organic compound. Fuel, 30 (1951) 253

39 H. H Horowitz, and G. Metzger.A New analysis of thermogravimetric traces. Anal. Chem., **35** (1963) 1464.

40 Dun Chen, Xiang Gao and David Dollimore. The application of non-isothermal methods of kinetic analysis to the decomposition of calcium hydroxide, Thermochimica Acta, **215** (1993) 65.

41 El-H. M. Diefallah, S. N. Basahel, A. A. El-Bellihi, Thermal decomposition of trioxalatoferrate(III) trihydrate in air, Thermochimica Acta, **290** (1996) 123.

42 J. M. Criado. Kinetic analysis of DTG data from master cuerves. Thermochimica Acta, **24** (1978) 186.

43 P. M. Madhusudanan, K. Krisshnan and K. N. Ninan. New Approximation for the p(x) function in the evaluation of non-isothermal kinetic data, Thermochimica Acta, **97** (1986) 189.

44 J. R. MacCallum and J. Tanner. The kinetics of thermogravimetry, Eur. Polym. J., **6** (1970) 1033.

45 H. E. Kissinger. Reaction kinetic in differential thermal analysis. Anal. Chem., **29** (1957) 1702.

46 S. Al-Thabaiti, A. A. El-Bellihi, and M. M. Moustafa, A. Y. Obaid, A. O. Alyoubi, A. A. samarkandy and El-H. M. Diehallah, KAU science (in press), 1998.

47 El-H. M. Diehallah. Kinetic analysis of thermal decomposition reactions. Part VI. Thrmal decomposition of manganese(II) acetate tetrahydate, Thermochimica Acta. **202** (1992) 1.

48 El-H. M. Diehallah, A. Y. Obaid, A. H. Qusti, a. A. El-Bellihi, M. Abdel Wahab and M. M. Moustafa. Gamma irradiation effects on the kinetic of the non-isothermal decomposition of manganese acetate tetrahydrate, Thermochimica Acta. **274** (1996) 165.

49 El-H. Diefallah, S. N. Basahel, M.M El-Fass,and E. A. Al-Sabban. Kinetic analysis of thermal decomposition reactions. Part 5. Gamma irradiation effects on the thermal decomposition of potassium nickel oxalatw, Thermochimica Acta. **184** (1991) 141.

50 A. Romero, E. Garcia Calvo, Pleton and M. A. Arranz. A differential method for kinetic of non-isothermal solid decomposition. Thermochimica Acta, **182** (1991) 235

51 Jiri Malek. A computer program for kinetic analysis of non-isothermal thermoanalytical data, Thermochimica Acta, **138** (1989) 337.

52 Oana Caprp and Segal. Basic program to discriminate among mechanism of solid-gas decomposition (DISCRIM 2), Thermochimica Acta, **185** (1991) 111.

53 J. S. Zsako and J. S. Zsako. Kinetic analysis of thermogravimtric data XIV. J., Therm. Anal., **19** (1980) 333.

54 L. Reich and S. S. Stivala. Computer analysis of non-isothermal TG data for mechanism and activation energy. Part 1, Thermochimica Acta, **73** (1984) 165.

55 J. P. Elder. A computer program system for kinetic analysis of non-isothermal thermogravimetry data. II. Generallized kinetic analysis and application to coal pyrolysis. Thermochimica Acta, **95** (1985) 41.

56 E. Eftimie and E. Segal. Basic language program to evaluate non-isothermal kinetic parameters from thermoanalytical data, Thermochimica Acta, **105** (1986) 247.

57 P. K. Sahoo, S. K. Mohanty, V. Chakravortty and K. C. Dash. Computer evaluation of non-isothermal kinetic parameters from TG data, Thermochimica Acta, **130** (1988) 369.

58 T. J. Taylor and Y. P. Khanna. The distinguishability of kinetic models using single, non-isothermal thermal analysis experiment, Thermochimica Acta, **136** (1988) 219.

59 S. Ma, G. Huang and J. O. Hill, KNIS- a computer program for the systematic kinetic analysis of non-isothermal thermogravimetric data, Thermochimica Acta, **184**(1971) 233.

60 J. Malek. A computer program from kinetic analysis of non-isothermal thermoanalytical data. Thermochimica Acta, **138** (1989) 337.

61 Leo Reich. Use of spreadsheets in thermal analysis. Part 4, Thermochimica Acta, **164** (1990) 1.

62 Leo Reich. Use of spreadsheets in thermal analysis. Part 6, Thermochimica Acta, **173** (1990) 253.

63 Leo Reich. Use of spreadsheets in thermal analysis. Part 3, Thermochimica Acta, **143** (1989) 311.

64 M. A. Omar, " Elementary Solid State Physics, Addison-Wesley Publishing company, First Edition (1975).

65 G. I. Epifanov, Solid State Physics, Mir Publishers Moscow, First Published 1979.

66 M. E. Green. Charge-Carrier injection and the ore-exponential factor in semiconducting organic substances, J. Chem. Phys., **51**, 8, (1969) 3279.

67 J. R. Allan, H. J. Bowley, D.L. Gerrard, A. D. Paton and K. Turveym. Thermal, spectral, magnetic and electrical studies of cobalt(II) and nickel(II) with 3-(3-Pyridyl) acrylic acid. Thermochimica Acta, **137** (1989) 205.

68 J. R. Allan and A. D. Paton. Preparation, structural, thermal and electrical studies of the chloro complexes of cobalt, nickel, and copper with 4-pyridinealdoxime, Thermochimica Acta, **228** (1993) 71.

69 J. R. Allan D. H. Brown, R. H. Nuttall, and D. W. Sharp. Pyridine complexes of iron(II), copper(II),zinc(II), and cadmium(II) halides, J. Chem. Soc. (A), (1993) 1031.

70 P. Knuuttila and H. Knuuttila. Crystal and molecular structures of thermal decomposition of calcium(II) complexes with pyridine monocarboxylic acid N-oxides, Act Chemica Scandinavica, A, **39**, (1985) 307.

71 J. R. Allan, M. Barron and A. R. Werninnck. Thermal studies on pyridine-2-3 dixarboxylic acid compounds of manganese(II), iron(II), cobalt(II),and nickel(II), Thermochimica Acta, **116** (1987) 275.

72 Y. Suzuki, T. Yamada and K. Sawada. Thermal decomposition of solid complexes of cadmium chloride with substituted pyridine, Thermochimica Act, **128** (1988) 225.

73 E. E. Sileo, P. J. Morando, Carlos O. Della Vedova, and Micuel A. Blesa. The thermal decomposition of copper(II) nicotinate and isonicotinate, Thermochimica Act, **138** (1989) 233.

74 J.R. Allan, W. C. Geddes, C. S. Hindel and A. E. Orr. Thermal analysis studies on pyridine carboxylic acid complexes of zinc(II), Thermochimica Act, **153** (1989) 249.

75 J. R. Allan, A. D. Paton and K. Yurvey. Structural, thermal and electrical studies of some transition metal compounds of 2,3-cyclododecenopyridine, Thermochimica Act, **184** (1991) 193.

76 G. Liptay, J. Mink, and G. Kenessey. Pyridine type complexes pf transition-metal-halides II. Preparation, characterization, and thermal analysis studies of cobalt(II)-bromides and iodides with 2-,3-,4-methylpyridine, Thermochimica Act, **214** (1993) 71.

77 E. E. Sileo, P. J. Morando, Erwin C. Baumgartner, and Miguel A. Blesa. Comparison of the thermal behaviour of the metal salts of simple and polymeric carboxylates, Thermochimica Acta, **184** (1991) 295.

78 A. M. G. Macdonald and P. Sirichanya. The determination of metals in organic compounds by oxygen-flask or wet combustion, Microchemical J. **14**, (1969) 199.

79 Marilena Ferbinteanu, Fanica Cimpoesu, Michaeta Stanescu, Marius Andruh, M. Badescu and E. Segal, On the thermal stability and non-isothermal decomposition kinetic of some coordination compounds of cobalt, nickel, and copper with a β-dicarbonylic compound and 4-benzoylpyridine or 4,4′-dipyridyl as ligands, Thermochimica Acta, **221**(1993) 237.

80 J. R. Allan and J. Dalrymple. Structural characterisation of bis(suberate) cobalt(II) 1.5 hydrate and a thermal analysis study of suberic acid and bis(suberate) cobalt(II) 1.5 hydrate, Thermochimica Act, **221** (1993) 195.

81 J. R. Allan, P. C. Beaumont, G. H. W. Milburn and I. Wood. Preparation, structural characterisation and thermal analysis studyies of vinylacetic acid compounds of some first row transition metals, Thermochimica Acta **230** (1993) 137.

82 J. R. Allan, A. D. Paton, and K. Turvey. Preparation, structural characterisation, thermal and electrical studies of complexes of cobalt and copper with methyl-3-pyridyl-carbamate, Thermochimica Acta, **240** (1994) 215

83 J. R. Allan, P. C. Beaumont, G.H. W. Milbrun and I. J wood. Preparation, structural characterisation, thermal and electrical studies of cobalt(II) chloride and zinc(II) chloride compounds of poly(acrylamide), Thermochimica Acta, **230** (1993) 129.

84 J. R. Allan, B. McCloy and A. D. Paton. Preparation, thermal, structural and electrical studies of dichlorohexa (anthraanilamide) cobalt(II) and dichloro (anthraanilamide) copper(II), Thermochimica Acta, **231** (1994) 121.

85 J. R. Allan and A. D. Paton. Thermal, electrical and structural properties of chloro complexes of cobalt, nickel, copper and zinc with 6,7-dimethyl-2,3-di(2-pyridyl) quinoxaline, Thermochimica Acta, **166** (1990) 177.

86 J. R. Allan and A. D. Paton. Thermal, structural, magnetic and electrical studies of cobalt(II) and nickel(II) with 3-(3-pyridyl) acrylic acid. Thermochimica Acta, **137** (1989) 205.

87 M. A. Ahmed, M.Sc. thesis, Gamma irradiation effects on the electrical conductivity behaviour of some sciff base chelats and double complex, Chemistry department, Faculty of science, Assiut University, 1984.

88 J. R. Allan, B. Carson, A. D. Paton, K. Turvey, H. J. Bowley and D. L. Gerrard. Electrical studies and characterisation of complexes of cobalt(II), copper(II) and zinc(II) with diphenyl-2-pyridyl-2-pyridylmethane, Inorganica Chimica Acta, **158** (1989) 249.

89 David E. Goldberg and Clyde R. Dillard, College chemistry , Collier Macillan publishers, London,1974.

90 Powder diffraction file search manual Hanawalt method. Inorganic, 1976. Joint committee on powder diffraction standard, U.S.A.

91 W. Brzyska and A.Krol. Properties and thermal decomposition in air atmosphere of Co(II), Ni(II), Cu(II), and Zn(II) benzene-1,2-dioxyacetates, Thermochimica Acta **223** (1993) 241.

92 H.M. Al-Hazmi and S. Al-SheWman, Principle in spectrum of organic compounds,

93 Xiang Gao and Daivd Dollimore. The thermal decomposition of oxatates. Part 26. A kinetic study of the thermal decomposition of manganese(II) oxalate dihydrate, Thermochimica Acta **215** (1993) 47.

94 J. R. Allan and J. Dalrymple. Preparation, structural characterisation and thermal analysis studies of the cobalt(II), nickel(II), and copper complexes of benzylmalonic acid, Thermochimica Acta **231** (1994) 129.

95 C. J.Keattch and D. Dollimore, An introduction to thermogravimetry, 2nd , Heyden, London, 1975.

96 M. N . Figgis and J. Lewis, Modern coordination chemistry, Eds. Lewis and R. G. Wolkins, intrescience, New York (1960).

97 J. R. Allan, and B. McClot. Thermal, structural and electrical studies of the chloro complexes of cobalt, nickel, and copper with 1,10-phenanthroline, Thermochimica Acta **214** (1993) 219.

98 J. R. Allan, P. C. Beaumont, G. H. W. Milburn and I. Wood. Structural and thermal studies of the chloro complexes of cobalt, nickel, and copper with 1.6-hexanediamine, Thermochimica Acta **219** (1993) 159.

99 A. B. P. Lever, "Inorganic electronic spectroscopy", Elsevier science Publishers B. V. The Netherlands (1984). 2nd edition.

100 J. R. Allan, P. C. Beaumont, G. H. W. Milburn and I. Wood. Preparation, structural characterisation and thermal analysis of complexes of cobalt, nickel, and copper with nonylamone, Thermochimica Acta **214** (1993) 243.

101 W. Brzyska and A. Krol, The properties and thermal decomposition in air of Co(II),Ni(II), Cu(II), and Zn(II) bezene-1,3-dioxyacetates, Thermochimica Acta **237** (1994) 111.

102 J. R. Allan and J. Dalrymple. The thermal, spectral and magnetic studies of oxamic acid compounds of cobalt(II), nickel(II), and copper(II) ions, Thermochimica Acta **221** (1993) 199.

103 Ram chand paul and S. L. Chandha. Structure of donoriaccerptor complexes-IX coordination comopunds of imides with metal halides. J. Inorg. Nucl. Chm., **31**(1969) 2753.

104 Seham A. A. Mansour. Spectroscopic and microscopic investigations of the thermal decomposition course of nickel oxysalts. Part 3. Nickel oxalate dihydrate, Thermochimica Acta **230** (1993) 243.

105 M. K. El-Mansy, N. M.Shash, M. H. Makld and E.M. Diefallah. Effect of growning barium ferrite phase on the electrical conduction in $Fe_2/BaCO_3$ composite, Materials Chemistry and Physics **52**(1998) 71.

106 W. A. England, M. G. Cross, A. Hamnett, P. J. Wiseman and J. B. Goodenough. Fast proton conduction in inorganic ion-exchange compounds, Solid state ionics 1 (1980) 231.

107 U. Chowdhry, J. R. Barkley, A. D. English and A. W. Sleight. New inorganic proton conductors, Material Res. Bull., 17 (1982)917.

108 U. Chowdhry, J. R. Barkley, A. D. English and A. W. Sleight, Material Res. Bull., 17 (1982)917.

109 Cleafield, A.. Role of ion exchange in solid-state chemistry, Chem. Rev., 88(1988) 125.

110 N. M. Shash and H. M. Aly. Electrical-conductivity behavior in crystalline cerium (IV) phosphates, IL Nuovo Ciments, 19 D, No 7, (1997) 92

APPENDIX

Appendix 1:

X-ray data for cobalt(II) picolinate(a), cobalt(II) nicotinate(B) cobalt(II) isonicotinate.

Picolinic acid

P. No.	2q	d-sp	I	I/I°
1	8.5	10.4023	13.8	15.5
2	12.9	6.86244	9.3	10.4
3	13..2	6.70714	60.9	68.4
4	17.3	5.12573	89	100
5	18.4	4.83473	73	82
6	23.9	3.7308	9.6	10.8
7	24.1	3.69267	5.7	6.4
8	24.9	3.58289	18.1	20.3
9	25.2	3.53392	4.4	4.94
10	26.4	3.38224	81.3	91.3
11	27.7	3.2261	31.2	35.1
12	30.2	2.95926	15.1	17
13	30.7	2.91219	3.5	3.93
14	31.4	2.85328	7	7.87
15	31.8	2.81392	7.2	8.09
16	33.3	2.69052	57.4	64.5
17	36.1	2.488	7.4	8.31
18	36.8	2.44227	14.2	16
19	37.4	2.40446	3.5	3.93
20	37.8	2.37993	1.3	1.46
21	38.8	2.32086	24.8	27.9
22	40.6	2.22203	35.6	40
23	44.8	2.02299	6	6.74
24	45.4	1.99764	4.7	5.28
25	49.2	1.8188	10.4	11.7

Nicotinic acid

P. No.	2q	d-sp	I	I/I°
1	15	5.90609	55.5	67
2	1.9	4.46152	34.4	41.5
3	20.8	4.27046	19.5	23.6
4	24.4	3.64794	82.8	100
5	25.5	3.49302	75	90.6
6	26.5	3.36968	63	76.1
7	27.6	3.23758	57.8	69.8
8	28.8	3.09984	8.5	10.3
9	33.7	2.65949	14	16.9
10	35.4	2.53558	7.9	9.54
11	37.9	2.37388	22.7	27.4
12	38.9	2.31513	4.1	4.95
13	39.5	2.28133	7	8.45
14	40.9	2.20642	18	21.7
15	44.8	2.02299	2.4	2.9
16	50.3	1.81561	6.5	7.85
17	50.9	1.79395	17	20.5
18	54.8	1.67655	6.6	7.97
19				
20				
21				
22				
23				
24				
25				

Isonicotinic acid

P. No.	2q	d-sp	I	I/I°
1	13.9	6.37091	2.7	4.16
2	15.1	5.86721	4.2	4.72
3	16.3	5.43787	89	100
4	19.5	4.55212	13	14.6
5	21.5	4.1425	9	10.1
6	24.3	3.66272	14	15.7
7	25.8	3.45308	87.4	98.2
8	27.7	3.2261	83.4	93.7
9	30.8	2.90296	3.8	4.27
10	33.4	2.68269	8.2	9.21
11	35.1	2.55656	4	4.49
12	37.2	2.41692	27.9	31.3
13	40.1	2.24857	36.1	40.6
14	42.8	2.11277	20.1	22.6
15	48.1	1.89162	3.8	22.6
16	48.9	1.86253	4.5	5.06
17	52.8	1.73378	10.8	12.1
18	56.4	1.63269	4.9	5.51
19				
20				
21				
22				
23				
24				
25				

Appendix 2:

X-ray data for the cobalt(II) picolinate, cobalt(II) nicotinate, and cobalt(II) isonicotinate.

Cobalt picolinate complex

P. No.	2θ	d - Spacings	I	(I / I°)
1	10.5	8.4250	3.6	14.4578
2	11.2	7.8999	5	20.0803
3	11.8	7.4996	6.6	26.5060
4	12.8	6.9158	7.2	28.9157
5	15.8	5.6088	3.9	15.6627
6	16.9	5.2461	17	68.2731
7	17.7	5.0108	3.2	12.8514
8	18.1	4.9009	1.9	7.6305
9	18.7	4.7450	3.9	15.6627
10	20.1	4.4176	3.1	12.4498
11	21.4	4.1521	3.8	15.2610
12	22.9	3.8834	3.6	14.4578
13	24.3	3.6627	24.9	100.0000
14	25.4	3.5065	4.4	17.6707
15	26.2	3.4013	8.7	34.9398
16	30	2.9785	2.7	10.8434
17	31	2.8847	8.4	33.7349
18	39.6	2.2758	9.5	38.1526
19	44.4	2.0403	3.5	14.0562
20	47.4	1.9179	1.5	6.0241
21	50.3	1.8139	2.9	11.6466
22	51.8	1.7649	2.4	9.6386
23	53.1	1.7247	2.5	10.0402
24	53.7	1.7068	4.2	16.8675
25	54.7	1.6780	2.8	11.2450
26				

Cobalt nicotinate complex

P. No.	2θ	d - Spacings	I	(I / I°)
1	14	6.3256	2.9	9.6026
2	15.6	5.6803	30.2	100.0000
3	25.9	3.4400	10.8	35.7616
4	27.4	3.2550	8.2	27.1523
5	28.1	3.1755	9.1	30.1325
6	28.6	3.1211	4	13.2450
7	29.7	3.0079	3.6	11.9205
8	30.6	2.9215	2.8	9.2715
9	32.9	2.7223	3	9.9338
10	34.1	2.6292	3	9.9338
11	36.1	2.4880	4.4	14.5695
12	39.3	2.2925	5.6	18.5430
13	43.6	2.0758	4.3	14.2384
14	44.6	2.0316	3.5	11.5894
15	44.8	2.0230	3.3	10.9272
16	47.1	1.9294	3.4	11.2583
17	47.6	1.9103	2.1	6.9536
18	47.9	1.8991	2.6	8.6093
19	48.2	1.8879	3.1	10.2649
20	50.8	1.7972	4.9	16.2252
21	52.2	1.7523	2	6.6225
22	55.2	1.6639	3.4	11.2583
23	58.1	1.5876	1.8	5.9603
24	59.2	1.5607	3.5	11.5894
25				
26				

Cobalt nicotinate complex

P. No.	2θ	d - Spacings	I	(I / I°)
1	11.5	7.6945	2.7	13.5678
2	12	7.3750	1.7	8.5427
3	13.2	6.7071	10.7	53.7688
4	14.3	6.1936	9.7	48.7437
5	20.6	4.3115	7	35.1759
6	22.1	4.0221	9.2	46.2312
7	22.6	3.9342	3.2	16.0804
8	25.5	3.4930	19.9	100.0000
9	26.3	3.3886	7.5	37.6884
10	29.2	3.0583	5.3	26.6332
11	32.9	2.7223	3.9	19.5980
12	33.3	2.6905	6.7	33.6683
13	34.3	2.6143	2.8	14.0704
14	35.7	2.5150	4.7	23.6181
15	37.5	2.3983	2.8	14.0704
16	38.5	2.3383	2.8	14.0704
17	39.8	2.2648	2.2	11.0553
18	41.1	2.1961	11.6	58.2915
19	41.9	2.1560	4.1	20.6030
20	42.6	2.1222	5.3	26.6332
21	46.4	1.9569	7	35.1759
22	51	1.7907	4.1	20.6030
23	52.8	1.7338	6.2	31.1558
24	59.7	1.5488	3.6	18.0905
25				
26				

X-ray data for the nickel(II) picolinate, nickel(II) nicotinate, and nickel(II) isonicotinate.

Nickel picolinate complex

P. No.	2θ	d - Spacings	I	(I / I°)
1	10.5	8.4250	59.9	66.5556
2	11.8	7.4996	90	100.0000
3	17.7	5.0108	25.9	28.7778
4	18.9	4.6953	5.1	5.6667
5	20.1	4.4176	61.4	68.2222
6	21.7	4.0953	14.8	16.4444
7	22.4	3.9689	30.5	33.8889
8	25.4	3.5065	24.7	27.4444
9	26.4	3.3759	29.4	32.6667
10	27.6	3.2318	24.7	27.4444
11	27.8	3.2090	22.5	25.0000
12	31	2.8847	61	67.7778
13	31.9	2.8053	19	21.1111
14	33	2.7143	9.9	11.0000
15	34.5	2.5996	14.1	15.6667
16	35.1	2.5566	4.9	5.4444
17	36.3	2.4748	8.9	9.8889
18	37.3	2.4107	6.6	7.3333
19	38.7	2.3266	29.8	33.1111
20	39.9	2.2594	11.9	13.2222
21	41	2.2013	15.6	17.3333
22	41.4	2.1809	4.8	5.3333
23	42	2.1511	2	2.2222
24	42.3	2.1366	2.1	2.3333
25	43.5	2.0804	2.1	2.3333
26	44.6	2.0316	19.2	21.3333

Nickel nicotinate complex

P. No.	2θ	d - Spacings	I	(I / I°)
1	11.6	7.6284	9.6	17.9104
2	13.2	6.7071	53.3	99.4403
3	14.4	6.1508	46.1	86.0075
4	16.4	5.4049	8.9	16.6045
5	20.6	4.3115	16.6	30.9701
6	22.2	4.0042	50.5	94.2164
7	25.5	3.4930	53.6	100.0000
8	26.5	3.3634	20.6	38.4328
9	28.2	3.1644	5.6	10.4478
10	29.3	3.0481	25.9	48.3209
11	31.6	2.8313	6.8	12.6866
12	33.4	2.6827	25.3	47.2015
13	35.8	2.5082	13.7	25.5597
14	37.7	2.3860	5.5	10.2612
15	41.2	2.1910	34.2	63.8060
16	44.7	2.0273	7.1	13.2463
17	45.8	1.9811	11.8	22.0149
18	46.6	1.9490	11	20.5224
19	51.1	1.7874	14.5	27.0522
20	52.8	1.7338	8.7	16.2313
21	54.6	1.6808	6.2	11.5672
22	56.1	1.6394	2.1	3.9179
23	60.8	1.5234	4.3	8.0224
24	65.9	1.4173	9.5	17.7239
25				
26				

Nickel nicotinate complex

P. No.	2θ	d - Spacings	I	(I / I°)
1	10	8.8451	3.5	4.0509
2	14.2	6.2370	7.6	8.7963
3	15.8	5.6088	86.4	100.0000
4	17.9	4.9552	2.9	3.3565
5	19.4	4.5754	8.5	9.8380
6	20	4.4394	2.7	3.1250
7	21.8	4.0768	3.7	4.2824
8	24.4	3.6479	21.8	25.2315
9	25.9	3.4400	57	65.9722
10	27.7	3.2204	22.7	26.2731
11	28	3.1866	7.5	8.6806
12	28.7	3.1104	7.2	8.3333
13	30.1	2.9689	9.3	10.7639
14	32.2	2.7799	11.8	13.6574
15	32.9	2.7223	12.3	14.2361
16	36.6	2.4552	8	9.2593
17	39.6	2.2758	30.8	35.6481
18	41.4	2.1809	9.8	11.3426
19	47.6	1.9103	5.2	6.0185
20	49.9	1.8275	9.9	11.4583
21	53.4	1.7157	11.1	12.8472
22	67.6	1.3858	3.7	4.2824
23				
24				
25				
26				

X-ray data for the copper(II) picolinate, copper(II) nicotinate, and copper(II) isonicotinate.

Copper picolinate complex

P. No.	2θ	d - Spacings	I	(I / I°)
1	9.6	9.2127	10.9	12.3723
2	11.7	7.5634	88.1	100.0000
3	13.9	6.3709	2.6	2.9512
4	18.3	4.8478	6.1	6.9240
5	20.1	4.4176	42	47.6731
6	22.9	3.8834	45.8	51.9864
7	27.4	3.2550	52.2	59.2509
8	36.8	2.4423	11	12.4858
9	37.9	2.3739	4.7	5.3348
10	45.9	1.9770	3	3.4052
11	47.5	1.9141	7.5	8.5131
12	52.9	1.7307	2.2	2.4972
13	55.2	1.6639	2.4	2.7242
14	57	1.6156	3.3	3.7457
15	62.4	1.4881	1.9	2.1566
16				
17				
18				
19				
20				
21				
22				
23				
24				
25				
26				
27				
28				
29				

Copper nicotinate complex

P. No.	2θ	d - Spacings	I	(I / I°)
1	12.4	7.1380	17.6	21.1031
2	15.1	5.8672	7.5	8.9928
3	16.6	5.3403	7.5	8.9928
4	19.8	4.4838	7	8.3933
5	24.3	3.6627	83.4	100.0000
6	25.6	3.4796	6	7.1942
7	28.9	3.0893	4.8	5.7554
8	37.4	2.4045	15.9	19.0647
9	43	2.1034	1.8	2.1583
10	50.4	1.8106	2	2.3981
11				
12				
13				
14				
15				
16				
17				
18				
19				
20				
21				
22				
23				
24				
25				
26				
27				
28				
29				

Copper nicotinate complex

P. No.	2θ	d - Spacings	I	(I / I°)
1	10.1	8.7577	4.5	5.0000
2	13.7	6.4635	9.8	10.8889
3	15.3	5.7910	90	100.0000
4	16.4	5.4049	5.2	5.7778
5	18.5	4.7959	9.3	10.3333
6	19.2	4.6226	7.1	7.8889
7	20.1	4.4176	5.5	6.1111
8	22.7	3.9171	9.1	10.1111
9	24.4	3.6479	5	5.5556
10	25.6	3.4796	18.9	21.0000
11	26.4	3.3759	61.3	68.1111
12	27.1	3.2903	22.4	24.8889
13	27.9	3.1978	15.9	17.6667
14	29.8	2.9981	8.2	9.1111
15	31.9	2.8053	15.1	16.7778
16	33.4	2.6827	5.6	6.2222
17	34.1	2.6292	14.5	16.1111
18	36.9	2.4359	7.9	8.7778
19	37.8	2.3799	4	4.4444
20	39.6	2.2758	28.1	31.2222
21	42.1	2.1463	7	7.7778
22	43.4	2.0849	10.3	11.4444
23	44.2	2.0490	5.3	5.8889
24	45.7	1.9852	5.4	6.0000
25	48.2	1.8879	11.7	13.0000
26	51.2	1.7841	6.5	7.2222
27	52.8	1.7338	15.3	17.0000
28	54.2	1.6923	2.4	2.6667
29	54.8	1.6751	2.7	3.0000

Appendix 3:

The values of α for free ligands:

HPA

T	5	10	15	20
439	0.0530			
441	0.0710			
443	0.0894			
445	0.1080			
447	0.1280			
449	0.1480			
451	0.1690			
453	0.1900			
455	0.2130			
457	0.2380			
459	0.2650			
461	0.2950	0.0579		
463	0.3290	0.0738		
465	0.3700	0.0908		
467	0.4160	0.1090		0.0507
469	0.4850	0.1300	0.0498	0.0752
471	0.5730	0.1600	0.0672	0.1010
473	0.6630	0.1970	0.0854	0.1270
475	0.7500	0.2400	0.1050	0.1540
477	0.8250	0.2880	0.1250	0.1820
479	0.8750	0.3390	0.1460	0.2110
481	0.9090	0.3930	0.1700	0.2420
483	0.9380	0.4500	0.1980	0.2740
485		0.5090	0.2330	0.3070
487		0.5690	0.2740	0.3410
489		0.6300	0.3180	0.3780
491		0.6890	0.3630	0.4170
493		0.7480	0.4130	0.4570
495		0.8050	0.4630	0.5000
497		0.8570	0.5140	0.5450
499		0.9000	0.5640	0.5910
501		0.9330	0.6160	0.6400
503		0.9600	0.6660	0.6890
505			0.7170	0.7360
507			0.7660	0.7800
509			0.8110	0.8190
511			0.8540	0.8490
513			0.8920	0.8760
515			0.9260	0.9030
517			0.9540	0.9280
519				0.9500

HNA

T	5	10	15	20
525.0	0.0651			
527.0	0.1320			
529.0	0.2030			
531.0	0.2770			
533.0	0.3550			
535.0	0.4370			
537.0	0.5240	0.0839		
539.0	0.6160	0.1270		
541.0	0.7110	0.1720		
543.0	0.8110	0.2190		
545.0	0.9140	0.2690		
547.0		0.3210	0.0796	
549.0		0.3760	0.1200	0.0617
551.0		0.4340	0.1630	0.0822
553.0		0.4950	0.2070	0.1030
555.0		0.5590	0.2540	0.1250
557.0		0.6270	0.3040	0.1480
559.0		0.6990	0.3560	0.1730
561.0		0.7740	0.4110	0.1980
563.0		0.8520	0.4690	0.2250
565.0		0.9310	0.5310	0.2530
567.0			0.5960	0.2830
569.0			0.6650	0.3150
571.0			0.7370	0.3490
573.0			0.8120	0.3860
575.0			0.8880	0.4250
577.0			0.9430	0.4660
579.0				0.5110
581.0				0.5600
583.0				0.6120
585.0				0.6690
587.0				0.7310
589.0				0.7980
591.0				0.8680
593.0				0.9260
595.0				0.9580

HIA

T	5	10	15	20
483	0.0473			
485	0.0568			
487	0.0664			
489	0.0760			
491	0.0857			
493	0.0956			
495	0.1060			
497	0.1160			
499	0.1260			
501	0.1360			
503	0.1470			
505	0.1580			
507	0.1690	0.0501		
509	0.1800	0.0576		
511	0.1920	0.0653		
513	0.2040	0.0731		0.0457
515	0.2160	0.0811		0.0505
517	0.2290	0.0849		0.0553
519	0.2420	0.0979		0.0602
521	0.2550	0.1070		0.0651
523	0.2700	0.1160		0.0701
525	0.2840	0.1250		0.0752
527	0.3000	0.1350	0.0490	0.0804
529	0.3160	0.1450	0.0566	0.0857
531	0.3330	0.1560	0.0643	0.0911
533	0.3510	0.1670	0.0722	0.0966
535	0.3690	0.1780	0.0803	0.1020
537	0.3890	0.1910	0.0887	0.1080
539	0.4100	0.2030	0.0973	0.1140
541	0.4320	0.2170	0.1060	0.1200
543	0.4560	0.2310	0.1160	0.1270
545	0.4810	0.2460	0.1250	0.1340
547	0.5080	0.2630	0.1350	0.1400
549	0.5360	0.2800	0.1460	0.1480
551	0.5670	0.2980	0.1560	0.1550
553	0.6000	0.3180	0.1680	0.1630
555	0.6350	0.3390	0.1800	0.1710
557	0.6730	0.3610	0.1920	0.1800
559	0.7130	0.3850	0.2030	0.1890
561	0.7570	0.4110	0.2190	0.1990
563	0.8030	0.4390	0.2340	0.2090
565	0.8510	0.4690	0.2490	0.2190
567	0.8990	0.5020	0.2660	0.2310
569	0.9470	0.5370	0.2840	0.2430
571		0.5750	0.3030	0.2560
573		0.6170	0.3240	0.2700
575		0.6610	0.3460	0.2850
577		0.7100	0.3690	0.3010
579		0.7620	0.3950	0.3180
581		0.8180	0.4220	0.3370
583		0.8800	0.4520	0.3580
585		0.9430	0.4840	0.3800

T	5	10	15
587			0.5190
589			0.5570
591			0.6000
593			0.6460
595			0.6970
597			0.7540
599			0.8150
601			0.8710
603			0.9250
605			0.9590
607			
609			
611			
613			